

The dynamic behaviour of hydraulic structures caused by wave impact loads

Enhancing the present design method in time and space

S. Sleuwaegen

Figure 1: (Title page) Aerial photo of discharge sluice complex at Den Oever
([https://beeldbank.rws.nl/Rijkswaterstaat/Bart van Eyck](https://beeldbank.rws.nl/Rijkswaterstaat/Bart%20van%20Eyck), June 7, 2019, URL <https://beeldbank.rws.nl/MediaObject/Details/74790>)

The dynamic behaviour of hydraulic structures caused by wave impact loads

Enhancing the present design method in time and space

By

S. Sleenwaegen

in partial fulfilment of the requirements for the degree of

Master of Science
in Civil Engineering

at the Delft University of Technology
January 2020

Supervisor:

Thesis committee:

Ir. O.C. Tieleman

Dr. ir. R. Abspoel

Ir. E. de Almeida

Dr. ir. B. Hofland

Dr. ir. A. Tsouvalas

Delft University of Technology

An electronic version of this thesis is available at <http://repository.tudelft.nl/>.

Preface

This thesis report is the final project to complete my study Civil Engineering at the Delft University of Technology. In the thesis work the dynamic behaviour of gates subjected to impulsive wave impacts is investigated, and propositions are made to improve the current design method. This thesis subject makes it possible to graduate in two master tracks within the master program of Civil Engineering, Structural- and Hydraulic Engineering.

I would like to thank all the members of my graduation committee for their guidance and feedback. The feedback and help I received from the committee members helped me a lot throughout the whole process, and made it possible to achieve this thesis report.

Furthermore, I thank Thomas for his support during the entire process.

Special thanks to my family for their support and giving me the possibility to achieve my goals.

*Shannon Sleeuwaegen
Delft, January 2020*

Abstract

In the Netherlands many hydraulic structures are present, a lot of these structures are outworn and close to the end of their lifetime. At the end of the (theoretical) lifespan of a structure, the structural safety is under discussion, so that new structures have to be designed and built, or the old structure has to be renovated to elongate its lifetime. One of these structures that is in need of renovation is the Afsluitdijk. Important loads on hydraulic structures, are wave loads. Wave loads can be divided into impulsive and quasi-static loads. The impulsive wave impacts are very intense and of short duration (typically 10-100 ms), and can cause dynamic response of the structure. For the Afsluitdijk, impulsive wave impacts are important loads.

At this moment hydraulic structures are designed based on a simple method: the Dynamic Amplification Factor (DAF) method or Kolkman method (Kolkman and Jongeling, 1996). This method does not consider the full dynamic interaction between the wave impacts, structure and water. The research project DynaHicS focusses on the dynamic behaviour of hydraulic structures, taking into account fluid-structure interaction (FSI). The main goal of the DynaHicS project is to develop new design guidelines to identify dynamic behaviour of hydraulic structures, so that more economical designs can be made in the future. Within the DynaHicS project already a lot of new knowledge is obtained. An advanced semi-analytical model of a bending gate is developed by Tieleman (2019) to determine the dynamic response of hydraulic structures, taking into account fluid-structure interaction. Also, a lot of new knowledge on impulsive wave impact loads is developed by studying the results of combined structural-hydraulic lab tests.

The main goal of this master thesis is to make improvements to the current design method, which can contribute to the development of a new design method for hydraulic structures in the future. The current design method, DAF method, does not consider the full dynamic interaction between the wave impacts, structure and water. In this method, the structure is simplified as a one dimensional structure, and the maximum response is based on the wave impact with the highest peak force. In this master thesis the DAF method is extended in time and space. To improve the DAF method in time, it is suggested to look at the maximum deflection that is obtained by running the force-time signal for multiple wave impacts (a whole wave field), instead of only looking at the maximum deflections for the wave impact with the highest peak force (as is done for the DAF method). To be able to use the whole force-time signal for multiple wave impacts, a first version of a method to compose a 'model' force-time signal for multiple wave impacts is described and validated in chapter 6. When this method is further developed and validated, no scale model tests are needed to determine the force-time series of wave impacts in the future, and the improvement of the DAF method in time can easily be implemented.

The DAF method does not take into account the spatial distribution of the wave impact force over the gate surface. The improvement in space consists of the implementation of a width distribution of the wave impacts force over the gate width. A new parameter, the skewness parameter, is introduced to describe the distribution of the wave impact force over the gate width. An equivalent SDOF model is set up to be able to compare the results (maximum deflections) that are obtained with the semi-analytical (MDOF) model and equivalent SDOF model, and to be able to investigate for which situations the SDOF model suffices for the determination of the maximum deflection. The equivalent SDOF model only takes mode (1,1) into account and the semi-analytical model can take an infinite (or specified finite) number of modes into account. It is found that the amount of modes that contribute to the response depends on the ratio of the impact duration and eigen period of the gate (τ/T_1).

A lower limit for the ratio of τ/T_1 can be determined for which an SDOF model suffices for the determination of the maximum deflection, and when it is necessary to use the more complicated semi-analytical (MDOF) model developed by Tieleman (2019). It is found that for the use of both the semi-analytical (MDOF) model and SDOF model, the skewness has to be taken into consideration.

Concluding, with the research performed in this master thesis the current design method can be improved in time and space. The improvement in time consist of the use of a force-time signal for multiple wave impacts instead of only looking at the response for the maximum peak force. The developed method to compose a force-time signal for multiple wave impacts (see chapter 6) makes it possible to also do this when no measurement data is available. The improvement in space consists of the implementation of a width distribution of the wave impacts force over the gate width, by using a skewness parameter. The improvements to the current design method, and knowledge that is obtained during this master thesis, can already be used by itself. However, more important the investigation that is done for this master thesis can contribute to the development of a new, more accurate, design method for hydraulic structures in the future.

Contents

Preface	v
Abstract	vii
1 Introduction	1
1.1 The Afsluitdijk project	1
1.2 Problem description	3
1.3 Research questions	4
1.4 Research methodology	5
1.5 Scope	6
1.6 Report structure.....	6
2 Wave impacts	8
2.1 Wave impact load	8
2.2 Using the wave impact impulse in design	12
3 Structural dynamics	15
3.1 Single degree of freedom systems (SDOF).....	15
3.2 Multiple degree of freedom systems (n-DOFS)	21
3.3 Plate theory.....	26
3.4 Semi-analytical model developed by Tieleman (2019).....	27
4 SDOF model – time investigation DAF method	33
4.1 Model schematisation	33
4.2 Triangular impact force schematisation	35
4.3 Maximum response to a wave field determined with the DAF method	38
4.4 Maximum response to a wave field determined with the SDOF model.....	42
4.5 Conclusions	48
5 Statistical description of wave impact data in time and space	51
5.1 Statistical description of pressure sensor data in time.....	51
5.2 Wave impact data from a wave field measured in scale experiments – load cell data.....	54
5.3 Statistical description of load cell data in space	56
5.4 Statistical distribution of (wave) parameters.....	57
6 Composition and validation of ‘model’ 3D force-time signal for multiple wave impacts 62	
6.1 Composition ‘model’ 3D force-time signal	62
6.2 Composition ‘real’ 3D force-time signal.....	69
6.3 Validation of ‘model’ 3D force-time signal.....	70
6.4 Sensitivity analysis – Triangular schematisation in time (rising time).....	74
7 SDOF vs MDOF model – space investigation DAF method	76
7.1 Model schematisation	77
7.2 Validation equivalent SDOF model.....	78
7.3 Comparison response for SDOF and MDOF model	79
7.4 Skewness parameter analysis	81
7.5 Improvements in time and space to the DAF method.....	86

8 Conclusions and recommendations	87
8.1 Conclusions	87
8.2 Recommendations.....	91
Bibliography	95
Nomenclature.....	99
List of Figures.....	103
List of Tables.....	107
A Quasi-static wave loads	109
A.1 Analytical methods for slender structures	109
A.2 Analytical methods for non-slender structures	110
B The hydrodynamic terms	112
B.1 Factors influencing the added terms	112
B.2 Determination of the hydrodynamic mass	113
B.3 Determination of the hydrodynamic damping	116
B.4 Determination of the hydrodynamic stiffness	117
C Time vs frequency domain analysis	119
D Scale experiment measurements	120
D.1 Pressure sensor data	120
D.2 Load cell data	122
E Splitting method for the wave impact force.....	124
F Statistics – basic formulations	126
G Afsluitdijk case	128
H Composition of ‘real’ 3D force signal over the full gate surface.....	131
H.1 Extrapolation of load cell data	131
H.2 Prediction force signal for the right half of the gate	133
H.3 Definition of individual waves in time	134
I Skewness parameter analysis.....	136
I.1 Correction factor average force	136
I.2 Structural modal shapes case study	137
J Equivalent SDOF model.....	138

1 Introduction

In this chapter some background information about the Afsluitdijk project is given in paragraph 1.1 . In paragraph 1.2 a description of the problem that is solved in this master thesis is given. This problem is translated into a main research question and a couple of sub-questions in paragraph 1.3 . In paragraph 1.4 the research method is discussed, and in paragraph 1.5 the most important limitations of this research are discussed. Finally, in paragraph 1.6 the structure of this report is explained.

1.1 The Afsluitdijk project

In the Netherlands many hydraulic structures are present, a lot of these structures are outworn and close to the end of their lifetime. At the end of the (theoretical) lifespan of a structure, the structural safety is under discussion, so that new structures have to be designed and built. One of these structures that is in need of renovation is the Afsluitdijk. The Afsluitdijk is a very important structure for the Netherlands, it closes the IJsselmeer from the Wadden Sea and protects The Netherlands from flooding. The structure must be renovated in order to comply with the structural safety requirements. Figure 2 shows the structure that lies between Den Oever and Kornwerderzand.



Figure 2: Overview Afsluitdijk (Google Maps, February, 2019, URL <https://www.google.nl/maps>)

The government planned a large-scale renovation of the Afsluitdijk (from 2018 to 2022). This renovation consists of reinforcement of the dam at the outer side in the form of a new stronger, more robust and higher revetment, reinforcement of the sluices at Den Oever and Kornwerderzand, and the addition of pumps at the discharge sluice complex at Den Oever to increase the discharge capacity from the IJsselmeer to the Wadden Sea. Figure 3 shows the sluice complexes at Den Oever and Kornwerderzand. The main goal of the renovation is to make sure that the Afsluitdijk meets the 1:10.000 year requirement. This means that the Afsluitdijk has to withstand the most unfavourable combination of waves and water levels with a probability of occurrence of 1 in 10.000 years (Publieksbrochure Project Afsluitdijk. Rijkswaterstaat, August 2016).



Figure 3: Sluice complexes at Den Oever (left) and Kornwerderzand (right)
([https://beeldbank.rws.nl/Rijkswaterstaat/Bart van Eyck](https://beeldbank.rws.nl/Rijkswaterstaat/Bart%20van%20Eyck), February 28, 2019,
URL <https://beeldbank.rws.nl/MediaObject/Details/2787> ,
URL https://beeldbank.rws.nl/MediaObject/Details/Luchtfotoserie_ljsselmeer_2794)

The sluice complexes at Den Oever and Kornwerderzand contain slender gates which are prone to complicated dynamic behaviour due to the hydrodynamic loading. The research project DynaHicS focusses on the dynamic behaviour of this slender parts, and not on the design of the whole Afsluitdijk, taking into account fluid-structure interaction (FSI). In current engineering practice only the simple Dynamic Amplification Factor (DAF) method or Kolkman method (Kolkman and Jongeling, 1996) is available for the dynamic design of hydraulic structures. The main goal of the DynaHicS project is to develop new design guidelines to identify dynamic behaviour of hydraulic structures, so that more economical designs can be made in the future. Within the research project DynaHicS there are two research lines: structural dynamics (structural engineering) and wave impacts (hydraulic engineering). The research line on structural dynamics focusses on the development of a semi-analytical model to identify the dynamic behaviour of hydraulic structures (especially flood- and lock gates). The second research line focusses on the development of new knowledge on wave impacts, especially on wave impact impulses, this knowledge can be used within the structural model. The problem that is solved during this master thesis is related to both research lines. In paragraph 1.2 the problem is described in more detail.

1.2 Problem description

Important loads on hydraulic structures are wave loads. Wave loads can be divided into impulsive and quasi-static loads. The impulsive wave impacts are very intense and of short duration (typically 10-100 ms), and can cause dynamic response of the structure. This means that the reaction force can become larger than the impact force. In other words the impact force may be amplified. The DynaHicS project mainly focusses on the response of hydraulic structures to these impulsive wave impacts. The present Afsluitdijk gates contain monumental concrete defence beams at the sea side. These protruding parts are the main cause of impulsive wave impacts on the Afsluitdijk gates, and it is therefore decided to remove this beams in the new design of the Afsluitdijk. In Figure 4 the typical impulsive wave impacts on the defence beams of the old sluice gates of the Afsluitdijk are displayed.

At this moment hydraulic structures are designed based on a simple method: the Dynamic Amplification Factor (DAF) method or Kolkman method (Kolkman and Jongeling, 1996). This method does not consider the full dynamic interaction between the wave impacts, structure and water. In this method, the structure is simplified as a one dimensional structure, and the maximum response is based on the wave impact with the highest static pressure/force. For the DAF method, the most important factors for the determination of the behaviour of the structure are the duration of the wave impact, τ , and the eigen-period(s) of the structure, T_n . For a more extensive description of this method reference is made to paragraph 3.1.2.



Figure 4: Wave impacts on the defence beams of the old sluice gates of the Afsluitdijk (Thijsse (1972))

An advantage of this quasi-static method with amplification factor, is that it is a quick method to deal with the dynamic behaviour of structures. However, the accuracy of this method is limited and may lead to an under- or overestimation of the maximum stresses, and subsequently a uneconomical or unsafe design. Secondly, the method does not give insight in the actual motion of the gate in time due to the wave impact. When the methods to deal with the dynamic behaviour of hydraulic structures can be improved, this leads to more economical designs. Concluding, there is a need for a more accurate prediction of the actual dynamic behaviour of hydraulic structures due to wave loads. The main goal of the DynaHicS project is to fill in this knowledge gap by characterising the loads on hydraulic structures and developing a better design method with respect to the dynamic behaviour of these structures taking into account fluid-structure interaction.

At this moment, already a lot of knowledge is obtained within the project. An advanced semi-analytical model of a bending gate is developed by Tieleman (2019) to determine the dynamic response of hydraulic structures, taking into account fluid-structure interaction. Numerical models based on finite element methods do exist to determine the dynamic response of hydraulic structures. However, the developed semi-analytical model is much more computationally efficient than the existing numerical models, which makes it more suitable for design purposes.

Also, combined structural-hydraulic lab tests will be performed to validate the developed semi-analytical model and other approaches developed during the project. Besides the semi-analytical model also a first method to determine a design load from the wave impact impulse instead of the wave impact peak pressure/force is developed by Chen et al (2018). With this method one characteristic value for the wave impact impulse can be found for a whole wave field.

In the past more attention is paid to the peak forces of the wave impacts instead of the impact impulses. However, Bagnold (1939) already observed that identical waves working on the same structure can give a different impact peak force. So it can be concluded that the peak forces/pressures are very unpredictable and because of this not convenient to use for design purposes. According to different literature sources (e.g., Cooker and Peregrine (1990,1995), Cuomo et al. (2010b), Hofland et al. (2010)) the impact impulse is better predictable, so when the impact impulse is used this can lead to simplified but much more stable models for the wave impact load on a structure. For now the developed method only applies to a simple single-degree of freedom model, so this method can be improved by including complex geometries (using the work of Tieleman (2019)). In paragraph 2.2 the developed method by Chen et al (2018) is discussed in more depth.

The next step in the DynaHicS project is to continue on the work of Chen et al (2018). This master thesis focuses on the next steps in the development of a new design approach (taking into account the dynamic behaviour of structures). Improvements in time and space are made to the present design method, which can contribute to the development of a new design methods for hydraulic structures in the future.

1.3 Research questions

The problem formulated in the previous paragraph is translated into a main research question and sub-research questions. The main goal of this master thesis is to make improvements to the present design method, which can contribute to the development of a new design methods for hydraulic structures in the future. This is translated into the following main research question:

How can the present design method, the DAF method, be improved in time and space to be able to predict the dynamic behaviour of a vertical steel gate with more accuracy?

The improvement of the current design method will be the first step in the development of a completely new design method, and the knowledge that is gained during this master thesis can be used as a basis for the development of the new method. A couple of sub-questions are formulated to find out how to improve the current design method in time and space, and to help answering the main research question:

1. *What is the applicability of the current design method, the DAF method, for a vertical steel gate subjected to wave impacts?*
 - a) *Can the wave impact load be simplified as a triangular impulse, and when is this schematisation valid?*
 - b) *Does the wave with the highest peak force in a storm also result in the largest dynamic response or should other factor be taken into account?*
2. *How can a force-time signal be predicted theoretically for a whole wave field, avoiding the use of results from scale model tests?*

3. *What is the distribution of the wave impact force over the gate width?*
 - c) *Does the width distribution of the wave impact force affect the response of a vertical steel gate?*
 - d) *Does the width distribution of the wave impact force affect the importance of higher modes for the response of a vertical steel gate, and when is it necessary to take the higher modes into account during the design of a structure?*

1.4 Research methodology

The research of Chen et al (2018) will be used as a base for this research. The research will continue on the knowledge on wave impact impulses that is obtained during the research of Chen et al (2018). The main goal of this master thesis is to extend and improve the current design method (DAF method). This improved method can be used by itself. However, more important the knowledge that is obtained by making the adjustments can be used to develop a completely new design method (which takes into account fluid-structure interaction and the dynamic behaviour of hydraulic structures).

The current method (DAF method) consist of a simple SDOF model for a single wave. The present method will be extended by enhancing the statistical description of the wave impact loads in time and space and the prediction of the subsequent structural design response. The most important tool that is used during the research is the semi-analytical model that is developed by Tieleman (2019). The model makes it possible to look at the dynamic behaviour of a plate structure, taking fluid-structure interaction into account. The research can be split into two phases: the investigation and extension of the present design method in time, and the investigation and extension of the present design method in space. Below, the work that is done during the two phases is described in more detail.

Phase 1: Investigation and extension of the current design method in time

First the method developed by Kolkman (DAF method) is investigated in time to develop an idea of the limitations of the current method used for dynamic design of structures. In paragraph 3.1.2 a more detailed theoretical description of the DAF method is given. To investigate the current design method, a simple SDOF model is set up in Matlab. A force-time series (consisting of typical wave impacts) obtained from scale measurements is used for this analysis. Combined structural-hydraulic lab tests are performed already, so results from these tests are used for this research. The main goal of this step is to compare the DAF method, for which the maximum response for a single triangular pulse is determined, with the maximum response determined by running a whole wave field (1000 waves) with the SDOF model. From this analysis first conclusions are drawn about the validity of the current design method (DAF method) in time.

The second part of this phase consist of the development of a method to compose a 'model' force-time signal for multiple wave impacts based on wave parameters only, to be able to improve the current design method in time.

Phase 2: Investigation and extension of the current design method in space

The second phase of this research focusses on the investigation and extension of the current design method in space. In this phase the focus will be on the importance of taking into account higher modes of vibration for the determination of the response of the structure, and the influence of the spatial variation of the impact force on this.

The differences (based on maximum deflections) between the SDOF model (used for the DAF method) and MDOF model (semi-analytical model) will be investigated. With this, the influence of higher modes of vibration on the response will be investigated. For this comparison, the model signal composed in phase 1 will be used as input for both the SDOF and MDOF model. For the SDOF model all the energy is in mode (1,1), while the semi-analytical model takes an infinite (or specified finite) number of modes into account. To be able to make this comparison, an equivalent SDOF model is set up and validated. Then, the results obtained with the SDOF and MDOF model are compared, and conclusions are drawn about the importance of taking into account higher modes (and by this using the more complicated semi-analytical model for design instead of the simple SDOF model) when the maximum response is determined. Next, the influence of taking into account the skewness of the wave impact force, and by this possible changes in the contribution of the different modes, on the response will be investigated. This phase will end with suggestions for possible improvements that can be made to the current design method.

1.5 Scope

For the design of hydraulic structures the ultimate limit state (ULS) situation and fatigue are two important failure mechanisms. This research focusses on the ultimate limit state only. Wave impacts with the highest peak forces and impulses are considered during this research. Failure mechanisms caused by fatigue are not taken into consideration.

This research focusses on the dynamic behaviour of vertical steel gates due to wave impacts. The case that is considered is based on the Afsluitdijk case study described in appendix G. It has to be noted that the structure that is used for this research is a simplification of a 'real' structure. For this research a 'real' gate structure with vertical and horizontal stiffeners, as shown in Figure 86a in appendix G, is simplified as a flat thin plate in the semi-analytical model developed by Tieleman (2019) (shown in Figure 86b in appendix G).

1.6 Report structure

The structure of this master thesis report follows the research method described in paragraph 1.4 . Figure 5 shows a schematic overview of the report structure.

Chapters 2 and 3 give an overview of theoretical background and past research on wave impacts and structural dynamics. Chapter 4 contains an analysis performed with a model based on a single degree of freedom mass-spring-dashpot system, based on which some shortcomings (in time) of the present design method are identified. In chapter 5, a statistical analysis in time and space of the wave impact data used for this research is performed. In chapter 6, the compositions of a 'real' 3D force-time signal based on scale experiment data, and of a 'model' 3D force-time signal are described. In this chapter the 'model' signal will also be validated based on the 'real' signal. Subsequently, chapter 7 will focus on the importance of taking into account higher modes of vibration for the determination of the response of the structure, and the influence of the spatial variation (skewness) of the impact force on this. Finally, in chapter 8 the conclusions and recommendations of the research will be given.

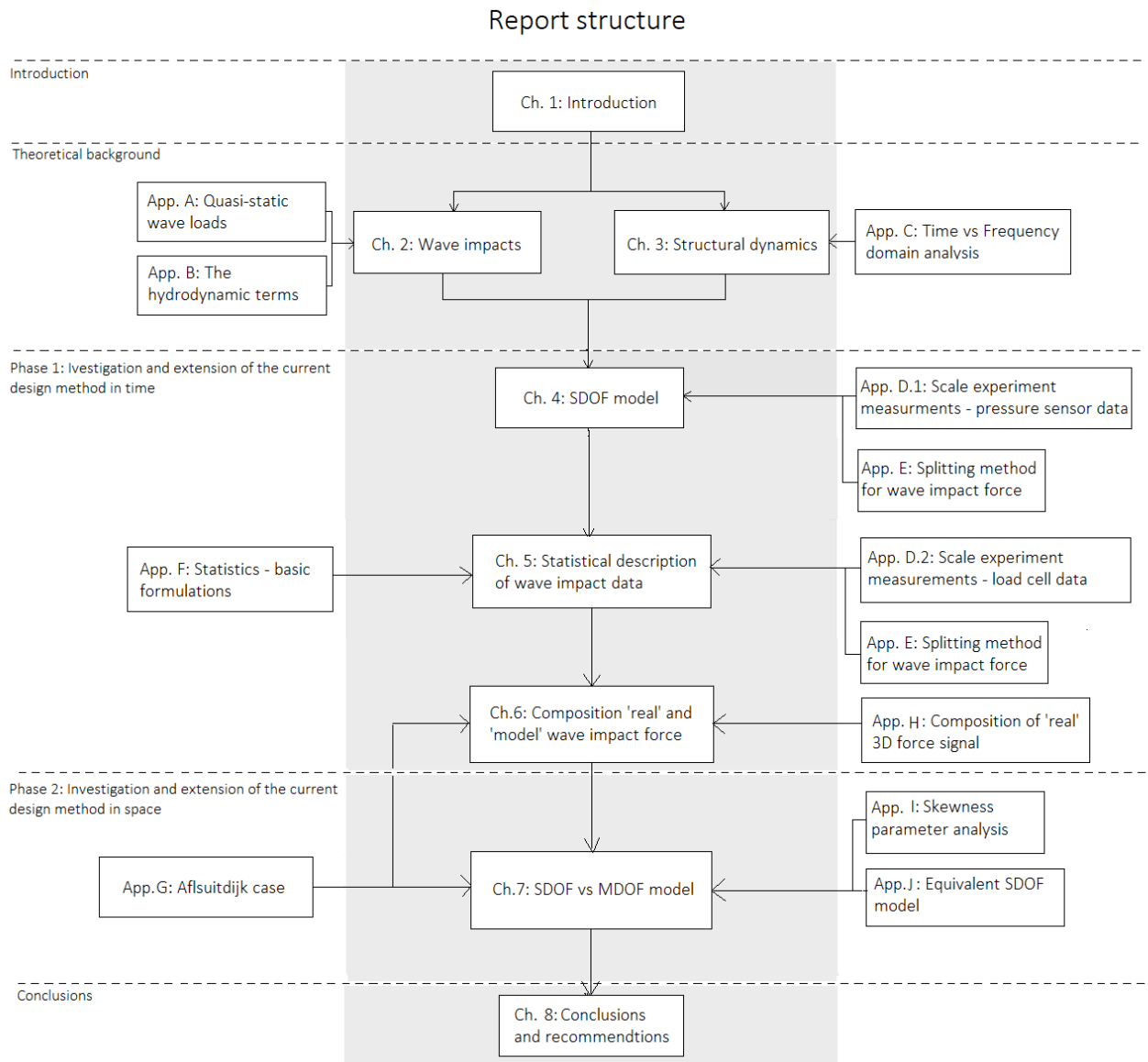


Figure 5: Overview of report structure

Figure 6 shows the improvements that are made to the current design method, and the chapters in the report that describe this phases of the research.

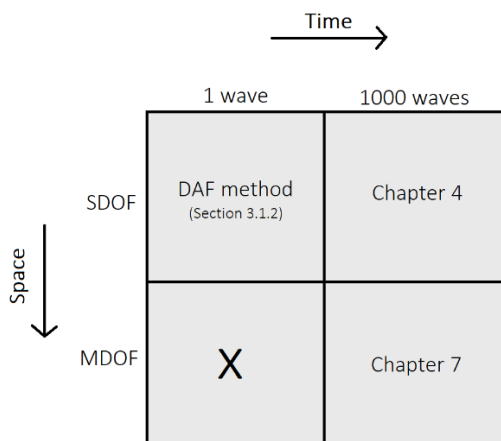


Figure 6: Improvements of the DAF method in time and space, report structure

2 Wave impacts

In this chapter the main load on hydraulic structures will be discussed: waves. Wave loads can be divided into two different loads:

- 1) Quasi-static wave loads
- 2) Wave impact loads

The quasi-static wave loads go with the same period as the waves. The quasi-static wave loads vary over the time and the loads depend on the wave height, - period and - direction. The load also depends on the magnitude of the construction surface on which the wave pressures are active. Also the geometry of the structure, foreland geometry and the presence of other structures play a role in connection with reflection, diffraction, wave overtopping and dissipation of wave energy. Attention have to be paid for waves with excitation frequencies near the eigenfrequencies of the structure, because this can cause resonance of the system which is undesirable. Wave impact loads occur when a wave is abruptly stopped, for instance when the wave front hits the structure. This kind of wave loads are much faster and occur only a short part of the wave period (indication wave impact duration: 10-100 ms). After the wave impact pressures are gone, the quasi-static wave pressure will be left. This research mainly focusses on the wave impact loads, in paragraph 2.1 some theoretical background on this type of loads is given, and in paragraph 2.2 the design approach developed by Chen et al (2018) is discussed in more depth. Some theoretical background on the quasi-static wave loads is given in appendix A.

2.1 Wave impact load

2.1.1 Basic theory on wave impact loads

Wave impacts occur when the movement of a quantity of water is suddenly stopped by a structure blocking the water movement. The impulse of the moving water will be converted into a force. In practice a large part of the water may run off sideways, so that a part of the impulse will move in another direction. According to second Newton's law the structure has to deliver an equal force, this force is equal to the first derivative to time of the impulse of the wave impact (equation 2.2). The impulse of a wave impact is given by equation 2.1, the impulse is not equal to the total impulse of the moving water mv (m = water mass [kg] and v = water velocity [m/s]). This is due to the change of direction of part of the impulse due to the sideways run off of part of the water.

$$I_{im} = \int_{\tau} \int_A p(t) dA dt \quad (eq 2.1)$$

$$F = m * a = \frac{d(mv)}{dt} \quad (eq 2.2)$$

In which: I_{im} = impulse of a wave impact [Ns]
 τ = wave impact duration [s]
 A = affected surface area [m^2]
 p = wave impact pressure [N/m^2]
 F = force delivered by the structure equal to the load working locally and perpendicular to the structure [N]
 m = water mass undergoing decelerating movement [kg]
 v = water velocity component perpendicular to the affected surface area [m/s]

Theoretically when no water can run off sideways and the water is considered incompressible, the wave impact pressures are going to infinity. In practice this does not happen because of the presence of elastic elements:

- The water is compressible
- Air bubbles in the water ensure a higher compressibility of the water
- Air pockets enclosed between the water surface and the structure, the air pockets can be considered as spring elements
- The structure itself is elastic

The weakest element of this list is determining the magnitude of the wave impact pressure. The structure can take the wave impact loads by deforming elastic or not-elastic, this deformations are depending on the stiffness of the structure, part of the load is also transferred to the supports. The deformations consist of deformations of the structure itself, however also the entrapped air and air bubbles in the water can deform. The deformations of the structure are considered as the response of the structure to the wave impact, this response can influence the magnitude of the wave impact, this can be seen as a kind of feedback of the response to the load. During the response (vibrations of the structure), also passive interaction forces are developed. In Figure 7 a schematisation of the relationships between the load and response is given. The interaction forces are an inertia force (added water mass) and damping force (added damping), this forces will be discussed in more depth in appendix B. The feedback from the response to the load will be discussed in paragraph 3.1.2. For very stiff structures the deformations will be small and the feedback to the load will be negligible. (Kolkman and Jongeling (1996))

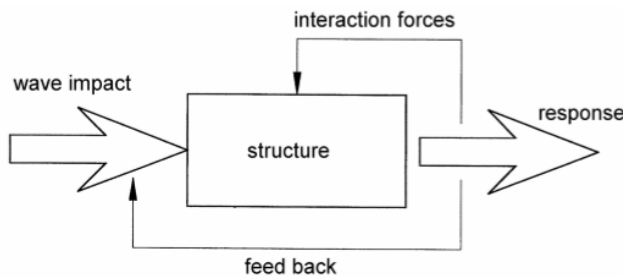


Figure 7: Schematisation of relationship between load and response (Kolkman and Jongeling (1996))

2.1.2 Factors influencing wave impact loads

Wave impact loads can lead to very high loads on a structure, because of this a designer will always try to design a structure in such a way that wave impact load will be avoided. There are different factors influencing wave impact loads. These factors determine if wave impacts will occur, the magnitude of the wave impact pressures and the development of the wave impact pressures in time and space. The following factors can be distinguished:

- *Geometrical factors*: these are the depth and geometry of the foreland (influencing the propagation of the waves, causing for instance refraction and breaking), the shape of the structure (in connection with the entrapment of air, sideways run off of water and the magnitude of the affected surface area), the angle with the water surface (for instance a slope or a vertical wall).
- *Factors connected with stiffness*: these are the elasticity of the structure, compressibility of the water and the presence of air pockets between the water surface and structure (or air bubbles).
- *Factors connected with the incoming wave*: these are the wave height (H) and wave period (T) (the higher the wave and the shorter the wave period, the higher the velocity of the water surface, the wave direction (when the angle between the incoming waves and the structure is larger than 20 degrees, the chance of wave impact is small due to the possibility of sideways run off of the water), the shape of the local wave.
- *Factors related to the water*: these are the salt content of the water (this is affecting the magnitude of the air bubbles in the water), flow (influencing the wave field and local waves near the structure), water level.

It appears that the geometrical factors (the geometry of the structure and the surroundings) are the most important factors determining the occurrence of wave impacts. The incoming wave factors are the most important factors determining the magnitude of the wave impact impulse. When the wave period is longer, more water mass is involved in the wave impact. The wave height and wave period also influence the velocity of the water mass. So it can be concluded that the highest waves do not always give the largest wave impacts.

From this influence factors it can be concluded that vertical structures (like gates) with ascending foreland (decreasing water depth) are promising wave impact situations. So for the case study of the Afsluitdijk (for this master thesis) it is important to investigate the foreland to determine whether there is a large chance of wave impacts. The most important check that has to be made is when the waves start breaking. Another important point that has to be taken into account for the Afsluitdijk case study are protruding parts of the structure, especially the parts near the water line are vulnerable for wave impacts. Near the still water line the vertical water velocity is the largest, so when protruding elements are near the still water line the wave impacts are the largest. (Kolkman and Jongeling (1996))

2.1.3 Wave impact characteristics

Wave impacts are impact loads at which, due to the abrupt stopping of the water movement, the load amplitude quickly increases in time. When the wave impact pressure falls away, only the quasi-static pressure remains. This pressure is considerably lower than the wave impact pressure. Distinction can be made between two wave pressure developments:

- 1) No air is entrapped during the wave impact
- 2) Air is entrapped during the wave impact

In practice mixed forms of this two types will occur. In Figure 8a a schematic pressure development of type 1 (no entrapped air) is displayed and in Figure 8b a schematic pressure development of type 2 (entrapped air) is displayed. For the type 2 impact load it can be seen that the downward flank shows strong oscillations. This oscillations are due to the entrapped air between the water surface and the structure, and/or due to air bubbles in the water. It can also be seen that the maximum pressure is lower when air is entrapped.

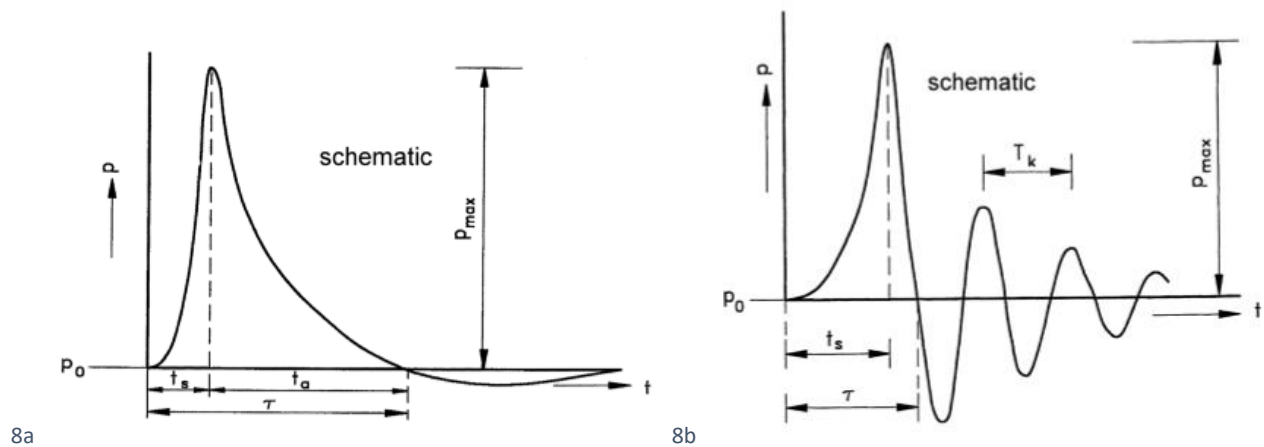


Figure 8: Schematic wave impact pressure developments in time, a) No entrapped air, b) Entrapped air (Kolkman and Jongeling (1996))

In Figure 8 a couple of characteristic quantities of wave impacts are indicated:

τ = impact duration (10 - 100 ms, with outliers until 1 ms) [s]

t_s = rise time (1-30 ms, with outliers until 0.1 ms) [s]

t_a = decay time [s]

p_0 = ambient pressure [N/m²]

p_{max} = maximum impact pressure (for extreme conditions 100-150 kN/m², however locally the pressure can be two times higher) [N/m²]

T_k = period of the oscillations in the downward flank [s]

(Kolkman and Jongeling (1996))

2.2 Using the wave impact impulse in design

2.2.1 Splitting of the wave impact force

In current engineering practice the design of hydraulic structures is mainly structural. The ratio of the impact duration τ and eigen period(s) of the structure mainly determines the dynamic part of the design at this moment (this is described in more detail in paragraph 3.1.2). However this method is very simplified and does not properly take into account the wave impact forces, the designs made based on this 'old' method can be very conservative and expensive. The current methods to determine the impact wave force (impulsive part with short duration) are the use of numerical or physical model tests. The forces that are determined with this methods are then used as design forces. There is a lack of knowledge how to deal with the impulsive wave impact forces, the use of the determined forces with numerical or physical models can lead to an overestimation of the design load. However not using the forces can give an underestimation of the design load.

In the paper of Chen et al (2018) a first attempt is made to develop a design method by which a design load can be derived from an impact wave load. The method is based on the approach of using the impulse of the wave impact instead of the peak force/pressure of the wave impact. In the paper of Chen et al (2018) the wave impact force is divided into two parts:

- F_{im} = impulsive force, this force changes quickly over time
- F_{qs} = quasi-static force, this force varies slowly over time

The impulsive force can be up to 10 times higher than the quasi-static force. In the left panel of Figure 9 the impulsive and quasi-static part of a wave impact force can distinguished well. The impulsive force is measured for a (vertical) wall with overhang, the overhang causes the impulsive wave impacts. The quasi-static force is measured for a (vertical) wall without overhang, by the lack of the overhang no impulsive wave impacts are caused. In the right panel of Figure 9 an example of a vertical wall with overhang is shown. The impact impulse I_{im} is the impulse cause by the impulsive force, and can be defined as the time integral of the impulsive force over the impact duration (τ).

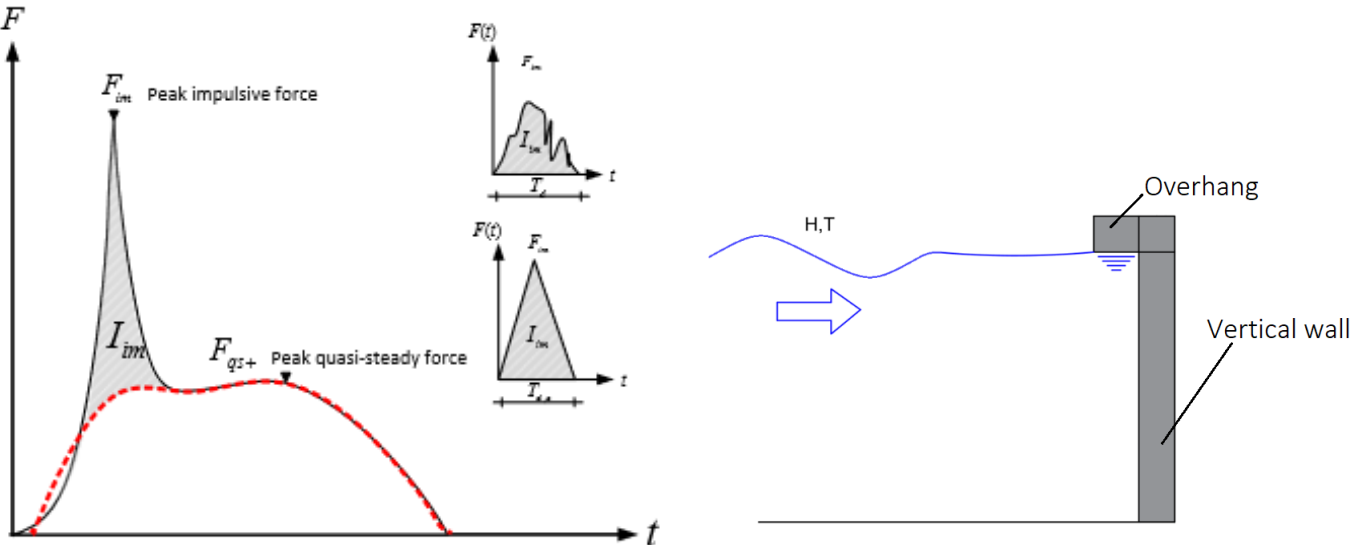


Figure 9: Typical time history of a wave impact on a (vertical) wall with or without a horizontal overhang, I_{im} denotes the impact impulse. (Chen et al (2018)) (left), vertical wall with overhang (right)

2.2.2 Envisaged method to determine the design reaction force based on wave impact impulse (developed by Chen et al (2018))

As said before, the paper of Chen et al (2018) focusses on the use of the impact impulse instead of the peak force/pressure of the wave impact. The peak forces of the impulsive impact on a vertical wall show large variations when laboratory measurements are compared (for instance the results from Bagnold, 1939). This large variation is partly caused by scale and model effects, however besides that impact loads itself are naturally very variable. Bagnold (1939) observed that identical waves working on the same structure can give a different impact peak force, so it can be concluded that the peak forces/pressures are very unpredictable and by this not convenient to use for design purposes. According to different literature sources (e.g., Cooker and Peregrine (1990, 1995), Cuomo et al. (2010b), Hofland et al. (2010)) the impact impulse is better predictable, so when the impact impulse is used this can lead to simplified but much more stable models for the wave impact load on a structure.

The wave impact load can be divided into three loading domains (according to Humar, 2002):

- Quasi-static: when the load is in this loading domain the structure reaches its maximum deflection well before the load is over, $\tau \gg T_n$ and $F_r = F_{max}$
- Dynamic: when the load is in this loading domain the maximum deflection of the structure is reached near the end of the loading time, the reaction force can become larger than the maximum loading amplitude, $\tau \approx T_n$ and $F_r > F_{max}$
- Impulsive: when the load is in this loading domain the load is long over before the structure reaches its maximum deflection, $\tau \ll T_n$ and $F_r < F_{max}$

In which: F_r = reaction force [N]
 F_{max} = wave impact force [N]

The optimal approach (used in current engineering practice) to determine the design reaction force (described in the paper of Chen et al., 2018) can be described by the following steps:

- Step 1: Determine the time series, $F(t)$, of the wave impact load from physical/numerical model tests.
- Step 2: Determine the reaction force time series, $F_r(t)$, in prototype scale with a structural model (for instance a finite element model).
- Step 3: Determine the design reaction force, for instance $F_{r,0.1\%}$, by means of a statistical model (for instance an extreme value analysis).

In practice obtaining the reaction force record in the time domain ($F_r(t)$), requires too much computational effort. The following simplified approach is mostly used in practice:

- Step 1: Determine the time series, $F(t)$, of the wave impact load from physical/numerical model tests.
- Step 2: Determine the design force, for instance $F_{0.1\%}$, by means of a statistical model.
- Step 3: Determine the design reaction force, for instance $F_{r,0.1\%}$, with a structural model.

A disadvantage of this simplified approach is that most of the times it leads to overestimation of the design load, so over dimensioning of the construction.

An envisaged method is developed to determine the design reaction force, the most important alteration is that the impact force is split in an impulsive part and a quasi-static part. By doing this the impact impulse can be used as an input to estimate the response of a structure (for instance the reaction force), instead of the wave impact peak force. As discussed before the wave impact impulse is much better predictable than the wave impact peak force, so this makes the method much more stable. The envisaged method consists of the following steps:

- Step 1: Determine the time series, $F(t)$, of the wave impact load from physical/numerical model tests.
- Step 2: Split the input force in an impulsive and quasi-static part, using a low-pass filter by using an impulse model. The quasi-static force is separated from the time series obtained at step 1. The result is the separation of: I_{im} (wave impact impulse of each wave impact) and F_{qs+} (quasi-static force of each wave impact). For the research described in this master thesis another (simplified) method is used to split the quasi-static and impulsive part of the load, see appendix E for a more detailed description of this simplified splitting method.
- Step 3: Determine the characteristic value with a certain exceedance probability of this two quantities, for instance $I_{im,0.1\%}$ and $F_{qs+,0.1\%}$, with a statistical model.
- Step 4: Determine the reaction force of the impulsive part based on $I_{im,0.1\%}$. This can be done by using a structural model. The reaction force: $F_{r,im,0.1\%}$ is obtained.
- Step 5: Calculate the design value of the total wave force as: $F_{tot,r,0.1\%} = F_{im,r,0.1\%} + F_{qs+,0.1\%}$

It has to be noted that the quasi-static force F_{qs+} is assumed within the static loading domain of the structure, so the dynamic response of the structure due to quasi-static loading is not considered and the reaction force to the quasi static impact ($F_{qs+,r}$) is the same as the quasi-static load (F_{qs+}). While the impulsive impact part may be amplified due to dynamic effects (so $F_{im,r} \neq F_{im}$). It also has to be noted that the structural model used within this study does not consider the exact structural components of the gate structure (so the model is only based on simple geometries). The gate in this study is assumed rigid with one degree of freedom (horizontal translation). The study of Tieleman (2019) can be used to extend the model for more complex structural geometries (and more structural component, like overhangs, can be included (this is done in the thesis work of Vorderegger, 2019)). The envisaged design method is validated by comparing the results (obtained total reaction forces) to the total reaction forces obtained from a single-degree of freedom mass-spring model. The results show that the proposed method can provide a good estimation of the reaction force for structures excited by impulsive wave impacts, and that the method of splitting the impulsive and quasi-static forces can be applied. The model can still be improved by improvement of the structural model (include more complex geometries) and improvement of the statistical model.

3 Structural dynamics

In this chapter some basic theory about structural dynamics, and theoretical background that is needed to understand and use the semi-analytical model of Tieleman (2019) will be discussed. The understanding of the basics is essential to understand the more complicated semi-analytical model, and to be able to identify situation for which for instance simple single degree of freedom models can be used. In paragraph 3.1 the simple single degree of freedom system is explained, this will be done for a dry condition and for a wet condition. In paragraph 3.2 some background theory on multiple degree of freedom systems, in dry condition and submerged in water, is given. In this paragraph distinction is made between discrete systems and continuous systems. Then in paragraph 3.3 some background information on plate theory is discussed, and finally in paragraph 3.4 the semi-analytical model developed by Tieleman (2019) is discussed. The most important equations that are used, and assumptions that are made for the semi-analytical model will be discussed. For more information about the semi-analytical model reference is made to the literature (Thesis work of Tieleman (2015), and the work done by Tieleman et al (2019)).

3.1 Single degree of freedom systems (SDOF)

3.1.1 Basic formulations – in dry condition

In this first paragraph the basic mass-spring-dashpot single degree of freedom (SDOF) system will be discussed. This is a very basic theoretical dynamical system. A single degree of freedom system has freedom of movement in one single direction, in the system described below the degree of freedom is the displacement in y-direction. The mass-spring-dashpot SDOF system is displayed in Figure 10 and can be described with the following equation of motion:

$$m \frac{d^2y}{dt^2} + c \frac{dy}{dt} + ky = F(t) \quad (\text{eq 3.1})$$

In which:

- m = mass [kg]
- c = damping [Ns/m]
- k = spring stiffness [N/m]
- y = displacement [m]
- F(t) = excitation force [N]
- t = time [s]

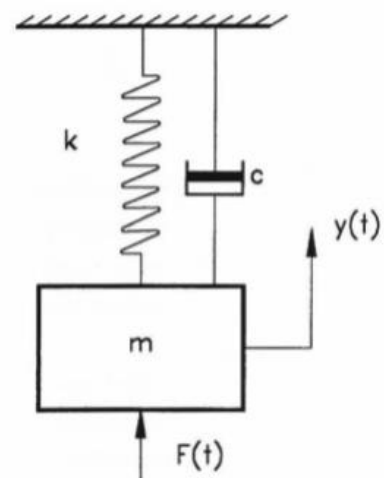


Figure 10: Mass-spring-dashpot single degree of freedom system (Jongeling and Erdbrink (2010))

Two important characteristics of such a mass-spring-dashpot SDOF system are the eigenfrequency or natural frequency f_n , and the dimensionless damping γ . The eigenfrequency is defined as the frequency of a free vibrating system in the absence of damping. The eigenfrequency is given by the following equation:

$$f_n = \frac{\omega_n}{2\pi} = \frac{1}{2\pi} \sqrt{\frac{k}{m}} \quad (\text{eq 3.2})$$

In which: f_n = eigenfrequency or natural frequency [1/s = Hz]
 $\omega_n = 2\pi * f_n$ = radial eigenfrequency or natural radial frequency [rad/s]

The relative damping is defined as:

$$\gamma = \frac{c}{c_{crit}} = \frac{c}{2\sqrt{km}} = \frac{c}{2m\omega_n} \quad (\text{eq 3.3})$$

In which: c_{crit} = critical damping [Ns/m]

The dimensionless damping can also be expressed with the parameter ζ , the damping ratio. The damping ration is also defined as: $\zeta = c/c_{crit}$. (Erdbrink and Jongeling (2010), Kolkman and Jongeling (1996))

3.1.2 Response of SDOF systems

In general the amplification factor A indicates the response of a simple mass-spring-dashpot SDOF system. The amplification factor A can be defined as the maximum force in the system ($k * y_0$, with k = spring stiffness and y_0 = maximum displacement of the mass (m)) divided by the maximum amplitude of the excitation (F_0). The amplification factor is a function of the relative damping (as defined in equation 3.3) and the ratio of the excitation frequency over the eigenfrequency (f/f_n). The maximum amplification factor is given by equation 3.4.

$$A = \frac{k * y_0}{F_0} = \frac{1}{2\gamma} \quad (\text{eq 3.4})$$

Resonance is a very important phenomena for the design of structures, and it must be prevented. Resonance is defined as the response at the frequency for which the amplification factor is maximum, as said before most of the times this is at $f/f_n \approx 1$. So when the eigenfrequency of the system/structure is close to the excitation frequency resonance is likely to occur. For $\gamma = 0$, no damping is present, so no energy will dissipate and the response will grow to infinity. For higher values of the relative damping the amplification factor becomes smaller.

When a structure is hit by a wave impact load, one or more eigenmodes of the structure may be hit simultaneously, then the response will consists of a superposition of several eigenmodes. The response of a structure to wave impact is depending on the following factors:

- The magnitude and duration of the wave impact load
- The dynamic characteristics of the structure
- The transfer of the load to the supports

The most important factors of this list are the duration of the wave impact load (τ) and the eigen-period(s) of the structure (T_n), the ratio of this two factors determines the dynamic behaviour of the structure. Another factor that is important for the response of the structure is the damping. When the structure is schematised as a single-degree of freedom mass-spring system, forced by an impact load, the influence of the wave impact duration, impact shape and eigen period of the structure can be investigated. For this system the eigen period is given by: $T_n = 2\pi \sqrt{\frac{m}{k}}$. The main distinction can be made between relatively stiff and not-stiff systems:

- $\tau \ll T_n$: This means that the structure is not very stiff and that there is not enough time for the structure to react on the load. This results in small response.
- $\tau \gg T_n$: This means that the structure is stiff, the maximum amplitude of the displacement is much higher than for relatively not-stiff systems. Theoretically the maximum displacement during loading or after the load falls away is given by:

$x_{maxmax} = \frac{2F_0}{k} = 2x_{stat}$, in which F_0 is the amplitude of the load and x_{stat} is the displacement of the system for a static load F_0 . It can be seen that the dynamic maximum response can be two times higher than the maximum static response for the same load. The dynamic response can be expressed by means of the dynamic amplification factor (DAF), the dynamic amplification factor lies between 0 and 2, and can be defined as:

$$DAF = \frac{x_{maxmax}}{x_{stat, wave\ impact}} \quad (eq\ 3.5)$$

In which: x_{maxmax} = maximum displacement of the structure [m]
 $x_{stat, wave\ impact}$ = displacement of the system for a static load with the magnitude of the amplitude of the wave impact [m]

In current engineering practice the DAF is used as a design tool to account for the dynamic behaviour of structures. In Figure 11 the graph of Harris and Crede (1961) is given. This graph shows the normalized maximax response (x_{maxmax}/x_{stat} , with x_{stat} as the displacement due to a static force with amplitude F_0) for different load shapes as a function of τ/T . The load shapes are chosen so that the impulse I is the same for all loads: $I_{im} = \int_{\tau} F dt = \frac{2}{\pi} F_0 \tau$. From the graph it can be seen that for loads with the same impulse and impact duration, but another shape (development in time) the response differs. For relatively not-stiff systems ($\tau/T < 0.25$) the differences are small. For stiff systems ($\tau/T > 3$) the dynamic amplification factor is about one, this means that the load can be seen as a quasi-static load for stiff systems (see appendix 0 for more explanation about quasi-static loads). The dynamic amplification factor is for none of the load shapes larger than two, so this is the upper limit for an undamped mass-spring system. Another important factor is the rise time (t_s) of the wave impact, this factor becomes important for impacts with $\tau/T > 0.7$. The shorter the rise time, the larger the response of a relatively stiff system. Harris and Crede (1961) also developed a figure showing the influence of the rising time on the maximax response, this is shown in Figure 12. This maximax response curves can be made for every load shape. The last factor influencing the response is the damping, damping ensures a systematically lower response. (Kolkman and Jongeling (1996))

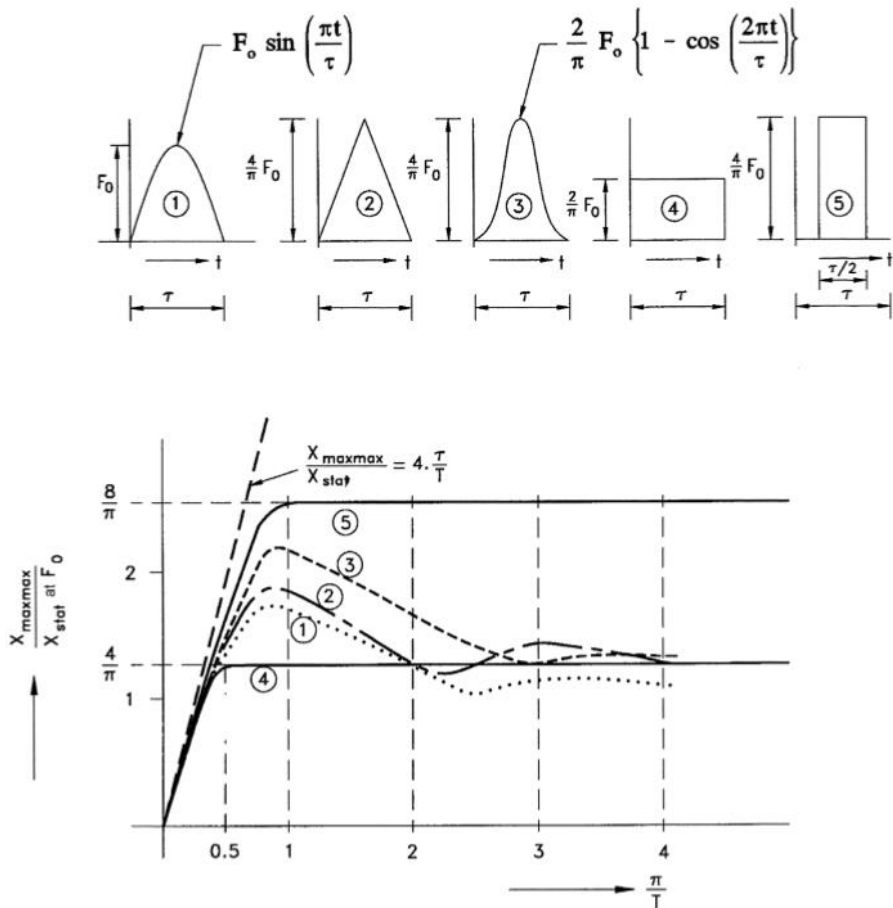


Figure 11: Maximax response curves for different load shapes (Harris and Crede (1961))

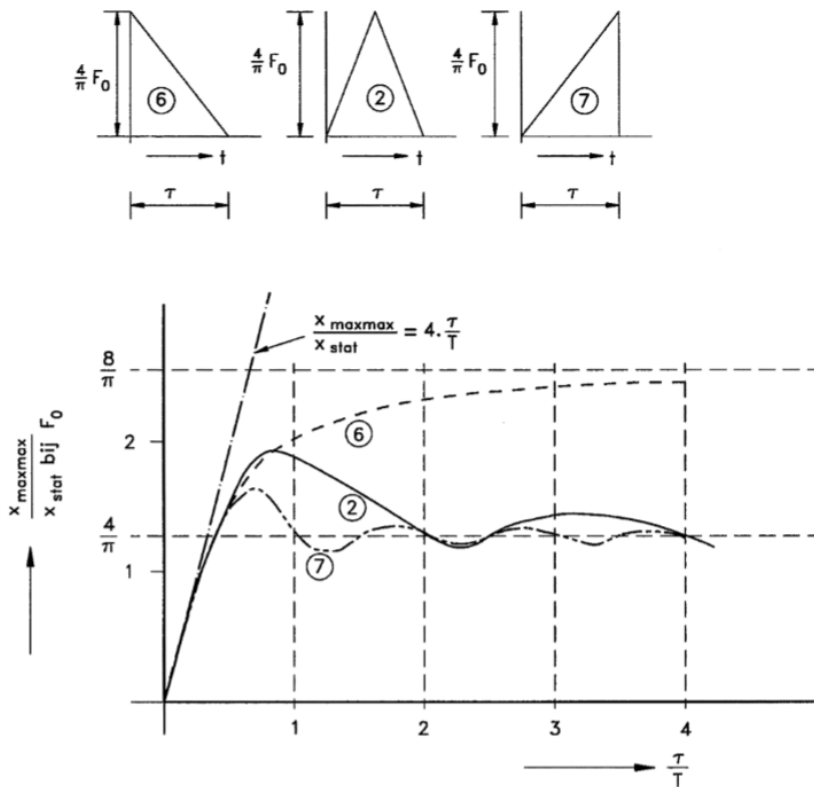


Figure 12: Maximax response curves for different triangular load shapes (Harris and Crede(1961))

In Figure 11, Figure 12 and Figure 13a, the dynamic amplification factor is determined based on the maximum wave impact force. However, as already described in paragraph 2.2, the use of the wave impact impulse (I_{im}) can lead to much more reliable results. In Figure 13b maximax response curves are plotted for different triangular load shapes, based on the impact impulse instead of the maximum peak force. In equation 3.6 the dynamic amplification factor is related to the wave impact impulse.

$$DAF_M = \frac{F_r}{I_{im} * \omega_n} \tag{eq 3.6}$$

- In which: DAF_M = dynamic amplification factor related to impact impulse [-]
- F_r = dynamic response of the structure [N]
- I_{im} = wave impact impulse [Ns]
- ω_n = natural radial frequency [rad/s]

From Figure 13b it can be seen that in the impulsive domain ($\tau/T < 0.25$) the dynamic response of the system (F_r) depends on the wave impact impulse with a factor 1. In the impulsive domain the dynamic response does not depend on the impact duration and on the shape of the impact force. This is an advantage of using the wave impact impulse instead of the wave impact peak force for the determination of the dynamic amplification factor, because the determination of the impact duration is difficult in the impulsive domain.

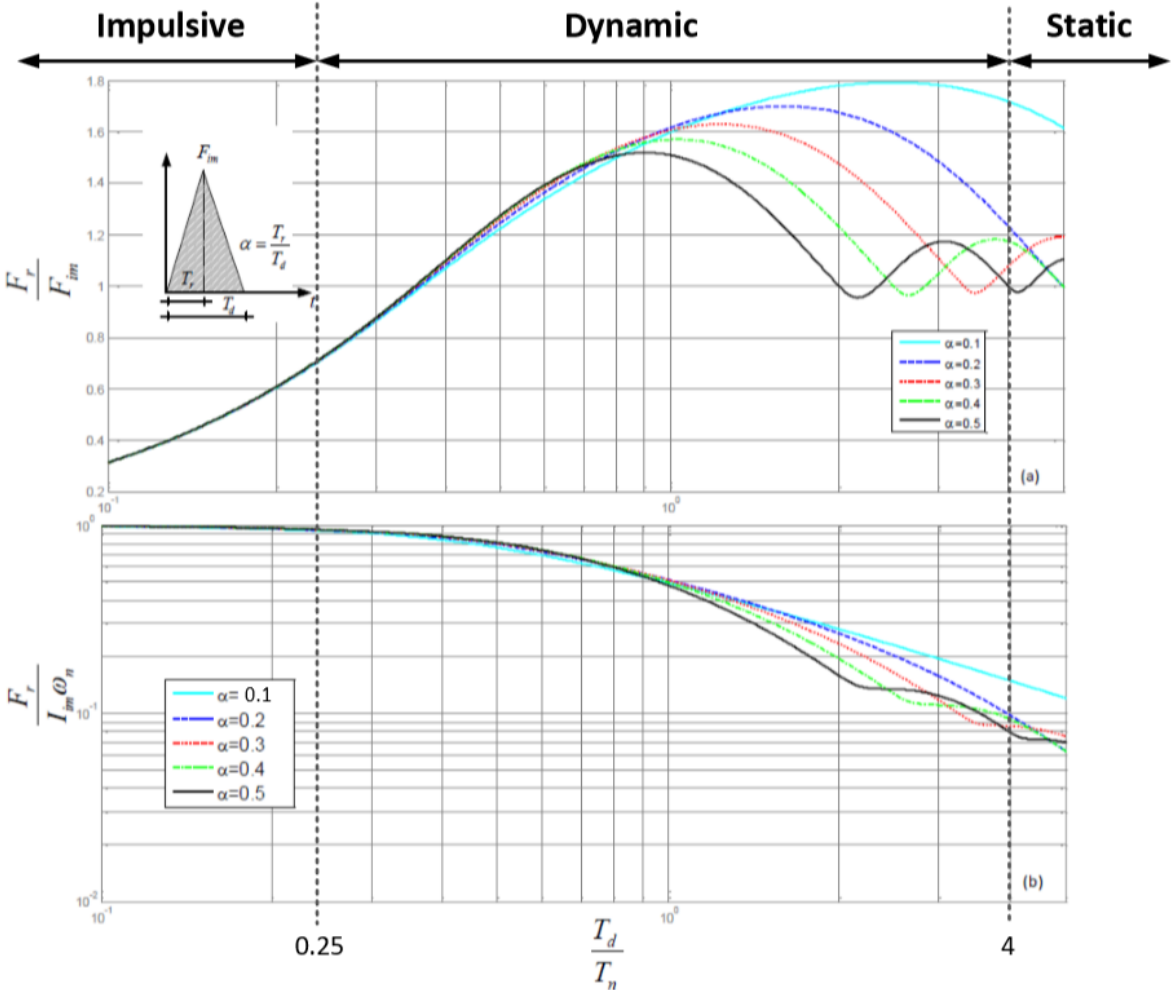


Figure 13: Maximax response curves for different triangular load shapes, a) based on maximum wave impact force, b) based on wave impact impulse, $\alpha = \tau/\tau$ (Chen, Hofland, Molenaar, Capel and Van Gent (2018))

3.1.3 Basic formulations – in water

When a structure that is submerged in water is vibrating, additional forces working on the mass/structure have to be taken into account. In this paragraph the single degree of freedom mass-spring-dashpot system described in paragraph 3.1.1 will be rewritten for the new situation.

For the single degree of freedom system described in paragraph 3.1.1 ,equation 3.1 has to be rewritten for the same system submerged in water:

$$(m + m_w) \frac{d^2y}{dt^2} + (c + c_w) \frac{dy}{dt} + (k + k_w)y = F_w \left(t, y, \frac{dy}{dt}, etc \right) \quad (eq 3.7)$$

In which the index w denotes the quantities that relate to the water:

m_w = added water mass [kg]

c_w = added damping [Ns/m]

k_w = added stiffness [N/m]

In appendix B some background information and methods to determine the hydrodynamic terms (added terms) are given.

The force F_w can be split into two components: $F_{w1}(t)$ and $F_{w2}(y, dy/dt, etc)$. The term $F_{w1}(t)$ represents the forces that are not related to the movement of the mass/system. The term $F_{w2}(y, dy/dt, etc)$ represents the non-linear coupled forces, so this forces are coupled to the movement of the mass/system. In practice the non-linear terms (F_{w2}) can be left out, as long as the vibration has a small amplitude, the vibration only causes a small disturbance on an average situation. The assumption of small amplitudes is allowed most of the times, because vibrations with large amplitudes has to be prevented anyway. (Kolkman and Jongeling (1996))

The eigenfrequency or natural frequency of this single degree of freedom system submerged in water is:

$$f_n = \frac{\omega_n}{2\pi} = \frac{1}{2\pi} \sqrt{\frac{k + k_w}{m + m_w}} \quad (eq 3.8)$$

Added water mass is a kind of virtual mass, actually it is a inertia effect which causes an additional force on the system that is in phase with the movement. The added water mass ensures a reduction of the eigenfrequencies of the system. It is very important to take this reduction into account to prevent the eigenfrequency of the system to come close to the excitation frequency (as discussed before this will result in resonance). According to Jongeling and Erdbrink (2010) the following equation can be used to determine the added water mass based on the eigenfrequency of the system in water (f_{wet}) and in dry condition (f_{dry}) :

$$\frac{m + m_w}{m} = \left(\frac{f_{dry}}{f_{wet}} \right)^2 \quad (eq 3.9)$$

For hydraulic structures the added water mass can be a multiple of the mass of the structure, especially for plate constructions (like gates) vibrating perpendicular to their plane the added water mass can be considerably. (Jongeling and Erdbrink (2010))

3.2 Multiple degree of freedom systems (n-DOFS)

When structures are more complex, single degree of freedom systems are not able to accurately describe the dynamic behaviour of the structures. Systems with more than one degree of freedom are then used to describe the dynamic behaviour of a structure, distinction can be made between discrete systems and continuous systems. Discrete systems are systems with a finite number of degrees of freedom, while continuous systems have an infinite number of degrees of freedom. In paragraph 3.2.1 discrete systems are shortly discussed, in paragraph 3.2.2 continuous systems are discussed.

3.2.1 Discrete systems

When a structure is described with a discrete system with n degrees of freedom, n eigenfrequencies and eigenvectors can be determined. When large numbers of degrees of freedom are used, it is a lot of work to find the solutions by hand and computer programs will be used to find the eigenfrequencies and eigenvectors. Discrete systems can be described by means of a coupled set of ordinary differential equations, the equations of motion can be noted down in a systematic way by means of a matrix notation:

$$\underline{M}\ddot{\underline{y}} + \underline{C}\dot{\underline{y}} + \underline{K}\underline{y} = \underline{F}(t) \quad (\text{eq 3.10})$$

In which: **M** = mass matrix [kg]
 C = damping matrix [Ns/m]
 K = stiffness matrix [N/m]

The mass-, damping- and stiffness matrices are diagonal, this means that there is no coupling of the different eigenmodes of the system. (Spijkers, Vrouwenvelder and Klaver. Lecture notes structural dynamics (2005))

When a structure is submerged in water, the water will couple the different eigenmodes. The coupling of the different terms can be illustrated with Figure 14. In Figure 14 the flow field of a vertically vibrating L-shaped gate is displayed. This flow field is strongly asymmetrical, so the pressures at both sides of the vertical plate will be different. When the gate accelerates upwards, additional pressure will develop on top of the horizontal plate. This results in a horizontal force to the left on the vertical plate. Similar to this when the gate accelerates in horizontal direction, a vertical downward force will develop on top of the horizontal plate. This additional forces are developed due to the presence of the water. This illustrates that for structures in water the mass terms are coupled, in contrast to structures in dry conditions for which the mass terms are decoupled as to acceleration forces.

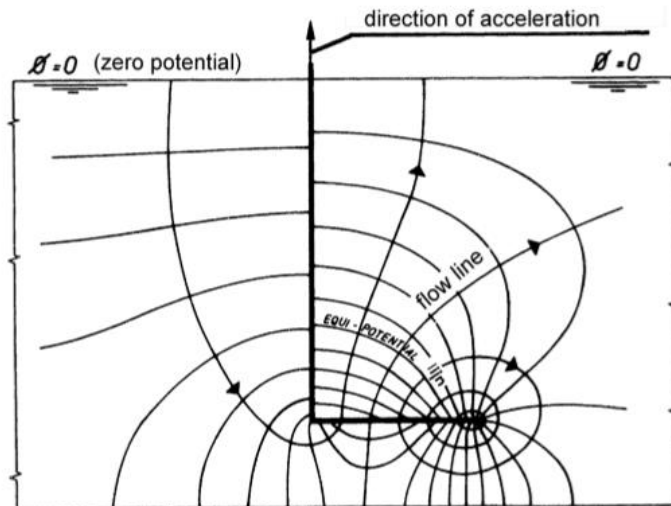


Figure 14: Flow field of vertically vibrating L-shaped gate in an added water mass. (Kolkman and Jongeling (1996))

Equation 3.10 can be rewritten for a system submerged in water:

$$(\mathbf{M} + \mathbf{M}_w)\ddot{\underline{y}} + (\mathbf{C} + \mathbf{C}_w)\dot{\underline{y}} + (\mathbf{K} + \mathbf{K}_w)\underline{y} = \underline{F}(t) \quad (\text{eq 3.11})$$

In which: \mathbf{M}_w = hydrodynamic mass matrix [kg]
 \mathbf{C}_w = hydrodynamic damping matrix [Ns/m]
 \mathbf{K}_w = hydrodynamic stiffness matrix [N/m]

The coupling between the eigenmodes can be found in the hydrodynamic mass-, damping- and stiffness matrices. These matrices are not diagonal and contain terms outside the main diagonal. These terms are the terms that establish the coupling between the different eigenmodes. (Jongeling and Erdbrink (2010))

3.2.2 Continuous systems – beam theory

Continuous systems have an infinite number of degrees of freedom. Continuous systems are systems whereof the dynamic behaviour can be described by means of partial differential equations. Some examples of structures which can be described with continuous systems are: the bending beam, shear beam, the torsion shaft, the bar and the cable. In this paragraph the discussed theory is limited to the two dimensional bending beam or Euler-Bernoulli beam. An assumption that is made for this beam model is that the cross-section always remains perpendicular to the neutral axis, also after bending of the beam. In Figure 15a a schematisation of the bending beam undergoing transverse motion is shown. The bending beam can be described with a fourth-order partial differential equation:

$$EI \frac{\partial^4 w(x, t)}{\partial x^4} + \rho A \frac{\partial^2 w(x, t)}{\partial t^2} = f(x, t) \quad (\text{eq 3.12})$$

In which: E = elasticity modulus [N/m²]
 I = moment of inertia [m⁴]
 ρ = density [kg/m³]
 A = cross-sectional area of the beam [m²]
 $w(x,t)$ = deflection of the beam at location x and time t [m]
 $f(x,t)$ = distributed force [N/m]

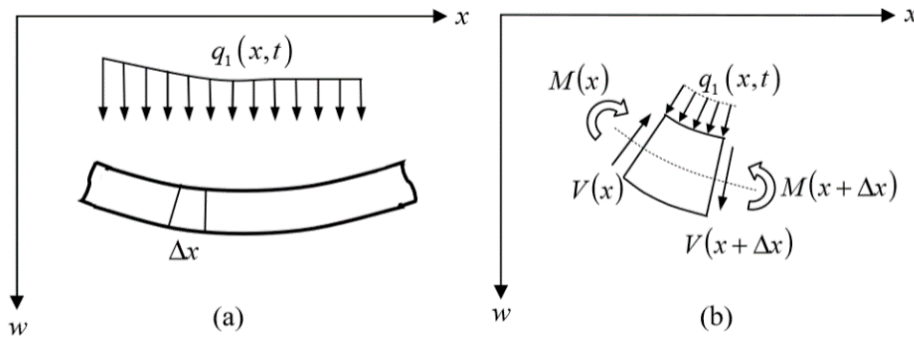


Figure 15: a) Schematisation of bending beam undergoing transverse motion, b) Differential element of the bending beam subject to shear force (V), bending moment (M) and an external load (q_1) (Metrikine Lecture notes Dynamics, Slender Structures and an Introduction to Continuum Mechanics (2006))

Two other important relations are the relations for the bending moment (equation 3.13) and shear force (equation 3.14) in the beam. In Figure 15b a differential element of a bending beam subject to shear force, bending moment and an external load is shown.

$$M = -EI \frac{d^2 w}{dx^2} \quad (\text{eq 3. 13})$$

$$Q = -EI \frac{d^3 w}{dx^3} \quad (\text{eq 3. 14})$$

3.2.2.1 Eigenfrequencies of a bending beam

The eigenfrequencies of a bending beam follow from the analysis of the free vibration of the beam. The free vibration of the beam represents the movement of the beam when it is unloaded, the free vibration is described by the homogeneous partial differential equation:

$$EI \frac{\partial^4 w(x,t)}{\partial x^4} + \rho A \frac{\partial^2 w(x,t)}{\partial t^2} = 0 \quad (\text{eq 3. 15})$$

This equation can be solved with the separation of variables method. When this is done the following eigenvalue problem (equation 3.16) and eigenfunction (equation 3.18), which is the solution to the eigenvalue problem, are obtained:

$$\frac{d^4 w(x)}{dx^4} - \beta^4 w(x) = 0 \quad (\text{eq 3. 16})$$

$$\beta^4 = \frac{\rho A \omega^2}{EI} \quad (\text{eq 3. 17})$$

$$w(x) = A\cosh(\beta x) + B\sinh(\beta x) + C\cos(\beta x) + D\sin(\beta x) \quad (\text{eq 3. 18})$$

In which: ω = eigenfrequency or natural frequency [rad/s]
 A, B, C, D = unknown constants

The unknown constants A, B, C, D and β depend on the support type of the beam, and thus on the applied boundary conditions. Two types of boundary conditions can be distinguished: kinematic boundary conditions and dynamic boundary conditions. The first is about the geometrical character of the beam and is about deflections (w) and slopes ($w' = \partial w / \partial x$), the latter is about bending moments (M , see equation 3.13) and shear forces (Q , see equation 3.14).

For a simply supported beam, the unknowns A, B, C and β can be simply determined by using the boundary conditions. This gives the following equation for the eigenfrequencies of a simply supported bending beam:

$$\omega_n = n^2 \left(\frac{\pi}{l} \right)^2 \sqrt{\frac{EI}{\rho A}} \quad (\text{eq 3. 19})$$

In which: l = length of the beam [m]

The following equation for the eigenfunction of the simply supported bending beam is found:

$$w_n(x) = D_n \sin\left(\frac{2\pi x}{\lambda_n}\right) \quad (\text{eq 3. 20})$$

With: $\lambda_n = 2l/n$ = wavelength of the n^{th} eigenfunction [m]

The unknown D can be determined using the initial conditions, D_n is the amplitude of the eigenmode. In Figure 16 the first (lowest) three eigenmodes of the simply supported bending beam are drawn. It can be seen that the wavelength of the fundamental (first) eigenfunction $w_1(x)$ is equal to twice the length of the beam, that the wavelength of the second eigenfunction $w_2(x)$ is equal to the length of the beam, and that for all the higher frequencies the wavelengths are shorter than the beam.

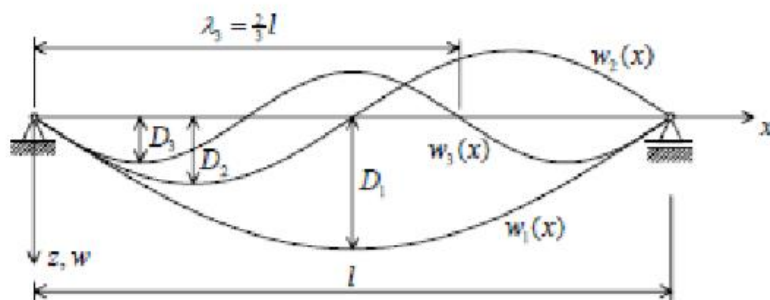


Figure 16: The first three eigenmodes of a simply supported bending beam (Spijkers, Vrouwenvelder, and Klaver. Lecture notes structural dynamics (2005))

From equation 3.19 it can be seen that theoretically there is an infinite number of eigenfrequencies for the simply supported bending beam. Earlier it was already stated that a continuous system has an infinite number of degrees of freedom, so this is in line with that. However in reality there is an upper limit of the number of eigenfrequencies which describe the dynamic behaviour accurately.

When the order of magnitude of the wavelength ($\lambda = 2l/n$) is about 10 times the height of the beam height H , then shear deformation starts to play a role. For the analysis of a bending beam shear deformation is not considered, so the following upper limit of n can be considered:

$$n < \frac{2l}{10H} \tag{eq 3. 21}$$

When it is necessary to determine higher eigenfrequencies than this limit it is important to elaborate the bending beam model with shear deformations, this is done in the Timoshenko beam model. Additional terms are added to equation 3.12 to account for the shear deformations. From this limit it can be concluded that when a dynamic design is made it is important to know if the higher eigenmodes have to be taken into account. Most of the time the lower (first) eigenmodes are governing, so the bending beam will be sufficient, however it is important to check this. (Spijkers, Vrouwenvelder, and Klaver. Lecture notes structural dynamics (2005))

3.2.2.2 Boundary conditions of a bending beam

In the previous paragraph it is mentioned that the eigenfrequencies and eigenmodes of a bending beam mainly depend on the boundary conditions (support type). In Figure 17 the first four eigenfrequencies and eigenmodes of a bending beam are given for different support types. It can be seen that the support type has a big influence on the dynamic behaviour of the beam. From the figure it can be concluded that clamped edges provide the highest eigenfrequencies, and thus the 'stiffest' behaviour.

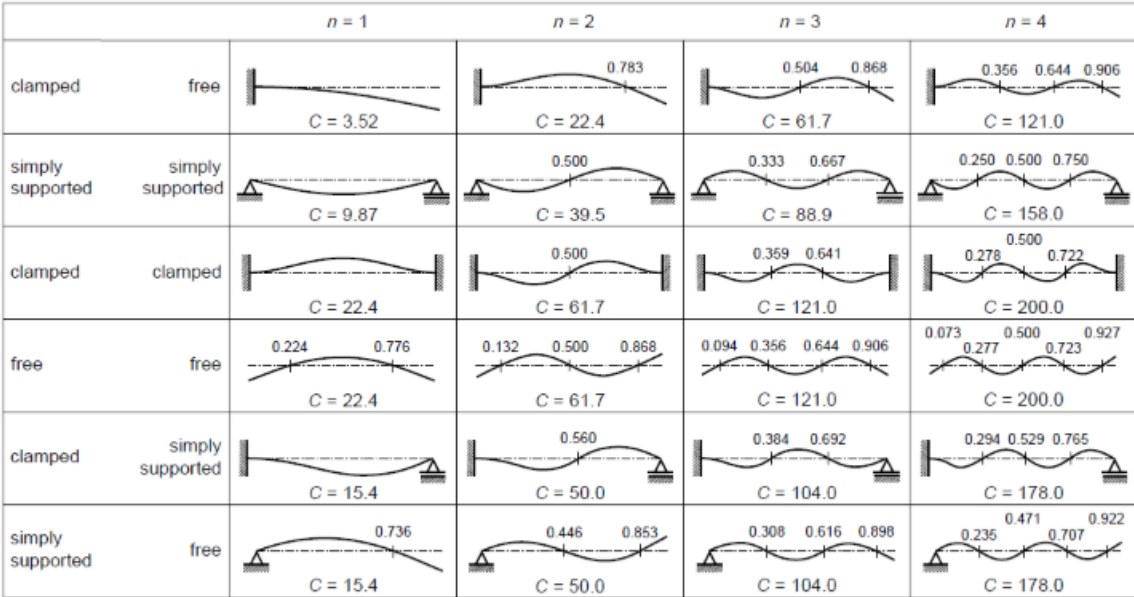


Figure 17: Eigenfrequencies and eigenmodes of bending beam for different support types.

$$\omega_n = C \sqrt{\frac{EI}{\rho A l^4}} \text{ [rad/s] (with the value of C from the figure)}$$

(Spijkers, Vrouwenvelder, and Klaver. Lecture notes structural dynamics (2005))

3.3 Plate theory

In the previous paragraph the one-dimensional bending beam is discussed, in plates the forces are transferred into two directions. For the gate structure in the semi-analytical model (see paragraph 3.4), a homogeneous isotropic thin plate is used. A plate can be considered thin if the thickness to span ratio is smaller than 1/5. The plate (gate) will be loaded perpendicular to its plane in the model (see Figure 18), so in this paragraph the basic formulations for thin plates loaded perpendicular to their plane are given.

Three main categories of basic equations can be distinguished:

- *Kinematic equations*: these equations give a relation between the deformations and the strains.
- *Constitutive equations*: these equations give information about the material behaviour, the relation between the stresses and strains is provided by these relations.
- *Equilibrium equations*: these equations give the relation between the loads and the stress resultants.

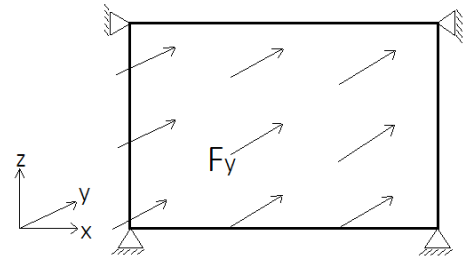


Figure 18: Plate loaded perpendicular to its plane

In Figure 19 the relations between these equations are shown.

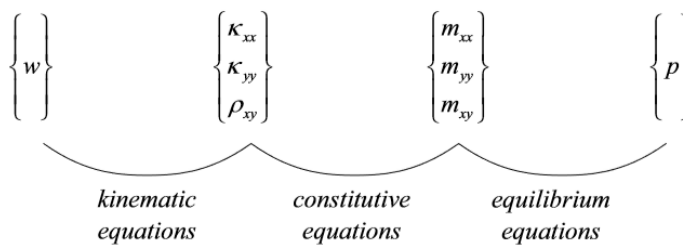


Figure 19: Relation scheme for thin plates loaded perpendicular to their plane (Blaauwendraad. Lecture notes Plate analysis, theory and application (2006))

When a plate is considered as thin, the shear deformations ($\gamma_x=0$, $\gamma_y=0$) are neglected. The following kinematic relations hold for thin plates loaded perpendicular to their plane:

$$\kappa_{xx} = -\frac{\partial^2 w}{\partial x^2}, \kappa_{yy} = -\frac{\partial^2 w}{\partial y^2}, \kappa_{xy} = -\frac{\partial^2 w}{\partial x \partial y} \quad (\text{eq 3. 22})$$

In which κ is the curvature, and w is the displacement of the plate. The following constitutive relations hold for thin plates loaded perpendicular to their plane:

$$m_{xx} = D(\kappa_{xx} + \nu\kappa_{yy}), m_{yy} = D(\nu\kappa_{xx} + \kappa_{yy}), m_{xy} = (1 - \nu)D\kappa_{xy} \quad (\text{eq 3. 23})$$

Or in terms of stresses and strains:

$$\sigma_{xx} = \frac{Et^3}{1 - \nu^2}(\epsilon_{xx} + \nu\epsilon_{yy}), \sigma_{yy} = \frac{Et^3}{1 - \nu^2}(\nu\epsilon_{xx} + \epsilon_{yy}), \sigma_{xy} = \frac{E}{2(1 + \nu)}\gamma_{xy} \quad (\text{eq 3. 24})$$

In which m is the bending moment per unit length in the plate, σ is the stress in the plate, and D is the uniform bending rigidity ($= Et^3/(12(1-\nu^2))$), E is the modulus of elasticity and ν is the Poisson's ratio). Finally the equilibrium relation is given by:

$$-\frac{\partial^2 m_{xx}}{\partial x^2} + 2\frac{\partial^2 m_{xy}}{\partial x \partial y} + \frac{\partial^2 m_{yy}}{\partial y^2} = p \quad (\text{eq 3. 25})$$

In which p is the load per unit area. When equation 3.22 is substituted in equation 3.23, and equation 3.23 is substituted in equation 3.25 the following fourth order differential equation is obtained for thin plates loaded perpendicular to their plane:

$$D \left(\frac{\partial^4}{\partial x^4} + 2\frac{\partial^4}{\partial x^2 \partial y^2} + \frac{\partial^4}{\partial y^4} \right) w = p \leftrightarrow D \nabla^2 \nabla^2 w = p \quad (\text{eq 3. 26})$$

This equation is called the biharmonic plate equation, and is for the first time derived by Lagrange in 1811. (Blaauwendraad (2006))

The most important relation that is used for the semi-analytical model, is the relation between the deflections and the stresses. When the structural deflection field, and by this the curvature field (see eq 3.22), is known from the calculations with the semi-analytical model, the stresses in a homogeneous thin plate can be described with the following system of equations:

$$\begin{bmatrix} \sigma_{xx} \\ \sigma_{yy} \\ \tau_{xy} \end{bmatrix} = -\frac{Dt_y}{I} \begin{bmatrix} 1 & \nu & 0 \\ \nu & 1 & 0 \\ 0 & 0 & (1-\nu) \end{bmatrix} \begin{bmatrix} \kappa_{xx} \\ \kappa_{zz} \\ \kappa_{xz} \end{bmatrix} \quad (\text{eq 3. 27})$$

3.4 Semi-analytical model developed by Tieleman (2019)

In this paragraph the semi-analytical model developed by Tieleman (2019) is described, and the most important equations and assumptions that are used for the model are summarized. For more information about the semi-analytical model reference is made to the work of Tieleman et al (2019).

3.4.1 Model description

The semi-analytical model of Tieleman is developed for the typical situation of a closed flood gate in a (infinitely long) discharge sluice. In Figure 20 a three dimensional overview of the gate model in space is shown. The gate structure in the model is represented by a homogeneous and isotropic thin plate, with equally distributed stiffness and mass. It is assumed that the sluice has impermeable walls, and a horizontal bottom, so that the cross-section of the water body will be rectangular. The sluice is assumed to be infinitely long in y-direction (to simplify the analytical derivations made to develop the model), and the contact surface between the gate and the fluid is assumed as a continuous vertical plane (on both sides of the gate). The fluid system is assumed to be stationary at both sides of the gate, and the free surface will be at h_l and h_r .

Below, the most important parameters used in the model are summarized:

- L_x = gate width (is equal o sluice width) [m]
- L_z = gate height [m]
- ρ_s = distributed mass per unit surface [kg/m^2]
- D = uniform bending rigidity = $Et^3/(12(1-\nu^2))$ [Nm^2]
- E = modulus of elasticity [N/m^2]
- t = thickness of the gate [m]
- ν = Poisson's ratio [-]
- h_l = water depth at the left side of the gate ($y < 0$) [m]
- h_r = water depth at the right side of the gate ($y > 0$) [m]

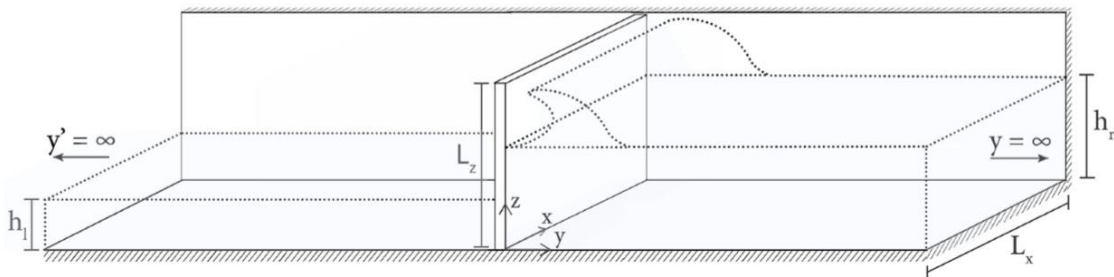


Figure 20: Overview of the plate model in space (O.C. Tieleman, A. Tsouvalas, B. Hofland, Y. Peng, S.N. Jonkman (2019))

As already described above the gate structure used in the model is a thin plate. It is also possible to predict the dynamic behaviour for more complex geometries (gate designs) with the model, however to do so the model has to be coupled to FE packages. For more information about adding more complex geometries to the model, reference is made to the Thesis work of Vorderegger (2019). For this research the simple model geometry shown in Figure 20 will be used (a isotropic and homogeneous thin plate).

Different types of boundary conditions can be incorporated in the model. In this paragraph the theoretical formulations for a simple set of boundary conditions will be discussed. The gate is simply supported at the vertical boundaries ($x = 0$ and $x = L_x$) and bottom ($z = 0$), and the top edge ($z = L_z$) is stress free.

In the following paragraphs the derivation of the method is summarized, and the most important formulations used for this derivation are given.

3.4.2 Theoretical formulations

The analysis of a system can be done in the frequency- or time domain. The semi-analytical model operates in the frequency domain, so the equations that are given are presented in the frequency domain. A transformation from the time domain to the frequency domain can be made using a Fourier transform. The main reasons to analyse the semi-analytical model in the frequency domain, are the frequency dependence of the hydrodynamic response, and the mathematical advantage that is obtained. In appendix C a short overview of the advantages and disadvantages of analysing in the frequency- and time-domain is given. In this paragraph the governing equation describing the motion of the gate and fluid are given.

3.4.2.1 Structural model

The Equation of motion describing the linear bending vibration of a homogeneous isotropic rectangular thin plate is as follows:

$$-\rho_s \omega^2 \tilde{w}(x, z, \omega) + D \left[\frac{\partial^4 \tilde{w}(x, z, \omega)}{\partial x^4} + \frac{\partial^4 \tilde{w}(x, z, \omega)}{\partial x^2 \partial z^2} + \frac{\partial^4 \tilde{w}(x, z, \omega)}{\partial z^4} \right] = \quad (eq 3. 28)$$

$$-\tilde{f}_i(x, y = 0, z, \omega) + \tilde{f}_r(x, y = 0, z, \omega) + \tilde{f}_e(x, z, \omega)$$

In which:

- w = displacement of the mid-surface of the plate [m]
- ρ_s = distributed mass per unit area [kg/m²]
- f_e = time signal of the external force distribution on the plate (for instance of a wave impact) [N/m²]
- f_i, f_r = fluid pressures at either sides acting on the surface of the gate [N/m²]

In equation 3.28, the shear deformation is neglected (due to the assumption of a thin plate). The boundary conditions of the gate structure described in paragraph 3.4.1 are described as follows in the frequency domain:

$$\tilde{w}(x = 0, z, \omega) = M_{xx}(x = 0, z, \omega) = \tilde{w}(x = L_x, z, \omega) = M_{xx}(x = L_x, z, \omega) = 0 \quad (eq 3. 29)$$

$$\tilde{w}(x, z = 0, \omega) = M_{zz}(x, z = 0, \omega) = M_{zz}(x, z = L_z, \omega) = V_{zy}(x, z = L_z, \omega) = 0 \quad (eq 3. 30)$$

In which:

- M_{xx}, M_{zz} = bending moments in x- and z-direction [Nm]
- V_{zy} = net shear force in y-direction [N]

3.4.2.2 Fluid model

The fluid is considered inviscid and irrotational. The Equation of motion describing the motion of the compressible fluid is described by equation 3.31. The fluid pressure is related to the velocity potential, and described by equation 3.32. The velocity vector of the fluid is given by equation 3.33.

$$\nabla^2 \tilde{\varphi}(x, y, z, \omega) + k_f^2 \tilde{\varphi}(x, y, z, \omega) = 0 \quad (eq 3. 31)$$

$$\tilde{p}(x, y, z, \omega) = -\rho_f i \omega \tilde{\varphi}(x, y, z, \omega) \quad (eq 3. 32)$$

$$\tilde{v}(x, y, z, \omega) = \nabla \tilde{\varphi}(x, y, z, \omega) \quad (eq 3. 33)$$

In which:

- φ = velocity potential [m²/s]
- ∇ = Nabla operator [-]
- c_p = sound velocity in water [m/s]
- ρ_f = fluid density [kg/m³]
- $k_f^2 = \omega^2 / c_p^2$

The boundary conditions of the fluid system are described by equations 3.34-3.36. The velocity at the impermeable sluice walls will be zero (eq 3.34). The free surface condition will be applied at the still water level (eq 3.35), and at the structure-fluid interface velocity compatibility will be enforced (eq 3.36). Finally at $y \rightarrow \infty$, the radiation condition should be satisfied at all times.

$$\left. \frac{\partial \tilde{\varphi}(x, y, z, \omega)}{\partial x} \right|_{x=0} = \left. \frac{\partial \tilde{\varphi}(x, y, z, \omega)}{\partial x} \right|_{x=L_x} = \left. \frac{\partial \tilde{\varphi}(x, y, z, \omega)}{\partial z} \right|_{z=0} = 0 \quad (\text{eq 3. 34})$$

$$\left. \frac{\partial \tilde{\varphi}(x, y, z, \omega)}{\partial z} \right|_{z=h} = \frac{\omega^2}{g} \tilde{\varphi}(x, y, z, \omega) \Big|_{z=h} \quad (\text{eq 3. 35})$$

$$\left. \frac{\partial \tilde{\varphi}(x, y, z, \omega)}{\partial y} \right|_{y=0} = i\omega \tilde{w}(x, z, \omega) \quad (\text{eq 3. 36})$$

3.4.3 Modal expansion and -coupling

The semi-analytical model is able to solve the interaction between the structure (gate) and the fluid. To solve the fluid-structure interaction (FSI) problem, a coupled modal analysis will be performed. With the coupled modal analysis, an analytical solution to the system of equations that is described in the previous paragraph will be obtained. In this paragraph, the steps that are followed during the coupled modal analysis will be discussed.

First the structural response will be described in terms of modes of vibration. The displacement of the plate is described as the summation of an infinite number of in-vacuo modal shapes (W_{km}) multiplied with modal coefficients (A_{km}). The first step is to describe the structural response in terms of in-vacuo modal shapes (W_{mk}) and coefficients (A_{mk}). The in-vacuo modal shapes and coefficient can be found by solving the homogeneous part of the Equation of motion of the plate (eq 3.28). This can be done either numerically or analytically.

$$\tilde{w}(x, z) = \sum_{m=1}^{\infty} \sum_{k=1}^{\infty} A_{km} W_{km}(x, z) \quad (\text{eq 3. 37})$$

To obtain the fluid response in terms of modal shapes (Φ_{pr}) and coefficients (B_{pr}), the modal expansions in the different directions (x,y,z) will be combined. The fluid problem will be solved completely analytically.

$$\tilde{\varphi}(x, y, z) = \sum_{p=1}^{\infty} \sum_{r=1}^{\infty} B_{pr} \cos(k_{z,p}z) \cos(k_{x,r}x) e^{-ik_{y,pr}y} = \sum_{p=1}^{\infty} \sum_{r=1}^{\infty} B_{pr} \Phi_{pr}(x, z) e^{-ik_{y,pr}y} \quad (\text{eq 3. 38})$$

Then the kinematic interface condition (eq 3.36) are applied to describe the fluid modal coefficient (B_{pr}) fully in terms of structural modal coefficients (A_{km}).

$$B_{pr} = -\frac{\omega}{k_{pr} \Delta_{pr}} \sum_{k=1}^{\infty} \sum_{m=1}^{\infty} A_{km} Q_{km,pr} \quad (\text{eq 3. 39})$$

With:

$$Q_{km,pr} = \int \int_{S_w} W_{mk}(x, z) \Phi_{pr}(x, z) dx dz \quad (\text{eq 3. 40})$$

The modal coefficients will be substituted in the solutions for the velocity potential and Bernoulli's pressure equation. Now the fluid pressure (eq 3.41) and structural deflection (3.37) are known in terms of structural coefficients only.

$$p_f(x, y, z) = i\omega^2 \rho_f \sum_{m=1}^{\infty} \sum_{k=1}^{\infty} A_{mk} \sum_{p=1}^{\infty} \sum_{r=1}^{\infty} \frac{Q_{km,pr}}{k_{y,pr} \Delta_{pr}} \Phi_{pr}(x, z) e^{-ik_y, pr y} \quad (\text{eq 3. 41})$$

3.4.4 Forced system of equations

From the previous paragraph, the solutions for \tilde{w} and p_f are known in terms of structural coefficients only. An infinite system of analytical equations in terms of the modal coefficients only is obtained by the substitution of the solutions for \tilde{w} and p_f in the (forced) Equation of motion of the plate (eq 3.28):

$$\sum_{k=1}^{\infty} \sum_{m=1}^{\infty} [\rho_s (\omega_{km}^2 - \omega^2) \delta_{kl} \delta_{mn} \Gamma_{ln} - L_{km,ln} + R_{km,ln}] A_{ln} = F_{ln} \quad (\text{eq 3. 42})$$

With:

$$L_{km,ln} = i\omega^2 \rho_f \sum_{p=1}^{\infty} \sum_{r=1}^{\infty} \frac{Q_{km,pr} Q_{ln,pr}}{k_{y,pr} \Delta_{pr}} \Big|_{h=h_l} \quad (\text{eq 3. 43})$$

$$R_{km,ln} = i\omega^2 \rho_f \sum_{p=1}^{\infty} \sum_{r=1}^{\infty} \frac{Q_{km,pr} Q_{ln,pr}}{k_{y,pr} \Delta_{pr}} \Big|_{h=h_r} \quad (\text{eq 3. 44})$$

$$F_{ln} = \int \int_S \tilde{f}_e(x, y, \omega) W_{ln}(x, z) dx dz \quad (\text{eq 3. 45})$$

$$Q_{ln,pr} = \int \int_{S_w} W_{ln}(x, z) \Phi_{pr}(x, z) dx dz \quad (\text{eq 3. 46})$$

To be able to evaluate the system of equations described by equation 3.42, the infinite summation has to be truncated to a finite number of structural and fluid modes.

3.4.5 Input of time-dependent force distribution

The semi-analytical modal takes any spatial distribution of external forcing as input for the calculations. However it is important that only the amplitude of the forced and not the distribution is time-dependent. If the force distribution is time-dependent, applying additional measures is necessary to be able to use the force signal within the semi-analytical model. In this paragraph it will shortly be described how to use a time-dependent force signal in the model. The description will be given based on an example (wave impact) from the work of Tieleman et al (2019).

In Figure 21 the spatial distribution of the wave impact force over the vertical of the gate is shown for four moments in time. In the upper panel of Figure 22 the time-signal of the vertically integrated wave force is shown.

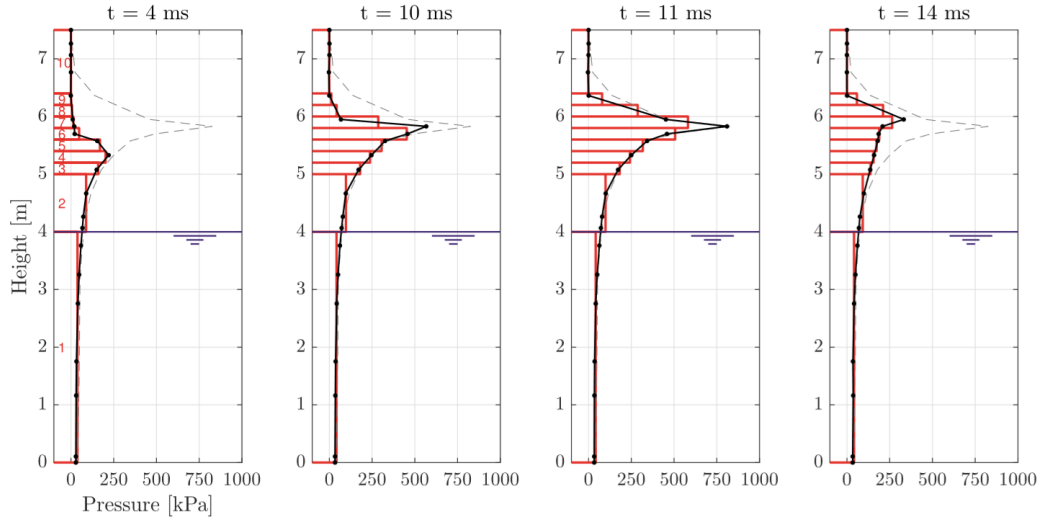


Figure 21: Spatial distribution of wave impact force, for four moments in time (Tieleman et al (2019))

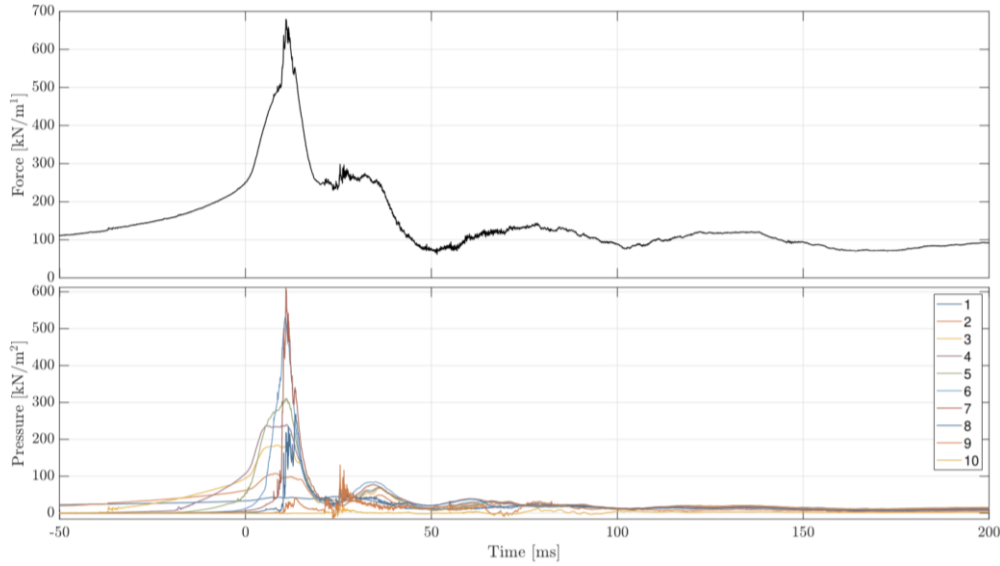


Figure 22: Vertically integrated wave force and the wave pressure amplitudes for the 10 intervals over the vertical of the gate as defined in Figure 21 over time (Tieleman et al (2019))

To perform a one-dimensional Fourier transform with respect to time, it is required to be able to split the wave force signal in a space- and time dependent part directly. When the force distribution (in space) changes over time this is not possible, so additional measures have to be applied, to be able to use the time-dependent force signal as input for the semi-analytical model. The wave force is divided into 10 intervals over the vertical, as shown in Figure 21. For every time step it has to hold that the applied value of the pressure results in an equal value of the vertically integrated force as for the original signal. In the lower panel of Figure 22 the wave pressure amplitudes for the 10 intervals are displayed over time. When the force has been split in different intervals with a constant value for the pressure (per time step), every interval has its own amplitude-time signal, and the one-dimensional Fourier transform can be performed. The total external force (f_e) is equal to the summation of the 10 signals in the intervals ($f_{n,t}$), and can be described with equation 3.47.

$$f_e(x, y, z) = \sum_{n=1}^{10} [H(z - z_n) - H(z - z_{n+1})] f_{n,t}(t) \quad (\text{eq 3. 47})$$

4 SDOF model – time investigation DAF method

In current engineering practice the most used method for the dynamic design of structures is the dynamic amplification factor method (DAF method or Kolkman method). In this chapter a simple SDOF model is set up in Matlab to investigate the validity of the DAF method 'in time'. As already described in paragraph 3.1.2, for the DAF method it is assumed that the maximum response (deflection) is obtained for the wave impact with the highest peak force. To investigate the validity of this assumption, in this chapter the maximum response (deflection) is also determined for a thousand waves, and compared to the maximum response determined with the DAF method. In Figure 23 the structure of the investigation of the DAF method in time and space is displayed. Figure 23 shows where chapter 4 is in the study of this master thesis.

First, in paragraph 4.1 the model schematisation that is used for the analysis is discussed. Then, the triangular impact force schematisation that is used for the DAF method is investigated in paragraph 4.2. The knowledge obtained from this analysis can be used for subsequent analyses. In paragraph 4.3 the SDOF model is used in the form of the DAF method, to determine the maximum response of a real wave field (force-time signal). In paragraph 4.4 the SDOF model is used to determine the real maximum response for the wave field (1000 waves). Finally, in paragraph 4.5 the most important conclusions are summarized, and the validity of the DAF method 'in time' will be discussed.

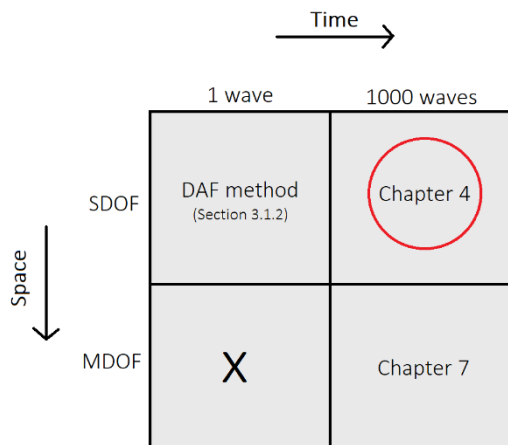


Figure 23: Improvements of the DAF method in time and space, report structure

4.1 Model schematisation

The SDOF mass-spring-dashpot system shown in Figure 24 is modelled in the time domain in Matlab. The second ordinary differential equation, representing the SDOF mass-spring-dashpot system, is solved numerically in Matlab. The standard ode solver function of Matlab, ode45, is used to determine the response of the SDOF in the time domain. The function ode45 implements a Runge-Kutta method with variable time step. Using the ode45 solver, results in the response of the system for a certain amount of time steps. It has to be noted that when the time step of the numerical calculation is chosen too large, the numerical error that arises will result in a certain resonant rise of the vibration.

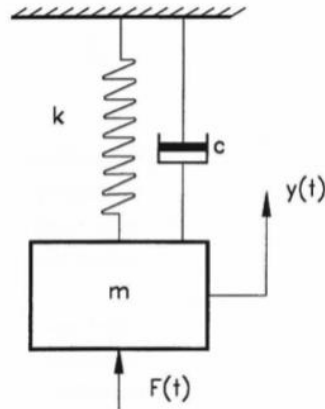


Figure 24: Mass-spring-dashpot single degree of freedom system (Jongeling and Erdbrink (2010))

The semi-analytical model of Tieleman is developed for the typical situation of a closed flood gate in a (infinitely long) discharge sluice. In Figure 25 an overview of this model is shown. The gate in the model is represented by a homogeneous and isotropic thin plate, with equally distributed stiffness and mass. The gate model is explained in more detail in chapter 3. In chapter 7 the semi-analytical model will be used to analyse the gate represented by a plate. For the analysis with the SDOF model (in this chapter), the gate is represented by a mass, the stiffness of the gate is represented by a single spring, and the (mechanical) damping of the gate is represented by a single dashpot.

When the gate is schematised as a plate in the semi-analytical model, the influence of the different vibration modes can be investigated and the deflection can be determined at different locations of the gate. When the gate is schematised as a SDOF, only the first vibration mode can be studied and the deflections are known for one single point in space.

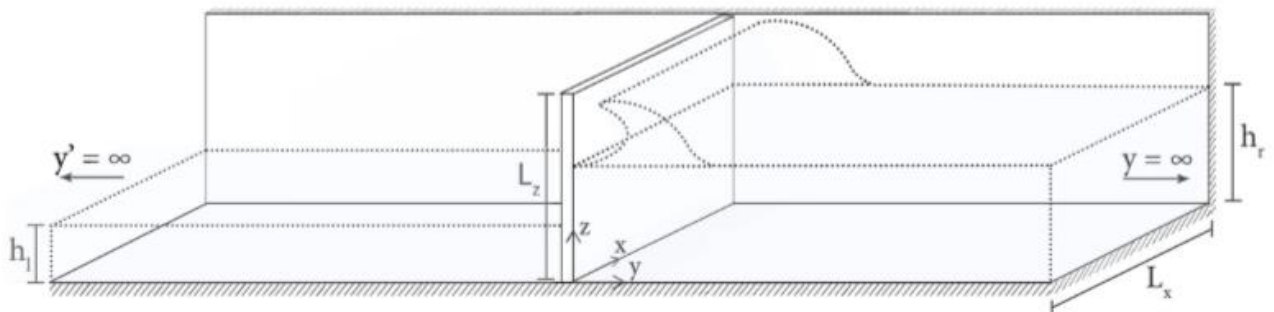


Figure 25: Overview of the plate model in space (Tieleman et al (2019))

For the analysis with the SDOF model in this chapter one of the gates of the Afsluitdijk will be studied as case study. The case study that will be studied during this chapter is the case study that is also studied in the PIANC report of Tieleman et al (2018). The only parameter values that are used during the analysis with the SDOF model are the width (L_x) and height (L_z) of the gate. These values are used for the scaling of the scale model wave data (from the lab-test) to a realistic situation (see also appendix D). The width of the gate that is studied is $L_x = 12.5$ m, and the height of the gate is $L_z = 7.25$ m.

4.2 Triangular impact force schematisation

In Figure 9, the shape of the wave impact force is shown. The impulsive part of the wave impact is schematised as a single triangular pulse in this part of the research in accordance with the DAF method by Kolkman and Jongeling (1996). In this paragraph, the response of the SDOF model to a single triangular impact force is analysed. This analysis is not based on real wave data, but will be a more general theoretical investigation to determine the influence of various factors like the impact duration (τ), rising time (t_s) and damping (ζ). The knowledge obtained from this analysis will be used to find a proper schematisation of real wave data. In paragraph 4.2.1 the SDOF model will be analysed for a dry condition and in paragraph 4.2.2 the influence of adding water will be explained.

4.2.1 SDOF model – in dry condition

First the influence of the wave impact duration will be investigated, using the SDOF model. Based on the studies of Tieleman (PIANC report, 2018) and Vorderregger (2019) a typical value for the fundamental eigen period of a gate in dry condition is chosen for this analysis, $T_1 = 45$ ms. Three situations are investigated:

- $\tau/T = 0.5$, a relatively slow system compared to the impact duration
- $\tau/T = 1.0$, an evenly fast system compared to the impact duration
- $\tau/T = 2.0$, a relatively fast system compared to the impact duration

The impact duration is varied to investigate the situations described above. In Figure 26a the triangular load schematisations for the different ratios of τ/T are shown. In Figure 26b the time responses for the different loads are shown, and in Figure 26c the maximax response curve for a symmetrical triangular load is given. A damping ratio of 5% is used for this analysis. In Figure 26c the three ratios of τ/T that are investigated are indicated with dashed vertical lines. The dynamic amplification factors from the maximax response curve correspond with the dynamic amplification factors found from the time responses. From the figures it can be concluded that the maximum deflection of the system, due to a triangular load, does not necessarily increase for a longer impact duration. The maximax response curve that is found with the model is in agreement with Figure 11 found by Harris and Crede (1961). So it can be concluded that the dynamic behaviour caused by a triangular load is quite hard to predict.

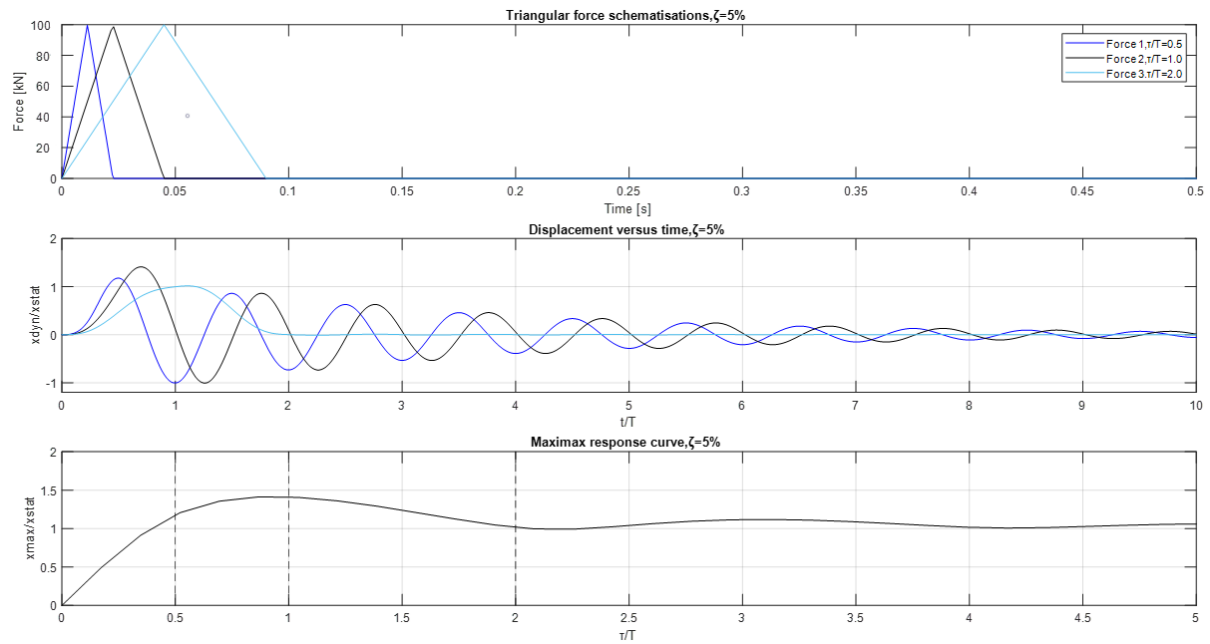


Figure 26: a) Triangular force schematisation, b) Time response of the SDOF, c) Maximax response curve for symmetrical triangular load, $\zeta = 5\%$

From Figure 26 it can already be concluded that the ratio of the impact duration and eigen period of the system is a really important factor determining the (maximum) response of the system. However, another important factor influencing the response is the rising time (t_r) in case the triangular load is non-symmetrical. Harris and Crede (1961) also developed a figure showing the influence of the rising time on the maximax response, this is shown in Figure 12. The SDOF model is used to reproduce the results of Harris and Crede (1961), the results are shown in Figure 27.

In the figure the maximax response curves for different rising times are plotted with ($\zeta = 5\%$) and without damping ($\zeta = 0\%$). It can be seen that the results are again in agreement with the results found by Harris and Crede. From this figure it can be concluded that the rising time of the (triangular) load is also an important factor for determining the (maximum) deflection of a structure. From the figure it can also be concluded that the maximax response curves shift downward due to the influence of damping, and that it is important to included damping in the model.

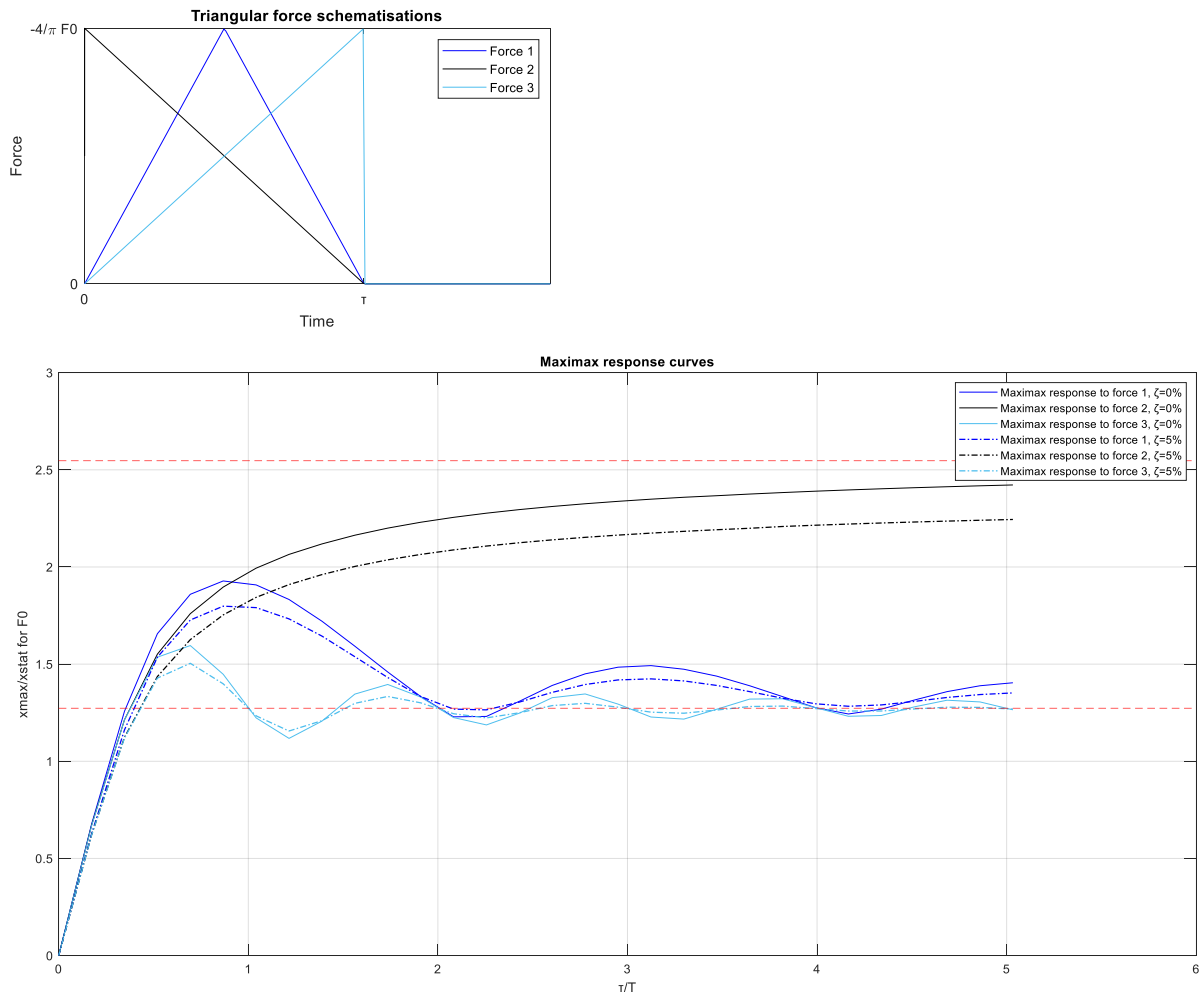


Figure 27: Maximax response curves for triangular loads with different rising time, with ($\zeta = 5\%$) and without ($\zeta = 0\%$) damping

4.2.2 SDOF model – in water

The behaviour of the system that is described in the previous paragraph is for a ‘dry’ structure. When the structure is submerged in water this behaviour will change. In paragraph 3.1.3 the equations that are used for a structure in water are given. For the simple SDOF model the only adjustment is the addition of the hydrodynamic mass, -damping and -stiffness to the mass-, damping- and stiffness terms, so these parameters will become larger. The adjustment of these terms also influences the eigenfrequency of the system (see equation 3.7), the added water mass leads to a reduction of the eigenfrequencies of the system. It is important to take this reduction into account in determining the amplification factor.

The added water mass depends on the vibration shape of the gate and the exact layout of the surrounding fluid domain. In appendix B.2 some methods to determine the added water mass are described. As said before, when the added water mass is included in the SDOF model the eigen period of the system will become longer. An important consequence of this increase of the eigen period is the change of the ratio τ/T , and by this the maximum deflection of the system (see Figure 27). So it can be concluded that due to the influence of the water the eigen period of the system will change, and by this the maximum deflection of the system will become larger or smaller (depending on the location in the maximax response curve, see Figure 27). When the influence of the water is not taken into account large under- or overestimations of the maximum deflections can be made, which will lead to uneconomical designs.

4.3 Maximum response to a wave field determined with the DAF method

In this paragraph the maximum response of the wave field is determined using the DAF method (Kolkman method). In current engineering practice, most of the time, the DAF method is used for the dynamic design of hydraulic structures. The DAF method is already described in more detail in paragraph 3.1.2. For this method the highest peak force of a whole force-time signal of a wave field is determined (F_{max}) and the static response for this force is determined ($x_{stat} = F_{max}/k$). From the literature the DAF can be determined, and the maximum dynamic response is obtained by multiplying the static response with the DAF. This method is based on the response of a simple SDOF mass-spring-dashpot system. In this paragraph the maximum response to a whole wave field (multiple wave impacts) is determined with the DAF method.

4.3.1 Impact pressures from a wave field measured in scale experiments – pressure sensor data

For the DynaHicS project there are already some scale experiments performed. Data obtained from these tests, is used for this research. For the analysis of a whole wave field with the SDOF model the result from the scale experiment (test A60) with the following specifications is used:

- An irregular wave field of 1000 waves is generated to test the structure shown in Figure 28 (a vertical plate with overhang).
- The structure is placed 30.8 m from the wave maker. In Figure 29 two fotos of the test setup in the WaterLab (at the faculty of Civil Engineering, TU Delft) are shown.
- Pressure measurements in 7 pressure sensors (PS2 to PS8) are performed, the positions of the pressure sensors are indicated in Figure 28.
- The data is filtered with a low-pass filter of 25 Hz, to make the results more smooth and easier to process.

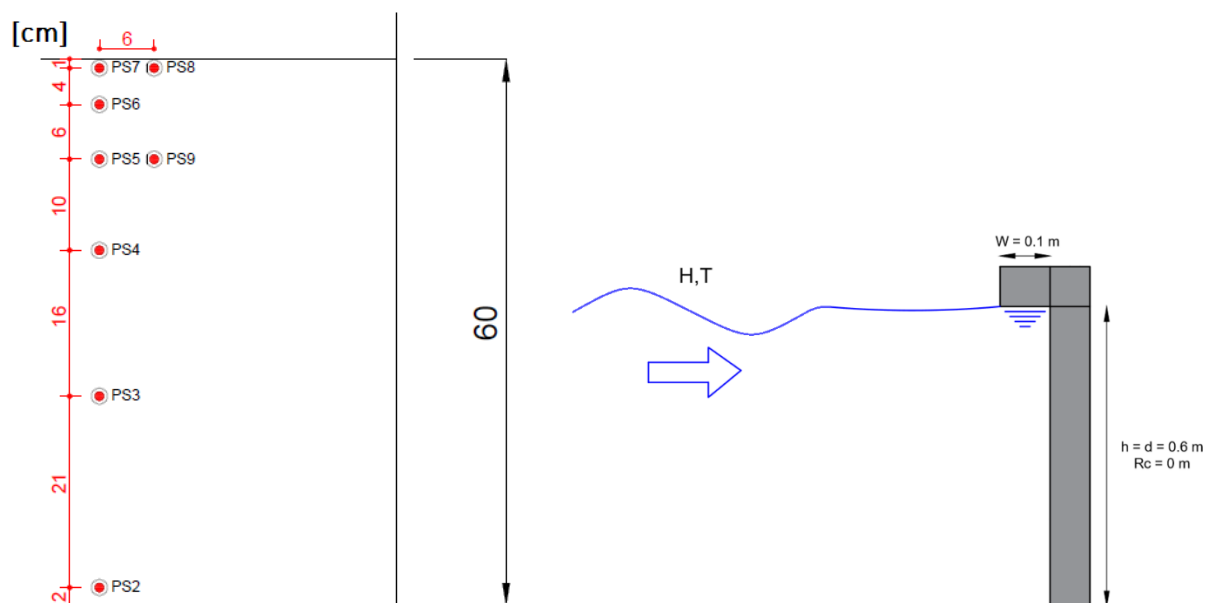


Figure 28: Position of the pressure sensors on the structure used during the lab-test (Left), schematisation test setup (right) (E. de Almeida, 2019)



Figure 29: Test setup wave flume with wall with overhang at the left (left), wall with overhang zoomed in (right) (E. de Almeida, 2019)

From the pressure signals from the 7 pressure sensors, one time series of the total force on the whole gate per meter width is calculated, taking the distance between the pressure sensors into account. The tests that are performed in the lab are scale tests, so to use the results for a real case study, scaling of the results is necessary. The scaling of wave impacts mainly uses the Froude scaling, the scaling factors for the different variables are given in Table 1. Also the scale model dimensions and wave quantities used for the scale experiments, and scaled values of this dimensions and quantities are given in the table. The height of the gate that is used during the lab-test is 0.6 m, the height of the gate used as case study is 7.25 m. So for the length a scaling factor of $\lambda = 12.08$ has to be used. In appendix D.1 the individual pressure signals obtained with the scale experiments, the original and scaled force signal are given. The time series of the total force on the gate per meter width is given in Figure 30, also the maximum peak force (103.06 kN) of the signal is indicated in this figure.

Table 1: Froude scaling for wave impact data

Variable	Unit	Scale model dimensions and quantities	Scaling factor	Scaling factor case study	Case study dimensions and quantities
Length	[m]	$H_s = 0.06$ $W = 0.1$ $L_z = 0.6$	λ	12.08	$H_s = 0.7$ $W = 1.2$ $L_z = 7.25$
Frequency	[Hz]		$\lambda^{-0.5}$	0.29	
Time	[s]	$T_p = 1.3$	$\lambda^{0.5}$	3.48	$T_p = 4.5$
Mass	[kg]		λ^3	1762.79	
Pressure	[Pa]		λ	12.08	
Force	[N]		λ^3	1762.79	
Force/m ¹	[N/m]		λ^2	145.93	

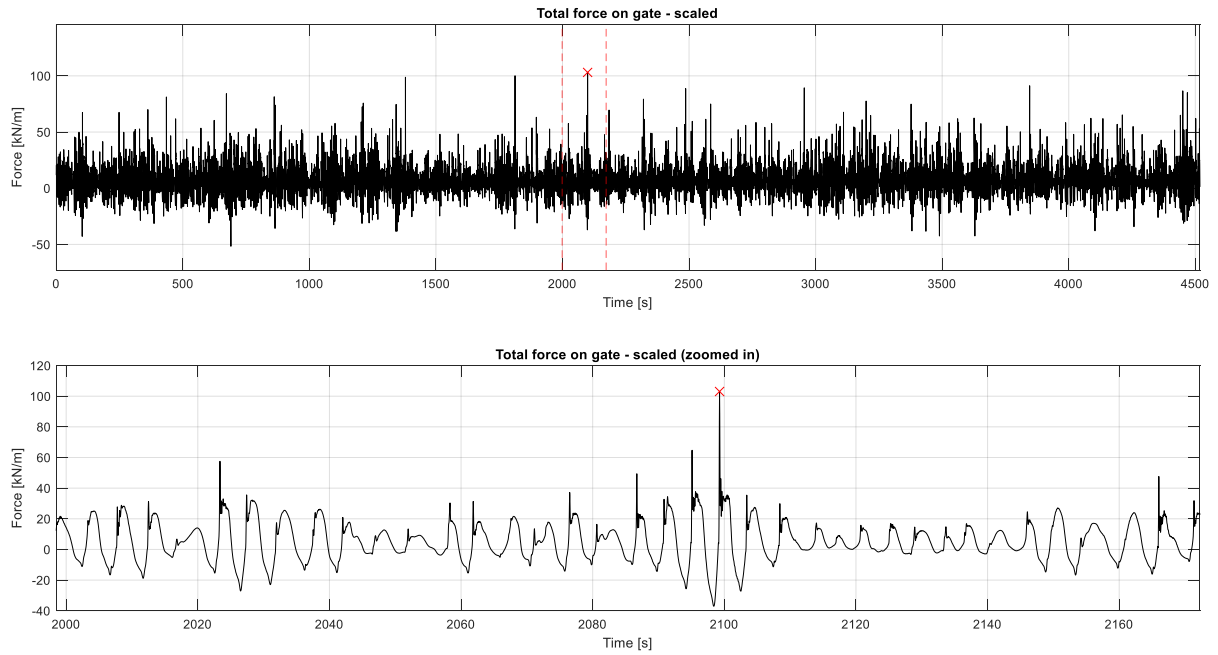


Figure 30: a) Time series of total force on the gate per meter width – scaled, b) Time series of total force on the gate per meter width – scaled and zoomed in

As said before, an irregular wave field consisting of 1000 waves is used for the lab-test, after scaling to the case study situation, a time signal with a total length of 4518 s (1 h 15 min 18 s) is obtained. It has to be kept in mind that in reality most of the time a storm lasts for several hours and consists of thousands of waves, so the wave field used to analyze the SDOF model is on the short side. However for now the duration of the lab-test is considered acceptable for the analysis. In Figure 32 (left) a histogram of the peak forces of the wave impacts is given, in Figure 32 (middle) a histogram of the wave impact durations is shown, and in Figure 32 (right) a histogram of the magnitude of the wave impact impulses is given. To calculate the wave impact impulse the force signal has been split into an impulsive part and a quasi-static part, see Figure 31. Thereafter, the wave impact impulse is calculated as the area under the wave impact peak (the green area in Figure 31). In appendix E the calculation of the wave impact durations, wave impact impulses, and the splitting method of the force signal are described in more detail.

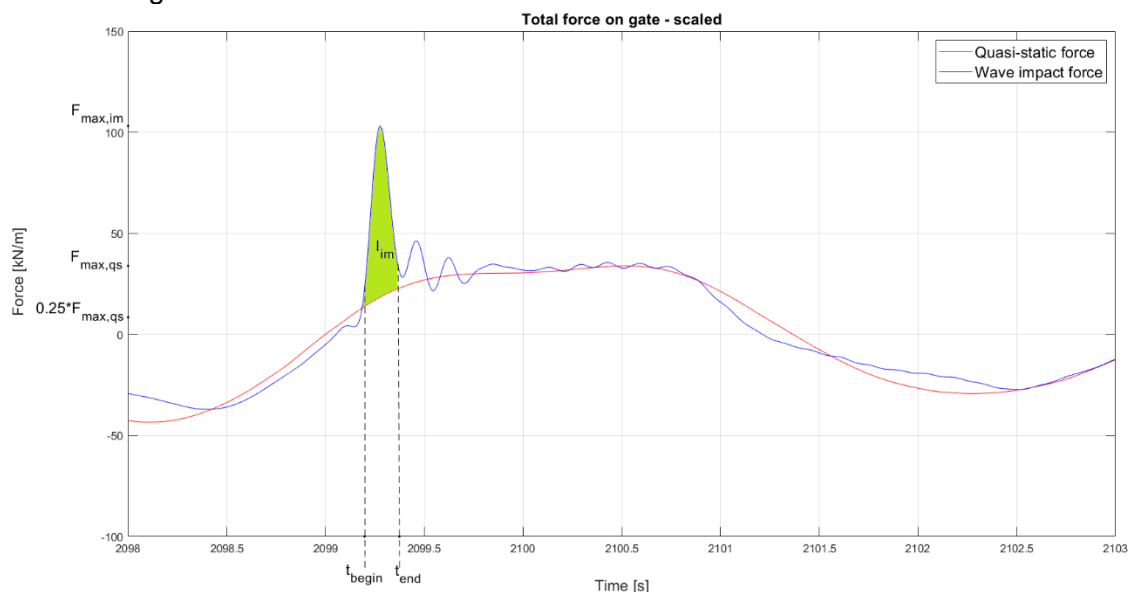


Figure 31: Used definition for the wave impact peak force ($F_{max,im}$), wave impact duration ($\tau = t_{end} - t_{begin}$), and wave impact impulse (I_{im}) (wave 311)

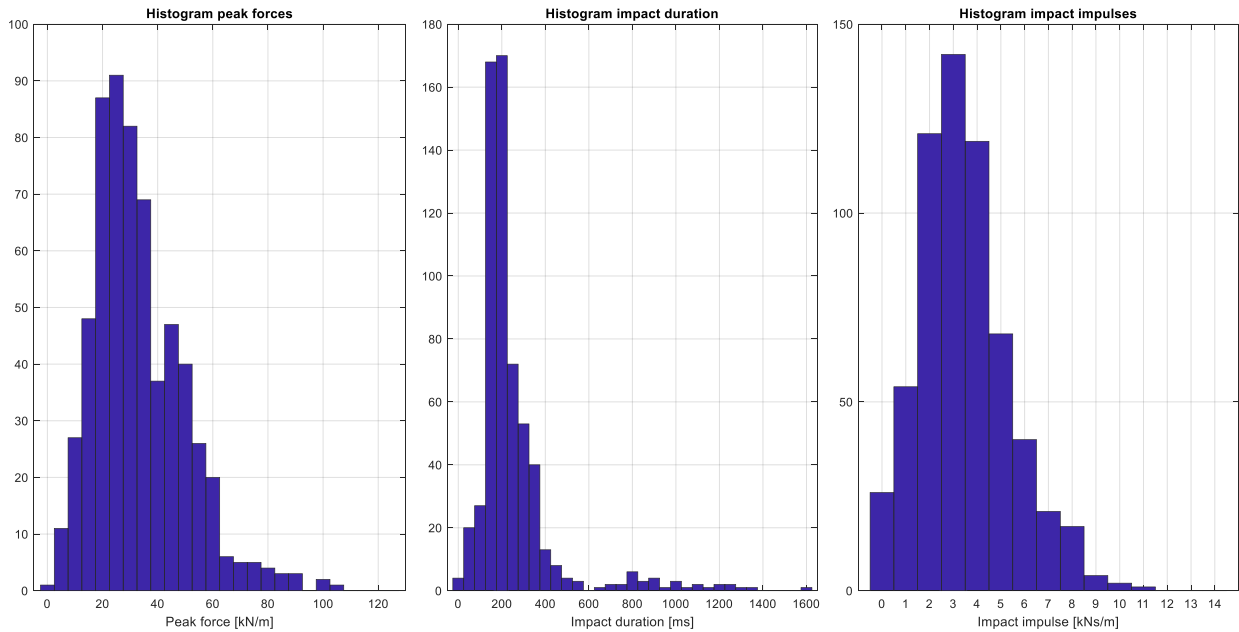


Figure 32: Histogram peak forces (left), histogram wave impact duration (middle), histogram wave impact impulses (right)

4.3.2 Maximum response to a wave field determined with the DAF method

The DAF method is used to determine the maximum deflection (response), and corresponding dynamic amplification factor (DAF) for the time signal of a whole wave field (Figure 30). The way that the method is used, is slightly different from the way that is described at the beginning of this paragraph. First the maximum peak force from Figure 30 is determined (wave 311, $F_{\max} = 103.06$ kN), then the corresponding force-time signal from this single (maximum) wave impact is isolated and schematised as a triangular load, see Figure 33. Next the response to this triangular load schematisation is determined with the SDOF model. The dynamic amplification factor is calculated by dividing the maximum deflection that is found ($x_{\max,DAF}$), by the static response for the maximum wave impact load ($x_{\max,static} = F_{\max}/k$).

For this part of the analysis three SDOF systems are investigated. All three of these systems are within the dynamic domain ($0.25 < \tau/T < 4$, see Figure 13).

- $\tau/T = 0.5$, a relatively slow system compared to the impact duration
- $\tau/T = 1.0$, an evenly fast system compared to the impact duration
- $\tau/T = 2.0$, a relatively fast system compared to the impact duration

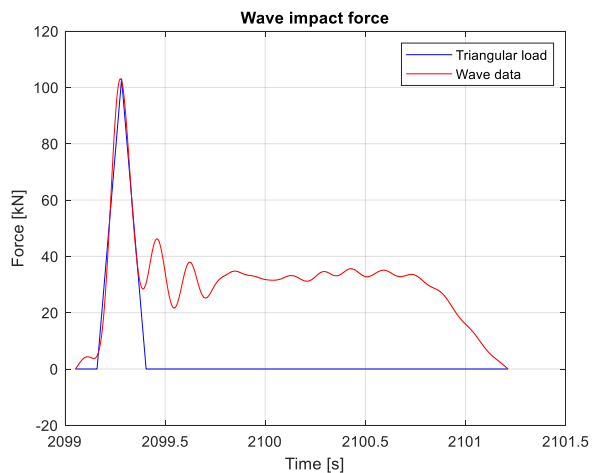


Figure 33: Triangular schematisation of maximum wave impact (wave 311)

From the wave data the impact duration can be determined, the impact duration of the schematised triangular load is approximately 250 ms. It has to be noted that this impact duration is quite high compared to the values known from the literature (10 ms -100 ms). This long impact duration is caused by the Froude scaling factor of $\lambda^{0.5}$ for the time variable.

From the study of Tieleman et al (PIANC report, 2018), typical values for the eigen period of gates in dry condition and submerged in water can be determined. For the dry gate studied in the paper of Tieleman et al (PIANC report, 2018) an eigen period of 45 ms is determined, and for the gate submerged in water an eigen period of 100 ms is found. When the cases above are investigated for an impact duration of 250 ms, the ratio of the mass and stiffness of the system has to be chosen such that the corresponding eigen periods are: $T = 500$ ms, $T = 250$ ms, $T = 125$ ms. Due to the relatively high impact duration value that is found from the wave data, these eigen periods are slightly higher than the values found in the report of Tieleman et al (PIANC report, 2018). However for this analysis they are considered within realistic limits for a gate submerged in water.

To obtain the different eigen periods for the systems, the ratio of the mass and stiffness have to be varied. For this analysis the mass is kept constant and the stiffness is chosen such that the desired eigen period is obtained. The dynamic amplification factors of the three systems, that are obtained with the DAF method (for the maximum wave impact force in the wave field), are compared to the dynamic amplification factors corresponding to the ‘real’ maximum deflections that are obtained for the whole wave field (in paragraph 4.4). For the three systems considered (with $\zeta=5\%$), the dynamic amplification factors that are obtained with the DAF method are given in Table 2 ($x_{\max,DAF}/x_{\max,static}$). In the table it is also indicated for which wave in the wave field the maximum response occurs for each system ($Wave_{DAF}$).

Table 2: Amplification factors obtained with the DAF method, and by running the whole force-time signal (wave field) with the SDOF model

	τ/T [-]	$x_{\max,DAF}/x_{\max,static}$ [-]	$Wave_{DAF}$ [-]	$x_{\max,real}/x_{\max,static}$ [-]	$Wave_{real}$ [-]
System 1	0.5	1.18	311	1.16	311
System 2	1.0	1.41	311	1.53	311
System 3	2.0	1.02	311	1.40	229

4.4 Maximum response to a wave field determined with the SDOF model

The following step of the analysis is to compare the amplification factors obtained with the DAF method (in the previous paragraph), to the amplification factors corresponding to the ‘real’ maximum deflections that are obtained by running the whole force-time signal (from Figure 30) with the SDOF model. This comparison is made to check the validity of the DAF method that is used as present design approach. The amplification factors that are determined, are compared for the three different systems described in the previous paragraph, to check whether different conclusions have to be drawn for systems with different stiffness (or ‘speed’).

4.4.1 Comparison maximum response DAF method and real maximum response

In Table 2, the amplification factors corresponding to the ‘real’ maximum deflections for the three systems (with $\zeta=5\%$) are also given ($x_{\max,real}/x_{\max,static}$). In the table it is again indicated for which waves in the wave field the maximum responses (and corresponding amplifications) occur ($Wave_{real}$).

When the amplification factors corresponding to the real maximum deflections are compared to the amplification factors obtained with the DAF method (Table 2), it can be seen that for system 1 the DAF method gives a slight overestimation of the amplification (and maximum deflection), and for systems 2 and 3 the DAF method gives a underestimation of the amplifications (and maximum deflections). The largest error is made for the stiffest/fastest system. It also has to be noted that the real maximum deflections (and corresponding amplification factors) for systems 1 and 2 are for the maximum force peak (that is also used for the DAF method), and that the real maximum deflection (and corresponding amplification factor) for system 3 is for a slightly lower force peak. It can be concluded that the maximum force does not necessarily give the largest response, and that lower peak forces can also cause quite high deflections. It can also be concluded that the DAF method gives a slight under- or over estimation of the maximum deflection and corresponding amplification factor. In the next paragraph, the cause of the difference between the maximum deflections/amplifications (found with the different methods) will be investigated.

4.4.2 Investigation of the difference between the maximum deflections and corresponding amplifications (found with the DAF method and for the whole wave field)

The difference between the two methods of determining the maximum deflection and corresponding amplification factor, that is found in the previous paragraph can have multiple causes. A couple of explanations of the difference can be:

- 1) In reality the vibration of the gate is not yet fully damped when the next wave impact already occurs (so this effect will be seen in the response obtained by running the whole time signal and this effect will not be seen by applying the DAF method).
- 2) The triangular schematisation used for the DAF method is not precise enough, so more effort should be paid on the schematisation of the load.
- 3) The wave impact with the highest peak force as used in the DAF method is not governing for the actual maximum dynamic response. In other words, the wrong wave impact is used within the DAF method.

Each of these three possible effects will be investigated in the following subsections.

4.4.2.1 Investigation vibration of the gate between two wave impacts

First, the vibration of the gate before the next wave impact occurs will be investigated. In Figure 34 the force signal and responses for the different systems obtained with the SDOF model are displayed for a certain time period. From this cut out the influence of the vibration of the gate from the previous wave impact on the response to the next wave impact can be seen for the different systems. For the relatively slow system (system 1), it can be clearly seen that the vibration of the first wave impact in the figure is not yet fully damped when the next wave impact already occurs. For the fastest system (system 3), it can be seen that the vibration from the first wave impact in the figure is almost fully damped when the next wave impact occurs. So it can be concluded that the influence of the vibration of the gate due to the previous wave impact depends on the stiffness (speed) of the system.

This conclusion is in agreement with the theory found in the literature (Kolkman and Jongeling, 1996). The amplitude of a damped SDOF systems damps with the following factor:

$$e^{-\gamma\omega_n t} \quad (\text{eq 4.1})$$

The time between two wave impacts (between the wave impact peak and start of the next wave impact) from the scale experiment is on average 3.5 s ($t = T_{wave}$). For this wave field (and $\zeta=5\%$), it can be assumed that the vibration from the previous wave impact is damped before the next impact occurs for systems with an eigen period smaller than 239 ms ($e^{-\gamma\omega_n t} < 1\%$). The damping factors for the 3 systems, at the beginning of the next wave impact, are given in Table 3. The damping factor indicates the magnitude of the amplitude of the vibration after a certain time period, as a percentage of the initial amplitude of the vibration. The damping factors calculated in Table 3 correspond with the results displayed in Figure 34 (the damping of the vibration amplitude between two wave impacts for the different systems). With equation 4.2 the amount of cycles that have to be made by the structure between two wave impacts can be calculated, so that the amplitude of the vibration is damped until 1%.

$$\frac{T_{wave}}{T_{structure}} > \frac{0.73}{\gamma} \tag{eq 4. 2}$$

For a damping ratio of 5%, 14.6 cycles are needed to be damped until 1%. It can be concluded that based on the wave period (time between two impact durations), eigen period of the structure, and damping, it can be determined whether the vibration of the structure is damped between two wave impacts.

Table 3: Damping factor for the amplitude of a damped SDOF system

	$T_{structure}$ [s]	ω_n [rad/s]	γ [-]	T_{wave} [s]	$e^{-\gamma\omega_n t}$ [%]
System 1	0.5	12.57	0.05	3.5	11.09
System 2	0.25	25.13	0.05	3.5	1.23
System 3	0.125	50.27	0.05	3.5	0.015
	0.239	26.29	0.05	3.5	1.00

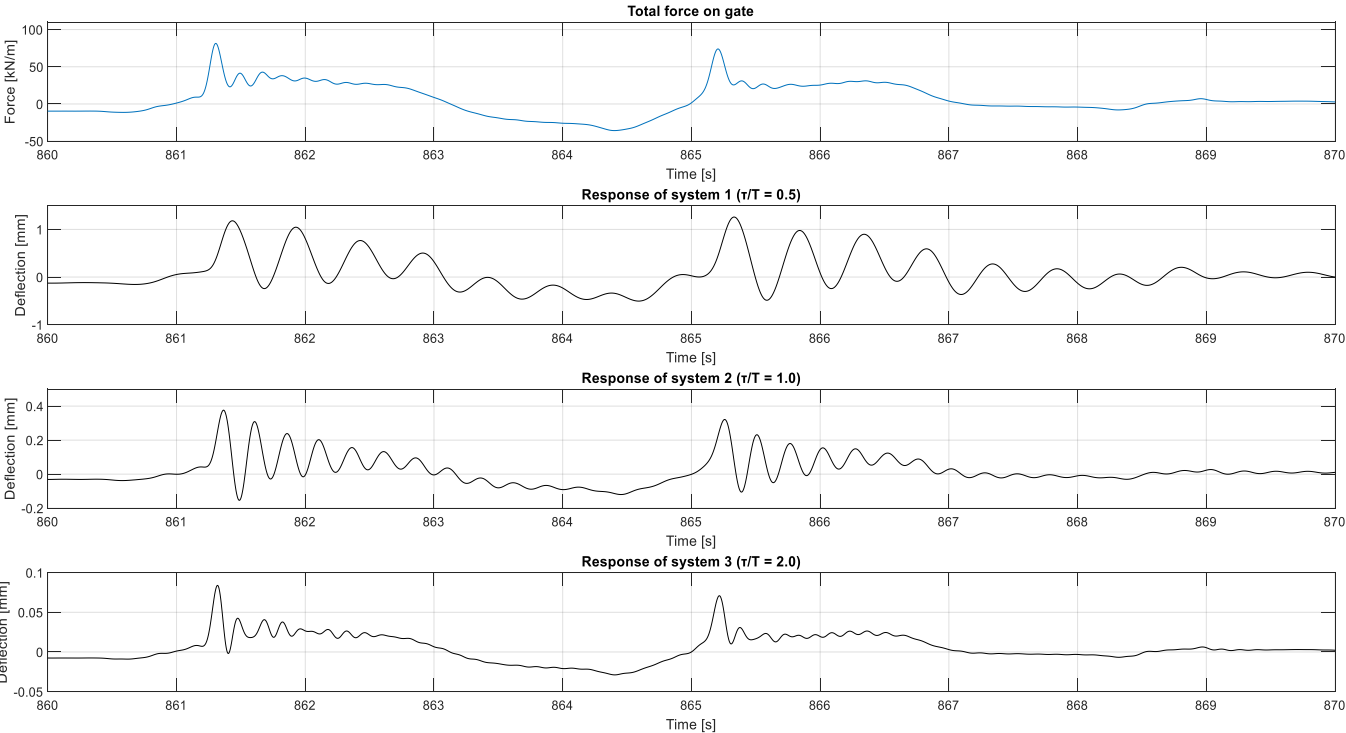


Figure 34: Influence of the vibration from the previous wave impact on the maximum response to the next wave impact (waves 141 and 142)

The next step is to investigate the influence of this not yet damped vibration on the maximum deflection for the next wave impact. To do this Matlab is used to calculate the maximum response for each force peak in the wave field with the DAF method ($x_{DAF} = DAF * F_{wave\ impact} / k$). This values are compared with the maximum deflections obtained with the SDOF model. From this analysis it can be concluded that for system 3, all the maximum responses that are calculated with the DAF method (for all of the force peaks) are systematically lower than the real maximum responses calculated with the SDOF model. For system 1, the maximum responses that are calculated with the DAF method are either lower or higher than the real maximum responses, depending on the position of the gate at the moment that the wave impact occurs. So it can be concluded that when the vibration is not yet fully damped, this has an influence on the maximum deflection for the next wave impact that is calculated with the SDOF model. For system 2 the vibration are also not fully damped between the wave impacts. Again it is found that for this system the maximum responses calculated with the DAF method are either lower or higher than the response found with the SDOF model. So the response calculated with the SDOF model is influenced by the not yet fully damped vibration from the previous wave impact. It can be concluded that the 'slower' the system, the higher the influence of the previous wave impact. This means that the DAF method will give more realistic and reliable results for relatively stiff/fast systems. However from Table 2 it can be seen that the DAF method give the larges error for system 3. This error is not caused by the not yet fully damped vibrations from the previous wave impact, and will be investigated in more depth in paragraphs 4.4.2.2 and 4.4.2.3.

The influence of the vibration of the previous wave impact is also tested in a different way. The response to a random wave impact from the data (wave 124) is analysed and compared to the response to the same wave impact with zero initial conditions ($w = 0\ m$ and $v = 0\ m/s$). By setting the initial conditions to zero, the influence (initial displacement and -velocity) of the previous wave impact on the response, is not present. A relatively fast (system 1) and slow (system 3) system are compared to check the influence of the vibration of the previous wave impact. In Figure 35 the responses of systems 1 and 3 are displayed for the wave impact in the upper panel of the figure. In the figure the real responses (black lines), and responses to the same wave impact with zero initial conditions (red lines) are shown. In Table 4 the results from this analysis are summarized.

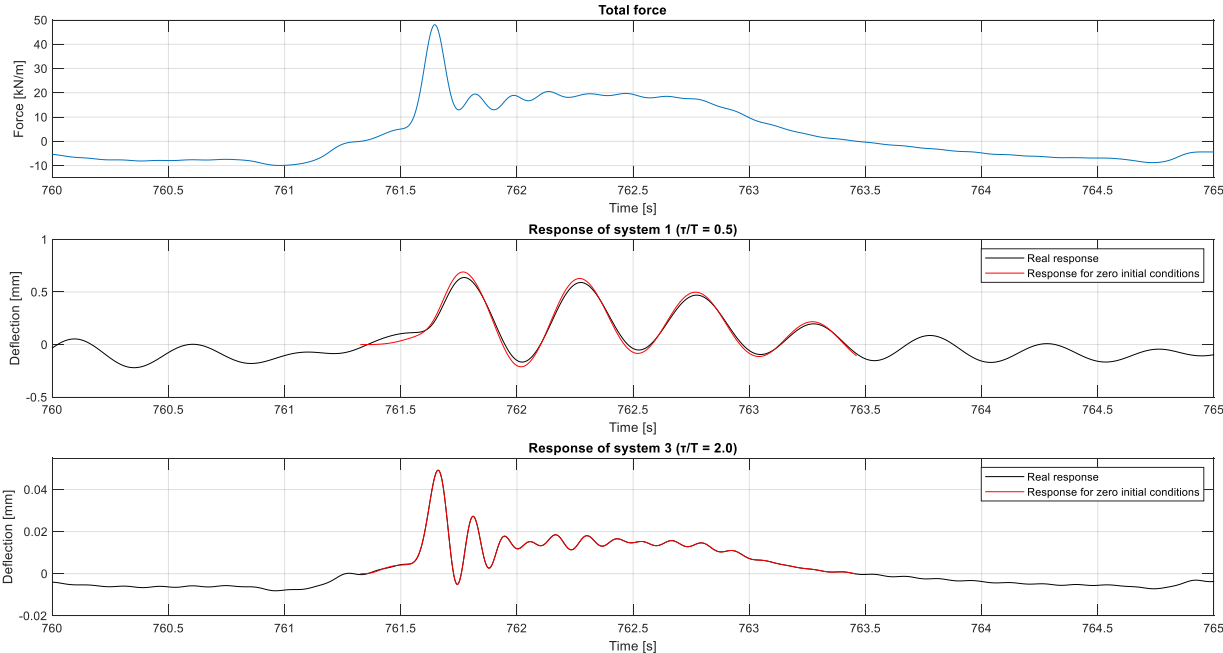


Figure 35: Comparison real response for wave impact 124 and response for wave impact 124 with zero initial conditions

Table 4: Comparison amplification factor for the real maximum response for wave impact 124, and amplification factor for the maximum response for wave impact 124 with zero initial conditions

	τ/T [-]	$x_{\max,\text{real}} / x_{\max,\text{static}}$ [-]	$x_{\max,v=0,w=0} / x_{\max,\text{static}}$ [-]	Wave [-]
System 1	0.5	1.05	1.13	124
System 3	2.0	1.28	1.28	124

From Figure 35 and

Table 4 it can be seen that the real (maximum) response of system 3 is similar to the response to the same wave impact with zero initial conditions. So it can indeed be concluded that the vibration from the previous wave impact is (almost) fully damped when the next wave impact occurs, and that the response is not affected by the previous wave impact for relatively fast/stiff systems. From the results it can also be seen that the not yet damped vibration from the previous wave impact has influence on the (maximum) response of relatively slow/not stiff systems. So based on this results it can also be concluded that the DAF method will give more realistic and reliable results for relatively stiff/fast systems.

4.4.2.2 Influence of the schematisation of the wave impact force on the validity of the DAF method

In the previous paragraph it was concluded that the DAF method gives more realistic results for relatively stiff/fast systems. However, when the results from Table 2 are compared, it is found that the DAF method gives the largest (systematic) underestimation for the maximum response and corresponding amplification factor for system 3. It appears that this underestimation is closely related to the schematisation of the wave impact force in the DAF method. In the previous analysis the impact duration is defined as τ_2 (=250 ms) in Figure 36. During the analysis the impact duration is determined graphically by fitting a triangular schematisation in the force-time signal of the wave impact (blue line in Figure 36). However, the impact duration can also be calculated with more accuracy following the numerical procedure described in appendix E (defined as $\tau_1 = 165$ ms in Figure 36). In this procedure the begin time of the wave impact is defined as the moment when the difference function between the wave impact data and quasi-static data (red and black line in Figure 36) becomes larger than a certain threshold value. For this research the threshold value is defined as 25% of the corresponding quasi-static force peak ($\text{diff} > 0.25 \cdot F_{\max,\text{qs}}$). The end time of the wave impact peak is defined as the moment at which the difference function becomes smaller than the threshold value. This other definition can give a larger or smaller value of the impact duration, compared with the graphical method used for this analysis. When the impact duration changes, the ratio of τ/T will change, and according to Figure 27 the dynamic amplification factor will change. Depending on the place on the x-axis in Figure 27 the dynamic amplification factor can be higher or lower for another impact duration. So when this other method is used for the determination of the impact duration (instead of using the same value of 250 ms for each wave impact), the schematisation that is used for the DAF method will be better, and better results will be obtained with the DAF method. When a triangular load schematisation with a shorter impact duration is used for the DAF method for system 3 ($\tau_1/T < \tau_2/T$), the dynamic amplification factor calculated with the DAF method is higher and closer to the calculated 'real' dynamic amplification factor. So when more effort is made on the wave impact schematisation for the DAF method (especially the wave impact duration), the results obtained with the DAF method for system 3 are closer to the 'real' response that is obtained by running the whole force-time signal with the SDOF model. Then this system gives indeed the most realistic results, as was expected based on the conclusions that are drawn in paragraph 4.4.2.

All three of the systems that are investigated are in the dynamic domain ($0.25 < \tau/T < 4$, see Figure 13). The optimization of the triangular load shape that is described above, gives better results for the DAF method for all three of these systems. However, for very long and short period systems (in the quasi-static and impulsive domain) the optimization of the schematisation does not necessarily give better results. When a system is in the quasi-static domain ($\tau/T > 4$), the structure starts moving very slowly and the response will be quasi-static. This means that the response has the same 'shape' as the load ('load in' is equal to 'response out'). When a system is in the impulsive domain ($\tau/T < 0.25$) the exact shape of the impact force also does not matter for the response (as can be seen in Figure 11). So it can be concluded that for systems in the dynamic domain, the load schematisation (especially the wave impact duration) is important for the correctness of the response that is determined with the DAF method.

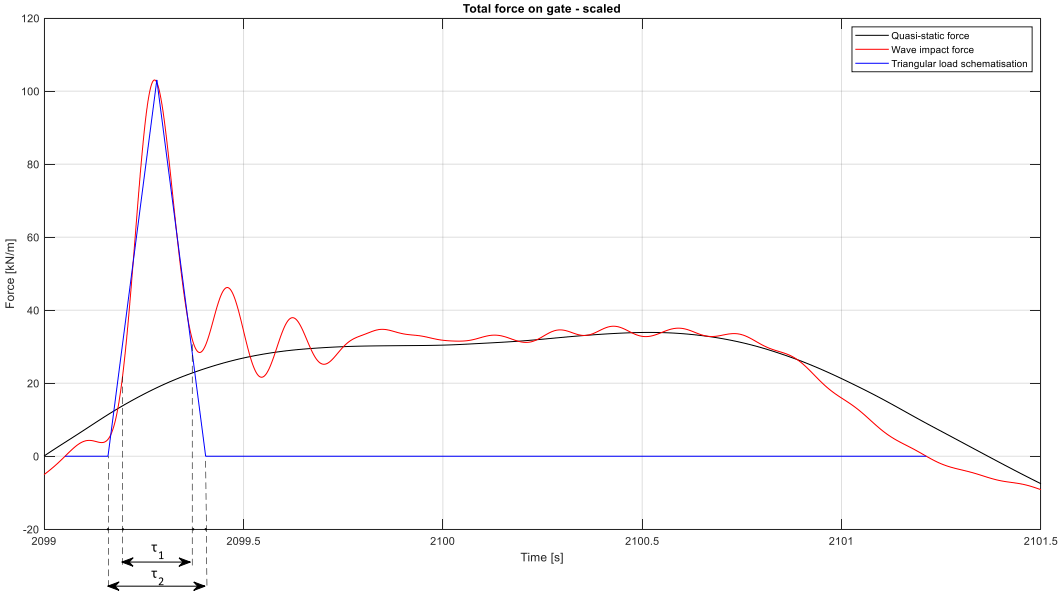


Figure 36: Two definitions of the impact duration (wave 311)

4.4.2.3 Design wave

From Table 2 it can be seen that the maximum response for system 3 is not found for the wave with the highest peak force (wave 311, $F_{max} = 103.06$ kN), but for a wave impact with a slightly lower peak force (wave 229, $F_{max} = 98.78$ kN). From paragraph 4.4.2.1 it can be concluded that the influence of the vibrations from the previous wave impact are negligible for system 3, so another explanation must be found for this phenomenon. Besides the difference in peak force, the waves (wave 311 and 229) also differ in impact duration. Wave 229 has a lower peak force and shorter impact duration than wave 311. In Figure 37 the maximum response curve for a symmetrical triangular impulse and damping ratio of 5% is again shown. In the figure the location of the 3 different systems is indicated. From the figure it can be seen that when the impact duration becomes shorter, the DAF for system 3 becomes larger, and the DAFs for systems 1 and 2 become smaller. When the increase of the DAF is larger than the decrease of the static deflection, the maximum response can indeed be found for a wave with a slightly lower peak force, with a shorter impact duration (for system 3).

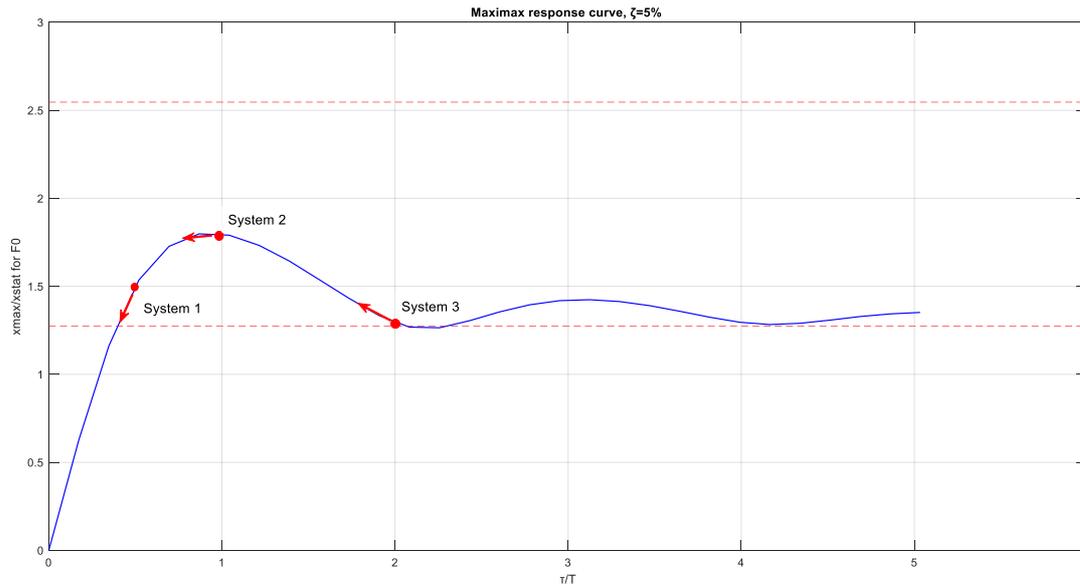


Figure 37: Influence of impact duration on DAF

It can be concluded that the wave with the highest peak force does not always give the largest maximum response. Based on the location in the maximax response curve (ratio of impact duration and eigen period of the structure), waves with a slightly lower peak force and shorter or longer impact duration can still give the largest response.

4.5 Conclusions

It can be concluded that the maximum deflection and corresponding dynamic amplification factor of a structure found with the DAF method, by which the response for a single triangular load schematisation (of the maximum wave impact in the wave field) is calculated with the SDOF model, differs from the 'real' maximum deflection and corresponding amplification factor obtained by running the whole force-time signal (wave field) with the SDOF model. The DAF method may give an over- or underestimation. The cause of this difference is a combination of the following three effects:

- 1) In reality the vibration of the gate is not yet fully damped (amplitude $<1\%$) when the next wave impact already occurs.
- 2) The triangular schematisation used for the DAF method is not precise enough, so more effort should be paid on the schematisation of the load.
- 3) The wave impact with the highest peak force as used in the DAF method is not governing for the actual maximum dynamic response. In other words, the wrong wave impact is used within the DAF method.

So, it can be concluded that the DAF method does not 'suffices in time'.

In Table 5 the percentual differences between the dynamic amplification factors corresponding to the maximum deflections found with the DAF method and by running the whole wave signal with the SDOF model are given. From the table it can be seen that the largest error is found for relatively fast systems compared to the impact duration (system 3). However, this error can be reduced tremendously when the impact duration of the wave impact causing the highest response, is determined with more accuracy than done for the analysis performed in paragraphs 4.3 and 4.4. During the analysis the impact duration is determined graphically by fitting a triangular schematisation in the force-time signal of the wave impact. However, when the numerical method described in appendix E is used to determine the wave impact duration with more accuracy, the error for relatively fast systems

compared to the impact duration will already be reduced to 6.1%. So, it can be concluded that, for systems in the dynamic domain ($0.25 < \tau/T < 4$), a proper definition of the impact duration has a large influence on the correctness of the load schematisation, and the corresponding calculated response (maximum deflection) and dynamic amplification factor. A method (described in appendix E), using the quasi-static force signal to split the wave force into an impulsive and quasi-static part, is proposed to determine the correct impact duration. When systems are in the quasi-static ($\tau/T > 4$) or impulsive ($\tau/T < 0.25$) domain, the influence of the definition of the impact duration (load schematisation) on the correctness of the response determined with the DAF method is much smaller. All three of the systems that are investigated are in the dynamic domain, so for all three of these systems a more accurate wave impact duration (better load schematisation) gives a more realistic result for the response that is determined with the DAF method. So, it can be concluded that when systems are in the dynamic domain, more realistic results are obtained with the DAF method, when the wave impact duration (load schematisation) is determined with more accuracy using a numerical method instead of a graphical method.

Table 5: Percentual differences between the dynamic amplification factors found with the DAF method and found by running the full wave signal in the SDOF model

	τ/T [-]	$\Delta_{\text{DAF,Real}}$ [%]
System 1 (slow)	0.5	1.7
System 2 (similar)	1.0	8.5
System 3 (fast)	2.0	37.3

In paragraph 4.4.2.1 it is concluded that based on the wave period (time between two impact durations), eigen period of the structure, and damping, it can be determined whether the vibration of the structure is damped between two wave impacts. As general rule it can be used that the vibration of the structure is damped out between two wave impacts when: $e^{-\gamma\omega_n t} < 1\%$. When this rule is met, the influence of the vibration of the structure due to the previous wave impact, on the response of the next wave impact can be considered negligible. The 'real' response that is calculated with the SDOF model can deviate considerably from the response calculated with the DAF method (higher or lower depending on the position of the gate at the moment that the new impact occurs) due to this effect. For systems 1 and 2 the vibrations between the wave impacts are not fully damped. Based on the position and velocity of the structure at the moment that the next wave impact occurs, the maximum deflection for the next wave impact is influenced. For system 1 only a small difference of 1.7% is found between the amplification factor determined with the DAF method and the dynamic amplification factor found by running the whole wave signal with the SDOF model. However it is important to keep in mind that the magnitude of this difference depends on the wave impact that occurs before the maximum wave impact, and the corresponding position and velocity of the structure caused by the not yet damped vibrations at the moment that the next wave impact occurs. So, this percentage can be increased significantly when the wave impact before the maximum wave impact results in another velocity or position of the gate when the governing wave impact occurs.

Finally, it can be concluded that the maximum peak force in the wave field does not always cause the largest response. The combination of the impact duration, maximum peak force, and eigen period of the structure (location in the maximax response curve), determines which wave causes the largest response (and amplification). So, it is important to also take some of the lower peak forces (with shorter or longer impact duration) into account when determining the maximum response and corresponding dynamic amplification factor with the DAF method.

From the analysis with an SDOF model in this chapter it can be concluded that the DAF method indeed not 'suffices in time', and that it is necessary to improve the DAF method in time. Only looking at the wave impact with the highest peak force (instead of looking at the response for a whole wave field), may result in over- or underestimations of the maximum deflection. To improve the DAF method in time, it is suggested to look at the maximum deflection that is obtained by running the force-time signal for multiple wave impacts (a whole wave field), instead of only looking at the maximum deflections for the wave impact with the highest peak force.

At this moment, the wave impact force-time signal is determined based on the results of scale model tests (measurements). So, when the use of a force-time signal for multiple wave impacts is incorporated into the design method, it is necessary to perform scale model tests for each individual design case. This makes the suggested improvement of the DAF method in time very uneconomical. In chapter 6 a first version of a method to easily determine the force-time signal of multiple wave impacts based on wave parameters only is described and validated. When this method is further developed and validated, no scale model tests are needed to determine the force-time series of wave impacts in the future, and the improvement of the DAF method in time can easily be implemented.

5 Statistical description of wave impact data in time and space

In chapter 4 it is concluded that the current design method (DAF method) does not 'suffices in time'. To improve the DAF method in time, it is suggested to look at the maximum deflection that is obtained by running the force-time signal for multiple wave impacts, instead of only looking at the maximum deflections for the wave impact with the highest peak force. In chapter 6 a first version of a method to easily determine the force-time signal of multiple wave impacts based on wave parameters only, that can be used for the improvement of the DAF method in time, is described and validated. To be able to also use this 'model' force-time signal (for multiple wave impacts) for the investigation of the influence of a spatial variation of the wave impact force over the gate surface on the response of the gate, in chapter 7 (and improve the current design method in space), the spatial distribution of the wave impact force over the gate surface is incorporated in the composition method of the 'model' force-time signal. In this chapter a statistical description of the wave impacts data from the scale experiments will be given in time and space, to be able to compose this 3D force-time signal for multiple wave impacts in chapter 6.

In paragraph 5.1 a statistical description of the pressure sensor data in time is given. In section 5.2 new scale experiment data (load cell data) will be introduced to be able to look at the spatial (width) variation of the wave impact force in section 5.3. Finally, in section 5.4 the statistical distributions of the wave parameters that are needed for the composition of the 'model' force-time signal in chapter 6 are discussed.

5.1 Statistical description of pressure sensor data in time

In this paragraph a statistical description of the (scaled) data set described in paragraph 4.3.1 is given. The data set represents a wave field consisting of a thousand waves. First, in paragraph 5.1.1 the correlation between the wave impact impulses and - peak forces is investigated. Then in paragraphs 5.1.2 and 5.1.3 extreme value distributions of the wave impact peak forces and -impulses are given. Appendix E explains how the force signal is split in an impulsive and quasi-static part, and how the wave impact peaks are identified. Figure 82 in appendix E shows the definitions of the wave impact peak force (F_{im}), quasi-static peak force (F_{qs}), and wave impact impulse (I_{im}).

5.1.1 Correlation between wave impact impulse and maximum wave impact force

In the paper of Chen et al (2018), a positive correlation is found between the wave impact impulse (I_{im}) and the wave impact peak force (F_{im}). However, the positive correlation between the peak force and the impulse is found for the data set that is used for that particular research. It is checked if the same positive correlation is found for the data set that is used for this research (the data set is described in paragraph 4.3.1). In Figure 38 the correlation between the wave impact peak forces and wave impact impulses is shown. It can be seen that there is some scatter in the data that is caused by double wave impact peaks. However, a positive correlation can be observed from the plot. So in general it can be concluded that, for the data set that is used for this research, larger values for the wave impact impulse can be expected for the wave impacts with higher peak forces.

It is important to keep in mind that the wave impact impulse is calculated as the area under the wave impact pressure graph. So, the magnitude of the wave impact impulse depends on the magnitude of the maximum wave impact pressure and on the magnitude of the wave impact duration. When the wave impact impulse is used for design, instead of the wave impact peak force, indirectly the wave impact duration is also included in the design method by this.

This research still focusses on the maximum wave impact pressure as input for design. However, when new design methods for dynamic design of structures are developed in the future, it is important to focus on the wave impact impulse as input for design, instead of the wave impact peak pressure.

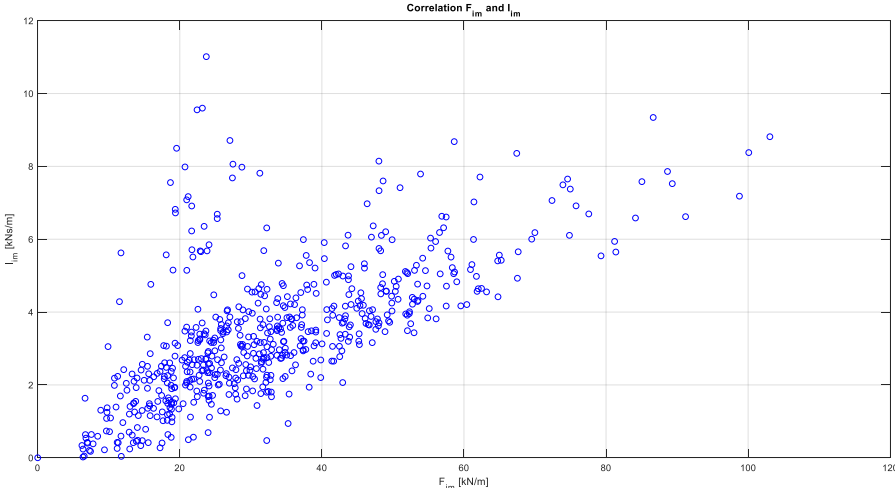


Figure 38: Wave impact peak forces versus wave impact impulses, (scaled, $\lambda = 12.08$)

5.1.2 Statistical description maximum wave impact force

In this paragraph the extreme value distribution of the wave impact peak forces (F_{im} [kN/m]) is investigated. The data set that is used consists of a thousand waves, however the number of actual wave impacts is on average 80% of the number of waves. In this paragraph an extreme value distribution is fitted based on the number of wave impacts. The paper of Chen et al (2018) shows that, for the data set that is used for that particular research, the wave impact impulses and maximum quasi-static wave forces are distributed according to a Weibull distribution (see appendix F). It is expected that this also holds for the data set that is used for this research.

For each data set the shape- and scale parameters a and b , giving the best fit, can be determined. In the upper panel of Figure 39 an exceedance probability curve for the wave impact peak forces is displayed. The peak forces from the wave signal that is used for this research, and corresponding exceedance probability are indicated with blue markers. From the figure it can be seen that the data set can also be described with a Weibull distribution. The best fit Weibull distribution is obtained for the following scale and shape parameters: $a = 36.0$, $b = 1.8$. On the x-axis the value of the wave impact peak force (F_{im}) is plotted, and on the y-axis the probability of exceedance of this peak force is plotted, so the probability that one of the wave impacts in the wave signal has a higher value for the wave impact peak force than the used value for F_{im} . From the plot a design value/characteristic value for the wave impact peak force can be determined, for instance $F_{im,0.1\%}$. In the lower panel of Figure 39 the probability density function of the wave data is plotted in blue, and the probability function for the best Weibull fit ($a = 36.0$, $b = 1.8$) is plotted in red.

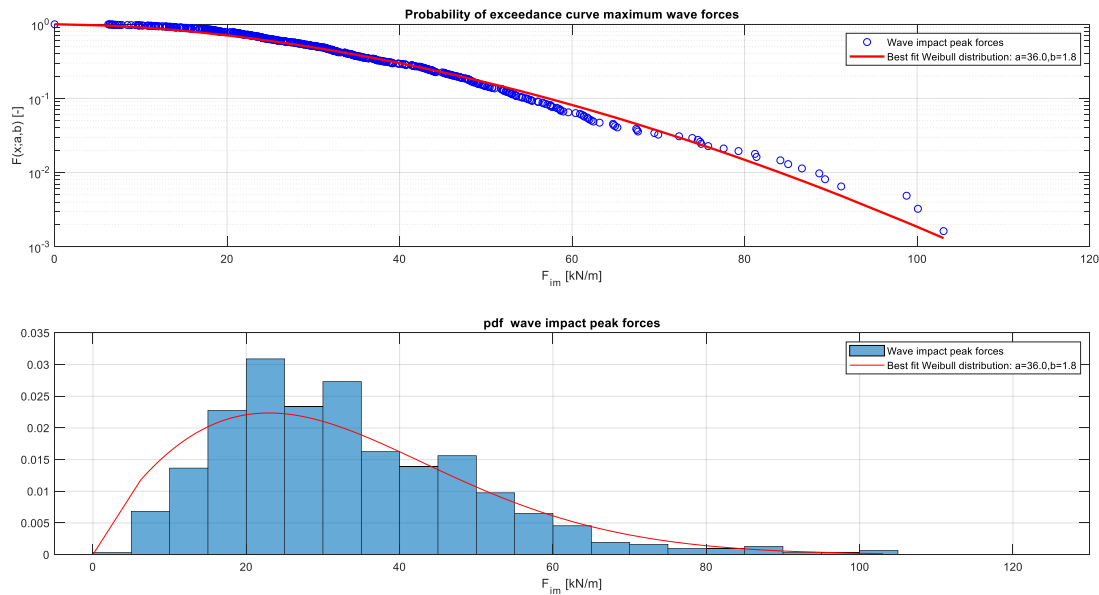


Figure 39: Weibull distribution fit for the wave impact peak forces, the best fit Weibull distribution is for $a = 36.0$ and $b = 1.8$, and pdf wave impact peak forces (F_{im}), (scaled, $\lambda = 12.08$)

5.1.3 Statistical description wave impact impulse

In this paragraph the extreme value distribution of the wave impact impulses (I_{im} [Ns/m]) is investigated. The same figure is made as for the wave impact peak forces, the results are shown in Figure 40. The best Weibull distribution fit is obtained for a scale factor $a = 4.0$, and a shape factor $b = 2.0$. When $b = 2.0$ the Weibull distribution can be related to the Rayleigh distribution, so actually the wave impact impulse is distributed according to a Rayleigh distribution. The wave impact impulse is linearly related to the wave velocity ($I_{im} \sim v$), and according to linear wave theory (see equation A.3) the wave velocity is linearly related to the wave height ($v \sim H$). From the literature it is known that the wave height is Rayleigh distributed (Holthuijsen (2007)), so this means that the wave impact impulse also has a Rayleigh distribution. The upper panel of Figure 40 can be used to obtain a design value for the wave impact impulse, for instance $I_{im,0.1\%}$.

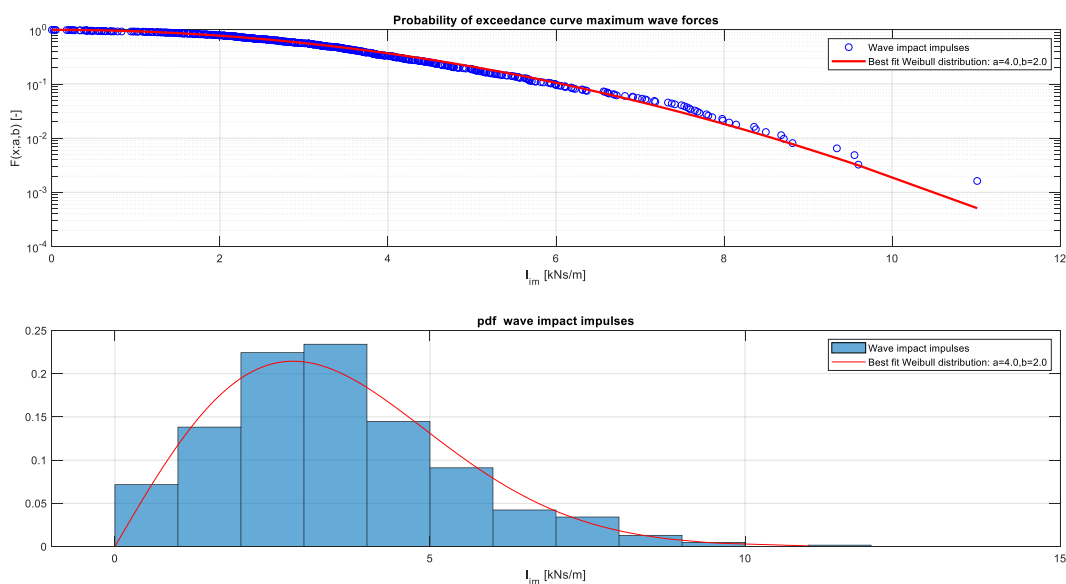


Figure 40: Weibull distribution fit for the wave impact impulses, the best fit Weibull distribution is for $a = 4.0$ and $b = 2.0$, and pdf wave impact impulses (I_{im}), (scaled, $\lambda = 12.08$)

5.2 Wave impact data from a wave field measured in scale experiments – load cell data

For investigation of a spatial distribution of the wave impact force, data from the scale experiment that is already described in paragraph 4.3.1 is used. In paragraph 4.3.1 data measured with pressure sensors (only over one vertical) is described. However, for the investigation of a spatial distribution of the wave impact pressure/force in chapter 7, data from load cell measurements is used as well. In Figure 41 the test set-ups for two scale measurements are shown: at the left a vertical wall subjected to wave impacts is shown, and at the right the same vertical wall with a short overhang ($W = 0.1 \text{ m}$) is shown. As already described in paragraph 4.3.1 using only the vertical wall will result in quasi-static wave data. This data can be used to determine the wave impact peak forces, -durations, and -impulses (see appendix E). The pressure sensors measure the pressure at one specific point, while the load cells measure the total force acting over a given area ($10 \times 10 \text{ cm}^2$ for load cells 2,3,4,5,6,7, and $10 \times 20 \text{ cm}^2$ for load cells 8,9,10).

The load cell- and pressure sensor data that is used for the investigation of width effects is filtered with a Butterworth filter 3rd order 150 Hz, this is done to simplify the analysis with the data. The raw data contains a lot of noise, which makes it more difficult to analyse the data. After filtering of the data, some vibrations are still present. This vibrations are caused by air bubbles in the water during impact. As already described in paragraph 2.1 (see Figure 8), air bubble/entrapped air in the water can cause large vibrations of the wave impact force.

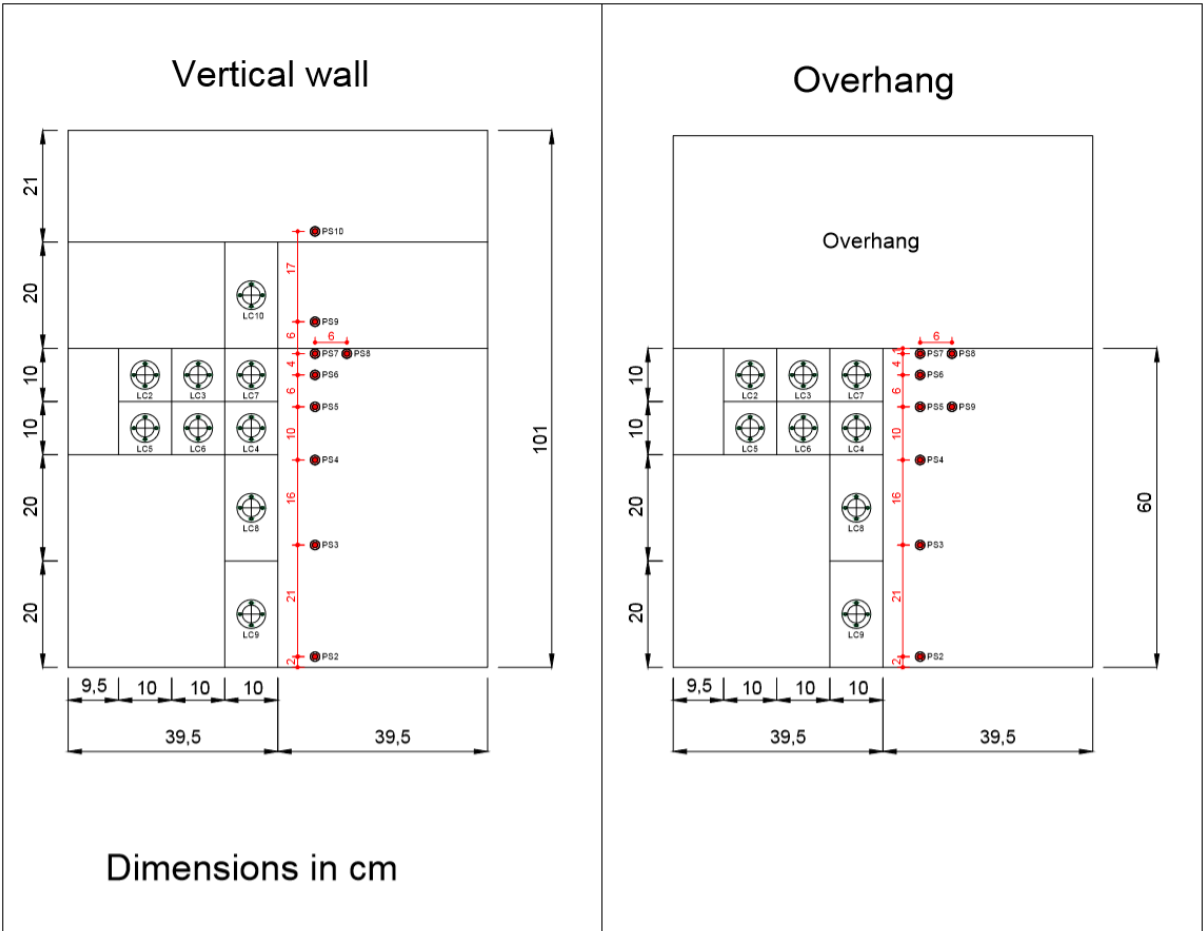


Figure 41: Overview test set-up load cells and pressure sensors (E. de Almeida, 2019)

The data is scaled to 'real' gate dimensions. The scaling to a realistic gate is inspired on the dimensions of the Afsluitdijk case study that is described in appendix G. The data is scaled using the Froude scaling (in paragraph 4.3.1 the scaling method is described in more detail). In Table 6 the scaling factors for the different variables, the original data values, and the corresponding scaled values are given.

Table 6: Froude scaling for load cell data

Variable	Unit	Scale model dimensions and quantities	Scaling factor	Scaling factor realistic gate	Realistic gate dimensions and quantities
Length	[m]	$H_s = 0.06$ $W = 0.1$ $L_z = 0.6$	λ	12.5	$H_s = 0.75$ $W = 1.25$ $L_z = 7.5$
Frequency	[Hz]		$\lambda^{-0.5}$	0.28	
Time	[s]	$T_p = 1.3$	$\lambda^{0.5}$	3.54	$T_p = 4.60$
Mass	[kg]		λ^3	1953.13	
Pressure	[Pa]		λ	12.5	
Force	[N]		λ^3	1953.13	
Force/m ¹	[N/m]		λ^2	156.25	

In the upper panel of Figure 42 the force measured, for one wave impact , with the different load cells is shown for the scaled data. In the lower panel of Figure 42 the force is converted to pressure. In appendix D.2 the original data and scaled data from the load cell measurements are shown.

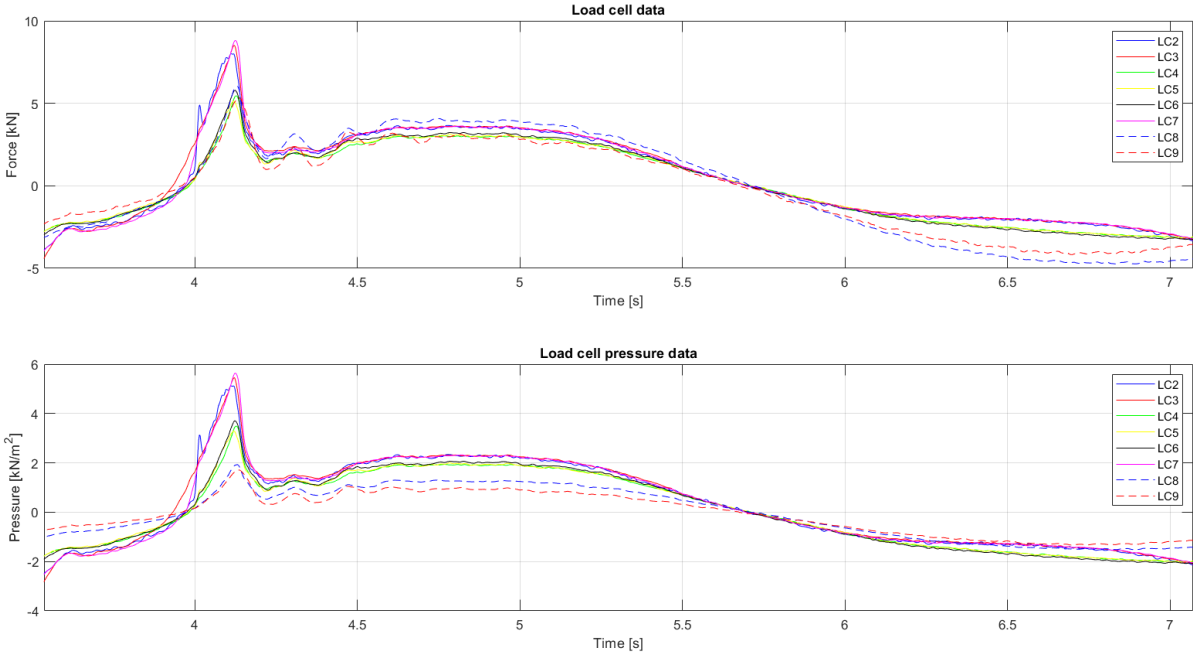


Figure 42: Load cell force data and load cell pressure data (scaled, $\lambda = 12.5$), wave 1

5.3 Statistical description of load cell data in space

In this paragraph the width distribution of the wave impact force is investigated. This research focusses on the wave impact force amplitude variation over the width of the gate. Another factor that may be important for the description of the width distribution of the wave impact force, is a small time shift of the wave impact peak time over the width that can be observed for some of the wave impacts in the wave signal described in the previous section. For wave 1, plotted in Figure 42, a really small time shift of 0.2% between load cells 2 and 7 of the top load cell row is observed. However, this research only focusses on the wave impact force amplitude variation over the width. For the possibilities for further research on the time shift of the wave impact peak time, and the influence of this time shift on the dynamic response of structures, reference is made to the recommendations in chapter 8.

The wave impact force amplitude variation over the width is investigated by introducing a skewness parameter. The skewness parameter is a dimensionless parameter describing the force amplitude variation over the width of the gate (based on the width distribution of the wave impact amplitude, the skewness parameter can be defined in a different way). The load cell data that is described in paragraph 5.3 is used for this investigation. The skewness parameter is determined for the top two rows of the load cell data (see Figure 41). The load cells are not present over the full width of the left gate half. So, at the left of the load cells, and in the centre of the gate extra points are defined (points 1- 4, see Figure 43). The pressure-time signals in this four points are determined by extrapolating the load cell data at the top two rows.

For the investigation of the width distribution of the load cell data over the left half of the gate the skewness parameter is defined with equation 5.1. For instance for the top row the skewness can be calculated with: $s = (F_{im,P3} - F_{im,P1})/F_{im,P3}$. The skewness is defined relative to the centre of the gate. At the centre the skewness is equal to 1. For instance, a skewness parameter of 0.5 means that wave impact amplitude in point 1 is 1.5 times the wave impact amplitude in the centre of the gate (at the right edge of load cell 7).

$$s = \frac{\Delta F}{F_{centre}} \tag{eq 5. 1}$$

In Figure 43 the definition of the skewness parameter for the different load cell rows is visualised.

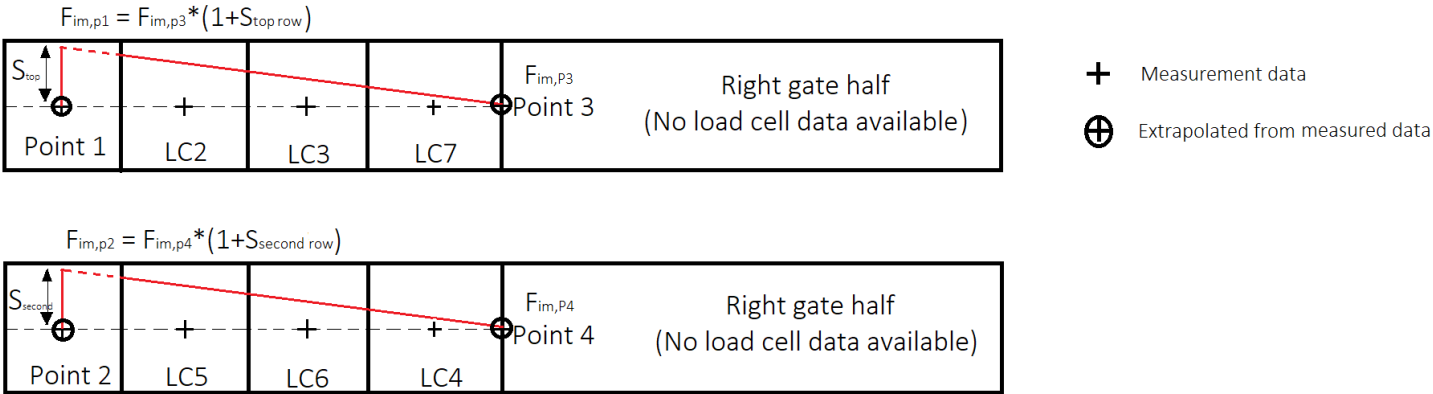


Figure 43: Definition skewness parameter for investigation width distribution of load cell data, front view of gate

In Figure 45 the skewness parameter is plotted against the mean value of the impact force over load cells 2,3,7 or load cells 4,5,6. From the figure it can be seen that the skewness parameter can be positive or negative:

- if $s > 0$: $F_{im,lc2} > F_{im,LC7}$ (or $F_{im,lc5} > F_{im,LC4}$)
- if $s < 0$: $F_{im,lc2} < F_{im,LC7}$ (or $F_{im,lc5} < F_{im,LC4}$)

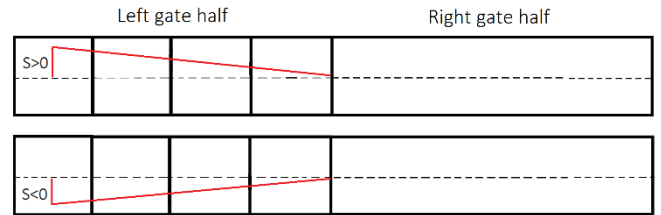


Figure 44: Positive and negative skewness, front view of gate

In Figure 44 the definitions of a positive skewness value and of a negative skewness value are visualised.

From Figure 45 it can be seen that the skewness parameter is slightly higher for the smaller waves. It can also be seen that for the wave data, positive- and negative skewness values occur. The skewness values that are found for the top row of the gate (LC 2,3,7) are higher than the values that are found for the 2nd row from the top (LC 4,5,6). So for the wave data the skewness is larger near the top side of the gate.

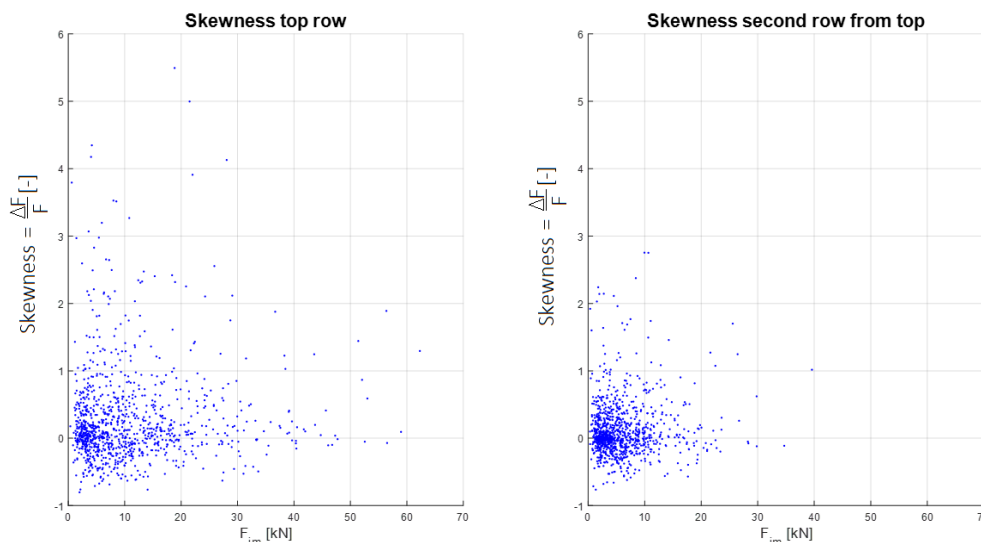


Figure 45: Relation between skewness and wave impact amplitude (scaled, $\lambda = 12.5$)

5.4 Statistical distribution of (wave) parameters

For the composition of the 'model' force signal in chapter 6, the statistical distributions of a couple of (wave) input parameters have to be known: wave height, wave period, wave impact duration and skewness. The statistical distributions are determined based on the pressure sensor- and load cell data, and on some knowledge that is known from literature.

5.4.1 Statistical distribution wave period

For the determination of the statistical distribution of the wave period the load cell data is used. The force-time signal of the load cell data is divided into individual waves (see appendix H.3 for a detailed description of the method that is used for this). The data from load cell 2 is used for the definition of the individual waves in the signal. For each wave the wave duration/wave period can be determined.

In the upper panel of Figure 46 the probability of exceedance is plotted for the wave periods from the scaled data of load cell 2. In the lower panel of Figure 46 the probability density function for the wave periods is shown. For the generation of the waves during the scale model testes a peak period of $T_p = 1.3$ s is used. When the period is scaled with $\lambda = 12.5$ this gives $T_p = 4.6$ s.

For this research it is assumed that the distribution of the wave period can be described with a Weibull distribution (see appendix F). For this data set (scaled load cell 2 data), the best Weibull fit is found for $a = 4.75$ and $b = 5.9$. The best Weibull fit is plotted in red in the upper- and lower panel of Figure 46. The best Weibull fit that is found for this data set is used as input for the composition of the 'model' force signal in paragraph 6.2. For the composition of the 'model' force signal in paragraph 6.2, for each generated wave in the wave field a wave period will be drawn randomly from this distribution.

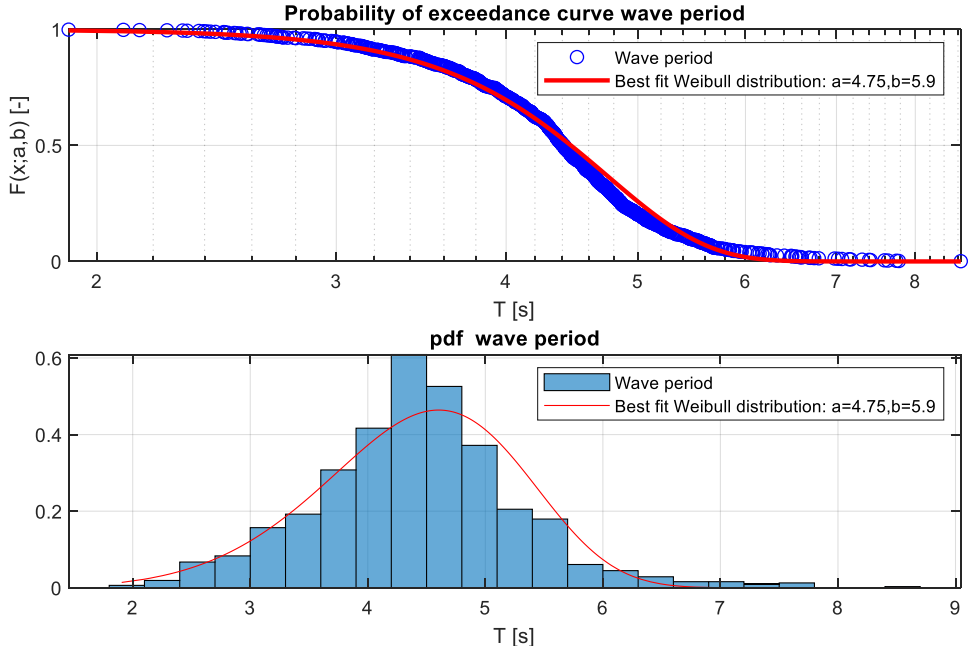


Figure 46: Weibull distribution fit for the wave period, the best fit Weibull distribution is for $a = 4.75$ and $b = 5.9$, pdf wave period (T), load cell 2 (scaled, $\lambda = 12.5$)

5.4.2 Statistical distribution wave height

One of the input parameters to make the 'model' force/pressure signal in paragraph 6.2, is the wave height. For the scale model testes a significant wave height of $H_s = 0.06$ m is used, after scaling with $\lambda = 12.5$, this gives $H_s = 0.75$ m. However, the distribution of the wave heights is not known from the data, so a more theoretical approach is used to determine the wave height distribution.

From the literature it is known that the wave height is Rayleigh distributed (Holthuijsen, 2007, see appendix F). In Figure 47a the exceedance probability graph of the generated wave heights (based on this significant wave height) is shown. In Figure 47b the corresponding pdf is shown.

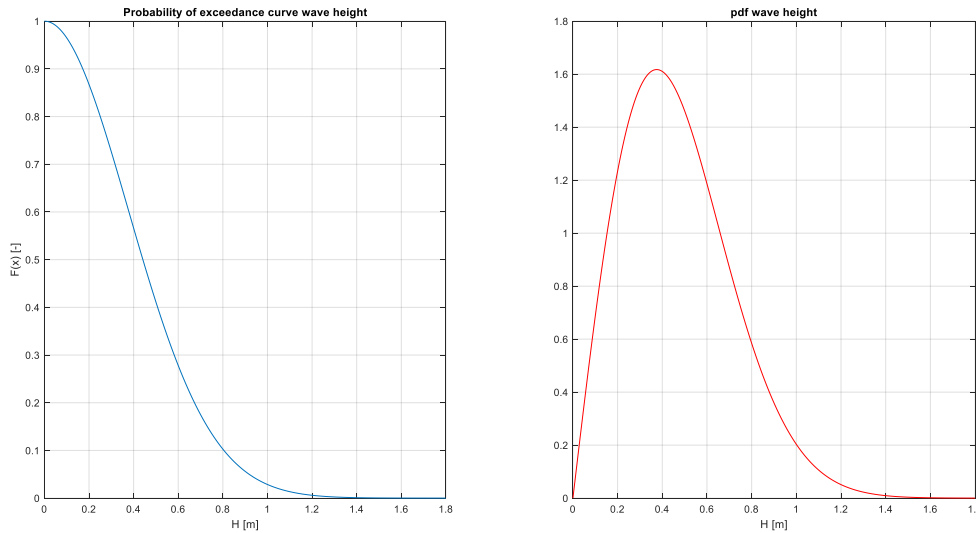


Figure 47: a) probability of exceedance curve wave height for $H_s = 0.75$ m, b) pdf for $H_s = 0.75$ m

For the composition of the ‘model’ force signal in paragraph 6.2, for each generated wave in the wave field a wave height will be drawn from this distribution. However, it is important to take the joint probability of the wave height and -period into account. In Figure 48 the relation between the wave height and wave period, that is present for the data that is used, is plotted in red ($T_p = 5.9 \cdot H^{1/3}$, this relation is fitted in Matlab for the data set used for this research). In general, the higher the wave period, the higher the wave height. The joint probability is included in a simplified way. This research focusses in the ultimate limit state (ULS), so the higher wave heights and periods are the most important. From the research of Longuet-Higgins (1983) it is known that for the higher wave heights and -periods, the scatter is quite small. For this research a scatter of $\sigma=10\%$ is used. So during the Monte Carlo simulation (the generation of the model wave field) a value for the wave period is drawn from the distribution indicated in Figure 46, and the wave height corresponding to this wave period is calculated with a maximum deviation of $\pm 10\%$, with the relation plotted in red in Figure 48. The relation between the wave height and -period for the model signal (1000 waves) is plotted in blue in Figure 48.

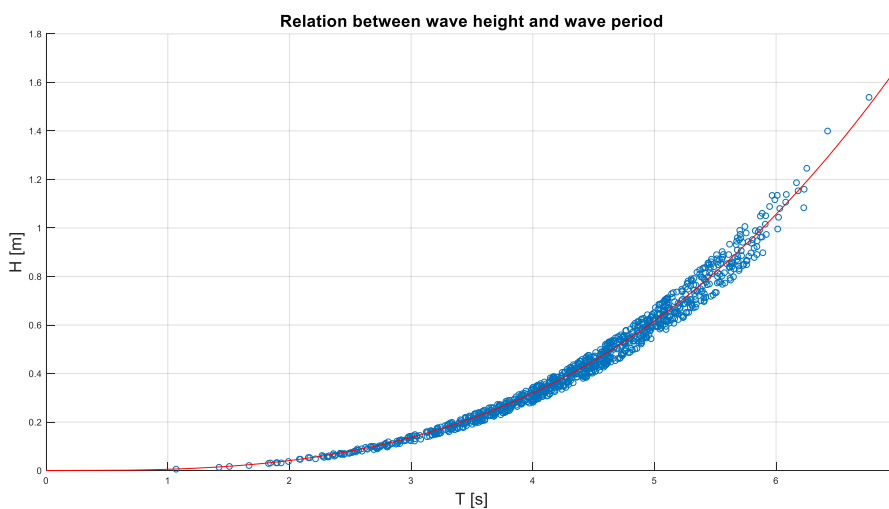


Figure 48: Relation between wave height and wave period

5.4.3 Statistical distribution wave impact duration

In Figure 49a the scaled histogram of the impact duration is given for load cell 2 (scaled, $\lambda = 12.5$). The wave impact durations measured with the other load cells are in the same order as shown in Figure 49a.

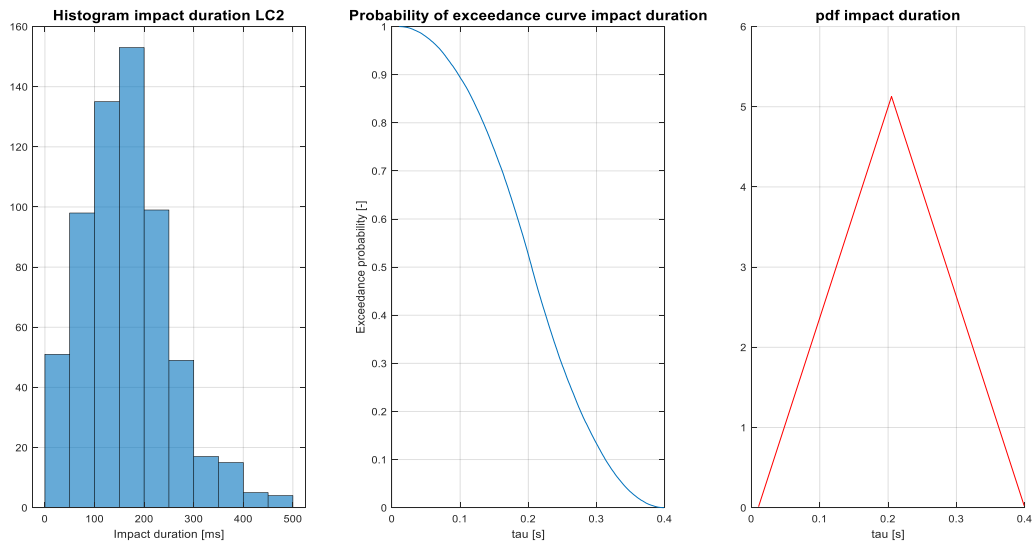


Figure 49: a) Histogram wave impact duration, load cell 2 (scaled, $\lambda = 12.5$), b) Probability of exceedance curve wave impact duration for $\tau_{min} = 0$ s, $\tau_{middle} = 0.2$ s and $\tau_{max} = 0.4$ s, c) pdf wave impact duration

It has been chosen to describe the impact durations with a symmetrical triangular distribution (see appendix F). From the scaled histogram in Figure 49a it can be seen that for most of the waves the impact duration lies approximately between 10 and 400 ms for the load cell data. These values are used as lower and upper limit for the statistical distribution of the wave impact duration (that is used for the composition of the 'model' force-time signal in chapter 6). So $a = 0.01$ s, $b = 0.2$ s and $c = 0.4$ s. In Figure 49b and c the statistical, symmetrical triangular, distribution that is used for the wave impact duration for this research is shown.

5.4.4 Statistical distribution skewness parameter

In paragraph 5.3 the definition of the skewness factor is already discussed. The statistical distribution of the skewness parameter that is used for the composition of the 'model' signal in paragraph 6.2 is determined based on the skewness of the force peaks of the top load cell row (Interpolation point 1 and LC2,3,7). From Figure 45 it can be seen that the skewness for the second row from the top (Interpolation point 2 and LC4,5,6) is lower than for the top row. So for this data set the skewness is not constant over the height. However, for the composition of the 'model' signal in paragraph 6.2 it is assumed that the skewness is constant over the height and varies only over the width of the gate. More research has to be done, and more data has to be analysed to be able to describe the skewness in a more general form in the future (see chapter 8, recommendations).

From the histogram/pdf that is made for the skewness parameter it can be seen that this parameter cannot be described with a Weibull distribution. The skewness parameter is determined for the maximum wave impacts, so another extreme value distribution has to be chosen to describe the skewness parameter. The best fit Gumbel distribution (see appendix F) is determined for the data.

In the upper panel of Figure 50 the probability of exceedance is plotted for the skewness parameters determined for the top load cell row. In the lower panel of Figure 50 the probability density function for the skewness parameters is shown. For this data set, the best Gumbel fit is found for $\alpha = 3.0$ and $u = 0.01$. The best Gumbel fit is plotted in red in the upper- and lower panel of Figure 50. The best Gumbel fit that is found for this data set is used as input for the composition of the 'model' force signal in paragraph 6.2. From the figure it can be seen that the fit is not perfect, however for now the found Gumbel fit is considered acceptable. More research has to be done to be able to better describe the statistics of the skewness parameter, and give a more general description of the skewness parameter (not only for this data set). For the composition of the 'model' force signal in paragraph 6.2, for each generated wave in the wave field a value for the skewness parameter will be drawn randomly from this distribution.

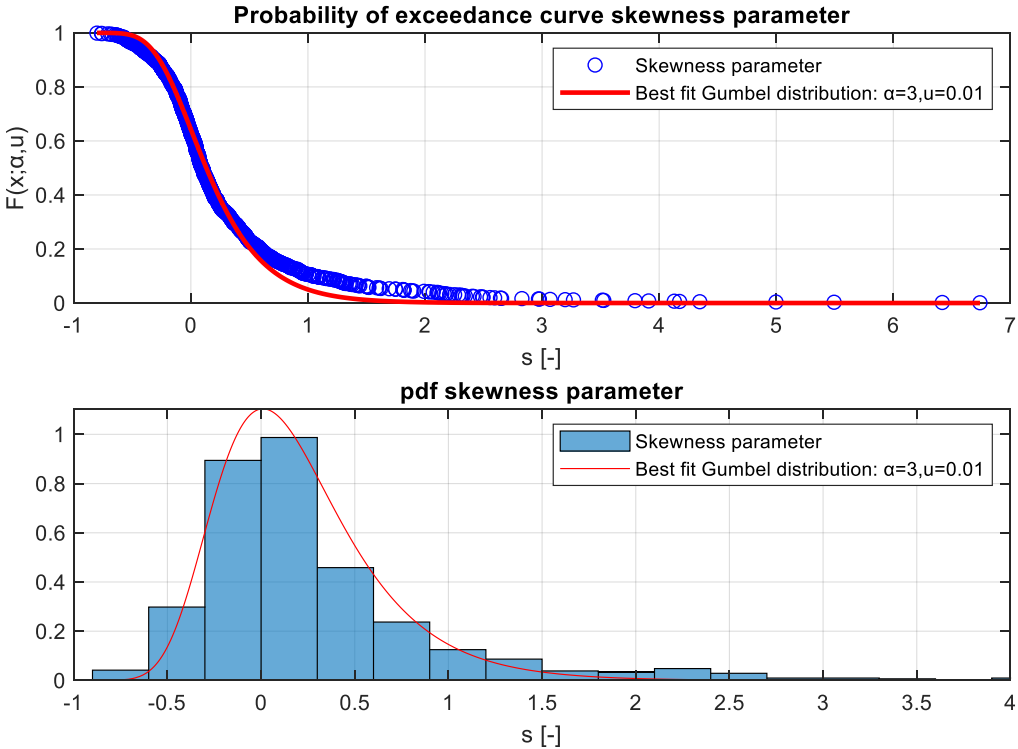


Figure 50: Gumbel distribution fit for the skewness parameter, the best fit Gumbel distribution is for $\alpha = 3.0$ and $u = 0.01$, pdf skewness parameter (s), based on skewness of top load cell row (LC 2,3,7)

6 Composition and validation of 'model' 3D force-time signal for multiple wave impacts

In chapter 5 a statistical description of the wave impacts data from the scale experiments is given in time and space. This statistical descriptions are used to compose a 'model' 3D force-time signal in this chapter. The goal of setting up the 'model' force-time signal, is to be able to generate a load in space and time, without using model test data as input. So that in the future, when the suggested method is further developed and validated, no scale measurement data is needed to compose a spatially varying force-time signal for multiple wave impacts. This 'model' force-time signal makes it possible to improve the current design method (DAF method) in time as described in chapter 4, to compare the deflection results determined with a simple SDOF model and with the more complicated semi-analytical model developed by Tieleman (2019) in chapter 7 (to be able to derive limits for the possibility of the use of a simple SDOF model), and to investigate the influence of a spatially varying wave impact force over the gate width on the response of the gate (and subsequently improve the DAF method in space) in chapter 7.

In paragraph 6.1, the suggested method to compose a 'model' 3D for force-time signal for multiple wave impacts, based on wave parameters only (wave height, wave period, skewness and wave impact duration), is described. Subsequently, in paragraph 6.2 the composition of the 'real' 3D force-time signal for multiple wave impacts is described. The 'real' force-time signal is composed from the scale measurement data of a selected test (see appendix D), and will serve as a reference signal to be able to validate the 'model' force-time signal in paragraph 6.3. Finally, in paragraph 6.4 a short sensitivity analysis is performed.

6.1 Composition 'model' 3D force-time signal

The purpose of this research is to be able to set up a wave signal based on a couple of (wave) input parameters only: wave height, wave period, wave impact duration and skewness. So that in the future, when the method is further developed and validated, no wave impact data (from for instance scale experiments) is needed to set up the force-time signal. In this chapter this force/pressure-time signal is called the 'model' signal. For the composition of the 'model' signal a probabilistic routine, consisting of the following steps, can be used:

- Step 1: Definition input parameters
- Step 2: A Monte-Carlo simulation will be used to generate a thousand waves (force-time signals). For each simulation one value will be drawn from each statistical distribution. Steps 3-5 will be performed with each parameter 'set' to create a wave field, consisting of for instance a thousand waves.
- Step 3: The next step is to determine the vertical pressure-impulse distribution for each wave, with the pressure-impulse theory (Cooker and Peregrine (1990, 1995)).
- Step 4: Than, the skewness parameter will be used to obtain the horizontal pressure-impulse distribution from the single vertical pressure-impulse distribution obtained with step 3, for each wave. The result for each wave: a spatially varying (3D) pressure-impulse field (that can be composed without model tests data).
- Step 5: Finally, the triangle schematisation (Chen et al (2018)) in time (impact duration) will be added, to obtain the pressure-time signal for each wave (that can be used as input for the semi-analytical model in chapter 7).

6.1.1 Definition input parameters

The 'model' signal can be composed based on a couple of input wave- and gate parameters only. The following parameters have to be defined:

Wave parameters:

- H_s [m] = Significant wave height, probabilistic (Rayleigh)
- T_p [s] = Peak wave period, probabilistic (Weibull)
- c_r [-] = Reflection coefficient, deterministic
- h [m] = Water depth, deterministic
- ρ_f [kg/m³] = Fluid density, deterministic
- s [-] = Skewness, probabilistic (Gumbel)
- τ [s] = Wave impact duration, probabilistic (Uniform)

Gate parameters:

- W [m] = Overhang width, deterministic
- L_x, L_z [m] = Gate width and -height, deterministic
- dx, dz [m] = Width- and height of gate intervals, deterministic

In the future the 'model' signal can be determined for different cases with different wave- and gate parameters (as input for design). For each parameter it is indicated whether one deterministic value, or a statistical distribution is used for the composition of the 'model' signal. When this method (to compose a 'model' signal) is used for design in the future, it can be chosen if a parameter is used as a statistical distribution or as one deterministic value. The statistical distributions that are used for this research are based on the model test data that is available, and on some knowledge from the literature. The statistical distributions are already discussed in more depth in paragraph 5.4. The unscaled- and scaled values of the input parameters that are used for the composition of the 'model' force-time signal are given in Table 7. The 'model' signal will be composed based on the parameter values that are used for the scale model tests (see Table 1). The 'real' force-time signal that is determined in the previous paragraph is also based on this scale model test results. In Figure 51 the probability density functions for the probabilistic parameters are shown.

Table 7: Parameters values used for the composition of the 'model' force-time signal

Gate parameters	Symbol	Scale model test value	Scaled value	Unit
Gate width	L_x	0.8	10	m
Gate height	L_z	0.6	7.5	m
Overhang width	W	0.1	1.25	m
Width interval	dx	0.1	1.25	m
Height interval	dz	0.1	1.25	m
Wave parameters	Symbol	Scale model test value	Scaled value	Unit
Significant wave height*	H_s	0.06	0.75	m
Peak wave period*	T_p	1.3	4.6	s
Reflection coefficient	c_r	1	1	-
Water depth	h	0.6	7.5	m
Fluid density	ρ_f	1025	1025	kg/m ³
Skewness*	s	0 – 2	0 – 2	-
Wave impact duration*	τ	0 - 0.1	0 - 0.4	s

* Probabilistic parameter

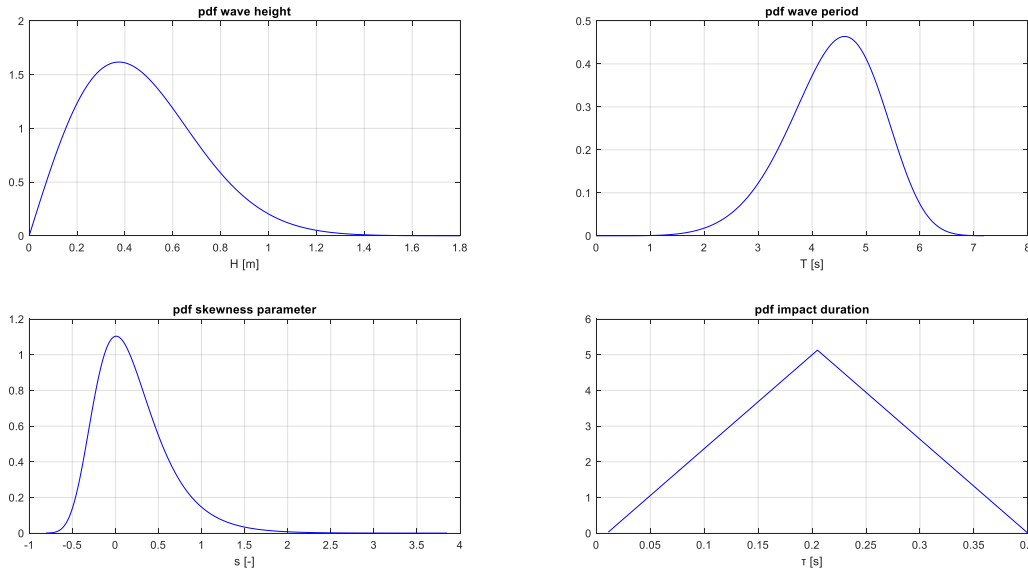


Figure 51: Probability density functions of the probabilistic input parameters: H, T, s and τ

6.1.2 Pressure-impulse theory

The impact impulse (I) of a pressure peak can be found by using the pressure-impulse (P) theory (Cooker and Peregrine, (1990, 1995)). As already discussed in chapter 2 the impact impulse is defined by equation 6.1, the pressure impulse is defined by equation 6.2.

$$I = \int_{\tau} \int_A p(t) dt dA \quad (eq 6.1)$$

$$P = \int_{\tau} p dt \quad (eq 6.2)$$

The pressure-impulse theory can be used to get the spatial (vertical) pressure impulse (P) distribution along a vertical gate. Chen et al (2018) showed that the pressure-impulse model can also be used to get the spatial (vertical) pressure impulse distribution along a vertical gate with an overhang.

The third step of the probabilistic routine is to determine the vertical pressure impulse distribution for for instance a thousand waves (a wave field). For each wave the vertical pressure impulse distribution is determined with the pressure-impulse theory. Ermano de Almeida provided the dimensionless results (from a Matlab script) of the pressure-impulse theory for a 1-6 configuration for the vertical wall with overhang, this configuration is shown in Figure 52b. In Figure 52c the scaled dimensions of the vertical wall that is used for the scale model tests, that are used for the composition of the 'real' force signal, is shown (this gate has a 1-6 configuration). This research will be limited to structures with the 1-6 configuration. When this composition method is used as a design tool, the pressure-impulse theory can be fully implemented in the method so that other gate configurations can also be used. The result from the pressure-impulse theory Matlab script is a vertical dimensionless pressure impulse (\bar{P}) distribution over the height of the gate.

The dimensionless pressure impulse can be converted to the pressure impulse with the following formula:

$$P = \bar{P} * \rho_f * U * W \quad (\text{eq 6.3})$$

With: P = pressure impulse [Ns/m²]
 \bar{P} = dimensionless pressure impulse [-]
 ρ_f = fluid density [kg/m³]
U = impact velocity [m/s]
W = overhang length [m]

The impact velocity can be estimated with an equation derived from Linear Wave Theory:

$$U = \omega \sqrt{A_w^2 - R_c} \quad (\text{eq 6.4})$$

With: ω = radial frequency = $2\pi/T$ [rad/s]
 A_w = amplitude of the incident wave [m]
 R_c = freeboard [m], see Figure 52a

For regular waves equation 6.5 can be used to determine the amplitude of the incident wave ($H_i = H_{s,i}$). For irregular waves the maximum wave ($H_{max,i}$) is used and equation 6.6 can be used to determine the amplitude of the incident wave. A common estimate for the maximum wave height is: $H_{max,i} = 2 * H_{s,i}$.

$$A_w = (1 + c_r) * \frac{H_i}{2} \quad (\text{eq 6.5})$$

$$A_w = (1 + c_r) * \frac{H_{max,i}}{2} = (1 + c_r) * H_{s,i} \quad (\text{eq 6.6})$$

With: c_r = reflection coefficient [-]
 H_i = incident wave height [m]
 H_s = significant wave height [m]
 H_{max} = maximum wave height [m]

For 100% reflection ($c_r = 1$) this gives: $A_w = H_i = H_{s,i}$ for regular waves, and $A_w = 2 * H_{s,i}$ for irregular waves.

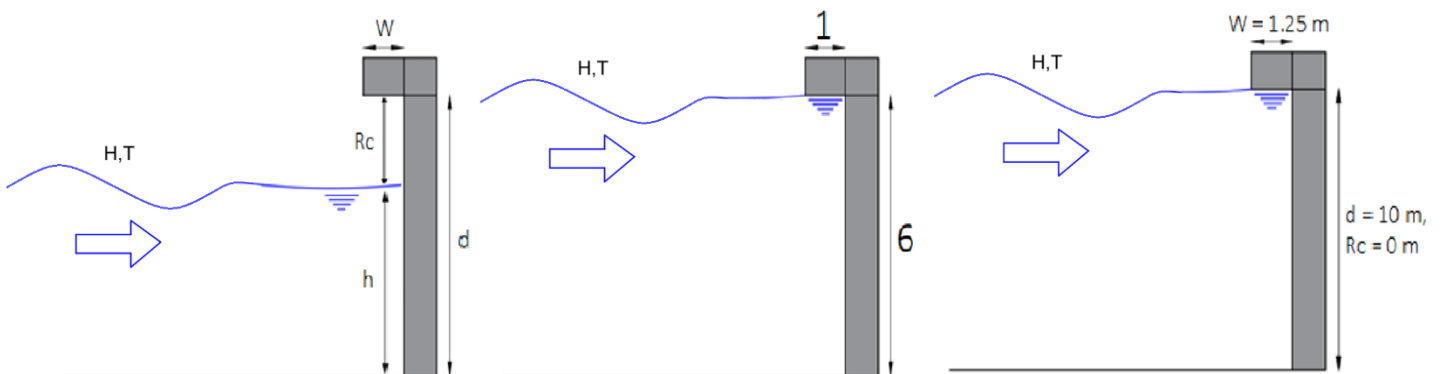


Figure 52: a) Definition parameters, b) Configuration 1-6, c) scaled ($\lambda = 12.5$) test set up in 1-6 configuration

With equations 6.3-6.6 the vertical pressure impulse distribution (P) over the gate height can be determined based on the input parameters described in paragraph 6.1.1 and the gate configuration only. In Figure 53 the vertical pressure impulse distribution determined with the pressure-impulse theory is shown for the scaled parameter values given in Table 7. The results are shown for regular waves and irregular waves. In the figures the pressure-impulse points in the middle of the defined grid ($dz = 1.25$ m) are indicated. From the figure it can be seen that over the full height of the gate, indeed the calculated pressure-impulse for irregular waves is higher than the calculated pressure-impulse for regular waves.

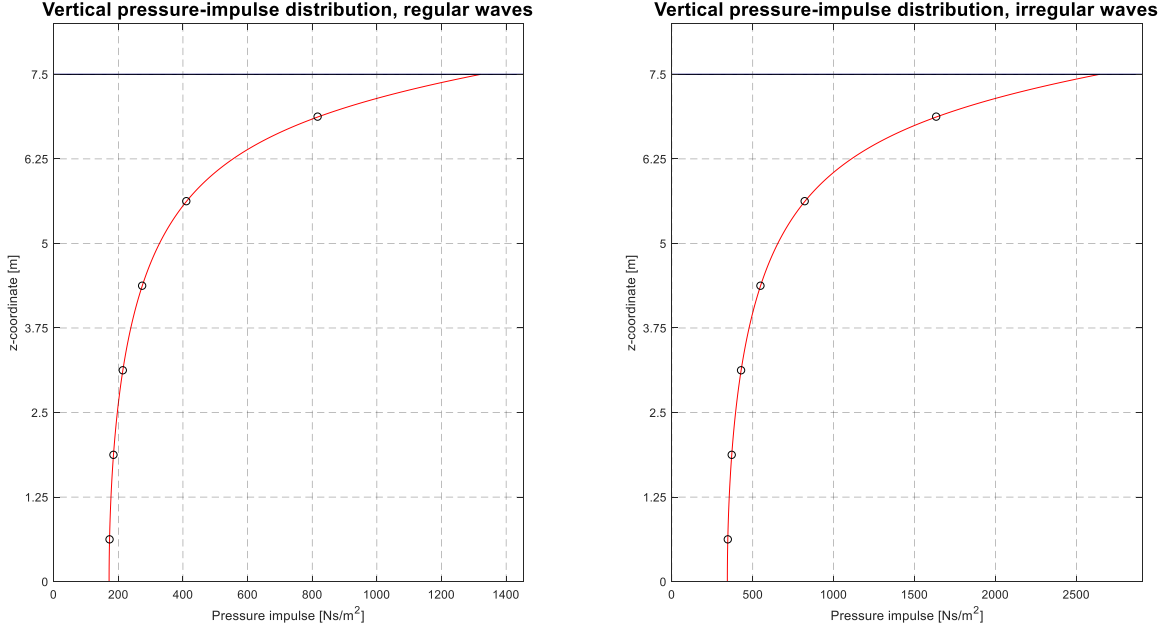


Figure 53: Vertical pressure impulse distribution for the scaled model test gate ($\lambda = 12.5$), for regular and irregular waves

In Figure 54 a typical height distribution of one of the wave impacts (wave 1) from the pressure sensor data (filtered with 150 Hz) is shown for a couple of moments in time (around the wave impact peak). To compare the results from the pressure-impulse theory with the real measurements, the vertical pressure distribution for wave 1 is calculated from the pressure-impulse distribution for irregular waves, and plotted in red in the third panel of Figure 54. From the third panel of Figure 54 it can be seen that the pressure-impulse theory indeed gives a good estimate of the pressure distribution over the gate height for this gate configuration. However, at the top of the gate the pressure-impulse theory overestimates the pressure.

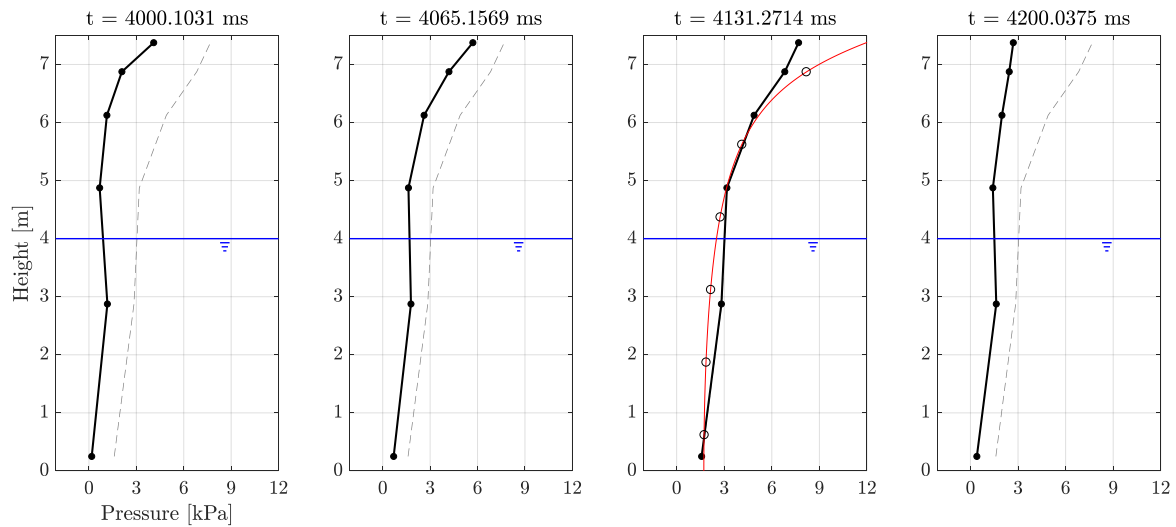


Figure 54: Height distribution of the wave pressure over the vertical of the gate at four moments during wave impact (from the scaled ($\lambda = 12.5$) pressure sensor data described in paragraph 4.3.1, wave 1). The dashed line indicates the envelope of the extreme pressure, the results from the pressure-impulse theory for irregular waves is plotted in red in the third panel

6.1.3 Definition skewness parameter

In step 3 the vertical pressure-impulse distribution is determined for each wave. The next step is to define the horizontal pressure-impulse distribution over the gate width. This is done using the skewness parameter. For each wave a value from the statistical distribution of this parameter is drawn. For the composition of the 'real' force-time signal in the previous paragraph it is chosen to mirror the known data for the left gate half, to obtain the data for the right gate half. So for the composition of the 'model' signal the definition of the skewness is chosen in such a way that a mirrored force distribution will be obtained.

It is assumed that the vertical pressure-impulse distribution that is obtained with step 3 is present in the middle of the gate (at $x = 5.0$ m). One value for the skewness will be drawn from the statistical distribution (s), from this value the skewness over the width ($s(x)$) will be determined and multiplied with the vertical pressure-impulse distribution that is known at the middle of the gate. After the multiplication of the vertical pressure-impulse distribution and the skewness parameter over the width, a three-dimensional pressure-impulse field over the full gate surface is obtained. In Figure 55 the definition of the skewness parameter is shown. For $s > 0$, the impact force in the middle of the gate is smaller than the impact force at the edges of the gate. For $s < 0$, the impact force in the middle of the gate is larger than the impact force at the edges of the gate.

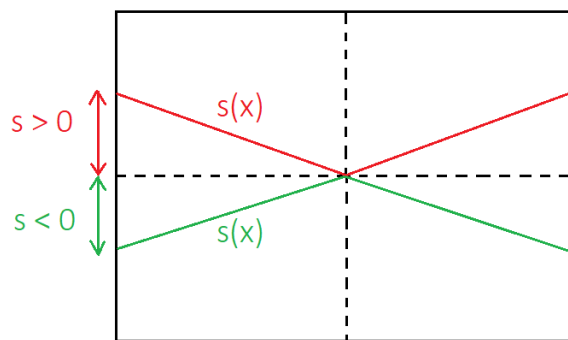


Figure 55: Definition skewness parameter 'model' signal

6.1.4 Triangular schematisation in time

After performing step 4, for each wave the pressure-impulse (P) is known for each point in the defined grid ($dx = 1.25$ m, $dz = 1.25$ m, see Figure 58b). The final step is to convert this single pressure-impulse value to a pressure-time signal. Based on the work of Chen et al (2018) a symmetrical triangular shape in time is assumed for this schematisation. For a symmetrical triangular schematisation the maximum pressure (p_{max}) can be calculated with the following equation:

$$p_{max} = \frac{2 * P}{\tau} \quad (eq 6.7)$$

A triangular pressure-time signal is generated based on this peak value (p_{max}) and the 'drawn' value for the impact duration. The triangular schematisation is shown in Figure 56. In this figure it is also shown that the pressure-impulse (P) is equal to the area under the pressure curve.

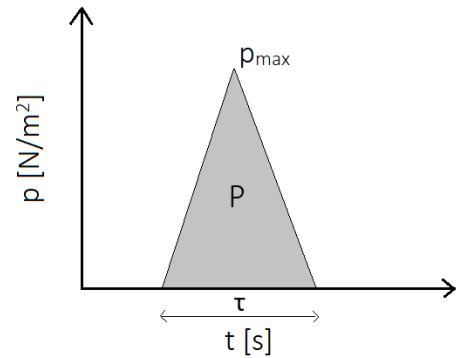


Figure 56: Triangular schematisation in time

In Figure 57 the final result of the composition of the pressure-time signal of a single wave of the 'model' signal is shown. The results are for the wave with the scaled parameter values given in Table 7, $s = -0.5$, and $\tau = 0.175$ s. The pressure field in Figure 57 can be converted into a force field by multiplying the pressure value that is known in the middle of each grid cell by the grid cell dimensions ($dx = 1.25$ m, $dz = 1.25$ m).

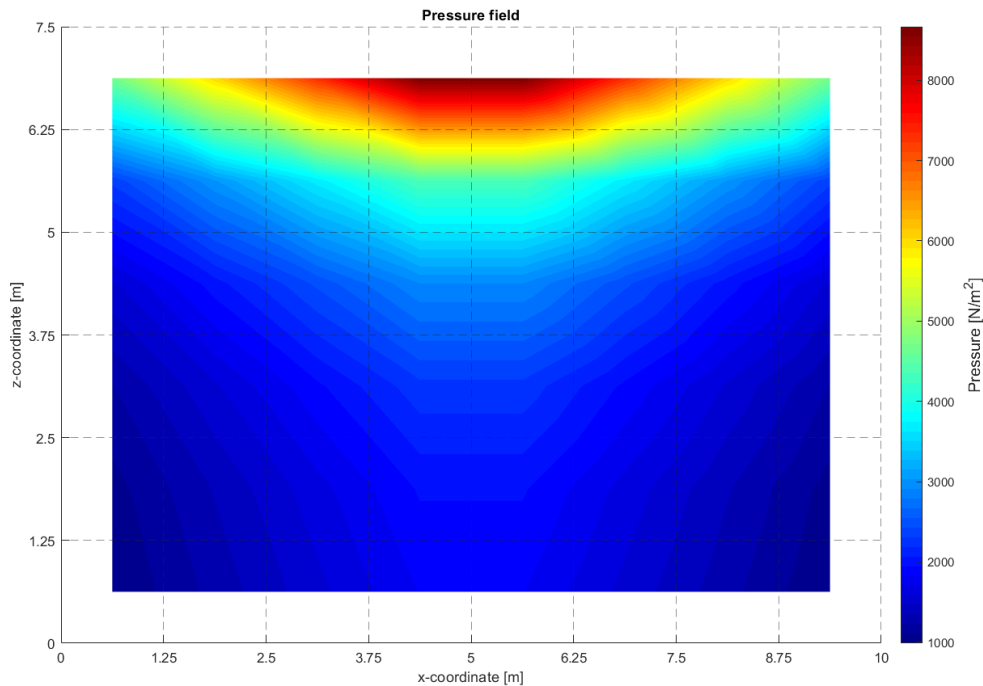


Figure 57: Mirrored 'model' 3D pressure field over the full gate surface during the maximum impact (p_{max})

6.2 Composition 'real' 3D force-time signal

The 'real' 3D force signal is obtained by inter- and extrapolation of the data that is obtained during the scale experiments (see paragraph 5.2). The composition of the 'real' force signal, that can be run with the semi-analytical model, consists of three steps:

- Step 1: Extrapolation of the load cell data to obtain a force signal over the left half of the gate.
- Step 2: Filling in the data points at the right half of the gate.
- Step 3: Definition of individual waves in time

In Figure 58a the final result of steps 1 and 2, a three-dimensional pressure distribution during maximum wave impact, is shown for the scaled gate (defined in step 3) and wave 1 (it has to be noted that this wave has different properties than the wave for which the pressure field is plotted in Figure 57, so this to pressure fields cannot be compared one to one for the comparison of the results from the 'model' signal and 'real' signal). The scaled gate ($L_x = 10$ m, $L_z = 7.5$ m) that is used for this research is shown in Figure 58b. In this figure the grid that is used is also indicated ($dx = 1.25$ m, $dz = 1.25$ m). First the known load cell data (described in paragraph 5.2) is used to obtain the force-time signals at the grid points specified for the left half of the gate. Then, it is assumed that the right half of the gate can be filled in by mirroring the data obtained for the left gate half (see appendix H.2). This assumption is made, due to the lack of data at the right gate half (see chapter 8, recommendations). It has to be kept in mind that the data is only known/extrapolated in the middle of each grid cell specified in Figure 58b. From the figure it can be seen that for wave 1 the wave impact force is higher in the middle of the gate than at the edge of the gate. However, it can also be seen that for the 2nd row from the top, the skewness cannot be described with a linearly increasing line from the middle to the edge of the gate. So it can be concluded that it is hard to specify the skewness based on this data set, and it is important to keep in mind that for the composition of the 'model' force in the next paragraph a lot of assumptions have to be made to include the skewness of the wave impact force.

For a detailed description of the composition of the 'real' force-time signal, the assumptions that are made for this, and the problems encountered during the composition process, reference is made to appendix H.

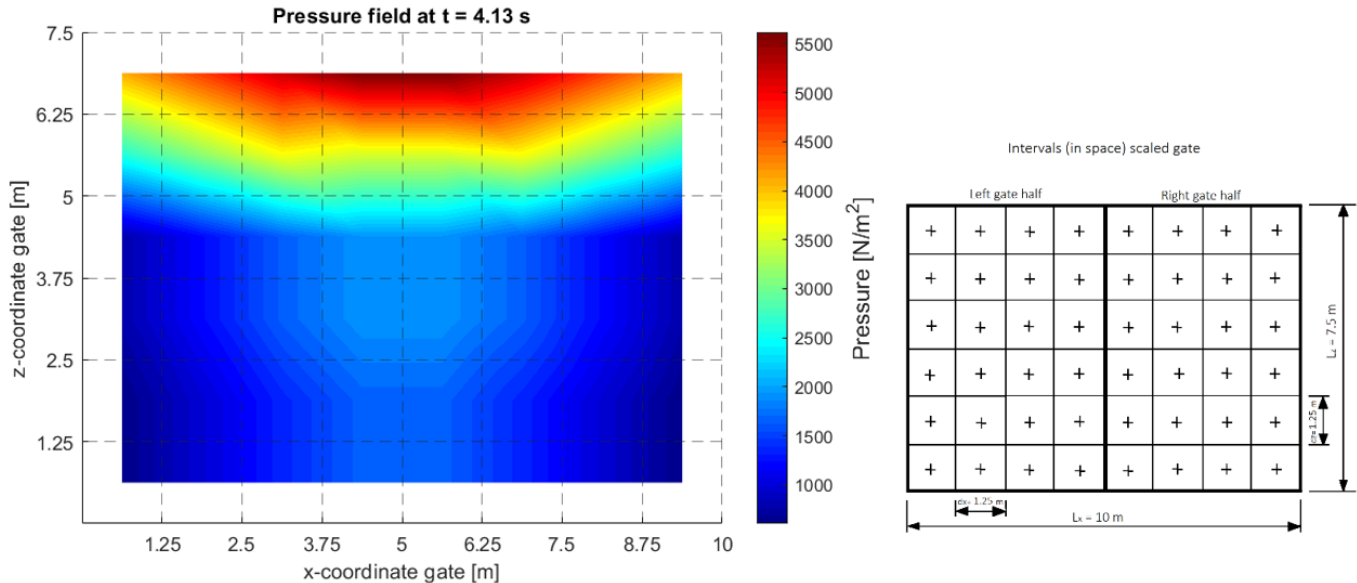


Figure 58: a) Mirrored 3D pressure field over the full gate surface during the maximum impact force (wave 1), b) Definition intervals (in space) over the gate (scaled, $\lambda = 12.5$)

The definition of the individual waves in time (step 3) is shown in Figure 59. For the analysis with the semi-analytical model the force-time signal has to be split shorter signals for individual waves, so that the model can be run separately for each individual wave. In appendix H the splitting method is described in more detail.

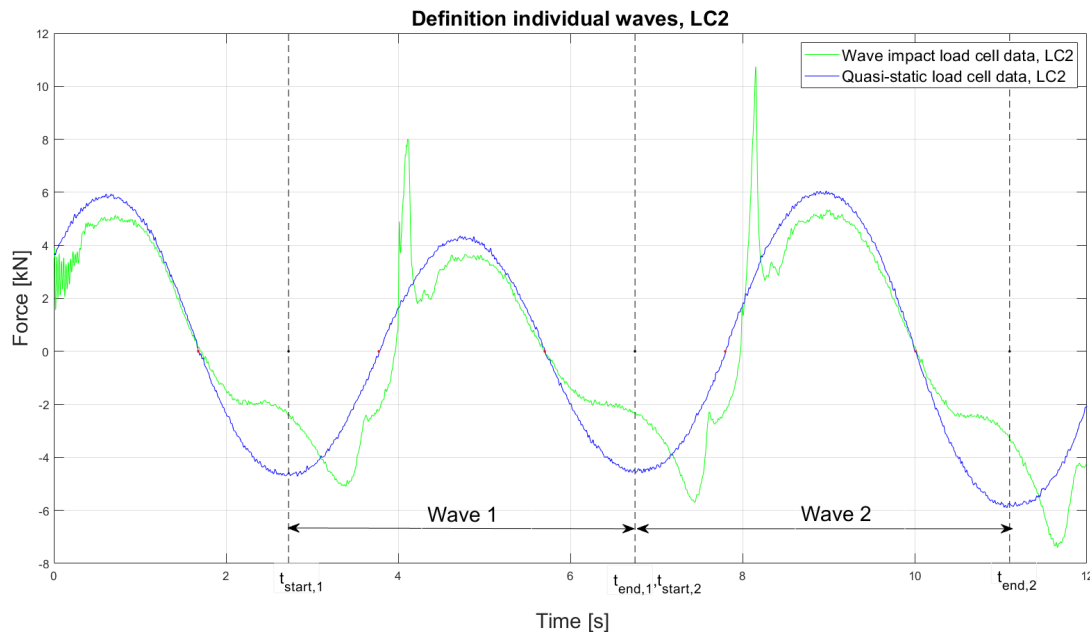


Figure 59: Definition individual waves, based on load cell 2 data (scaled, $\lambda = 12.5$)

6.3 Validation of 'model' 3D force-time signal

In paragraph 6.1 and 6.2, the compositions of a 'model' and 'real' force-time signal are discussed. The 'real' force-time signal will serve as a reference signal, to be able to validate the 'model' force-time signal in this paragraph. First, in section 6.3.1 the maximum pressures/forces of the individual wave impacts for the 'real' and 'model' signals are compared. Then, in section 6.3.2 the responses (maximum deflections) for the 'model' and 'real' force-time signal are determined with the semi-analytical model developed by Tieleman (2019), and compared. So, first the input pressure/force for the semi-analytical model is validated, and then the validation is completed by comparing the responses for the 'real' and 'model' signals.

6.3.1 Comparison 'real' and 'model' force signal

In Figure 60 the force-time signals of a single wave from the 'real' and 'model' signal are shown. In the 'model' signal the force-time signal consist of a symmetrical triangular schematisation of the wave impact only. Due to the random generation of the wave impacts in the model signal, the first wave that is generated (Figure 60b) in the 'model' signal has other properties (p_{max} , τ , etc) than the first wave in the 'real' signal. Figure 60 only indicates the difference of the course in time of the 'model' and 'real' signal. The properties of this two waves (first waves from both signals) cannot be compared one to one.

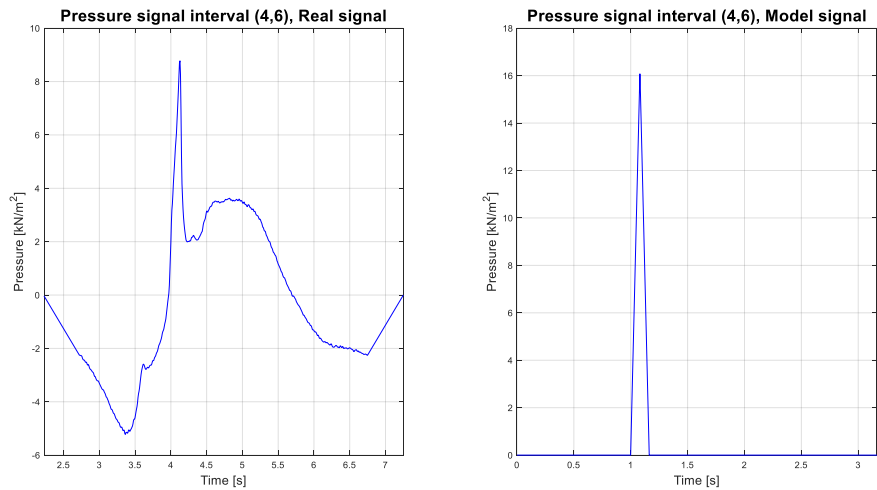


Figure 60: Force-time signals of a single wave from the 'real-' and 'model' signals, wave 1

The left panel of Figure 61 shows the histograms of the peak pressures for the individual waves of the 'model' (orange) and 'real' (blue) signals. In the right panel of Figure 61 the probability of exceedance curve of the maximum pressures for the 'model' (red) and 'real' (blue) signals are plotted.

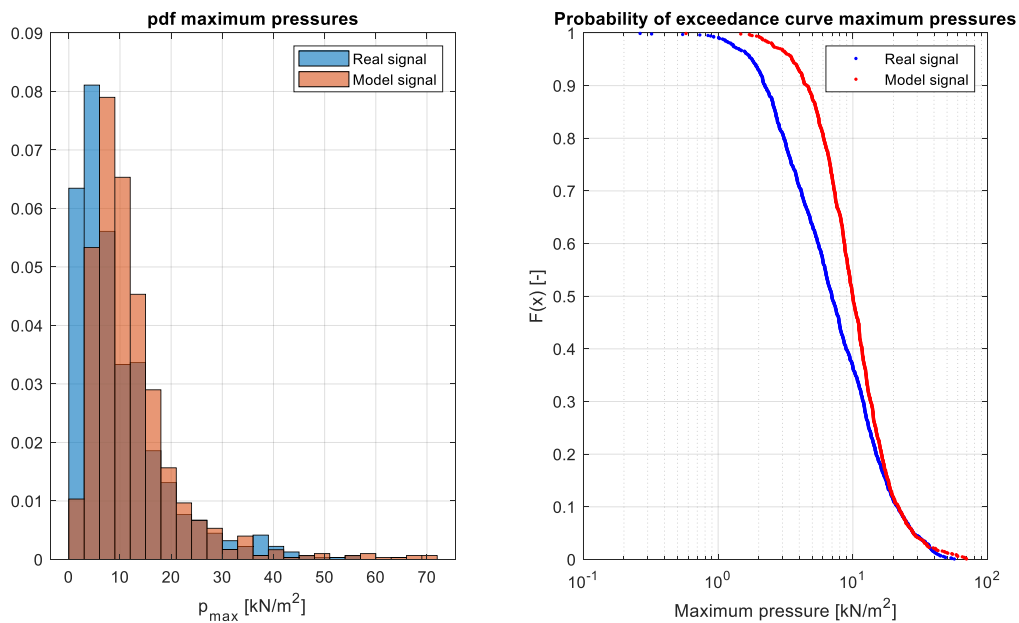


Figure 61: a) Histograms for the maximum pressures for the 'real' and 'model' signal, b) Probability of exceedance curves for the maximum pressures of the 'real' and 'model' signal

From Figure 61 it can be seen that overall the maximum pressures for the 'real' and 'model' signal are quite similar. However, in general the 'model' signal overestimates the peak pressure a bit. The most likely explanation for this overestimation is the overestimation of the pressure-impulse when the pressure-impulse theory is used. As can be seen from Figure 54, at the top of the gate the pressure-impulse theory gives a significant overestimation of the pressure-impulse, which probably results in the overestimation of the peak pressures of the 'model' signal. However, more research have to be performed to find out the exact cause of the overestimation of the peak pressures of the 'model' signal. The pressure-impulse theory that is used during this research is still in development, so when this method is further developed in the future, the composition method of the model signal can also be improved.

This research focuses on the ultimate limit state (ULS). When the higher peak pressures are compared ($> 11 \text{ kN/m}^2$), the best agreement is found between the results from the 'real' and 'model' signal. When a design pressure, for instance $p_{1\%}$, is determined from Figure 61b, for the same exceedance probability this pressure will be higher for the 'model' signal (plotted in red) than for the 'real' signal (plotted in blue). For the 'model' signal $p_{1\%,\text{model}} = 55 \text{ kN/m}^2$, and for the 'real' signal $p_{1\%,\text{real}} = 42 \text{ kN/m}^2$. This gives, $p_{1\%,\text{model}} / p_{1\%,\text{real}} = 1.31$. So, it can be concluded that, for ULS calculations, the model is a little bit on the safe side. When the 'model' signal will be used for for instance fatigue calculations, the amount of lower peak force impacts will be underestimated, and wrong conclusions about the importance of fatigue will be drawn.

6.3.2 Comparison response to 'real' and 'model' force signal

From the previous paragraph it can be concluded that when the peak pressures are compared, the 'model' signal that is generated with the probabilistic routine is in the same order of magnitude as the 'real' signal that is based on scale measurements. So, the input signals for the semi-analytical model are in the same order of magnitude. The next step is to further validate the 'model' signal and probabilistic routine, by which the 'model' signal is generated, based on the response of the gate to the 'model' signal. The response of the gate to 'real' signal is used as reference. Again the validation will focus on the ULS. The responses that are compared are in terms of maximum deflections of the gate.

The responses to the 'real' and 'model' force-time are determined with the semi-analytical model developed by Tieleman (2019). With the semi-analytical model the response and corresponding maximum deflection are determined for each wave impact of the two signals. In Figure 62 the first modal shape (1,1) for the gate is shown. For the gate with parameters as given in Table 12 (with $L_x = 10 \text{ m}$ and $L_z = 7.5 \text{ m}$), most of the energy will go to mode (1,1). So, for each wave impact in the 'model' and 'real' signal, the maximum deflection that is determined is at the location $(x,z) = (5,7.5) \text{ m}$. In Figure 63 the histograms for the maximum deflections per wave impact are plotted in the left panel for the 'real' (blue) and 'model' (orange) signal. In the right panel of Figure 63 the exceedance curves of the maximum deflections are plotted for the 'real' (blue) and 'model' (red) signal.

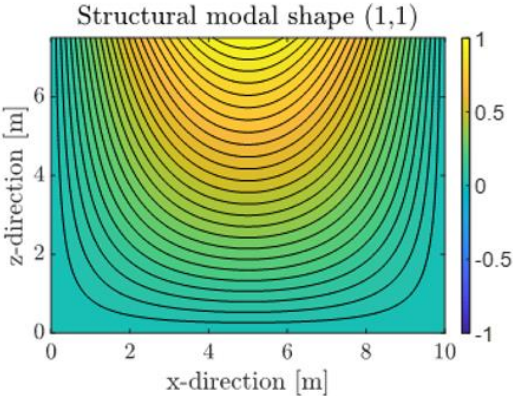


Figure 62: First modal shape of the case study gate, maximum deflection at $(x,z) = (5,7.5) \text{ m}$

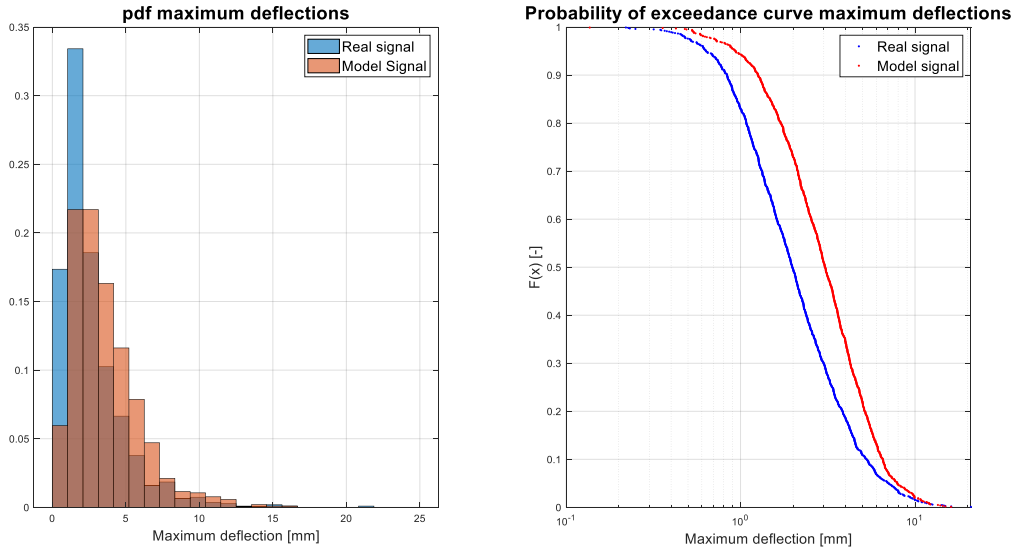


Figure 63: a) Histograms for the maximum deflections for the 'real' and 'model' signal, b) Probability of exceedance curves for the maximum deflections of the 'real' and 'model' signal

From Figure 63 it can be seen that the deflections for the 'real' and 'model' signal are quite similar, just like for the peak pressures. Again, in general the 'model' signal overestimates the maximum deflection a bit. For the 'model' signal $w_{1\%,\text{model}} = 11.8$ mm, and for the 'real' signal $w_{1\%,\text{real}} = 11.2$ mm. This gives, $w_{1\%,\text{model}}/w_{1\%,\text{real}} = 1.05$. So, the 1% design values of the maximum deflections (response) differ even less than the 1% maximum pressures ($p_{1\%,\text{model}}/p_{1\%,\text{real}} = 1.31$) of the 'model' and 'real' signal. When the ULS is considered, the model is on the safe side. When fatigue is considered, the 'model' signal caused too few small deflections (in the order of 0-2 mm) compared to the 'real' signal. As already discussed in the previous paragraph this can result in wrong conclusions about the importance of fatigue for the failure of the gate.

Based on the results from paragraphs 6.3.1 and 6.3.2, it can be concluded that for this case (input wave field and case study gate), the 'real' wave field can be schematised as a 'model' wave field. The input peak forces and corresponding responses (maximum deflections) to both signals are in the same order of magnitude. When the probabilistic method to compose a 'model' 3D force-time signal is further developed and validated, scale model tests are no longer required to determine the force-time series of multiple wave impacts in the future. So that in the future, the 3D force-time series for multiple wave impacts can be generated based on wave parameters only. For the composition of the 'model' force-time signal, the probabilistic distributions of the wave height, -period, skewness and wave impact duration are required as input only. This is an important step in the improvement of the current design method (DAF method) in time and space, and eventually the development of a new design method for hydraulic structures exposed to wave impacts.

As already discussed, there is still room for improvement for the probabilistic method to compose the 'model' signal. The amount of higher peak forces (> 10 kN/m², for this input wave field) for the generated 'model' is a bit too high. This results in a general overestimation of the maximum deflection that is obtained for each wave impact, with the semi-analytical model. However, more important, the amount of lower peak forces (< 10 kN/m², for this input wave field) is underestimated by the 'model' signal. This can result in wrong conclusions about the importance of fatigue for the failure of the gate. To obtain better resemblance between the peak pressures, and corresponding maximum deflections, for the 'model' and 'real' signal, a couple of modifications/improvements can be made to the probabilistic method. For instance, as already described in section 6.1.2, the Pressure-Impulse theory is still in development. Especially the pressure-impulse at the top region of the gate is still hard

to predict, and overestimated significantly when the Pressure-Impulse theory is used. Also, more attention can be paid to the joint probability of the wave height and wave period to improve the 'model' signal. Furthermore, more research have to be done to better describe the skewness parameter. In this research a lot of assumptions are made concerning the skewness parameter. More research have to be done, to investigate the course of the wave impact force over the full width of a gate, and to be able to give a more general description of the skewness parameter. In section 7.4 the influence of the skewness parameter on the correctness of the determined response is investigated. Finally, the simple triangular schematisation in time can be improved a bit by applying slightly other shapes. For instance a more smooth shape can be used. In section 6.4 the influence of the rising time of the triangular schematisation is investigated in a short sensitivity analysis.

6.4 Sensitivity analysis – Triangular schematisation in time (rising time)

In this section a short sensitivity analysis about the triangular schematisation of the wave impact force in time is performed. The influence of a non-symmetrical schematisation of the force signal in time on the response is investigated by adjusting the rising time of the input force-time signal.

In Figure 64a the 'symmetrical triangular schematisation' ($t_s = 0.5 \cdot \tau$) of the impact force in time for the 'model' signal is displayed. In Figure 64b the non-symmetrical triangular schematisation of the impact force in time for the 'model' signal that is investigated in this section is displayed ($t_s = 0.25 \cdot \tau$).

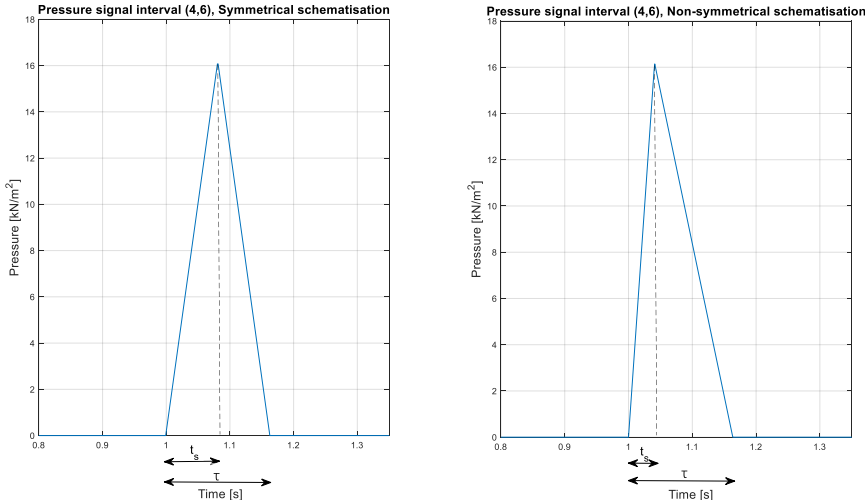


Figure 64: Force-time signals of symmetrical and non-symmetrical triangular schematisation of the 'model' signal, wave 1

The peak pressure histograms for both schematisations in time are the same, see Figure 61. Only the triangular schematisation in time (described in paragraph 6.1.4) is adjusted in this section. The different schematisations in time are compared based on the response histograms (maximum deflections of the gate). The location of the maximum deflection is the same for both schematisations, and is shown in Figure 62. In Figure 65 the results for the 'real signal' (plotted in blue in the left and right panel of Figure 65), original symmetrical 'model' signal (plotted in orange in the left panel and in red in the right panel of Figure 65) and for the adjusted non-symmetrical 'model' signal (plotted in yellow in the left panel and in black in the right panel of Figure 65) are shown. From the figure it can be seen that for this gate, a smaller rising time results in larger maximum deflections. So, when a smaller rising time is used (which results in a non-symmetrical triangular schematisation in time) for this gate, the difference between the results obtained for the 'real' signal and 'model' signal

become larger than for a 'model' signal with symmetrical schematisation in time. The gate that is used for the investigation has a thickness of 0.243 m and an eigen period of 0.153 s. The wave impact durations lies between 10 and 400 ms. For this gate almost all the wave impacts are in the dynamic loading domain (only wave impacts shorter than 38 ms are in the impulsive loading domain ($\tau/T < 0.25$)). For smaller gate thicknesses (higher eigen periods), for which all the waves are in the impulsive loading domain ($\tau/T < 0.25$), the rising time no longer effected the maximum deflections that are obtained. For this systems, the maximum deflections are the same for the different schematisations in time (rising times). So, based on the ratio of τ/T , the rising time can affect the maximum deflection that will be obtained with the semi-analytical model.

Concluding, for the investigated system ($t = 0.243$ m, $T = 0.153$ s) that is in the dynamic loading domain ($0.25 < \tau/T < 4$), the rising time affects the maximum deflection that is obtained. For a rising time of $t_s = 0.25 \cdot \tau$, the 1% design deflection is $w_{1\%,model\ sym} = 11.8$ mm, and for a rising time of $t_s = 0.5 \cdot \tau$, the 1% design deflection is $w_{1\%,model\ non-sym} = 12.3$ mm ($w_{1\%,model\ non-sym} / w_{1\%,model\ sym} = 1.04$). For the investigated system, this results in a larger error between the maximum deflections that are obtained than for the symmetrical schematisation in time ($w_{1\%,model\ sym} / w_{1\%,real} = 1.05$ and $w_{1\%,model\ non-sym} / w_{1\%,real} = 1.10$). So, it is chosen to use the symmetrical schematisation in time for the analysis performed in chapter 7.

When the method to compose a 'model' force time signal, that is described in this chapter, is further developed in the future, the rising time can be used as an additional stochastic input parameter. However, more research has to be performed to be able to draw more general conclusions about the influence of the rising time on the response. This small analysis only shows that the rising time can indeed affect the dynamic response of a structure.

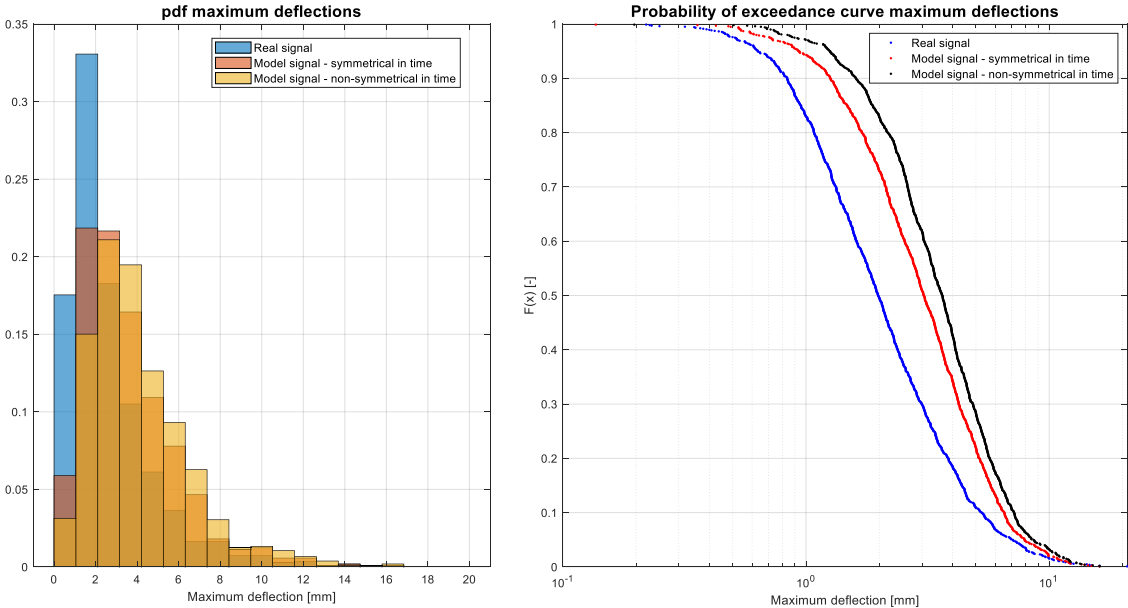


Figure 65: a) Histograms for the maximum deflections for model signals 1 and 2, b) Probability of exceedance curves model signals 1 and 2

7 SDOF vs MDOF model – space investigation DAF method

In chapter 4 it is concluded that the DAF method does ‘not suffices in time’. In this chapter the focus will be on the importance of taking into account higher modes of vibration for the determination of the response of the structure, and the influence of the spatial variation of the impact force on this. In this chapter the influence of higher modes of vibration on the response will be investigated by comparing the differences (based on maximum deflections) between the SDOF model (used for the DAF method) and MDOF model (semi-analytical model).

The model signal composed in chapter 6 (consisting of a thousand waves) will be used as input for both the SDOF and MDOF model. For the SDOF model all the energy is in mode (1,1), while the semi-analytical model takes an infinite (or specified finite) number of modes into account. To be able to make this comparison, an equivalent SDOF model is set up in section 7.1, and validated in section 7.2. Then in section 7.3, the results obtained with the SDOF and MDOF model are compared, and conclusions are drawn about the importance of taking into account higher modes (and by this using the more complicated semi-analytical model for design instead of the simple SDOF model) when the maximum response is determined. Next, in section 7.4 the influence of taking into account the skewness of the wave impact force, and by this possible changes in the contribution of the different modes, on the response will be investigated. Finally in section 7.5, all the (suggested) improvements that are made to the current deign method (DAF method) are summarized.

In Figure 66 the structure of the investigation of the DAF method in time and space is displayed. Figure 66 shows where chapter 7 is in the study of this master thesis.

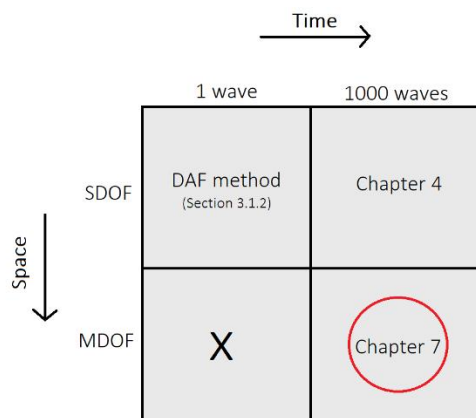


Figure 66: Improvements of the DAF method in time and space, report structure

7.1 Model schematisation

To be able to investigate the importance of taking higher modes of vibration into account for the determination of the maximum response of a gate, and to compare the results obtained with the semi-analytical model (MDOF model) in section 6.3.2 to the results obtained with an SDOF model, an equivalent SDOF model has to be set up. The semi-analytical model takes an infinite (or specified finite) number of modes into account, while an SDOF model only considers the first mode of vibration. In appendix J the complete derivation of the equivalent SDOF model is described. In this section only the most important formulations and assumptions are discussed.

The starting point of the derivation of the equivalent SDOF model is the plate equation of motion that is used for the semi-analytical model:

$$D\nabla^4 w(x, z, t) + (\rho_s + \rho_{s,w}) * \ddot{w}(x, z, t) = f_e(x, z, t) \quad (eq 7.1)$$

In which: w = displacement of the mid-surface of the plate [m]
 ρ_s = distributed mass per unit area [kg/m²]
 $\rho_{s,w}$ = distributed added water mass per unit area [kg/m²]
 f_e = time signal of the external force distribution on the plate (for instance of a wave impact) [N/m²]

The distributed added water mass can be calculated with equation 7.2 from Jongeling and Erdbrink (2010).

$$\frac{\rho_s + \rho_{s,w}}{\rho_s} = \left(\frac{f_{dry}}{f_{wet}} \right)^2 \quad (eq 7.2)$$

In which: f_{dry} = the in-vacuo natural frequency of the gate [Hz]
 f_{wet} = the natural frequency of the submerged gate [Hz]

For the time signal of the external force, the 'model' signal composed in chapter 6 is used. As discussed earlier the response determined with the semi-analytical model consists of the summation of the response for an infinite number of modes. For the SDOF model it is assumed that all the energy goes to the first mode of vibration, so that the response can be simplified as indicated in equation 7.3.

$$w(x, z, t) = \sum_{n=1}^{\infty} w_n(x, z) u_n(t) \approx w_0(x, z) * u_0(t) \quad (eq 7.3)$$

In which: w_0 = an assumed shape function of the response
 u_0 = an assumed time function of the response

For the plate with boundary conditions as indicated in Figure 67a, the following shape function is assumed to obtain the first mode of vibration for the SDOF model:

$$w_0(x, z) = \sin\left(\frac{\pi x}{L_x}\right) \sinh\left(\frac{0.88 * z}{L_z}\right) \quad (eq 7.4)$$

This shape function is shown in Figure 67b.

Support type: FSSS

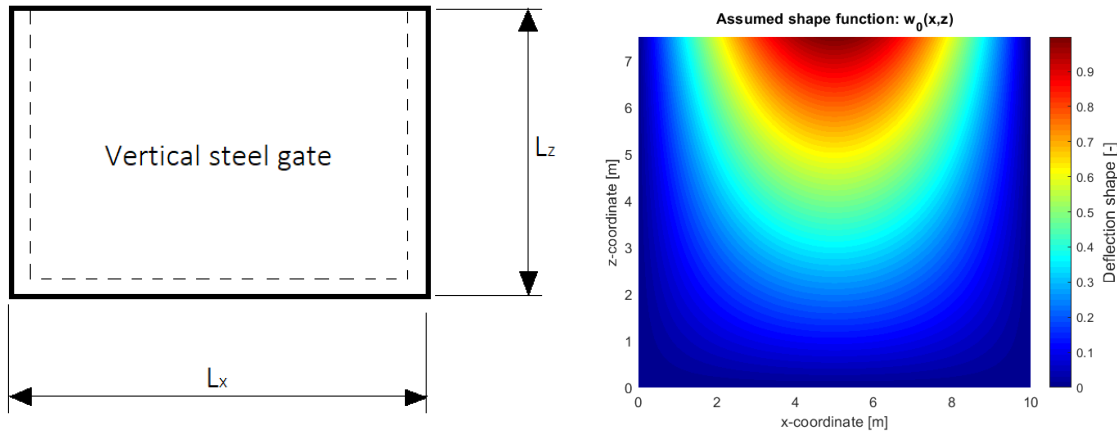


Figure 67: a) Boundary conditions of the case study gate, b) Assumed shape function $w_0(x,z)$ for the case study gate

After application of the orthogonality condition, and substituting an assumed response into the homogeneous equation of motion, the following generalised SDOF equation of motion is obtained:

$$\ddot{u}_0(t) + \omega_{n,w}^2 u_0(t) = \frac{\bar{F}_0}{L_0 \rho_s} * f(t) = \frac{\iint_S \bar{f}(x,z) * w_0(x,z) dS}{(\rho_s + \rho_{s,w}) \iint_S w_0(x,z)^2 dS} * f(t) \quad (eq 7.5)$$

In which the factor in front of the time signal of the wave impact force at the right hand side of the equation, is a constant which can be calculated. Also, the natural frequency of the submerged gate indicated in Figure 67a is known from the semi-analytical model. For a gate with thickness of $t = 0.243$ m and gate parameters as given in Table 12, the wet natural radial frequency is: $\omega_{n,w} = f_n * 2\pi = 6.71 * 2\pi = 42.16$ rad/s. With this data, Matlab can be used to solve equation 7.5, and calculate the maximum response (deflection) for each wave impact from the 'model' force-time signal. This results are used to compare the SDOF model with the semi-analytical (MDOF) model in the next section.

7.2 Validation equivalent SDOF model

The equivalent SDOF model is validated based on the semi-analytical model. The amount of modes that are taken into consideration can be set for the semi-analytical model, so to validate the equivalent SDOF model the semi-analytical has been run for only 1 mode. For this validation the options to include surface waves, and compressibility of the water are turned off in the semi-analytical model. In Figure 68 the probability of exceedance curves for the maximum deflections determined with the equivalent SDOF model and semi-analytical model run for 1 mode are given (for the gate parameters given in Table 12, $t = 0.243$ m). The model signal composed in chapter 6 is used as input for both models. Possible explanations for the small deviations between the models are the magnitude of the grid cells that are used for the two models, the hydrodynamic damping that is taken into account in the semi-analytical model, or small errors in the determination of the added water mass by using the simple formulation (equation 7.2) in the equivalent SDOF model.

When the 1% design values are compared for this gate, the difference between the maximum deflections obtained with the SDOF model and semi-analytical model run for only one mode is smaller than 1% ($w_{1\%,SDOF} = 13.1$ mm, $w_{1\%,1 \text{ mode}} = 13.2$ mm, $w_{1\%,SDOF}/w_{1\%,25 \text{ modes}} = 1.0076$).

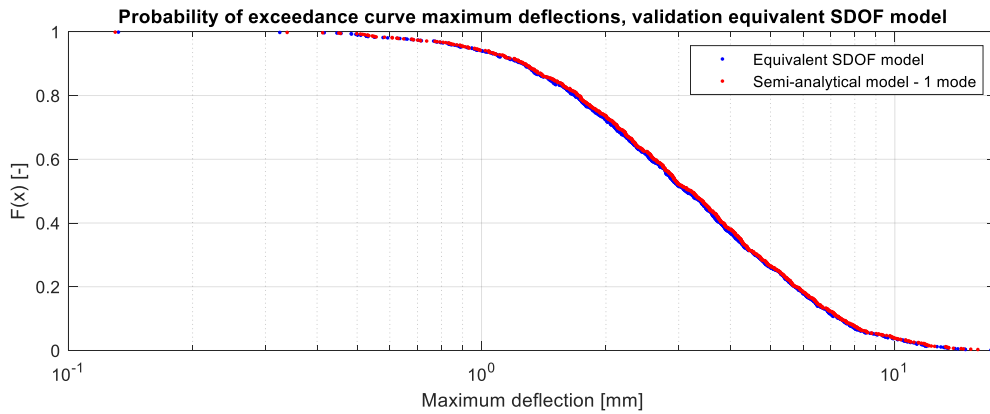


Figure 68: Probability of exceedance curve maximum deflection, validation equivalent SDOF model

7.3 Comparison response for SDOF and MDOF model

For the comparison of the maximum deflections obtained with the equivalent SDOF model and semi-analytical (MDOF) model, the model signal composed in chapter 6 (consisting of a thousand waves) will be used as input for both the SDOF and MDOF model. In Figure 69 the probability of exceedance curves for the maximum deflections determined with the equivalent SDOF model and semi-analytical model run for 25 modes, so as MDOF model, are given (for the gate parameters given in Table 12, $t = 0.243$ m). From the figure it can be seen that for the higher deflections, the results obtained with both models begin to show larger differences. This differences are caused by the small influence of mode (1,2) on the response for the semi-analytical model. The equivalent SDOF model assumes that all the energy is in mode 1, however in reality that does not always have to be the case. The contribution of the different modes on the response of the gate ($t = 0.243$ m) for the first wave of the model signal is shown in Figure 70a. For this gate, subjected to wave 1 from the model signal, 95.5% of the energy is in mode (1,1), 4.3% of the energy is in mode (1,2) and the rest of the energy is in the other modes. The amount of energy that is in other modes is limited for this gate subjected to the first wave of the model signal, however the ratio of the maximum deflections obtained with the SDOF model and semi-analytical model is still $w_{\max, \text{SDOF}}/w_{\max, 25 \text{ modes}} = 1.09$. So, an error of about 9% is made for wave 1 of the model signal when the SDOF model is used instead of the semi-analytical model for the gate width an (wet) eigen period of 0.15 s.

For this gate, the differences between the maximum deflections obtained with the different models are still limited ($w_{1\%, \text{SDOF}} = 13.1$ mm, $w_{1\%, 25 \text{ modes}} = 11.8$ mm, $w_{1\%, \text{SDOF}}/w_{1\%, 25 \text{ modes}} = 1.11$), however later in this section it is investigated whether the influence of higher modes becomes larger or smaller for gates with different characteristics (eigen period/stiffness).

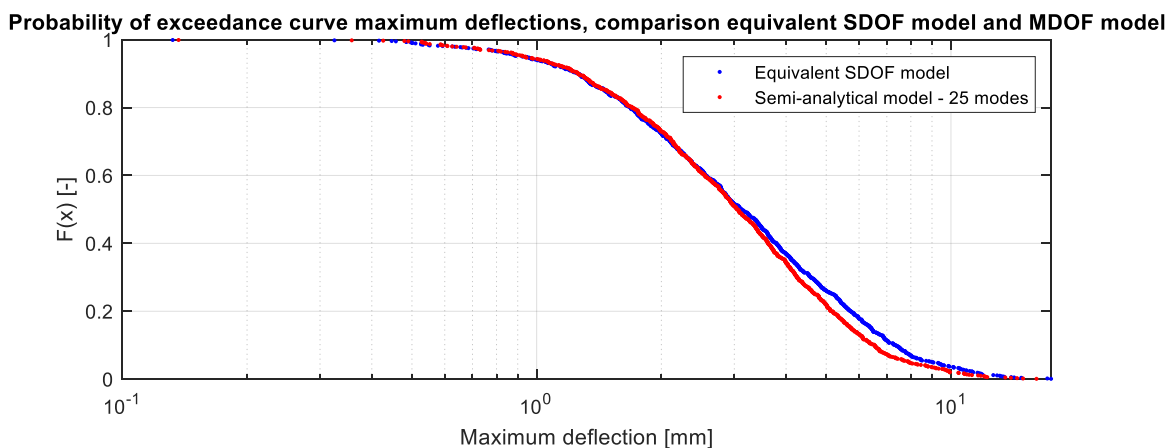


Figure 69: Probability of exceedance curve maximum deflection, comparison SDOF model and MDOF model

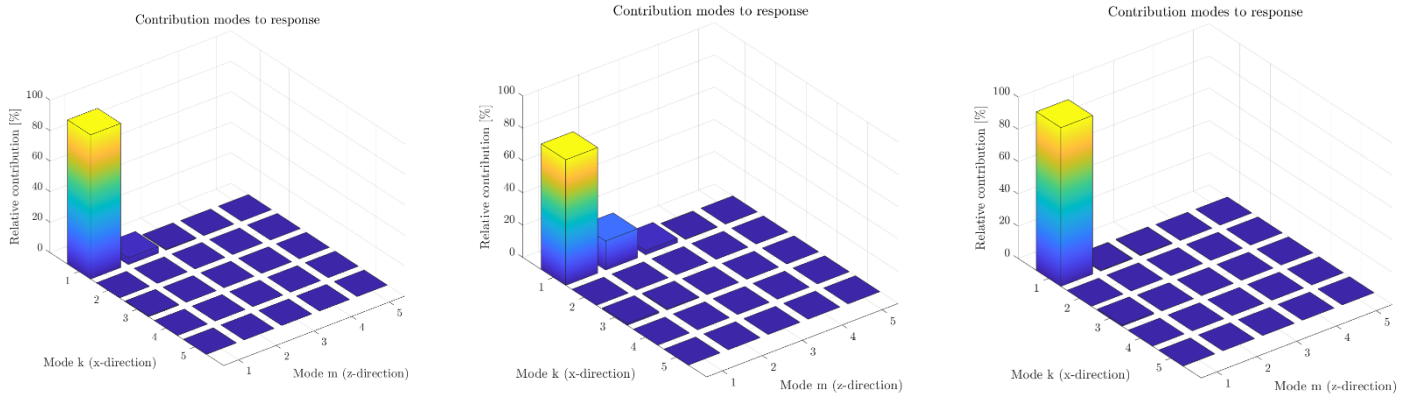


Figure 70: Contribution of the different modes on the response for three gates (a) $\tau/T = 1.1$, b) $\tau/T = 0.1$, c) $\tau/T = 5.0$, taking into account 25 structural modes

To investigate the influence of higher modes for submerged gates with different (wet) eigen periods, a small analysis is performed with the first wave of the model signal. So, the impact duration and skewness are constant during the analysis ($\tau_{\text{wave 1}} = 164 \text{ ms}$, $S_{\text{wave 1}} = 0.31$). By changing the (wet) eigen period of the gate, the ratio of τ/T_1 , and by this the domain in which the wave impact is (static, dynamic or impulsive), will change for the different gates. It is important to investigate the influence of higher modes on the response for different ratios of τ/T_1 , because in a wave field waves with larger and smaller impact durations are present. So, in a wave field the ratio of τ/T_1 is not constant, and the influence of higher modes (and by this the decision whether a SDOF model can be used for design) may be different for the different wave impacts.

In Table 8 the characteristics for the three gates that are investigated are given. The thickness, and by this eigen period, of the gates are chosen such that the wave impact (wave 1 from the model signal) is in the dynamic, impulsive or static loading domain. Gate 1 is an evenly fast system compared to the impact duration, gate 2 is a relatively slow system compared to the impact duration, and gate 3 is a relatively fast system compared to the impact duration. Also, the contributions of modes (1,1) and (1,2) are given for the three gates. In appendix I.2 the first six structural modal shapes for the case study gate are shown.

Table 8: Contribution of the different modes on the response for three gates, taking into account 25 structural modes

	τ/T_1 [-]	Loading domain	% mode (1,1)	% mode (1,2)
Gate 1 (similar)	1.1	Dynamic	95.5	4.3
Gate 2 (slow)	0.1	Impulsive	77.8	18.0
Gate 3 (fast)	5.0	Static	98.3	0.4

From Figure 70 and Table 8 it can be concluded that the lower the ratio of τ/T_1 , the larger the influence of higher modes for this case study gate and model wave signal. For the wave impact that is investigated the influence of higher modes is negligible (assumed when $<2\%$) for gates with: $\tau/T_1 > 1.5$. For this gates $W_{\text{max},25 \text{ modes}}/W_{\text{max},\text{SDOF}} = 1.0$, and an SDOF model can be safely used to determine the response. However, the boundary of $\tau/T_1 > 1.5$ is strictly determined for this specific gate case and wave impact. Further research have to be performed to be able to derive this kind of boundary conditions, which indicate when a SDOF model can be used for design instead of the more complicated MDOF model, for other situations (gates and wave fields). This research must also show whether this boundaries are fixed for all situations, or that the boundaries are different for different gates and wave fields.

Also, the wave impact that is used for the analysis has a relatively small skewness, $s = 0.31$. It is expected that not only the ratio of τ/T_1 , but also the skewness affects the importance of higher modes for a specific case. So, the determined boundary of τ/T_1 for which a SDOF model can be applied, can shift when higher or lower values for the skewness are used. In the next section the effect of the skewness parameter on the importance of higher modes is investigated.

7.4 Skewness parameter analysis

In section 7.3 it is investigated for which ratios of τ/T_1 the SDOF model suffices, and for which ratios it is necessary to use the semi-analytical model for the determination of the maximum deflection of the case study gate. However, for the whole analysis the skewness is kept constant at a quite small value of $s = 0.31$. In this section the influence of the skewness on the response and importance of higher modes will be investigated, and it will be checked whether the skewness influences the determined boundary of τ/T_1 for the case study gate. So, the combination of the skewness and ratio of τ/T_1 for which differences between the SDOF and MDOF model are visible will be investigated in this section. The skewness analysis is also made for the first wave of the model signal, only the skewness value of the force is adjusted.

7.4.1 Definition skewness parameter

For the analysis of the influence of the skewness parameter, two definitions for the skewness parameter are used and compared to the results for a uniform force distribution over the gate width. In Figure 71b and c the two definitions are shown. The symmetrical skewness definition is used for the composition of the model signal and already described in section 6.1.3. For this analysis also a linear, asymmetrical skewness definition will be investigated. As already described in section 6.1.3 no data is available for the right gate half, so an assumption of the force course for the right gate half has to be made. From Figure 45 in section 5.3 it can be seen that quite high skewness values are found ($s > 2$) for the wave impact data, so actually this indicated that the asymmetrical skewness definition shown in Figure 71c cannot be the case for this wave impact data. When the skewness value is larger than 2 for this definition, negative pressures are assumed at the right gate half. However, due to the lack of data it is impossible to say what the force distribution over the full gate width is, and it maybe a hasty conclusion to exclude the asymmetrical skewness definition from the analysis due to this reasoning. So, it is decided to include the asymmetrical skewness definition in this analysis to see how the behaviour of the gate is influenced by this. Further research has to point out the real course of the force over the full gate width, this research only focusses on showing the effects of including different skewness definitions in the analysis.

When for the symmetrical skewness definition shown in Figure 71b, a skewness value of for instance 2 is used, this means that the skewness is equal to 1 in the middle of the gate and equal to 3 at the left and right side of the gate. When for the asymmetrical skewness definition shown in Figure 71c, a skewness value of for instance 2 is used, this means that the skewness is equal to 1 in the middle of the gate, equal to 2 at the left edge of the gate and equal to 0 at the right edge of the gate.

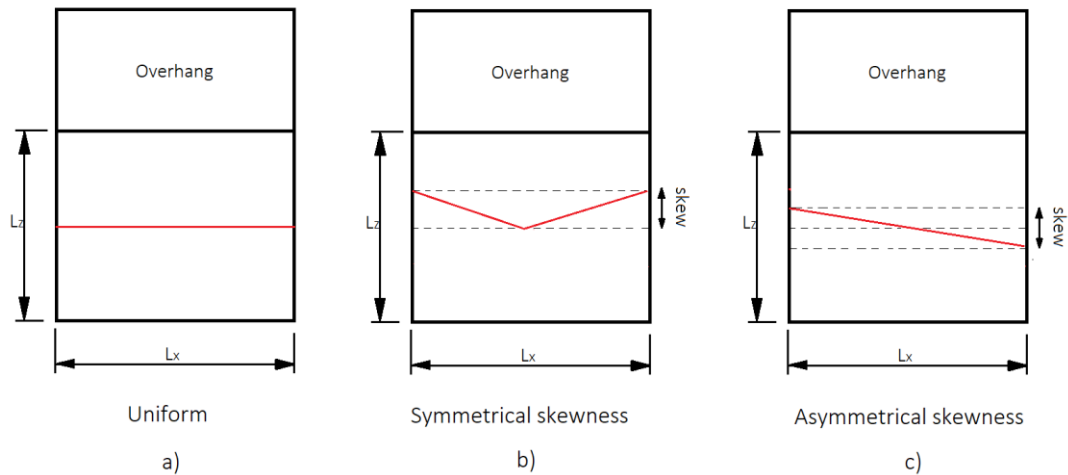


Figure 71: Definitions skewness parameter

From Figure 71 it can be seen that the symmetrical skewness definition increases the average force compared to the uniform case. The asymmetrical skewness definition gives the same average force as for the uniform case. To be able to compare the maximum deflections for the different gates and different skewness values, a correction factor is used. This correction factor is determined based on the force, and corrects the force so that the average force is the same as for the uniform case. The force and deflection are related, so that for instance a ten times higher force gives a ten times higher deflection. So, the correction factor that is determined for the force can also be used to correct the maximum deflection that will be obtained in the next section. As already said, the asymmetrical skewness definition does not increase the average force, so no correction of the maximum deflections is needed for this definition. In Table 9 the correction factors for the skewness values that are used for the analysis are given. In appendix I.1 the uncorrected and corrected values of the maximum deflections that are determined with the semi-analytical and SDOF model, and used in the next section are given.

Table 9: Correction factor average force, for symmetrical skewness definition

s [-]	Correction factor average force [-]
-0.5	0.71
2	2.14
4	3.29
8	5.57

7.4.2 Investigation gates with different characteristics

The same gates as in section 7.3 are used for the analysis with the different skewness definitions (see Table 8 for the gate characteristics).

In Table 10 the results from the skewness analysis are given for the three different gates. In the table the (corrected) maximum deflections determined with the semi-analytical model (w_{\max}) and SDOF model ($w_{\max, \text{SDOF}}$), the contribution of the most important modes, the location at the plate at which the maximum deflection occurs, and the ratio of the maximum deflection determined with the semi-analytical model and SDOF model ($w_{\max} / w_{\max, \text{SDOF}}$) for the different skewness values and definitions are given.

Table 10: Results from skewness parameter analysis, for MDOF and SDOF model

Gate 1 (similar) $\tau/T_1 = 1.1$									
	s	W_{max} [mm]	% mode (1,1)	% mode (1,2)	% mode (2,1)	% mode (3,1)	Location W_{max} (X,Z) [m]	$W_{max,SDOF}$ [mm]	$W_{max}/$ $W_{max,SDOF}$ [-]
Uniform	0	4.9	94.7	4.1	0.0	0.5	(5,7.5)	5.3	0.92
Symmetrical skewness	2	4.2	94.3	4.3	0.0	0.8	(5,7.5)	4.6	0.91
	4	4.0	94.1	4.3	0.0	0.9	(5,7.5)	4.4	0.91
	8	3.8	94.0	4.3	0.0	1.0	(5,7.5)	4.2	0.91
	-0.5	5.5	94.9	4.1	0.0	0.3	(5,7.5)	5.9	0.93
Asymmetrical skewness	1	4.9	93.4	4.1	1.2	0.5	(5,7.5)	5.3	0.92
	2	4.9	92.2	4.0	2.3	0.5	(4.75,7.5)	5.4	0.91

Gate 2 (slow) $\tau/T_1 = 0.1$									
	s	W_{max} [mm]	% mode (1,1)	% mode (1,2)	% mode (2,1)	% mode (3,1)	Location W_{max} (X,Z) [m]	$W_{max,SDOF}$ [mm]	$W_{max}/$ $W_{max,SDOF}$ [-]
Uniform	0	154.7	78.3	18.1	0.0	0.7	(5,7.5)	91.1	1.70
Symmetrical skewness	2	132.8	76.5	17.7	0.1	1.5	(5,7.5)	78.6	1.69
	4	126.2	75.9	17.6	0.1	1.6	(5,7.5)	74.8	1.69
	8	121.1	75.5	17.4	0.2	1.7	(5,7.5)	71.9	1.68
	-0.5	171.1	78.9	18.1	0.0	0.0	(5,7.5)	100.5	1.70
Asymmetrical skewness	1	155.1	73.1	16.9	3.1	0.6	(5,7.5)	91.4	1.70
	2	155.6	68.3	15.7	6.5	0.5	(4.75,7.5)	91.7	1.70

Gate 3 (fast) $\tau/T_1 = 5.0$									
	s	W_{max} [mm]	% mode (1,1)	% mode (1,2)	% mode (2,1)	% mode (3,1)	Location W_{max} (X,Z) [m]	$W_{max,SDOF}$ [mm]	$W_{max}/$ $W_{max,SDOF}$ [-]
Uniform	0	0.171	98.5	0.4	0.0	0.6	(5,7.5)	0.174	0.98
Symmetrical skewness	2	0.147	97.7	0.4	0.1	1.2	(5,7.5)	0.150	0.98
	4	0.140	97.4	0.4	0.1	1.4	(5,7.5)	0.143	0.98
	8	0.134	97.2	0.4	0.1	1.6	(5,7.5)	0.137	0.98
	-0.5	0.189	98.8	0.4	0.0	0.3	(5,7.5)	0.192	0.99
Asymmetrical skewness	1	0.172	96.0	0.4	2.2	0.6	(4.75,7.5)	0.174	0.99
	2	0.173	93.7	0.3	4.2	0.6	(4.75,7.5)	0.175	0.99

7.4.2.1 Conclusion symmetrical skewness

The conclusions that are drawn in this section, correspond to symmetrical skewness definition. From Table 10 it can be concluded that for positive values of the symmetrical skewness, for each gate, the (corrected) maximum deflections determined with the semi-analytical model and SDOF model are lower than the maximum deflections determined for the uniform case. For the negative skewness value, the maximum deflections that are determined for the semi-analytical model and SDOF model are higher than for the uniform case. This can be explained by the fact that also for the higher skewness values, mode (1,1) stays the most important mode for all three of the gates (>75 %). When the skewness is positive, the force works against the first vibration shape, and when the skewness is negative, the force has a similar shape as the first vibration mode. So, when the skewness is negative the largest force is at the same location as the largest deflection from the first modal shape, and this results in higher deflections. This is indicated in Figure 72. Figure 72a shows the first modal shape, Figure 72b shown the pressure field for a positive skewness value of 2, and Figure 72c shows the pressure field over the gate for a negative skewness value of 0.5.

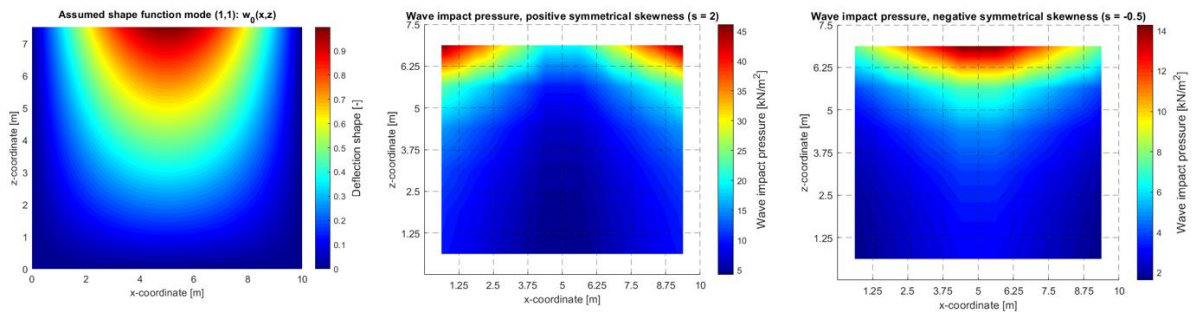


Figure 72: Influence of positive or negative symmetrical skewness on response

The first conclusion that can be draw is that it is important to take the skewness of the wave impact force into account for the determination of the maximum deflection. When the corrected maximum deflections that are obtained for a wave impact with skewness are compared with the deflection obtained for the uniform force, considerable differences are obtained for the three gates ($\pm 28\%$ for $s = 8$, for all three of the gates). However, as can be seen from Table 10 this effect of the skewness can also be taken into account with the simple SDOF model (For the calculation of the transformation factor for the force in the SDOF model, the spatial variation of the wave impact force can be included in the SDOF model, however the effect of this distribution is limited to the effect on the first vibration mode only). The ratio of $W_{max}/W_{max,SDOF}$ differs for the different gates, however it is constant for the different skewness values per gate. So, the difference between the semi-analytical model and SDOF model that is found for the uniform case (as shown in the previous section, this difference depends on the ration of τ/T_1) stays the same when the skewness becomes higher. This indicates that, despite the shift in the contribution of the higher modes that can be seen from the calculations with semi-analytical model, the amount of energy that goes to mode (1,1) is large enough for the SDOF model to be sufficient.

So, for the wave impact signal and case study gate that are investigated in this report, it can be concluded that the skewness affects the deflection that is obtained. However, as long as the shift in contribution of higher modes is limited (as for the three investigated gates), the effect of the symmetrical skewness can also be obtained with the SDOF model. So, the limit of τ/T_1 for which the SDOF model suffices that is determined in the previous section, is not affected when the values of the symmetrical skewness become higher.

7.4.2.2 Conclusions asymmetrical skewness

The conclusions that are drawn in this section, correspond to asymmetrical skewness definition. From Table 10 it can be seen that the same change in skewness (from $s = 0$ until $s = 2$) has a larger effect on the contribution of higher modes for the asymmetrical skewness definition. Also, as expected, other higher modes (for instance mode (2,1)) are hit due to the asymmetrical skewness definition. So, it can be concluded that based on the assumed shape of the skewness, other modes can become important for the response of the gate. However, despite the larger influence of higher modes for the asymmetrical skewness definition, the maximum deflection that is obtained differs less from the uniform deflection than for the symmetrical skewness case.

Again, it can be seen that still most of the energy goes to mode (1,1), and that the ratio of $W_{\max}/W_{\max,SDOF}$ is still the same for the different skewness values. So again, the limit of τ/T_1 for which the SDOF model suffices that is determined in the previous section, is not affected when the values of the asymmetrical skewness become higher.

However, for the asymmetrical skewness definition a small shift in the location of the maximum deflection can be observed. This shift is caused by the hitting of higher asymmetrical modes when the asymmetrical skewness definition is used. It can be concluded that, for this case study, the SDOF model can be used to determine the absolute value of the maximum deflection when $\tau/T_1 > 1.5$. However, the location of the maximum deflection cannot be determined exactly when the simple SDOF model is used (when the SDOF model is used, it is assumed that the maximum deflection occurs at $(x,z) = (5,7.5)$ for the case study gate).

7.4.3 Conclusions – effect of skewness on use of SDOF or MDOF model

From the analysis with the different skewness definitions and multiple gates, the most important conclusions that can be drawn are:

- It is important to take the skewness into account. The deflection determined for the uniform case, differs from the (corrected) deflection obtained for the different skewness definition cases (for both the semi-analytical model and SDOF model). Higher or lower values of the maximum deflection can be found for negative or positive values and different definitions of the skewness parameter.
- The contribution of the higher modes is affected by the skewness value that is used. Also, the shape of the skewness definition determines which of the higher modes will be hit. However, despite the shift in contribution in the higher modes, the skewness does not affect the limit of τ/T_1 for which the SDOF model suffices for this case study gate and wave impact force signal. So, a limit for τ/T_1 can be determined from which the SDOF model suffices for each value of the skewness parameter. The effect of the skewness is also in the SDOF model (when the contribution of mode (1,1) stays large enough (>70% during the analysis that is performed)).
- As already discussed, the definition of the skewness parameter determines which of the higher modes are hit. The hitting of higher modes can result in a shift of the location of the maximum deflection. This shift cannot be determined from the SDOF model, and the semi-analytical model is needed to determine the exact location of the maximum deflection.

It has to be kept in mind that this conclusion are based on the analysis of a single wave impact force signal and case study gate. So, more research has to be performed to be able

to generalise this conclusions, and to be able to developed guidelines which can be used for design. This research focusses on showing the effects on the response caused by including the skewness in the analysis, and can be used as a basis for the development of new design guidelines which can indicate for which ratios of τ/T_1 it is needed to use the semi-analytical model (include the effect of higher modes in the design) and when the SDOF model suffices, taking into account the skewness of the wave impact force.

7.5 Improvements in time and space to the DAF method

In this section the improvements that are made/suggested to the present design method (DAF method) are shortly summarized. From the analysis with an SDOF model in this chapter 4 it can be concluded that the DAF method not 'suffices in time', and that it is necessary to improve the DAF method in time. Only looking at the wave impact with the highest peak force (instead of looking at the response for a whole wave field), may result in over- or underestimations of the maximum deflection. To improve the DAF method in time, it is suggested to look at the maximum deflection that is obtained by running the force-time signal for multiple wave impacts, instead of only looking at the maximum deflections for the wave impact with the highest peak force. To be able to use the whole force-time signal for multiple wave impacts, a first version of a method to compose a 'model' force-time signal for multiple wave impacts is described and validated in chapter 6. When this method is further developed and validated, no scale model tests are needed to determine the force-time series of wave impacts in the future, and the improvement of the DAF method in time can easily be implemented.

Chapter 7 focusses on the improvement of the current design method in space. The DAF method does not take into account the spatial distribution of the wave impact force over the gate surface. In the semi-analytical model developed by Tieleman (2019), the spatial distribution of the wave impact force can be used as input. However, until now a uniform distribution was assumed for the width distribution of the wave impact force. For the wave impact force-time signal that is used during this research it is found that the width distribution of the wave impact force can be described with a skewness parameter (see section 5.3). The skewness is implemented in the method that is developed to compose a 'model' force-time signal or multiple wave impacts. In section 7.1, an equivalent SDOF model is set up to be able to compare the results (maximum deflections) that are obtained with the semi-analytical (MDOF) model and equivalent SDOF model, and to be able to investigate for which situations the SDOF model suffices for the determination of the maximum deflection. The equivalent SDOF model only takes mode (1,1) into account and the semi-analytical model can take an infinite (or specified finite) number of modes into account. In section 7.3 it is shown that the amount of modes that contribute to the response depends on the ratio of τ/T_1 . The influence of the ratio of τ/T on the contribution of the different modes, and by this on the possibility of using the SDOF model instead of the more complicated MDOF model, is already present for the uniformly distributed wave impact force (so, also when the skewness is not introduced yet). When the skewness is introduced, the maximum deflection that is found changes. Also, the contribution of the higher modes increases a bit by introducing the skewness. However, for the cases that are investigated, the shift of the contribution of the modes does not result in a change of the ratio of τ/T for which the SDOF model suffices.

Concluding, an upper bound for the ratio of τ/T_1 can be determined for which the equivalent SDOF model suffices for the determination of the maximum deflection. Based on the results found during this master thesis, it is suggested that a full force-time signal for multiple wave impacts always have to be used for design. It is also suggested that the skewness of the wave impact force will always be included for the semi-analytical (MDOF) model and equivalent SDOF model.

8 Conclusions and recommendations

The main goal of this master thesis was to extend and improve the present design method, the DAF method, in time and space. In section 8.1 the most important conclusions that can be drawn from the research, that is performed for this master thesis, are discussed. The research questions stated in section 1.3 are answered to formulate the most important conclusions. The second part of this chapter discusses some recommendations for further research.

8.1 Conclusions

This section follows the research questions stated in section 1.3 . First, the sub-research question are discussed in sections 8.1.1 - 8.1.2. Then, in section 8.1.4 the main-research question is answered.

8.1.1 Applicability of the present design method (DAF method) - time investigation

From the analysis with the SDOF system it can be concluded that the maximum deflection and corresponding dynamic amplification factor of a structure found with the DAF method, by which the response for a single triangular load schematisation (of the maximum wave impact in the wave field) is calculated with the SDOF model, differs from the 'real' maximum deflection and corresponding amplification factor obtained by running the whole force-time signal (wave field) with the SDOF model. The DAF method may give an over- or underestimation. In the remainder of this section three effects that are found and investigated, causing this difference, are shortly discussed.

The first effect that is investigated is the influence of the not yet fully damped (amplitude <1%) vibration of the gate when the next wave impact already occurs. Based on the wave period (time between two impact durations, T_{wave}), eigen period of the structure ($T_{structure}$), and damping (γ), it can be determined whether the vibration of the structure is damped between two wave impacts. Equation 8.1 can be used to determine the amount of structure cycles that are needed for the vibration amplitude to be damped till 1%. When this rule is met, the influence of the vibration of the structure due to the previous wave impact, on the response of the next wave impact can be considered negligible. The 'real' response that is calculated with the SDOF model can deviate considerably from the response calculated with the DAF method (higher or lower depending on the position of the gate at the moment that the new impact occurs) due to this effect. For instance, for wave 124 in the wave signal and the relatively slow system compared to the wave impact duration ($\tau/T = 0.5$), $x_{max,real}/x_{max,static} = 1.05$ and $x_{max,real}/x_{max,static} = 1.13$. However, for a relatively fast system compared to the wave impact duration ($\tau/T = 2.0$), this two values are the same $x_{max,real}/x_{max,static} = x_{max,real}/x_{max,static} = 1.28$. For this relatively fast system the vibration of the previous wave impact is damped (amplitude <1%) when the next wave impact occurs.

$$\frac{T_{wave}}{T_{structure}} > \frac{0.73}{\gamma} \quad (eq\ 8.1)$$

The second effect that is investigated is the influence of the triangular schematisation (wave impact duration) used for the DAF method on the correctness of the response. During the analysis in chapter 4 the impact duration is determined graphically by fitting a triangular schematisation in the force-time signal of the wave impact. However, when the numerical

method described in appendix E is used to determine the wave impact duration with more accuracy, the difference between the response determined with the DAF method and by running the whole force-time signal, reduces tremendously for systems in the dynamic domain ($0.25 < \tau/T < 4$). For instance for the fastest system that is investigated in chapter 4 (system 3, $\tau/T = 2.0$), the percentual difference between the maximum deflections obtained with the DAF method and by running the whole force time signal reduces from 37.3% to 6.1% when the impact duration that is determined with the numerical method is used as input for the DAF method, instead of the graphically determined wave impact duration. When systems are in the quasi-static ($\tau/T > 4$) or impulsive ($\tau/T < 0.25$) domain, the DAF method performs better. So, it can be concluded that when systems are in the dynamic domain, more realistic results are obtained with the DAF method, when the wave impact duration (load schematisation) is determined with more accuracy using a numerical method instead of a graphical method.

Finally it can be concluded that the maximum peak force in the wave field does not always cause the largest response. The combination of the impact duration, maximum peak force, and eigen period of the structure (location in the maximum response curve), determines which wave causes the largest response (and amplification). So it is important to also take some of the lower peak forces (with shorter or longer impact duration) into account when determining the maximum response and corresponding dynamic amplification factor with the DAF method.

The DAF method does not 'suffices in time', and it is necessary to improve the DAF method in time. Only looking at the wave impact with the highest peak force (instead of looking at the response for a whole wave field), may result in over- or underestimations of the maximum deflection. To improve the DAF method in time, it is suggested to look at the maximum deflection that is obtained by running the force-time signal for multiple wave impacts, instead of only looking at the maximum deflections for the wave impact with the highest peak force. To be able to use the whole force-time signal for multiple wave impacts, a first version of a method to compose a 'model' force-time signal for multiple wave impacts is proposed. When this method is further developed and validated, no scale model tests are needed to determine the force-time series of wave impacts in the future, and the improvement of the DAF method in time can easily be implemented.

8.1.2 Composition of a 'model' force-time signal

For the design of hydraulic structures, force-time signals consisting of multiple wave impacts (representing for instance a full storm) are used. This force-time signals can be determined with scale model tests. During this research a method is developed to compose a 'model' force-time signal of multiple wave impacts, based on wave parameters only (chapter 6). So that, in the future, when the suggested method is further developed and validated, no scale measurement data is needed to compose a spatially varying force-time signal for multiple wave impacts. For the composition of the 'model' force-time signal, the probabilistic distributions of the wave height, wave period, skewness and wave impact duration are required as input only (chapter 5). For the composition of the 'model' signal the Pressure-Impulse theory is used for the determination of the height distribution of the pressure-impulse based on the wave height and wave period. Also, the skewness of the wave impact force is included in the method. Due to the lack of knowledge on the course of the skewness over the full gate width, the force-time series on the right gate half are obtained by mirroring the data known at the left gate half (see Figure 55 in chapter 6). For the schematisation in time a symmetrical triangular shape is assumed (see Figure 56 in chapter 6).

To validate the method to compose a 'model' force-time signal for multiple wave impacts, first the maximum peak pressures are determined and compared. Then, the responses to a 'real' force-time signal and schematised 'model' signal are determined and compared. Good agreement between the peak pressures of both signals is found ($p_{1\%,\text{model}}/ p_{1\%,\text{real}} = 1.31$). Even better agreement is found between the maximum deflections for both signals ($W_{1\%,\text{model}}/ W_{1\%,\text{real}} = 1.05$).

The composition method of the 'model' signal still has to be improved to obtain even better resemblance between the peak pressures and correspondingly the maximum deflections that are obtained. For instance the Pressure-Impulse theory is still in development. Especially the pressure-impulse at the top region of the gate is still hard to predict. Also, more attention can be paid to the joint probability of the wave height and wave period to improve the 'model' signal. More research have to be done to better describe the skewness parameter. In this research a lot of assumptions are made concerning the skewness parameter. More research have to be done, to investigate the course of the wave impact force over the full width of a gate, and to be able to give a more general description of the skewness parameter for different wave fields. Finally, the simple symmetrical triangular schematisation in time can be improved a bit by applying slightly other shapes, and by using the rising time as a statistical input value for the composition of the 'model' force-time signal.

8.1.3 Influence of the width distribution of the wave impact force on the dynamic behaviour of a flat vertical steel gate

The DAF method does not take into account the spatial distribution of the wave impact force over the gate surface. In the semi-analytical model developed by Tieleman (2019), the spatial distribution of the wave impact force can be used as input. However, until now a uniform distribution was assumed for the width distribution of the wave impact force. For the wave impact force-time signal that is used during this research it is found that the width distribution of the wave impact force can be described with a skewness parameter (see section 5.3).

Also, for the uniform wave impact force, higher modes can become important for certain ratios of τ/T_1 . A lower limit of τ/T_1 is determined for the case study gate ($\tau/T_1 > 1.5$) for which the SDOF model suffices and gives the same deflection results as the semi-analytical model. The analysis with the skewness parameter has focussed on the effect of implementing a width distribution of the wave impact force, and a shift in the contribution of the higher modes, which can result in a shift of the ratio of τ/T_1 (where from the SDOF model suffices) that is found for the uniform case. In section 7.4 it is found that when the skewness of the wave impact force is implemented in the analysis, the maximum deflection that is obtained changes by this (a correction factor is used to make sure that the average force over the width is not increased by the use of the skewness parameter). Based on the definition and magnitude of the wave impact force, the deflection can be lower or higher than the maximum deflection obtained for a uniform wave impact force. It is found that when the skewness is implemented, a small shift in the contribution of the higher modes occurs. Also, the shape of the skewness definition determines which of the higher modes will be hit. However, despite the small shift in contribution in the higher modes (maximum difference of $\pm 10\%$), the skewness does not affect the limit of τ/T_1 for which the SDOF model suffices. So, a lower limit for τ/T_1 can be determined from which the SDOF model suffices for each value of the skewness parameter. The effect of the skewness is also in the SDOF model (see Figure 72) when the contribution of mode (1,1) stays large enough ($>70\%$ during the analysis that is performed)).

A final note that has to be made is that the definition of the skewness parameter determines which of the higher modes are hit. The hitting of higher modes can result in a shift of the location of the maximum deflection. This shift cannot be determined from the SDOF model, and the semi-analytical model is needed to determine the exact location of the maximum deflection. So, per wave another location of the maximum deflection can be found. A big advantage of the use of the 'model' signal for multiple wave impacts, instead of only looking at the single response for the highest peak force, is that this different locations can be determined from the analysis with the semi-analytical model.

It has to be kept in mind that this conclusions are based on the analysis of a single wave impact force signal and case study gate. So, more research has to be performed to be able to generalise this conclusions, and to be able to developed guidelines which can be used for design. This research focusses on showing the effects on the response caused by including the skewness in the analysis, and can be used as a basis for the development of new design guidelines which can indicate for which ratios of τ/T_1 it is needed to use the semi-analytical model (include the result of higher modes in the analysis) and when the SDOF model (only mode 1 is taken into consideration) suffices, taking into account the skewness of the wave impact force.

8.1.4 Improvements to the present design method in time and space

The main goal of this master thesis is to improve the present design method, the DAF method, in time and space. It is found that an upper bound for the ratio of τ/T_1 can be determined for which the equivalent SDOF model suffices for the determination of the maximum deflection. Based on the results found during this master thesis, it is suggested that a full force-time signal for multiple wave impacts always have to be used for design (improvement of the DAF method in time). A first version of a method to demine the force-time signal for multiple wave impacts, based on wave input parameters only, is proposed in the report. It is also suggested that the skewness of the wave impact force will always be included in the wave impact input force signal, for both the semi-analytical (MDOF) model and equivalent SDOF model (improvement of the DAF method in space).

So, for some ratios of τ/T_1 ($\tau/T_1 > 1.5$ for the studied case study), a simple SDOF model (as used in the DAF method) suffices. However, it is important to include the spatial distribution of the wave impact force in this SDOF model (by using the transformation factor in equation 7.5), and always look at the response for the whole force-time signal instead of only the wave impact with the highest peak force. For all other ratios of τ/T_1 (< 1.5 for the case study in this thesis), the contribution of higher modes is too large, and the semi-analytical model has to be used to determine the correct maximum deflection. Implementation of the skewness in the analysis does not change the ratio of τ/T_1 for which the SDOF model suffices. The skewness only changes that way that, especially, the first mode of vibration is hit in the SDOF and semi-analytical model (see Figure 72).

8.2 Recommendations

In this section some recommendations for further research are done. First, in section 8.2.1 suggestions for the performance of new scale model tests are done. With the results from this scale model tests, the width distribution of the wave impact force can be investigated further. Furthermore, suggestions are made for further improvements of the current design method, which can finally be used for the development of a completely new design method for hydraulic structures exposed to wave impacts.

8.2.1 Scale model tests

The width distribution of the wave impact force over the full gate width determines which of the higher modes becomes important when waves are in the impulsive loading domain. As described earlier, more energy goes to asymmetrical modes when the width distribution is asymmetrical, and more energy goes to symmetrical modes when the width distribution is symmetrical. It is recommended to do more scale model tests to determine the width distribution of the wave impact force over the full gate width. From the results of this scale model tests the skewness can be included in the new design method in a better and more general way. So, with the results from new (more complete) scale model tests conclusions can be draw about the course of the wave impact force over the full gate width, and conclusions can be draw about the magnitude and statistical distribution of the skewness of the wave impact force. In this master thesis a statistical distribution has been determined for the skewness parameter for a wave field attacking a certain case study gate. However, further research has to point out if the skewness parameter has a fixed distribution for different wave fields, or that different statistical distributions have to be used for different wave fields. In this case, methods to predict the skewness distribution for a certain wave field have to be developed.

In Figure 73a the locations of the load cells and pressure sensors for which data was available during this research are shown. It can be seen that, except for the pressure sensor data near the middle of the gate, no data was available at the right side of the gate. To be able to determine and investigate the width distribution (skewness) over the full gate width it is recommended to do more scale model tests. For this model tests the same structure can be used as for the model test used for this research. It is recommended to place load cells as indicated in Figure 73b. To prevent uncertainty in the results due to calibration of the load cells and pressure sensors, it is recommended to only use load cells for this tests. From the research it is already known that larger values of the skewness are found near the top of the gate (with the highest impact forces), so this is the most interesting region for the investigation. It is important to place enough load cells over the width near the top of the gate, to get a good indication of the width distribution (skewness shape) of the impact force. The load cells near the bottom are placed to check if the skewness globally follows the same shape as at the top of the gate. When the load cells are placed as indicated in Figure 73b, the width distribution of the wave impact force over the full gate can be investigated, and a possible variation of the magnitude of the skewness over the height can be determined.

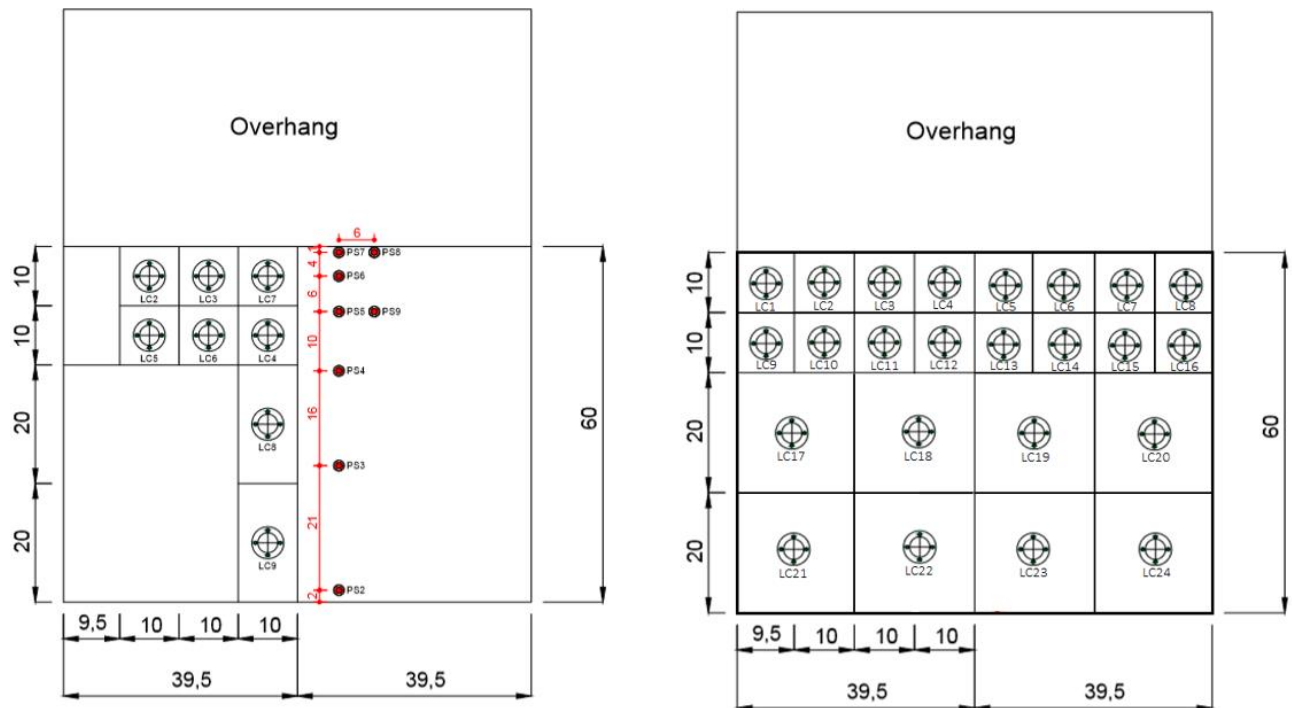


Figure 73: a) Data points 'old' scale model tests, b) recommended data points for 'new' scale model tests

8.2.2 Development of design guidelines – use of MDOF or SDOF model

This research has only focussed on one case study gate attacked by one wave impact force-time signal. However, for the dynamic design of structures in the future it is important to set up guidelines which indicate when the use of a simple SDOF model is sufficient and when it is really necessary to use the more complicated semi-analytical model developed by Tieleman (2019) (and include higher modes in the analysis), for different gates and wave impact force-time signals. Further research is needed to set up these guidelines, with ratios of τ/T_1 for different gates and wave impact force-time signals from which the use of an SDOF model is sufficient.

The focus of this master thesis was more on showing the possible improvements that can be made to the current design method based on a set of lab-data. So, no design guidelines can be set up from this thesis work. The work performed in this thesis can be used as a basis for the development of new design methods in the future.

8.2.3 Time shift of wave impact peak time

This research has focussed on the wave impact force amplitude variation over the width of the gate. Another factor that may be important for the description of the width distribution of the wave impact force is a small time shift of the wave impact peak time over the width that can be observed for some of the wave impacts in the wave signal described in section 5.2. Further research has to be performed to characterise the time shift of the wave impact peak time that is present in the data, and the possible influence of this time shift on the dynamic response of structures. When a significant effect is found, the time shift of the wave impact peak time has to be included in the proposed composition method described in chapter 6.

8.2.4 Fatigue

This research has only focused on the ultimate limit state (ULS). However, fatigue is another important failure mechanism for hydraulic structures. More research have to be done on this subject, to be able to include this failure mechanism in the new design method.

8.2.5 Stresses

The research performed in this master thesis has focussed on the response in terms of maximum deflections only. The next step is to look at the maximum stresses, and locations of the maximum stresses at the plate surface that can be determined with the semi-analytical model developed by Tieleman (2019). As already described in section 7.4, a small shift in the contribution of higher modes is found when the skewness is included in the analysis. However, this small shift does not affect the lower limit of τ/T_1 from which the SDOF model can be used when looking at the maximum deflections of the plate. Higher modes can give higher stresses for equal deflections. So, it may be the case that the skewness parameter does affect the maximum stresses that are obtained with the semi-analytical model, and that based on the stresses the limit of τ/T_1 will change when the skewness is introduced. Further research can focus on the effect of the skewness of the wave impact force amplitude, on the stresses that are obtained in the plate, and the corresponding lower limit of τ/T_1 from which the SDOF model can be used.

8.2.6 Comparison to 'wind' approach in the field structural engineering

Within the field structural engineering, a clear and extensive design approach is available to deal with wind loads on buildings (Eurocode NEN-EN 1991-1-4, 2005). For wide buildings a factor is introduced to determine the horizontal distribution of the wind load. The factor is used as a reduction factor of the maximum wind load on the building. Due to the use of this factor, the maximum wind load is spread out over the width of the building. The skewness parameter can be compared to this factor. When the maximum value of the wave impact load is used over the full width of a gate, the deflections are overestimated. However, besides the effect on the average wave impact force, the skewness also has an effect on the importance of higher modes.

When a new design method to deal with the dynamic behaviour of hydraulic structures exposed to wave impacts is developed, it may be useful to take a look at the similarities with the method that is used for wind loads in the field of structural engineering. This can give some insight in how to construct the new guidelines, and it may be useful to approach similar problems in the same way within the different fields of civil engineering.

Bibliography

R.A. Bagnold. Interim report on wave-pressure research. Institution of Civil Engineers, 1939.

<https://beeldbank.rws.nl>, Rijkswaterstaat / Bart van Eyck. Visited at 18-02-19. URL <https://beeldbank.rws.nl/MediaObject/Details/2787>

<https://beeldbank.rws.nl>, Rijkswaterstaat / Bart van Eyck. Visited at 18-02-19. URL https://beeldbank.rws.nl/MediaObject/Details/Luchtfotoserie_IJsselmeer_2794

<https://beeldbank.rws.nl>, Rijkswaterstaat / Bart van Eyck. Visited at 07-06-19. URL <https://beeldbank.rws.nl/MediaObject/Details/74790>

J. Blaauwendraad. Lecture notes Plate analysis, theory and application ct4180: Volume 1 Theory. Delft University of Technology, November 2006.

X. Chen, B. Hofland, W. Molenaar, A. Capel, M.R.A Van Gent. Use of impulses to determine the reaction force of hydraulic structure with an overhang due to wave impact. Delft University of Technology, December 2018.

M.J. Cooker and D.H. Peregrine. A model for breaking wave impact pressures. Coastal Engineering Proceedings 1, 1990.

M.J. Cooker and D.H. Peregrine. Pressure-impulse theory for liquid impact problems. Journal of Fluid Mechanics 297, 193, 1995.

G. Cuomo, W. Allsop, S. Takahashi. Scaling wave impact pressures on vertical walls. Coastal Engineering 57, 604–609, 2010b.

www.deafsluitdijk.nl. Visited at 06-06-29. URL <https://deafsluitdijk.nl/wp-content/uploads/2014/05/presentatie-RWS-en-Levvel-stakeholderbijeekomst-2018-04-23.pdf>

E. de Almeida. Results from scale model tests performed for DynaHicS project, 2019

Y. Goda. Random seas and design of maritime structures. University of Tokyo Press, 1985.

Google Maps. Visited at 18-02-19. URL <https://www.google.nl/maps>

C.M. Harris and C.E. Crede. Shock And Vibration Handbook. McGraw-Hill Engineering, 1961.

B. Hofland, M. Kaminski, G. Wolters. Large scale wave impacts on a vertical wall. Coastal Engineering Proceedings 1, 15, 2010.

www.hollandluchtfoto.nl. Visited at 06-06-19. URL <http://www.hollandluchtfoto.nl/-/galleries/dorpensteden/noord-holland/den-oever/-/medias/ed36592c-0bb8-4ed4-983e-9e699351bf5a-den-oever-luchtfoto>

L.H. Holthuijsen. Waves in oceanic and coastal waters. Cambridge University Press, Delft University of Technology, 2007.

- T.H.G. Jongeling and C. Erdbrink. Dynamica van beweegbare waterkeringen. Technical report, Deltares, 2010.
- S.N Jonkman, R.D.J.M Steenbergen, O. Morales-Nápoles, A.C.W.M Vrouwenvelder, J.K. Vrijling. Lecture notes Probabilistic design CIE4130: Risk and Reliability Analysis in Civil Engineering. Delft University of Technology, November 2016.
- P.A. Kolkman. Flow-induced gate vibrations: Prevention of self-excitation computation of dynamic gate behaviour and the use of models. Doctoral thesis, Technische Hogeschool Delft, 1976.
- P. A. Kolkman. A simple scheme for calculating added mass of hydraulic gates. Technical Report 439, Delft Hydraulics, December 1990.
- P.A. Kolkman and T.H.G. Jongeling. Dynamische gedrag van waterbouwkundige constructies. Delft Hydraulics, 1996.
- M.S. Longuet-Higgins. On the joint distribution of wave periods and amplitude. Proceedings of the Royal Society of London, Vol 389, Paper No 1797, pp 241-258, 1983.
- A.V. Metrikine. Lecture notes Dynamics, Slender Structure and an Introduction to Continuum Mechanics ct4145. Delft University of Technology, August 2006.
- R. Miche. Mouvements ondulatoires des mers en profondeur constante on décroissante. Annales des Ponts et Chaussées, 1944.
- J.R. Morison, J.W. Johnson, M.P. O'Brien, S.A. Schaaf. The Force exerted by surface waves on piles. Petroleum Transactions, American Institute of Mining Engineers, Vol. 189, pp.149-154, 1950.
- NEN-EN 1991-1-4: Eurocode 1: Actions on structures - Part 1-4: General Actions - wind actions. 2005.
- Publieksbrochure Project Afsluitdijk. Rijkswaterstaat, August 2016.
- L. Rundgren. Water wave forces – a theoretical and laboratory study. Kungliga Tekniska Hogskolans handlingar, 1958.
- G. Sainflou. Essai sur les digues maritimes verticales. École nationale des Ponts et Chaussées, 1928.
- J. Spijkers, A. Vrouwenvelder, E. Klaver. Lecture notes Structural Dynamics ct4140: Part 1 - Structural Vibrations. Delft University of Technology, January 2005.
- J. T. Thijsse. Een Halve Eeuw Zuiderzeewerken. 1972.
- O.C. Tieleman. The dynamic behaviour of pump gates in the Afsluitdijk. Master's thesis, Delft University of Technology, February 2015.
- O.C. Tieleman, A. Tsouvalas, B. Hofland, Y. Peng, S.N. Jonkman. A three dimensional semi-analytical model for the prediction of gate vibrations immersed in fluid. Elsevier, 2019.

O.C. Tieleman, B. Hofland, S.N. Jonkman. Bending Vibrations of the Afsluitdijk Gates Subjected to Wave Impacts: A Comparison of two Design Methods. Proceedings of the 34th PIANC World Congress, 2018.

M. Versluis. Hydrodynamic pressures on large lock structures. Master's thesis, Delft University of Technology, April 2010.

R.F. Vorderegger. Optimization of gate design in the Afsluitdijk based on dynamic wave impact: Application of fluid-structure interaction models coupled with FEM. Master's thesis, Delft University of Technology, April 2019.

H.M. Westergaard. Water Pressures on Dams During Earthquakes. Transactions, American Society of Civil Engineers (ASCE), Vol. 98, Paper No. 1835, pp. 418–433, 1933.

Witteveen+Bos. Herbeschouwing systeemontwerp noordelijke hefschuiven van spuicomplexen Den Oever en Kornwerderzand naar aanleiding van schaalmodelproeven Deltares. 2016.

Nomenclature

Roman

Symbol	Description	Unit
a	Shape parameter Weibull distribution	-
A	Amplification factor	-
A	Surface area	m^2
A_{km}	Structural modal coefficients	-
A_w	Amplitude of the incident wave	m
b	Scale parameter Weibull distribution	-
B_{pr}	Fluid modal coefficients	-
c	Damping	Ns/m
c_{crit}	Critical damping	Ns/m
C_d	Resistance coefficient	-
C_l	Lift coefficient	-
C_m	Inertia coefficient	-
c_p	Sound velocity in water	m/s
C_r	Reflection coefficient	-
C_w	Hydrodynamic damping/added damping	Ns/m
C_w	Coefficient for flow resistance	-
$C_{w,radiation}$	Added damping due to radiation per unit wave width	Ns/m
D	Plate bending stiffness	Nm^2
D_n	Amplitude of eigenmode n	m
dx	Gate interval width	m
dz	Gate interval height	m
E	Elasticity modulus	N/m^2
f	Excitation frequency	$Hz = s^{-1}$
F	Force	N
$f(x;a,b)$	Probability density function for Weibull distribution	-
$F(x;a,b)$	Cumulative distribution function Weibull distribution/Exceedance probability	-
F_0	Maximum force amplitude	m
$F_{im,0.1\%}$	Design wave impact force	N
f_e	Time signal of the external force distribution of the plate	N/m^2
F_{im}	Impulsive wave impact force	N
F_l	Lift force per unit length in vertical direction	N
$F_{max,im}$	Peak force of impulsive wave force	N
$F_{max,qs}$	Peak force of quasi-static wave force	N
f_n	Natural frequency/Eigen frequency	$Hz = s^{-1}$
F_{qs}	Quasi-static force	N
F_r	Reaction force/Dynamic response of the structure	N
F_y	Yield strength	N/m^2
h	Water depth	m
H	Wave height	m
H_i	Incident wave height	m
H_{max}	Maximum wave height	m
H_s	Significant wave height	m
I	Moment of inertia	m^4
I_{im}	Wave impact impulse	Ns
k	Spring stiffness	N/m
k	Wave number	m^{-1}

Roman (continued)

Symbol	Description	Unit
K_w	Hydrodynamic stiffness/added stiffness	N/m
$K_{w,flow}$	Added stiffness due to flow	N/m
$K_{w,immersion}$	Added stiffness due to immersion	N/m
$K_{w,sudden}$	Sudden stiffness	N/m
L	Wave length	m
L_x	Gate/structure width	m
L_z	Gate/structure height	m
m	Mass	kg
M	Bending moment	Nm
m_w	Hydrodynamic mass/added water mass	kg
p	Wave impact pressure	N/m ²
P	Pressure impulse	Ns/m ²
\bar{P}	Dimensionless pressure impulse	-
p_0	Ambient pressure	N/m ²
p_f	Fluid pressure	N/m ²
p_{max}	Maximum impact pressure	N.m ²
Q	Shear force	N
r	Reflection coefficient	-
R_c	Freeboard	m
s	Skewness parameter	-
s	Streamline element vector	m
t	Gate thickness	m
t	Time	s
t_a	Decay time of wave impact	s
t_{begin}	Start time wave impact	s
t_{end}	End time wave impact	s
T_k	Period of the oscillations of the downward flank	s
T_n	Eigen period of structure	s
T_p	Peak wave period	s
t_s	Rising time of wave impact	s
u	Horizontal orbital velocity in the axis of the structure	m/s
U	Impact velocity	m/s
u_0	Assumed time function of the response	-
v	Velocity	m/s
V	Fluid velocity vector	m/s
V	Shear force	N
w	Deflection in z-direction	m
W	Overhang width	m
w_0	Assumed shape function of the response	-
X_{dyn}	Displacement of a structure including dynamic effects	m
$X_{max,DAF}$	Maximum displacement determined with DAF method	m
$X_{max,max}$	Maximum displacement of structure	m
$X_{max,static}$	Static displacement corresponding to maximum wave impact force	m
$X_{max,real}$	'Real' maximum displacement determined for wave field	m
X_{stat}	Displacement of a structure due to a static force	m
$X_{stat,wave\ impact}$	Displacement of the system for a static load with the magnitude of the amplitude of the wave impact	m
y	Displacement in y-direction	m
y_0	Maximum displacement in y-direction	m

Greek

Symbol	Description	Unit
γ	Relative damping	-
$\Delta_{DAF,Real}$	Percentual difference between the dynamic amplification factor found with the DAF method and found by running the full wave signal in the SDOF model	%
ζ	Damping ratio	-
κ	Curvature	m^{-1}
λ	Froude scaling factor	-
λ_n	Wave length of the n^{th} eigenfunction	m
ν	Poisson's ratio	-
ρ	Density	kg/m^3
ρ_f	Fluid density	kg/m^3
ρ_s	Distributed mass per unit surface	kg/m^2
$\rho_{s,w}$	Distributed added water mass per unit surface	kg/m^2
σ	Stress	N/m^2
τ	Wave impact duration	s
φ	Velocity potential	m^2/s
ω_n	Dry natural radial frequency/Radial eigen frequency	Rad/s
$\omega_{n,w}$	Wet natural radial frequency/Radial eigen frequency	Rad/s

Notations

Symbol	Description
X	Matrix
x	Vector

Abbreviations

Symbol	Description
DAF	Dynamic amplification factor
DAF_M	Dynamic amplification factor related to wave impact impulse

List of Figures

Figure 1: (Title page) Aerial photo of discharge sluice complex at Den Oever	2
Figure 2: Overview Afsluitdijk	1
Figure 3: Sluice complexes at Den Oever (left) and Kornwerderzand (right)	2
Figure 4: Wave impacts on the defence beams of the old sluice gates of the Afsluitdijk	3
Figure 5: Overview of report structure	7
Figure 6: Improvements of the DAF method in time and space, report structure.....	7
Figure 7: Schematisation of relationship between load and response.....	9
Figure 8: Schematic wave impact pressure developments in time, a) No entrapped air, b) Entrapped air	11
Figure 9: Typical time history of a wave impact on a (vertical) wall with or without a horizontal overhang	12
Figure 10: Mass-spring-dashpot single degree of freedom system.....	15
Figure 11: Maximax response curves for different load shapes	18
Figure 12: Maximax response curves for different triangular load shapes.....	18
Figure 13: Maximax response curves for different triangular load shapes.....	19
Figure 14: Flow field of vertically vibrating L-shaped gate in an added water mass.	22
Figure 15: a) Schematisation of bending beam undergoing transverse motion, b) Differential element of the bending beam subject to shear force (V), bending moment (M) and an external load (q_1)	23
Figure 16: The first three eigenmodes of a simply supported bending beam	24
Figure 17: Eigenfrequencies and eigenmodes of bending beam for different support types	25
Figure 18: Plate loaded perpendicular to its plane	26
Figure 19: Relation scheme for thin plates loaded perpendicular to their plane	26
Figure 20: Overview of the plate model in space	28
Figure 21: Spatial distribution of wave impact force, for four moments in time.....	32
Figure 22: Vertically integrated wave force and the wave pressure amplitudes for the 10 intervals over the vertical of the gate as defined in Figure 21 over time	32
Figure 23: Improvements of the DAF method in time and space, report structure.....	33
Figure 24: Mass-spring-dashpot single degree of freedom system.....	34
Figure 25: Overview of the plate model in space	34
Figure 26: a) Triangular force schematisation, b) Time response of the SDOF, c) Maximax response curve for symmetrical triangular load, $\zeta = 5\%$	36
Figure 27: Maximax response curves for triangular loads with different rising time, with ($\zeta = 5\%$) and without ($\zeta = 0\%$) damping	37
Figure 28: Position of the pressure sensors on the structure used during the lab-test (Left), schematisation test setup (right)	38

Figure 29: Test setup wave flume with wall with overhang at the left (left), wall with overhang zoomed in (right).....	39
Figure 30: a) Time series of total force on the gate per meter width – scaled, b) Time series of total force on the gate per meter width – scaled and zoomed in.....	40
Figure 31: Used definition for the wave impact peak force ($F_{max,im}$), wave impact duration ($\tau = t_{end} - t_{begin}$), and wave impact impulse (I_{im}) (wave 311).....	40
Figure 32: Histogram peak forces (left), histogram wave impact duration (middle), histogram wave impact impulses (right)	41
Figure 33: Triangular schematisation of maximum wave impact (wave 311)	41
Figure 34: Influence of the vibration from the previous wave impact on the maximum response to the next wave impact (waves 141 and 142).....	44
Figure 35: Comparison real response for wave impact 124 and response for wave impact 124 with zero initial conditions	45
Figure 36: Two definitions of the impact duration (wave 311)	47
Figure 37: Influence of impact duration on DAF.....	48
Figure 38: Wave impact peak forces versus wave impact impulses, (scaled, $\lambda = 12.08$)	52
Figure 39: Weibull distribution fit for the wave impact peak forces, the best fit Weibull distribution is for $a = 36.0$ and $b = 1.8$, and pdf wave impact peak forces (F_{im}), (scaled, $\lambda = 12.08$)	53
Figure 40: Weibull distribution fit for the wave impact impulses, the best fit Weibull distribution is for $a = 4.0$ and $b = 2.0$, and pdf wave impact impulses (I_{im}), (scaled, $\lambda = 12.08$)	53
Figure 41: Overview test set-up load cells and pressure sensors	54
Figure 42: Load cell force data and load cell pressure data (scaled, $\lambda = 12.5$), wave 1.....	55
Figure 43: Definition skewness parameter for investigation width distribution of load cell data, front view of gate	56
Figure 44: Positive and negative skewness, front view of gate	57
Figure 45: Relation between skewness and wave impact amplitude (scaled, $\lambda = 12.5$)	57
Figure 46: Weibull distribution fit for the wave period, the best fit Weibull distribution is for $a = 4.75$ and $b = 5.9$, pdf wave period (T), load cell 2 (scaled, $\lambda = 12.5$)	58
Figure 47: a) probability of exceedance curve wave height for $H_s = 0.75$ m, b) pdf for $H_s = 0.75$ m.....	59
Figure 48: Relation between wave height and wave period	59
Figure 49: a) Histogram wave impact duration, load cell 2 (scaled, $\lambda = 12.5$), b) Probability of exceedance curve wave impact duration for $T_{min} = 0$ s, $T_{middle} = 0.2$ s and $T_{max} = 0.4$ s, c) pdf wave impact duration	60
Figure 50: Gumbel distribution fit for the skewness parameter, pdf skewness parameter (s), based on skewness of top load cell row (LC 2,3,7)	61
Figure 51: Probability density functions of the probabilistic input parameters: H, T, s and τ	64
Figure 52: a) Definition parameters, b) Configuration 1-6, c) scaled ($\lambda = 12.5$) test set up in 1-6 configuration.....	65
Figure 53: Vertical pressure impulse distribution for the scaled model test gate ($\lambda = 12.5$), for regular and irregular waves	66

Figure 54: Height distribution of the wave pressure over the vertical of the gate at four moments during wave impact	67
Figure 55: Definition skewness parameter 'model' signal.....	67
Figure 56: Triangular schematisation in time	68
Figure 57: Mirrored 'model' 3D pressure field over the full gate surface during the maximum impact (p_{max})	68
Figure 58: a) Mirrored 3D pressure field over the full gate surface during the maximum impact force, b) Definition intervals (in space) over the gate (scaled, $\lambda = 12.5$).....	69
Figure 59: Definition individual waves, based on load cell 2 data (scaled, $\lambda = 12.5$)	70
Figure 60: Force-time signals of a single wave from the 'real-' and 'model' signals.....	71
Figure 61: a) Histograms for the maximum pressures for the 'real' and 'model' signal, b) Probability of exceedance curves for the maximum pressures of the 'real' and 'model' signal.....	71
Figure 62: First modal shape of the case study gate, maximum deflection at $(x,z) = (5,7.5)$ m	72
Figure 63: a) Histograms for the maximum deflections for the 'real' and 'model' signal, b) Probability of exceedance curves for the maximum deflections of the 'real' and 'model' signal	73
Figure 64: Force-time signals of symmetrical and non-symmetrical triangular schematisation of the 'model' signal, wave 1	74
Figure 65: a) Histograms for the maximum deflections for model signals 1 and 2, b) Probability of exceedance curves model signals 1 and 2	75
Figure 66: Improvements of the DAF method in time and space, report structure.....	76
Figure 67: a) Boundary conditions of the case study gate, b) Assumed shape function $w_0(x,z)$ for the case study gate.....	78
Figure 68: Probability of exceedance curve maximum deflection, validation equivalent SDOF model.....	79
Figure 69: Probability of exceedance curve maximum deflection, comparison SDOF model and MDOF model	79
Figure 70: Contribution of the different modes on the response for three gates (a) $\tau/T = 1.1$, b) $\tau/T = 0.1$, c) $\tau/T = 5.0$, taking into account 25 structural modes.....	80
Figure 71: Definitions skewness parameter	82
Figure 72: Influence of positive or negative symmetrical skewness on response.....	84
Figure 73: a) Data points 'old' scale model tests, b) recommended data points for 'new' scale model tests	92
Figure 74: Frequency and water depth regions for which surface waves and compressibility play a role for two-dimensional fluid system.....	115
Figure 75: : Position of the pressure sensors on the structure used for the lab-test.....	120
Figure 76: Individual pressure signals of one wave impact	120
Figure 77: a) Time series of total force on the gate per meter width, b) Time series of total force on the gate per meter width - zoomed in	121
Figure 78: Time series of total force on the gate per meter width – scaled, b) Time series of total force on the gate per meter width – scaled and zoomed in.....	122

Figure 79: Load cell force data and load cell pressure data (unscaled), wave 1	122
Figure 80: Load cell force data and load cell pressure data (scaled, $\lambda = 12.5$), wave 1	123
Figure 81: Using the intersection points of the impulsive wave force signal and quasi-static wave force signal to define the wave impact duration	124
Figure 82: Used definition for the wave impact peak force ($F_{\max,im}$), wave impact duration ($\tau = t_{\text{end}} - t_{\text{begin}}$), and wave impact impulse (I_{im}) (wave 311)	125
Figure 83: a) Current discharge sluice complex at Den Oever, b) Design of the new discharge sluice complex at Den Oever by consortium Level	128
Figure 84: Top view of tower discharge sluices at Den Oever	129
Figure 85: a) Schematisation of the cross-section of the current situation at Den Oever (with defence beam), b) schematisation of the cross-section of the new situation at Den Oever (defence beam is removed)	129
Figure 86: a) Conceptual 'real' flood gate design for the Afsluitdijk, with horizontal and vertical stiffeners, b) Boundary conditions for simplified case study gate (flat thin plate) used for this research, F = free edge, S = simply supported edge	130
Figure 87: Definition extrapolation points at the left half of the gate	131
Figure 88: Time signal of one wave impact (wave 1) for load cell data and interpolated data points	132
Figure 89: Definition intervals (in space) over the gate, scaled $\lambda = 12.5$	132
Figure 90: Mirrored 3D pressure field over the full gate surface during the maximum impact force (scaled, $\lambda = 12.5$), wave 1	134
Figure 91: Definition individual waves, based on load cell 2 data (scaled, $\lambda = 12.5$)	135
Figure 92: Histogram wave duration (left), histogram impact duration (right), based on load cell data 2 (scaled, $\lambda = 12.5$)	135
Figure 93: Structural modal shapes for case study gate	137
Figure 94: a) Boundary conditions of the case study gate, b) Assumed shape function $w_0(x,z)$ for the case study gate	139

List of Tables

Table 1: Froude scaling for wave impact data	39
Table 2: Amplification factors obtained with the DAF method, and by running the whole force-time signal (wave field) with the SDOF model.....	42
Table 3: Damping factor for the amplitude of a damped SDOF system	44
Table 4: Comparison amplification factor for the real maximum response, and amplification factor for the maximum response for wave impact 124 with zero initial conditions	46
Table 5: Percentual differences between the dynamic amplification factors found with the DAF method and found by running the full wave signal in the SDOF model.....	49
Table 6: Froude scaling for load cell data	55
Table 7: Parameters values used for the composition of the 'model' force-time signal.....	63
Table 8: Contribution of the different modes on the response for three gates, taking into account 25 structural modes.....	80
Table 9: Correction factor average force, for symmetrical skewness definition	82
Table 10: Results from skewness parameter analysis, for MDOF and SDOF model	83
Table 11: Froude scaling factors for wave impact data	121
Table 12: Case parameters	130
Table 13: Correction factor average force, maximum deflections	136

A Quasi-static wave loads

When the wave conditions are known analytical methods are available to determine the wave loads. For the analytical methods a design wave with a certain height, period and direction is used. The determination of this design wave from a wave field is out of the scope of this research, and reference is made to the book 'Waves in oceanic and coastal waters' (Holthuijsen, 2007) for more information on this topic. A distinction can be made between slender and non-slender structures. For slender structures the wave field is almost undisturbed and the wave load will consist of an inertia term and a resistance term. For non-slender structures the wave forces are determined by diffraction and reflection phenomena. In the hydraulic sector the following definition of slender structures is used:

$$\frac{D}{L} < 0.05 - 0.2 \quad (A.1)$$

In which: D = dimension of the structure perpendicular to the wave direction [m]
L = wave length [m]

It has to be noted that the equations from the literature are strong simplifications from reality, so the equations have to be used with care. (Kolkman and Jongeling (1996))

A.1 Analytical methods for slender structures

For slender structure the equation of Morison (Morison, Johnson, O'Brien and Schaaf (1950)) is mostly used, this equation is given by equation A.2. With this equation the quasi-static wave load in the direction of the waves, for slender, vertical structure can be determined. The load consists of an inertia force and a resistance force.

$$F = C_m \rho V \frac{du}{dt} + C_d \frac{1}{2} \rho D u |u| \quad (A.2)$$

In which: F = quasi-static wave force per unit length in vertical direction [N/m]
C_m = inertia coefficient [-]
ρ = density of water [kg/m³]
V = volume of the structure per unit length in vertical direction [m³/m]
C_d = resistance coefficient [-]
D = transverse dimension of the structure perpendicular on the wave direction [m]
u = horizontal orbital velocity in the axis of the structure (calculated as if the structure is not present) [m/s]

The horizontal orbital velocity varies with the depth, at the water surface the velocity is the biggest and at the bottom the velocity is the smallest. This means that the wave load also varies with depth (the position below the water level). The horizontal orbital velocity used in equation A.2 is the maximum velocity u_m. Often linear wave theory is used to calculate the horizontal orbital velocity:

$$u = \frac{\omega H \cosh k(d+z)}{2 \sinh kd} \sin(\omega t - kx) \quad (A.3)$$

In which: ω = 2π/T = radial wave frequency [rad/s]

H = wave height [m]
 $k = 2\pi/L$ = wave number [m^{-1}]
 L = wave length [m]
 T = wave period [s]
 d = water depth (still water) [m]
 z = coordinate in vertical direction (positive upward and with the origin at the still water level) [m]
 x = horizontal coordinate in direction of propagation of the waves (zero if the origin is in the heartline of the structure) [m]

The velocity is harmonic (a sinus), so the acceleration (du/dt) is 90° out of phase with the velocity. This means that the extreme values of the inertia term and resistance term are also 90° out of phase, and the maxima of both terms will never occur at the same time. The inertia- and resistance coefficient (C_m and C_d) from equation A.2 differ for different structure geometries. Another factor influencing this coefficient is the roughness (k) of the structures. In the literature graphs are available for the determination of the inertia- and resistance coefficients, for different geometries.

The inertia- and resistance forces are working in the same direction as the wave propagation. For stationary flow also a force perpendicular to the wave direction is caused by the wave motion, this is a fluctuating lift force:

$$F_l = C_l \frac{1}{2} \rho D u^2 \quad (A.4)$$

In which: F_l = lift force per unit length in vertical direction [N/m]
 C_l = lift coefficient [-]

The lift coefficient C_l also depends on the geometry of the structure and the roughness. (Kolkman and Jongeling (1996))

A.2 Analytical methods for non-slender structures

For non-slender structures the quasi-static wave loads are mainly determined by diffraction and reflection phenomena. For infinitely long structures and wave crests, incoming perpendicular to the structure, the problem can be reduced to a two-dimensional reflection problem. For perpendicular reflection a standing wave pattern will be generated, according to linear wave theory the following equation holds for the pressure in the vertically standing wave:

$$p = -\rho g z + \rho g \frac{H \cosh k(d+z)}{2 \cosh kd} \cos(kx) \cos(\omega t) \quad (A.5)$$

In which: $H = (1+r)H_i$ = wave height of the standing wave [m]
 H_i = incoming wave height [m]
 r = reflection coefficient [-]
 x = horizontal coordinate from the reflection point (at the vertical wall: $x=0$) [m]

In this equation no mean water level increase is taken into account, it is a first order approach. For a global estimation of the quasi-static wave load on a vertical wall the following approximation can be used. The wave pressure from the free water surface until the still water level is assumed hydrostatic, and from the still water level until the bottom the wave pressure is assumed constant.

This wave pressure added to the hydrostatic water pressure gives also a hydrostatic total pressure, with a maximum and minimum value at the bottom of:

$$p_{max} = \rho g(d + A) \quad (A.6)$$

$$p_{min} = \rho g(d - A) \quad (A.7)$$

In which A is the local wave amplitude in meters.

There are also equation developed in which mean water level increase is taken into account, this gives a second order approach. One of this equations is the equation developed by Sainflou (1928), this equation gives the wave load on a vertical wall caused by a standing, non-breaking wave. When the waves are breaking wave impacts can occur, the wave impact pressures are much higher than the quasi-static wave pressures and will be discussed in paragraph 2.1. From measurements it is known that the equation developed by Sainflou (1928) gives an overestimation of the wave load for steep waves. The equations are adjusted by Rundgren (1958) based on the higher-order wave theory developed by Miche (1944). The equations of Sainflou and Rundgren/Miche are used in CERC (1984) in the form of graphs from which the wave load can be determined. The latest developments of the equation are made by Goda (1985), he developed equations to determine the wave loads on vertical breakwaters.

The equations described above are only valid for two dimensional reflection problems. When the structure has small dimensions the diffraction problem also has to be solved. This is mostly done by the use of numerical techniques (diffraction models). For quasi-static wave loads, working on supported structures it is a good starting point to assume that the construction is rigid and does not move relative to the supports. This assumption can be made due to the elastic properties of the structure. When for instance a structure bends due to wave pressures, this deflection does not have influence on the magnitude of the wave load. For hinged connections the movement of the structure due to the wave loads will be much larger, the quasi-static wave loads will be a function of the degree of movement in this case. (Kolkman and Jongeling (1996))

B The hydrodynamic terms

B.1 Factors influencing the added terms

There are a couple of factors that can influence the added terms (m_w , c_w and k_w). The most important factors are:

- The influence of the free water surface and wave radiation
- The influence of flow (compared to stagnant water)
- The presence of a wall or other closed plane in the vicinity of the vibrating structure

When a wall or other closed plane is present in the vicinity of the vibrating structure, the added water mass will increase. The influence of the other two factors require a little more explanation.

The free water surface can influence the added water mass and added damping. On the free water surface radiation surface waves can develop due to the vibration of a structure, the presence of this waves can make the added water mass and added damping frequency dependent. The wave pressures related to longer waves penetrate deeper than the pressures related to short waves, so the influence of long waves on the added terms will be much bigger than the influence of short waves. According to Jongeling and Erdbrink (2010) the added water mass will be strongly frequency dependent in the following low excitation frequency range:

$$\frac{\omega^2 h}{g} < 10 \quad (B.1)$$

In which: h = water depth [m]
 g = gravitational acceleration [m/s²]

However vibration problems mainly are about high vibration frequencies, this means that the developed waves have short wave lengths and the penetration depths are small. The influence of wave radiation on the added terms is small in this case, the added water mass will not be frequency dependent for high excitation frequencies (and will go to a constant value), and the added damping will even go to zero. In this case the pressure at the free water surface will be constant (equal to the atmospheric pressure), this means that the water surface will only move up and down with the movement of the vibration.

It can be concluded that the free water surface can influence the added terms considerably, but that for most of the vibration problems the vibration frequencies will be high enough to neglect the influence of the formed radiation waves. (Jongeling and Erdbrink (2010), Kolkman and Jongeling (1996))

Most of the time the added terms are determined in the stagnant water condition, this is because the determination of this terms in flowing water is very complex and requires the usage of the complete Navier-Stokes equation. To get an impression of the influence of the flow condition (compared to the stagnant water condition), the flow will be split into a permanent flow part and a periodic fluctuating flow part. The periodic fluctuations will be caused by the vibrating structure. In equation 2.6 The Navier-Stokes equation in x-direction is given. The velocities in x,y and z direction are u,v and w for the permanent flow field, and the dynamic components that are coupled to the vibrations are u',v' and w'. In equation B.2 the viscous terms are left out.

$$\frac{\partial(p + p')}{\partial x} = -\rho \frac{\partial(u + u')}{\partial t} - \rho(u + u') \frac{\partial(u + u')}{\partial x} - \rho(v + v') \frac{\partial(u + u')}{\partial y} - \rho(w + w') \frac{\partial(u + u')}{\partial z} \quad (B.2)$$

The first term on the right hand side is the local acceleration and the other terms are the convective accelerations. The local acceleration is the rate of change of the velocity with respect to time at a given point in the flow field, and the convective accelerations are the rate of change of the velocity due to the change of position of a fluid particle in the flow field. For non-permanent phenomena, like waves, the local acceleration term is the most important. For the permanent phenomena ($u' = 0$ and $\partial u' / \partial t = 0$) the convective acceleration terms are the most important. These terms lead to the stationary forces on a structure. The additional pressure field (p') that is caused by the vibrations of the structure is described by the following equation:

$$\frac{\partial p'}{\partial x} = -\rho \frac{\partial u'}{\partial t} - \rho \left(u' \frac{\partial u}{\partial x} + u \frac{\partial u'}{\partial x} \right) - \rho \left(v' \frac{\partial u}{\partial y} + v \frac{\partial u'}{\partial y} \right) - \rho \left(w' \frac{\partial u}{\partial z} + w \frac{\partial u'}{\partial z} \right) + \dots \quad (B.3)$$

The terms with a product of u' can be neglected when the vibration velocities (u') are small compared to the initial flow velocities (u). The terms that are proportional to $\partial u' / \partial t$, the acceleration of the vibrating structure, deliver the added water mass m_w . The terms that are proportional to u' , the velocity of the vibrations, deliver the added damping c_w . This type of damping is called flow damping.

It can be concluded that the added water mass is not depending on u , the initial flow field, so for the calculation of the added water mass it suffices to limit the calculations to the stagnant water condition. The added damping is proportional to the initial flow field. (Kolkman and Jongeling (1996))

B.2 Determination of the hydrodynamic mass

In sections B.2, B.3 and B.4 the hydrodynamic terms (added terms) are explained in more depth and possible calculation methods known from the literature are discussed. The determination of the added terms is a really difficult task and the different methods have a lot of restrictions. When a certain method is chosen it is important to know the restrictions and assumptions that are made during the derivation of the method.

In the previous section it is concluded that the calculation of the added mass is always for the stagnant water condition. When the calculation also assumes irrotational flow and neglect of viscosity of the water, there is potential flow. Potential flow can occur for both compressible and incompressible fluid. If wave radiation can also be neglected, so the influence of the waves generated by the vibrations of the structure can be neglected, the velocities in the whole flow field are in phase with each other, and also in phase with the velocity of the vibrations of the structure. In this case the flow pattern behaves like a periodically varying, quasi-permanent flow field. This means that potential flow is similar to permanent flow when wave radiation is neglected, so the available classical methods can be used to solve the flow.

The equations that are valid for potential flow can be used as a basis for the determination of the added water mass. The basic equation of potential flow is:

$$\frac{\partial \Phi}{\partial \mathbf{s}} = -\mathbf{V} \quad (B.4)$$

In which: Φ = velocity potential vector [m²/s]
 \mathbf{s} = streamline element vector [m]
 \mathbf{V} = fluid velocity vector [m/s]

For potential flow the following also applies:

$$u = -\frac{\partial \Phi}{\partial x}, v = -\frac{\partial \Phi}{\partial y}, w = -\frac{\partial \Phi}{\partial z} \quad (B.5)$$

In which u,v and w are the flow velocities in x,y and z direction. For incompressible flow the following continuity equation has to be fulfilled:

$$\frac{\partial u}{\partial x} + \frac{\partial v}{\partial y} + \frac{\partial w}{\partial z} = 0 \quad (B.6)$$

Combined with equation B.5 this gives the Laplace equation:

$$\frac{\partial^2 \Phi}{\partial x^2} + \frac{\partial^2 \Phi}{\partial y^2} + \frac{\partial^2 \Phi}{\partial z^2} = 0 \quad \text{or} \quad \nabla^2 \Phi = 0 \quad (B.7)$$

In literature various methods are described to determine the added water mass. The different methods all have their own validity, if a method can be used depends on the assumptions that are made during the derivation of the method. For instance is the water assumed compressible or incompressible, is wave radiation neglected (are surface wave taken into account, what is the geometry of the structure, is the structure fully submerged in water or is the water only at one side. In the Master thesis work of Tieleman (2015) equations are derived to determine the added water mass for a two-dimensional schematisation of a beam, this equations are compared to two well-known methods from the literature: the simple scheme of Kolkman (1990) to determine the added mass of hydraulic gates, and the method of Westergaard (1933). The method of Westergaard is developed to determine the hydrodynamic pressure for a vertical dam during earthquakes. The simplifications that are used for this model are: the dam is infinitely long and rigid, the reservoir extends to the infinity and the pressure at water level is zero (Thesis work of Versluis (2010)). However according to the Master thesis work of Versluis (2010) the expressions used in this method can also be used for large lock gates (which generally have a finite reservoir and smaller water levels), keeping all the made simplifications and assumptions in mind. In the Master thesis work of Tieleman (2015) distinction is made between three regions of radial excitation frequencies:

- | | | |
|--|--------------------|---------|
| a) Significant influence of surface waves | $\omega < 8$ | [rad/s] |
| b) Transition region with approximately zero surface pressure and incompressible fluid | $8 < \omega < 100$ | [rad/s] |
| c) Significant influence of fluid compressibility | $100 < \omega$ | [rad/s] |

For the transitional region the problem is simplified a lot by the assumptions of zero surface pressure and incompressible fluid, and an analytical solution for the hydrodynamic mass is derived for this region:

$$m_{w,total} = \rho_f \sum_{p=1}^{\infty} \frac{5}{18k_{z,p}^3}, \text{ with } k_{z,p} = \frac{(2p-1)\pi}{2h} \quad (B.8)$$

In which: ρ_f = fluid density [kg/m³]
 k_z = spring stiffness in z-direction [N/m]
 h = water depth [m]

This analytical solution differs a bit from the simplified Westergaard shape (Westergaard (1933)). In Figure 74 the limits of the different regions are displayed using 5% deviation lines. The red line on the left indicates a 5% deviation of the total added mass when surface waves are not included, and the red line on the right indicates a 5% deviation when compressibility of the water is not included. The dotted lines in Figure 74 indicate the maximum and minimum water level at Den Oever. The case study of the Master thesis work of Tieleman (2015) was the Afsluitdijk, and the master thesis of Shannon Sleuwaegen continuous with this case study. For example, for the maximum water level at Den Oever the transition region schematisation will be valid from approximately 8 to 103 rad/s. For wave excitations with lower radial frequencies the system cannot be schematized as the transition region, and surface waves have to be taken into account when the added mass is calculated. The simple analytical solution given in equation B.8 can not be used in this case.

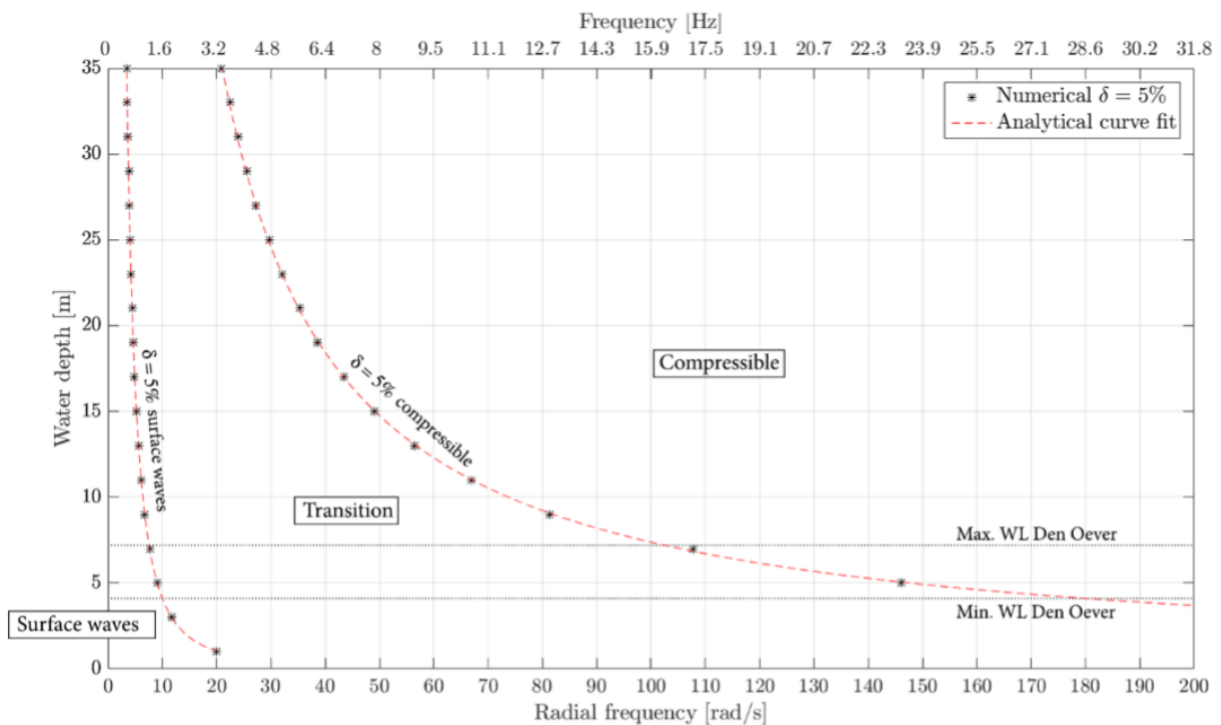


Figure 74: Frequency and water depth regions for which surface waves and compressibility play a role for two-dimensional fluid system. (Thesis work of Tieleman (2015))

Figure 74 can be used to get a quick indication of the validity regions for given excitation frequencies and water depths. From the validity region it is known which assumptions can be made in a certain two-dimensional case with closed bottom boundary and free surface (compressible or incompressible fluid and include or not include surface waves). When this is known it can be decided which methods from the literature are valid for this case, and if the analytical solution derived by Tieleman (2015) is valid. For instance the quick scheme from Kolkman (1990) is only valid in the transitional zone, because this scheme assumes zero surface pressure and incompressible flow.

B.3 Determination of the hydrodynamic damping

Strong damping ensures that the response of a structure is limited. The amplification factor is smaller for larger damping. Besides the mechanical damping of the structure (c), added damping (c_w) can be present due to the water. There are a couple of factors that can induce added damping:

- 1) Radiation waves: there will be energy loss due to the waves excited by the vibrations of the structure.
- 2) Viscous damping.
- 3) Strong flow: it is important to note that flow can induce strong damping, however the flow can also add energy to the structure by which the structure starts moving. So strong flow can lead to damping or excitation of the structure. According to Kolkman and Jongeling (1996) this factor is the most important one.

The added damping due to radiation waves for a horizontally vibrating, deep gate is given by equation B.9 (Kolkman (1976)).

$$c_{w,radiation} = \frac{2\rho g^2}{\omega^3} \quad (B.9)$$

In which $c_{w,radiation}$ is the added damping due to radiation per unit of gate width. From this equation it can easily be seen that for higher excitation frequencies the damping will soon become small.

For structures vibrating in the same direction as the flow direction the added damping can easily be derived. When a structure is vibrating the magnitude of the relative flow velocity (the flow velocity relative to the structure) and the flow angle will change. As long as the relative flow deviates little from the flow velocity in stationary conditions, linearization techniques can be used to solve the problem. The flow force (flow resistance) and flow velocity are related quadratic by the following equation:

$$F_{perm} = C_w \frac{1}{2} \rho V^2 L^2 \quad (B.10)$$

In which: C_w = coefficient for flow resistance [-]
 V = flow velocity in undisturbed condition [m/s]
 L = a measure for the frontal surface [m²]

When the structure is vibrating the relative flow velocity will change (equation B.11) which results in a change of the flow force (equation B.12).

$$V = V_{perm} - \frac{dy}{dt} = V_{perm} + dV \quad (B.11)$$

$$dF = \frac{\partial F}{\partial V} dV = -C_w \rho V L^2 \frac{dy}{dt} \quad (B.12)$$

The added damping can be calculated by dividing the 'counterforce' by the vibration velocity:

$$c_w = \frac{dF}{\frac{dy}{dt}} = C_w \rho L^2 V \quad \text{or} \quad c_w = \frac{2F_{perm}}{V} \quad (B.13)$$

When the vibration of the gate is not in the direction of the flow the added damping will change. However the gate is supported at both sides, so it is unlikely that vibration perpendicular to the flow will occur. It is important to note that the added damping can also be negative. When the mechanical damping of the structure is not big enough and the added damping is negative, a self-excitation mechanism can arise. (Kolkman and Jongeling (1996))

B.4 Determination of the hydrodynamic stiffness

In the literature (Kolkman and Jongeling (1996)) three forms of added stiffness can be distinguished:

- 1) Stiffness due to immersion.
- 2) Stiffness due to quasi-static flow forces
- 3) Stiffness due to a sudden change of position of an object, so called sudden stiffness.

The first of this list especially applies to floating objects/structures, and can easily be calculated with the following equation:

$$k_{w,immersion} = \rho g A_{intersection} \quad (B.14)$$

In which $A_{intersection}$ is the intersection surface with the water level.

The stiffness due to flow mainly depends on the position of the object relative to the flow direction. A deviation of the original position of the object will result in a restoring force. When a structure experiences a flow force in y-direction, than the stiffness in y-direction can be written as:

$$k_{w,flow} = \frac{\partial F_y}{\partial y} = \frac{\partial}{\partial y} \left(C_{Fy} \frac{1}{2} \rho V^2 L^2 \right) = \frac{1}{2} \rho V^2 L^2 \frac{\partial C_{Fy}}{\partial y} \quad (B.15)$$

In which: F_y = component of the flow force in y-direction [N]
 C_{Fy} = flow resistance coefficient in y-direction [-]

The last kind of stiffness, sudden stiffness, only applies to gates with over- or under flow. The sudden stiffness is a result of the inertia of the discharge (due to flow inertia the flow cannot immediately adjust to the new position of the gate). When the gate is opened, the same discharge will go through a larger gap. This results in a smaller flow velocity, and thus in a smaller flow force ($F \propto V^2$). The new flow force for a larger flow gap is given by:

$$F_{new} = F_{perm} \left(\frac{\delta^2}{(\delta + y)^2} \right) \quad (B.16)$$

In which δ is the old gap width. The stiffness can be determined by dividing the force change by the vibration magnitude. When the vibration magnitude (y) is small compared to the initial gap width the approximation given in equation B.17 can be used.

$$k_{w,sudden} = \frac{dF}{-y} = \frac{F_{new} - F_{perm}}{-y} = -F_{perm} \left(\frac{\delta^2}{(\delta + y)^2} - 1 \right) \frac{1}{y} \cong 2 \frac{F_{perm}}{\delta} \quad (B.17)$$

From this equation it can be seen that the sudden stiffness will be larger for a smaller gap. Again the added stiffness (k_w) can be negative. When the mechanical stiffness of the structure itself and its supports is not large enough in this case, suction of the gate can occur. The added stiffness is frequency dependent, and occurs especially at high frequencies. This is because for high frequencies the discharge tends to remain constant.

C Time vs frequency domain analysis

The analysis of a system can be done in the frequency- or time domain. In the time domain it is described how the signal changes over time, and in the frequency domain it is indicated to what extent a certain frequency is present in the signal (and what the amplitude and phase of the different frequencies are). In other words the signal in the frequency domain is the spectrum of the corresponding signal in the time domain. When a signal is analysed in one of the two domains it is possible to transform it afterwards to the other domain by means of a Fourier transform or Laplace transform.

In the book of Kolkman and Jongeling (1996) some advantages and disadvantages of analysing in the time domain are mentioned. The advantages of analysing in the time domain that are mentioned are:

- Not-periodic loads and loads with short duration can be analysed without complications, while in the frequency domain only long duration, periodic loads can be analysed.
- The equations that are used to make the analysis/calculations in the time domain are easy to adjust, so that non-linear terms can be fully included. In the frequency domain this is not possible, so the system has to be linear.
- It is possible to directly determine the response of a structure, at which the basic equations do not have to be adjusted.

The disadvantages that are mentioned in the report are:

- Added water mass and water damping are in principle only known in the frequency domain. To do the analysis in the time domain this factors have to be converted to the time domain, this is not an idea task and specialist knowledge is needed for this.
- For the analysis of vibrations small time steps have to be used, while the calculation have to take place over the whole vibration period before the equilibrium state is reached. This takes more computational effort than analysing in the frequency domain.
- Many calculations are needed to determine connections between different quantities.

Another advantage of analysing in the frequency domain is that frequency dependence of the response is included. To determine if it is best to analyse in the time- or frequency domain it has to be decided which advantage and disadvantages are the most important for that specific case.

For the development of the semi-analytical model of Tieleman (2019), the analysis is made in the frequency domain. The main reasons to do this are due to the frequency dependence of the hydrodynamic response and the mathematical advantage.

D Scale experiment measurements

In this appendix the data sets that are obtained from the scale experiments (performed in the Stevin 2 laboratory (Delft University of Technology)) are described in more detail. In appendix D.1 the data that is measured with pressure sensors is described, and in appendix D.2 the data that is measured with load cells is described.

D.1 Pressure sensor data

In this appendix the lab-test results of the scale test are shown in more detail. During the scale test the pressure on the vertical wall structure with overhang is measured with 7 pressure sensors. The position of the pressure sensors on the structure is shown in Figure 75. In Figure 76 the measured individual pressure signals of one wave impact are shown.

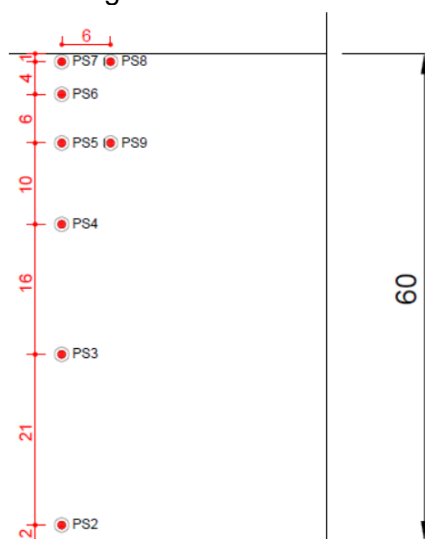


Figure 75: : Position of the pressure sensors on the structure used for the lab-test, (E. de Almeida, 2019)

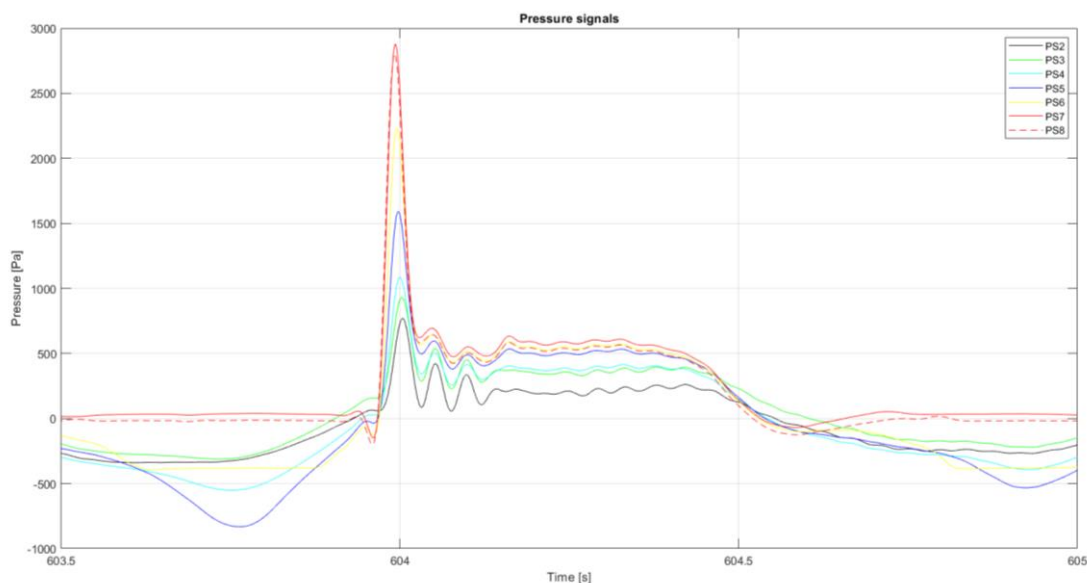


Figure 76: Individual pressure signals of one wave impact

From the pressure signals from the 7 pressure sensors, one time series of the total force on the whole gate per meter width is calculated, taking the distance between the pressure sensors (given in Figure 75) into account. In Figure 77a the total force-time signal of the whole wave field is shown (1300 s), to show the course of the force over the time more clearly Figure 77b zooms in on 50 s of this force-time signal.

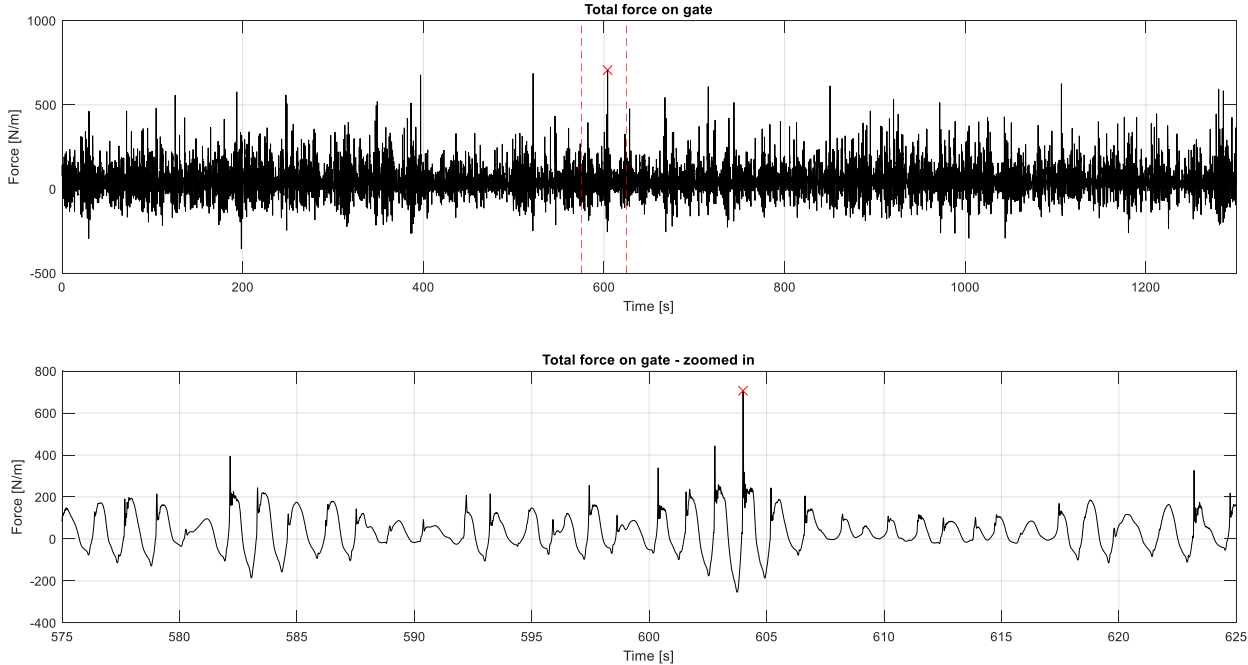


Figure 77: a) Time series of total force on the gate per meter width, b) Time series of total force on the gate per meter width - zoomed in

The tests that are performed in the lab are scale tests, so to use the results for a real case study, scaling of the results is necessary. As already discussed in paragraph 4.3.1 the scaling of wave impacts mainly uses the Froude scaling, the scaling factors for the different variables are given in Table 11.

Table 11: Froude scaling factors for wave impact data

Variable	Scaling factor	Scaling factor case study
Length	λ	12.08
Frequency	$\lambda^{-0.5}$	0.29
Time	$\lambda^{0.5}$	3.48
Mass	λ^3	1762.79
Pressure	λ	12.08
Force	λ^3	1762.79
Force/m ¹	λ^2	145.93

The height of the gate used during the lab-test is 0.6 m, the height of the gate used as case study is 7.25 m. So for the length a scaling factor of $\lambda = 12.08$ has to be used. In Figure 78 again the total force-time signal is shown, only now for the scaled situation.

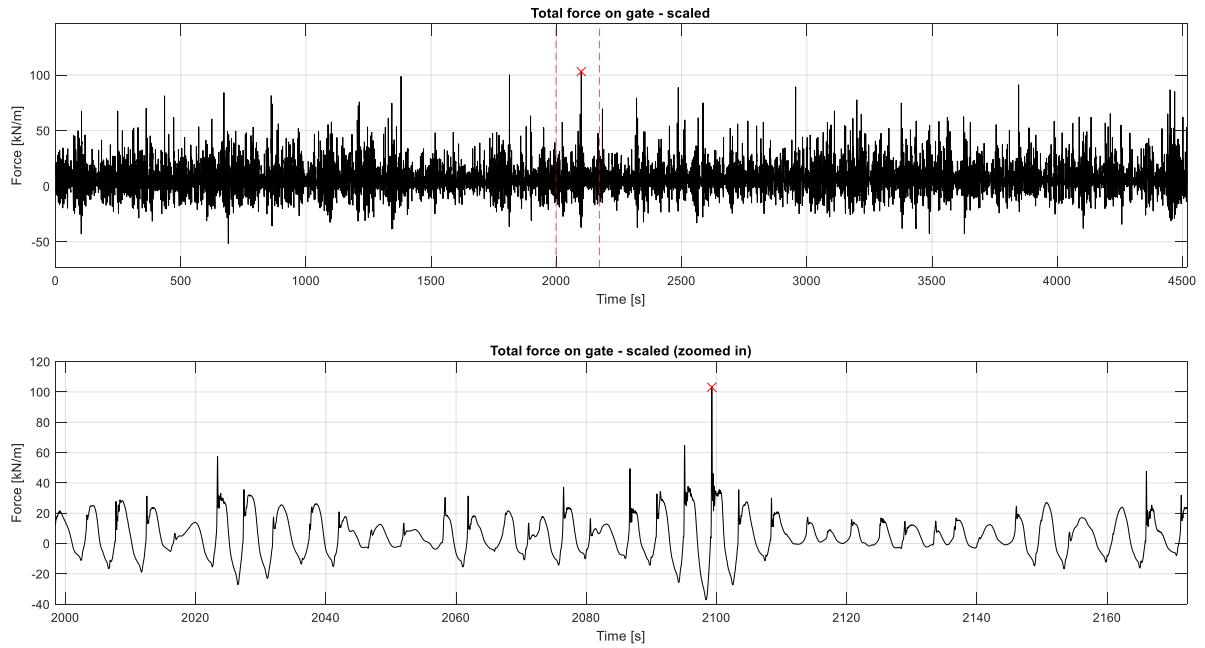


Figure 78: Time series of total force on the gate per meter width – scaled, b) Time series of total force on the gate per meter width – scaled and zoomed in

D.2 Load cell data

Figure 79 shows the unscaled load cell data (for one wave impact). In the upper panel the force that is measured with the load cells is plotted, and in the lower panel the load data is converted to pressure data.

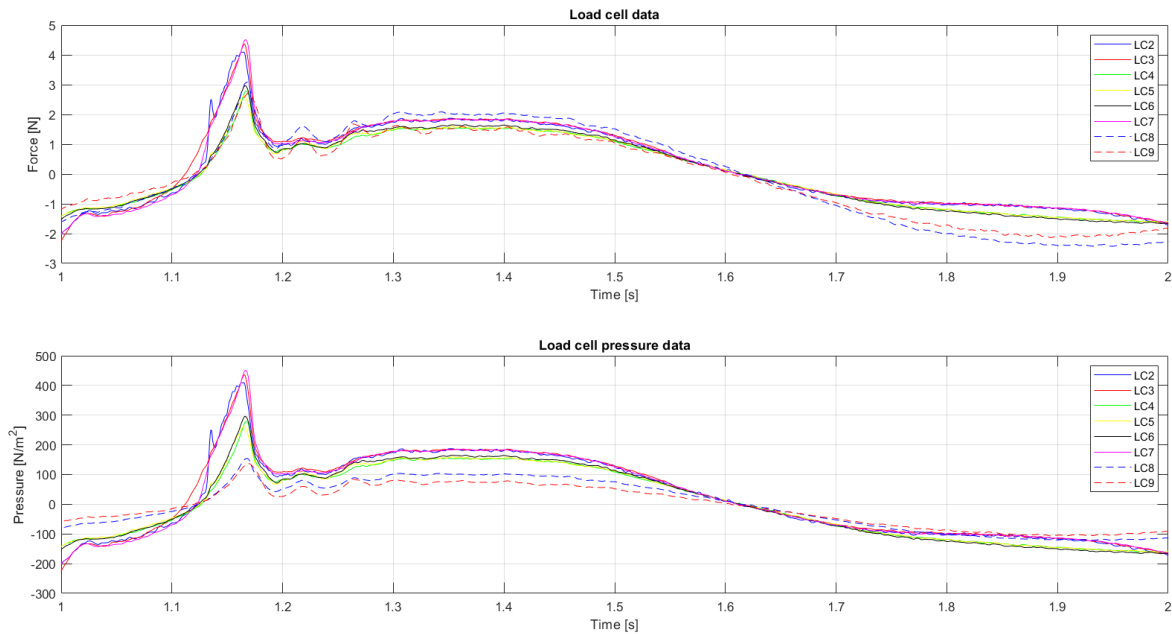


Figure 79: Load cell force data and load cell pressure data (unscaled), wave 1

Table 11 shows the Froude scaling that is used to scale the load cell data. In Figure 80 the scaled ($\lambda = 12.5$) load cell data is shown for one wave impact.

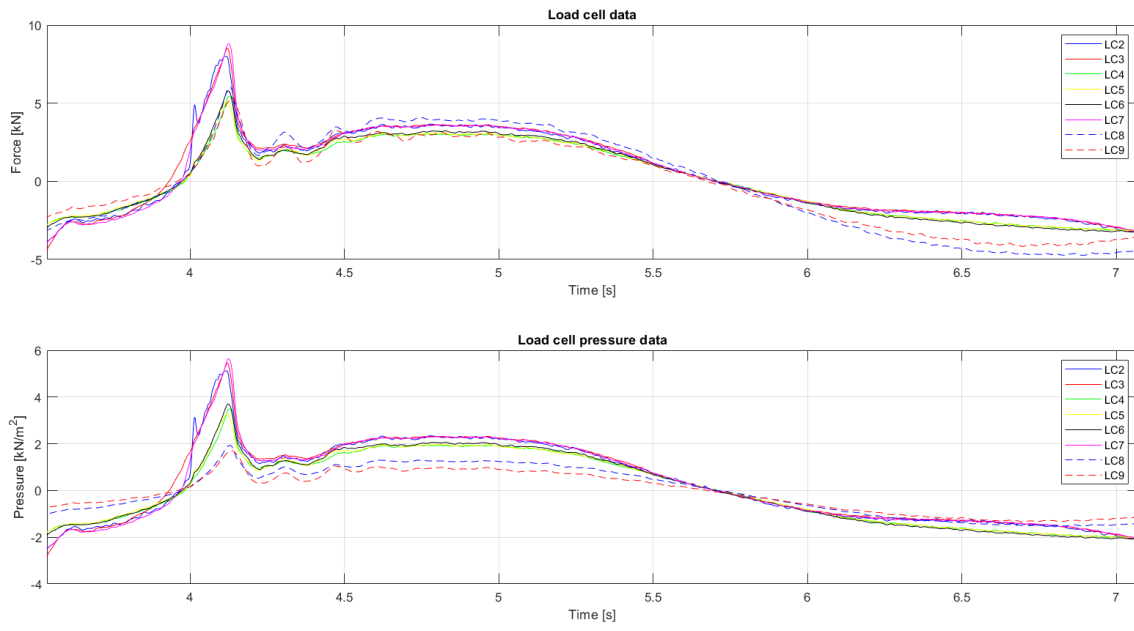


Figure 80: Load cell force data and load cell pressure data (scaled, $\lambda = 12.5$), wave 1

E Splitting method for the wave impact force

In the research of Chen et al (2018) filters (low pass and high pass filters) are used to split the wave force in an impulsive part and a quasi-static part. However, for this research another (simplified) method is used to split the wave force. To split the wave force, two sets of lab-tests are used: one test series with impacts caused by the overhang (this is the data described in appendix D), and another test series for the same situation without the overhang and thus without the wave impacts (quasi-static wave force). In Figure 81 and Figure 82 the two test series (with and without wave impacts) are plotted.

When the wave force has been split into an impulsive part and quasi-static part, the wave impact peak forces, wave impact durations, and wave impact impulses can be defined. In theory the begin- and end time of the impact can be defined as the intersection points of the two data sets (see Figure 81 (left)), however as can be seen in Figure 81 (right) large errors in estimating the wave impact durations can be made when using this definition. Instead of this definition, the begin- and end times are defined as the points where the differences between the quasi-static force signal and impulsive force signal are larger or smaller than a certain threshold.

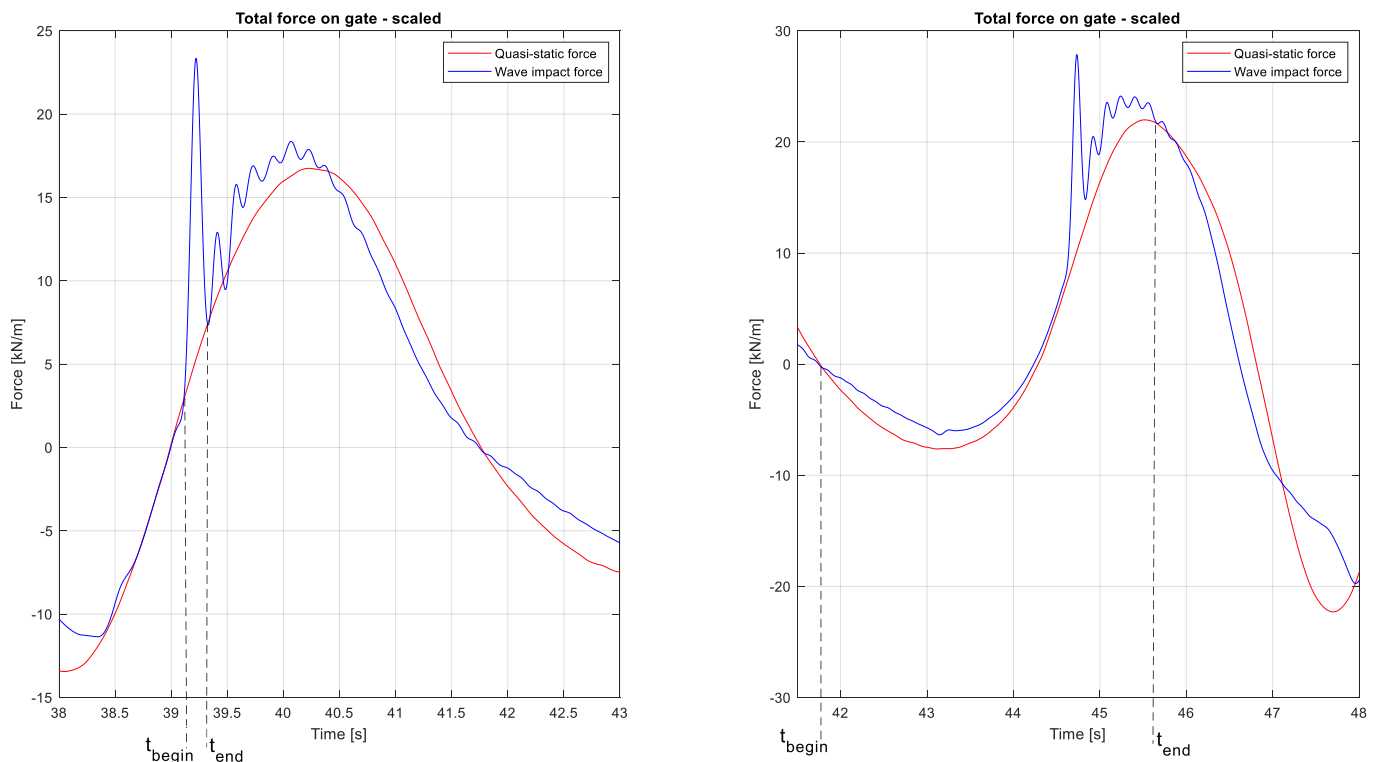


Figure 81: Using the intersection points of the impulsive wave force signal and quasi-static wave force signal to define the wave impact duration (wave 9 (left) and wave 10 (right))

The first step of this method is to define the force peaks in the quasi-static force signal. It is more convenient to search for the force peaks of the quasi-static force signal (instead of the actual wave impact force peaks), because this data is more smooth and by this less errors are made by defining the local maxima. A minimum peak height of 14.6 kN is used as lower limit for the quasi-static force peaks (for the unscaled force signal the lower limit is set to 100 N, this gives $100 \cdot 12.08^2 / 1000 = 14.6$ kN as lower limit for the scaled force signal). The next step is to define a difference function (equation D.1), considering only values higher than zero.

$$diff = F_{im} - F_{qs} \tag{D.1}$$

The begin time of the wave impact is defined as the moment when the difference function becomes larger than a certain threshold value. For this research the threshold value is defined as 25% of the corresponding quasi-static force peak ($diff > 0.25 \cdot F_{max,qs}$). The end time of the wave impact is found in the same way, only now the difference function has to become smaller than the set threshold value ($diff < 0.25 \cdot F_{max,qs}$). The impact duration is defined as:

$$\tau = t_{begin} - t_{end} \tag{D.2}$$

The force peak of the impulsive wave signal is found by searching for the maximum impulsive force between the begin- and end time of the wave impact. Finally the wave impact impulse can be calculated. The impact impulse I_{im} is the impulse caused by the impulsive force, and can be defined as the time integral of the impulsive force over the impact duration (τ). In Figure 82 the begin- and end time, maximum force peaks of the impulsive and quasi-static signals, and wave impact impulse (shaded green) are shown for the maximum wave impact in the wave field. In Figure 32 in chapter 4, histograms of the peaks force, impact duration, and impact impulse are displayed.

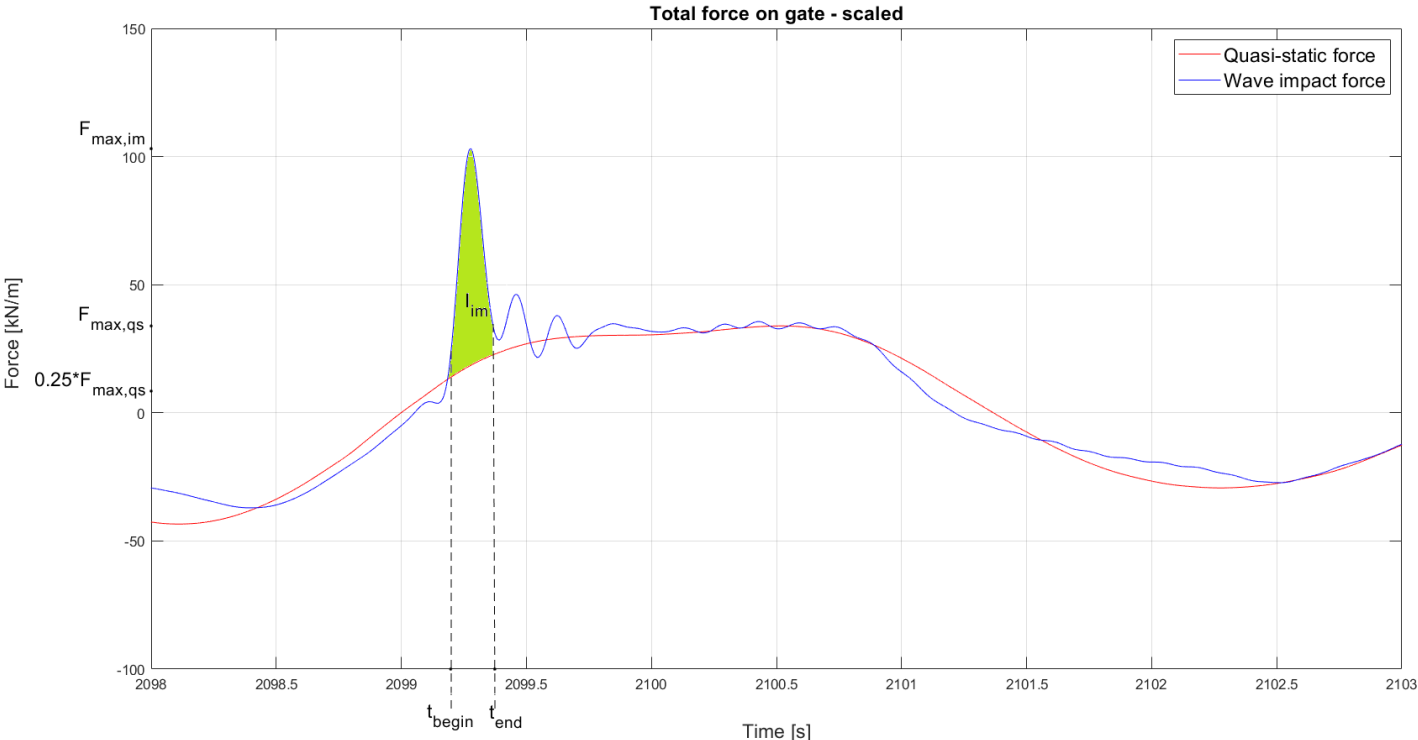


Figure 82: Used definition for the wave impact peak force ($F_{max,im}$), wave impact duration ($\tau = t_{end} - t_{begin}$), and wave impact impulse (I_{im}) (wave 311)

F Statistics – basic formulations

In this appendix the basis formulations of the used statistical distributions in chapter 5 are summarized.

Weibull distribution:

The probability density function (pdf) for the Weibull distribution is given by equation F.1, and the cumulative distribution function (cdf), describing the exceedance probability of a certain value of the wave impact peak force, is given by equation F.2 (Jonkman et al., 2016).

$$f(x; a, b) = \frac{b}{a} \left(\frac{x}{a}\right)^{b-1} e^{-\left(\frac{x}{a}\right)^b} \quad (\text{eq F. 1})$$

$$F(x; a, b) = P(x \geq X) = e^{-\left(\frac{x}{a}\right)^b} \quad (\text{eq F. 2})$$

Rayleigh distribution:

The probability density function (pdf) for the Rayleigh distribution (in general) is given by equation F.3, and the cumulative distribution function (cdf), describing the exceedance probability of a certain value of the wave impact peak force, is given by equation F.4 (Jonkman et al., 2016).

$$f(x; \sigma) = \frac{x}{\sigma^2} e^{-\frac{x^2}{2\sigma^2}} \quad (\text{eq F.3})$$

$$F(x; \sigma) = P(x \geq X) = e^{-\frac{x^2}{2\sigma^2}} \quad (\text{eq F.4})$$

From the literature it is known that the wave height is Rayleigh distributed (Holthuijsen, 2007). For wave heights equation F.5 can be used to describe the relation between the exceedance probability and the significant wave height (H_s) (Holthuijsen, 2007).

$$P(\underline{H} \geq H) = e^{-\frac{2H^2}{H_s^2}} \quad (\text{eq F. 5})$$

To be able to generate a wave height distribution, equation F.5 can be written as:

$$H = \sqrt{-\frac{1}{2} * \ln(P(\underline{H} \geq H))} * H_s \quad (\text{eq F. 6})$$

Triangular distribution:

Equation F.7 describes the probability density function of the triangular distribution, and equation F.8 describes the cumulative distribution function of the triangular distribution (Jonkman et al., 2016).

$$f(x; a, b, c) \begin{cases} \frac{2(x-a)}{(c-a)(b-a)} & a \leq x \leq b \\ \frac{2(c-x)}{(c-a)(c-b)} & b < x \leq c \\ 0 & \text{otherwise} \end{cases} \quad (\text{eq F. 7})$$

$$F(x; a, b, c) \begin{cases} 0 & x < a \\ \frac{(x-a)^2}{(c-a)(b-a)} & a \leq x \leq b \\ 1 - \frac{(c-x)^2}{(c-a)(c-b)} & b < x \leq c \\ 1 & x > c \end{cases} \quad (\text{eq F. 8})$$

Gumbel extreme value distribution for maxima:

The Gumbel extreme value distribution for maxima can be described with the following equations (Jonkman et al., 2016):

$$f(x; \alpha, u) = \exp [-e^{-\alpha(x-u)}] \quad (\text{eq F. 9})$$

$$F(x; \alpha, u) = \alpha * \exp [-\alpha(x-u) - e^{-\alpha(x-u)}] \quad (\text{eq F. 10})$$

With scale parameter α and location parameter u .

G Afsluitdijk case

In this appendix the case study that is used as inspiration for scaling of the scale measurement data to a realistic gate, that will be used for the analysis with the semi-analytical model, is described. Typical parameter values for the Afsluitdijk case are described. These parameters describe a realistic gate (schematised setting), and multiple realistic cases (schematisations) can be investigated with the semi-analytical model by applying small variations to this parameters.

The case study that is used as inspiration is the same case study that is studied in the thesis work of Vorderegger (2019). The design case that is used, is the design of the Northern gate of the tower discharge sluice at den Oever. The design and execution of the reinforcement of the Afsluitdijk will be performed by the consortium Level. At this moment, a new design of the discharge sluice complex at Den Oever is already made by Level. The new design consists of three sections of tower discharge sluices, separated by two islands containing new discharge sluices. Also, at both sides of the sluice complex a new pumping station will be build. In Figure 83a the current sluice complex at Den Oever is displayed, and in Figure 83b the design made by Level is shown.



79a



79b

Figure 83: a) Current discharge sluice complex at Den Oever, b) Design of the new discharge sluice complex at Den Oever by consortium Level
([www.hollandluchtfoto.nl](http://www.hollandluchtfoto.nl/-/galleries/dorpensteden/noord-holland/den-oever/-/medias/ed36592c-0bb8-4ed4-983e-9e699351bf5a-den-oever-luchtfoto), June 6, URL <http://www.hollandluchtfoto.nl/-/galleries/dorpensteden/noord-holland/den-oever/-/medias/ed36592c-0bb8-4ed4-983e-9e699351bf5a-den-oever-luchtfoto>)
([www.deafsluitdijk.nl](https://deafsluitdijk.nl/wp-content/uploads/2014/05/presentatie-RWS-en-Level-stakeholderbijeenkomst-2018-04-23.pdf), June 6, URL <https://deafsluitdijk.nl/wp-content/uploads/2014/05/presentatie-RWS-en-Level-stakeholderbijeenkomst-2018-04-23.pdf>)

In Figure 84 a top view of one of the three sections containing tower discharge sluices is displayed. Each section consists of five tower discharge sluices, which contain two gates each: a Northern gate at the Wadden Sea-side and a Southern gate at the IJsselmeer-side. In the figure the case that will be used for further analysis, the Northern gate, is highlighted in red.

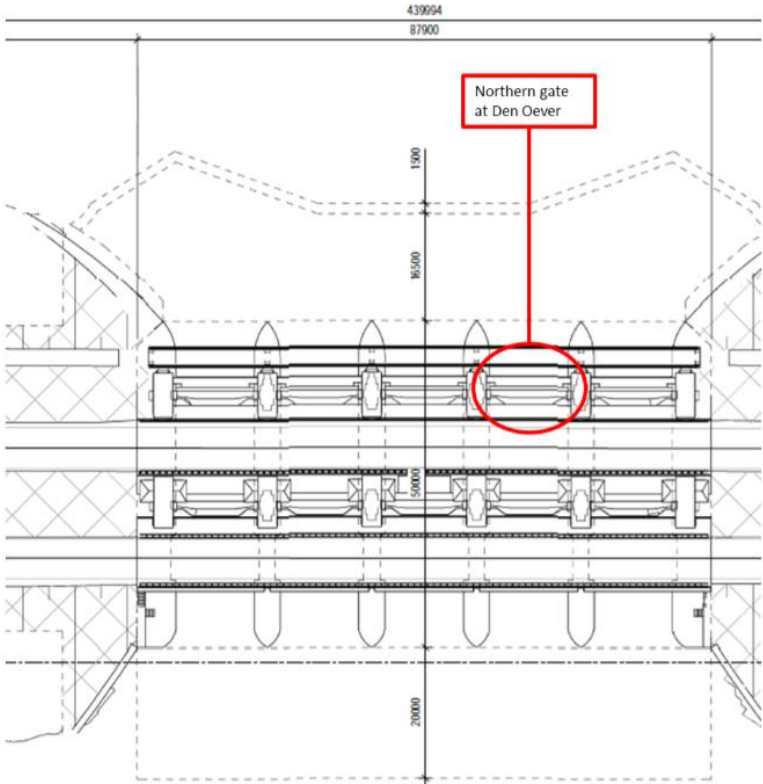


Figure 84: Top view of tower discharge sluices at Den Oever, the case is highlighted in red (Thesis work of Vorderegger (2019))

An important adjustment that is made in the new design of the discharge sluice complex, is the removal of the defence beam at the frontside of the Northern gate. The defence beam can cause very intense impulsive loading of the gate. This is the main reason of the removal of this part of the structure. In Figure 85a a schematisation of the old sluice design is given, and in Figure 85b a schematisation of the new design made by Level is given. For this master thesis the old situation will be studied (the situation with the defence beam). This will be done because model test are already performed for this situation (the defence beam causes the impulsive wave impacts that are studied), so this results can be used for the analysis.

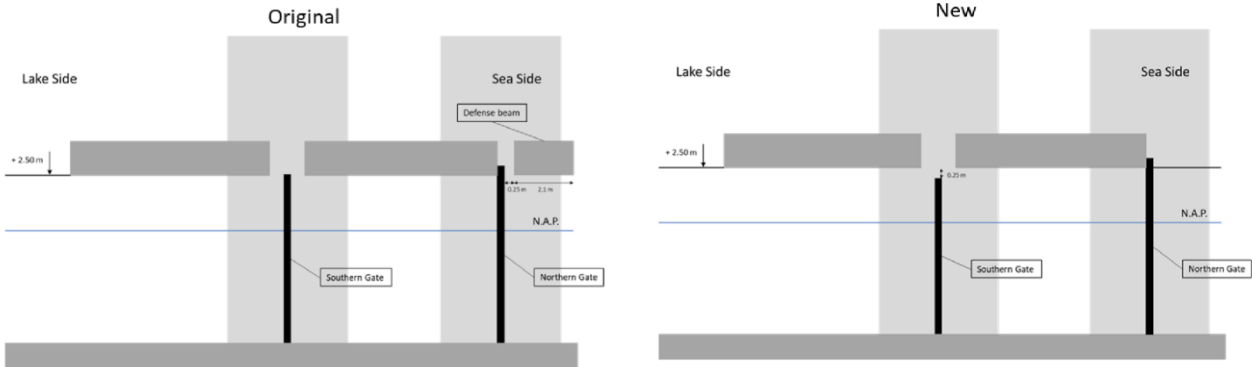


Figure 85: a) Schematisation of the cross-section of the current situation at Den Oever (with defence beam), b) schematisation of the cross-section of the new situation at Den Oever (defence beam is removed) (Thesis work of Vorderegger (2019))

As described before, further research focusses on the Northern gate only. All the parameters and their values corresponding to the Northern gate case, are given in Table 12. The structure that will be studied and investigated with the semi-analytical model in chapter 7 will be inspired by the data given in Table 12. However, some variations to this data will be applied. For instance, the width that will be used is $L_x = 10$ m instead of 12 m. Also, the thickness of the gate and by that the distributed mass will be varied during the analysis performed in this report.

Table 12: Case parameters

Structural parameters	Symbol	Value	Unit	Fluid parameters	Symbol	Value	Unit
Gate width	L_x	12	m	Sluice width	L_x	12	m
Gate height	L_z	7.5	m	Water level sea	h_l	7	m
Gate thickness	t	0.243	m	Water level lake	h_r	4	m
Bending stiffness	D	$2.63 \cdot 10^8$	Nm^2	Fluid density	ρ_f	1025	kg/m^3
Distributed mass	ρ_s	95	kg/m^2	Fluid sound velocity	c	1500	m/s
Modulus of elasticity	E	$200 \cdot 10^9$	N/m^2	Gravitational constant	g	9.81	m/s^2
Moment of inertia	I	0.0012	m^4				
Poisson's ratio	ν	0.3	-				
Yield strength (steel)	f_y	$255 \cdot 10^6$	N/m^2				
Material damping (steel)	η	0.01	-				

It has to be noted that the structure that is used for this research is a simplification of a 'real' structure. For this research a 'real' gate structure with vertical and horizontal stiffeners, as shown in Figure 86a, is simplified as a flat thin plate in the semi-analytical model developed by Tieleman (2019) (shown in Figure 86b). An assumption that has to be made before the semi-analytical model can be applied, is how the gate is supported at its edges. It is assumed that the gate is simply supported at its bottom, at the right edge and at the left edge, and that the top edge of the gate is free (FSSS), see Figure 86b.

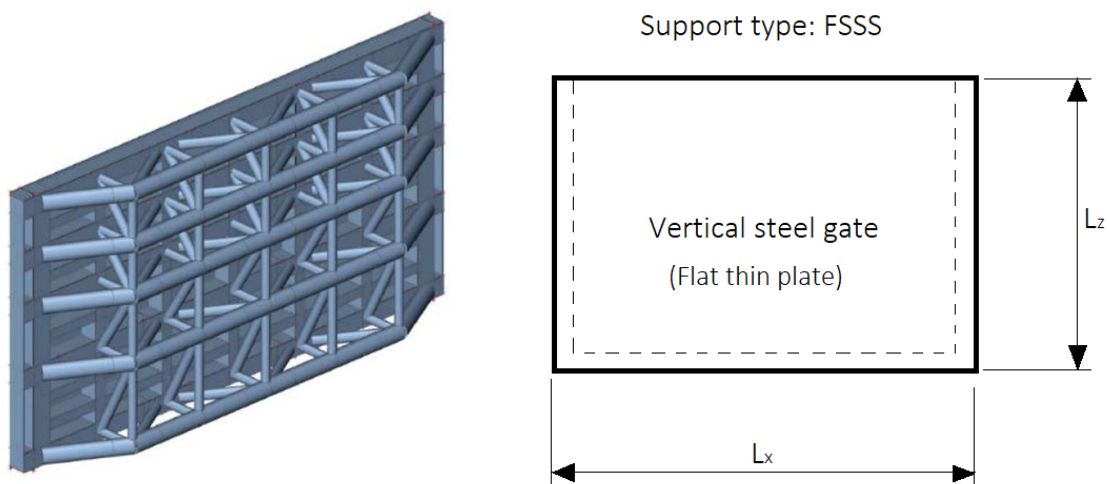


Figure 86: a) Conceptual 'real' flood gate design for the Afsluitdijk, with horizontal and vertical stiffeners (Witteveen+Bos, 2016), b) Boundary conditions for simplified case study gate (flat thin plate) used for this research, F = free edge, S = simply supported edge

H Composition of 'real' 3D force signal over the full gate surface

As discussed in section 5.2 the scale experiments provide a number of data sets measured with load cells and pressure sensors (see Figure 87 for the locations of the load cells and pressure sensors). For the investigation of a distribution of the impact force over the width of the gate, a three-dimensional force signal over the full gate surface is needed. In this appendix the composition of the 'real' 3D force-time signal will be described. This 'real' signal will be used to validate the 'model' signal that is composed in section 6.2. The 'real' 3D force signal is obtained by inter- and extrapolation of the data that is obtained during the scale experiments. The composition of the 3D force signal, that can be run with the semi-analytical model, consists of three steps:

- Step 1: extrapolation of the load cell data to obtain a force signal over the left half of the gate.
- Step 2: filling in the data points at the right half of the gate.
- Step 3: Definition of individual waves in time

H.1 Extrapolation of load cell data

In Figure 87 the locations of the extrapolation points at the left half of the unscaled gate are shown. The Matlab functions 'scatteredInterpolant' and 'interp1' are used to extrapolate the known data, to obtain a force signal at the extrapolation points defined in Figure 87. Linear inter- and extrapolation are used as method in Matlab. First, points 1-4 are found by using the function 'scatteredInterpolant'. Then the points 5-8 are found by using the function 'interp1'. The force signals that are obtained for extrapolation points 1,2,3,4,7, and 8 are divided by two in Figure 88, to correct for the size of the assumed loading plate (10*20 cm², instead of 10*10 cm²), this is also done for load cells 8 and 9.

In Figure 88 the extrapolation results (for the left half of the unscaled gate) are shown for one wave impact. In the left and middle panels of Figure 88 the force-time signals of the load cell data and extrapolation points are shown. The maximum wave impact force is indicated with the red vertical line. In the right panel the three-dimensional force field over the left side of the gate during the maximum wave impact force is shown.

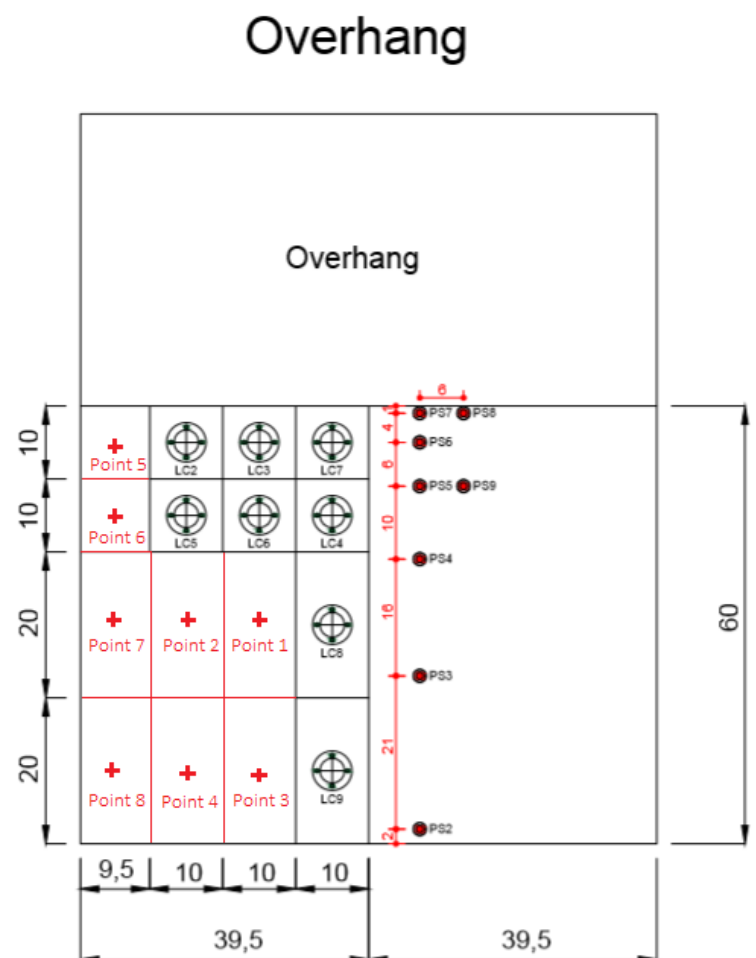


Figure 87: Definition extrapolation points at the left half of the gate

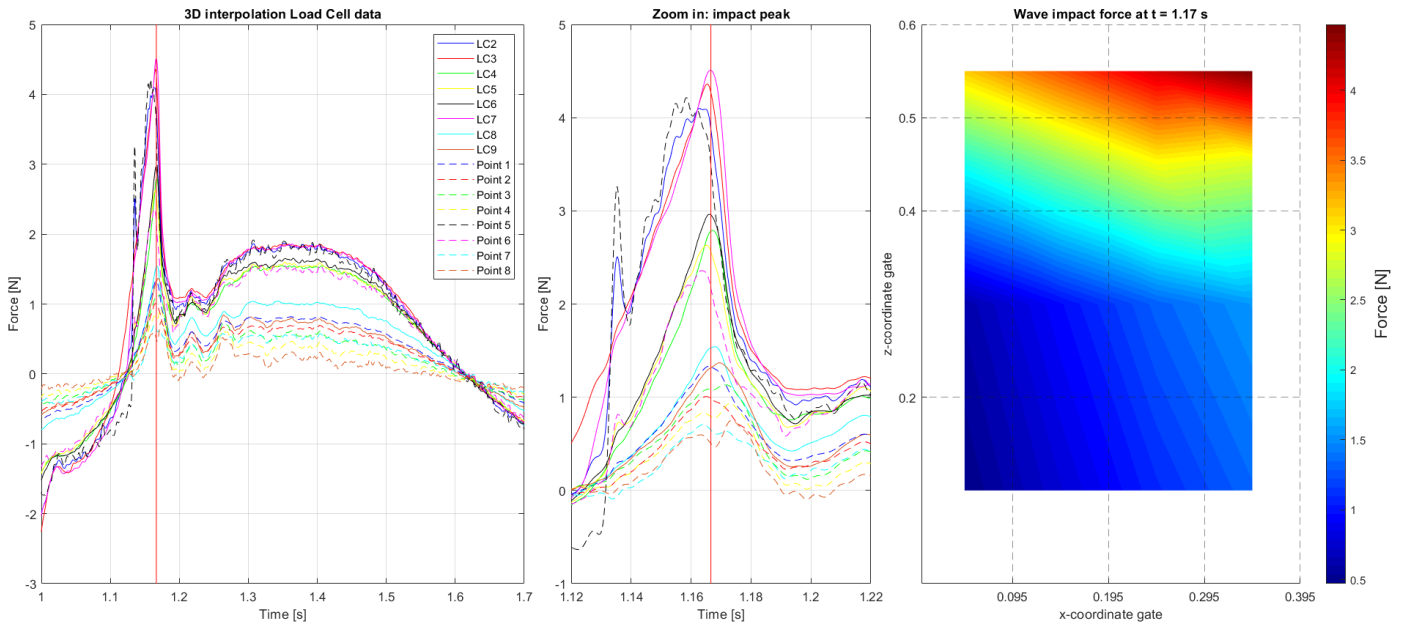


Figure 88: Time signal of one wave impact (wave 1) for load cell data and interpolated data points, the maximum wave impact force is indicated with the vertical red line (left and middle), 3D force field over the left side of the gate during the maximum impact force, unscaled

The next step is to scale the inter/extrapolation results to a realistic gate situation (inspired on the Afsluitdijk case described in appendix G). The gate that is used for the scale measurements has a width of $L_{x, \text{scale}} = 0.79 \text{ m}$ and a height of $L_{z, \text{scale}} = 0.6 \text{ m}$. A scaling factor of $\lambda = 12.5$ is used, this gives $L_{x, \text{scaled}} = 10 \text{ m}$ and $L_{z, \text{scaled}} = 7.5 \text{ m}$ for the 'real' case study gate.

After scaling of the data, the following parameters are defined as input for the semi-analytical model:

- Gate dimensions: $L_x = 10 \text{ m}$, $L_z = 7.5 \text{ m}$.
- Interval accuracy (definition of the grid that is used for the calculations with the semi-analytical model, in the middle of each grid cell a force-time signal is known):
 $dx = 1.25 \text{ m}$, $dz = 1.25 \text{ m}$.
 Number of intervals in x-direction = 8,
 number of intervals in z-direction = 6.
 In Figure 89 the defined intervals (in space) are shown.

Intervals (in space) scaled gate

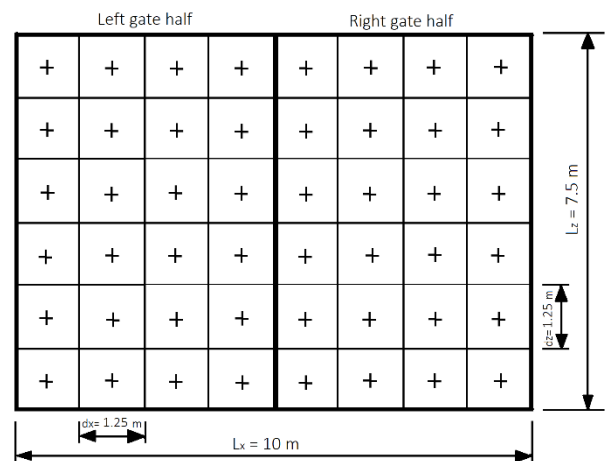


Figure 89: Definition intervals (in space) over the gate, scaled $\lambda = 12.5$

In the original grid (see Figure 87), load cells 8 and 9, and points 1,2,3,4, 7 are twice as large as load cells 2,3,4,5,6 7, and points 5,6. In the grid that is defined for the 'real' gate (see Figure 89), all the cells have the same size. One larger load cell has been split into 2 equally sized smaller cells. First the force-time signals for the large load cells are scaled for the real gate (with λ^3). Then, the scaled force-time signals are divided by two to obtain the force-time signals at the small cells (it is assumed that the measured force can be split into two to get the force at the equally sized smaller cells).

H.2 Prediction force signal for the right half of the gate

The force-time signal for the left half of the gate is determined based on the load cell data. On the right half of the gate, only one vertical of pressure sensor data is present. The most optimal method to fill in the data points on the right half of the gate, is to use the pressure sensor data to make a prediction of the further course of the load cell data at the left half.

The data is measured with two different measuring instruments, pressure sensors and load cells. An amplitude difference error (5-10%) is present between the data measured with the pressure sensors and the load cells. So, first the load cell data and pressure sensor data are calibrated. However, also after calibration of the load cell and pressure sensor data, no clear trend is found for the course of the data at the right half of the gate. For different wave impacts, the load cell data shows a decay or increase of the impact force amplitude towards the middle of the gate, however the pressure sensor data always shows an increase of the wave impact force amplitude towards the middle of the gate. So no conclusions about the course of the data at the right half of the gate can be drawn based on the pressure sensor data that is available.

From Figure 90 it can be seen that for wave 1 the wave impact force is higher in the middle of the gate than at the edge of the gate. However, it can also be seen that for the 2nd row from the top, the skewness cannot be described with a linearly increasing line from the edge to the middle of the gate (the wave force at load cell 6 is higher than at load cell 4). Also, from Figure 45 in section 5.3 it can be seen that quite high skewness values are found ($s > 2$) for the wave impact data, so actually this indicated that an asymmetrical linear skewness definition (shown in Figure 71c) cannot be the case for this wave impact data. When the skewness value is larger than 2 for this definition, negative pressures are assumed at the right gate half.

So, it can be concluded that it is hard to specify the skewness based on this data set, and to make a prediction of the width distribution of the data on the right half of the gate. For this research it has been chosen to mirror the data from the left gate half to construct the force-time signal for the right gate half. The other option was to extrapolate the data from the left gate half, to obtain the data at the right gate half (see Figure 71b). However, due to the 'irregularities' in the load cell data described above (higher force in load cell 6 than in load cell 4) it is really hard to simulate the correct width distribution of the force on the right half of the gate when the data is extrapolated. It is recommended to do more scale model tests to determine the 'real' course of the data on the right gate half (see chapter 8, recommendations). In Figure 90 the mirrored three-dimensional pressure field over the full gate surface during the maximum wave impact pressure from wave 1 is shown for the scaled gate displayed in Figure 89.

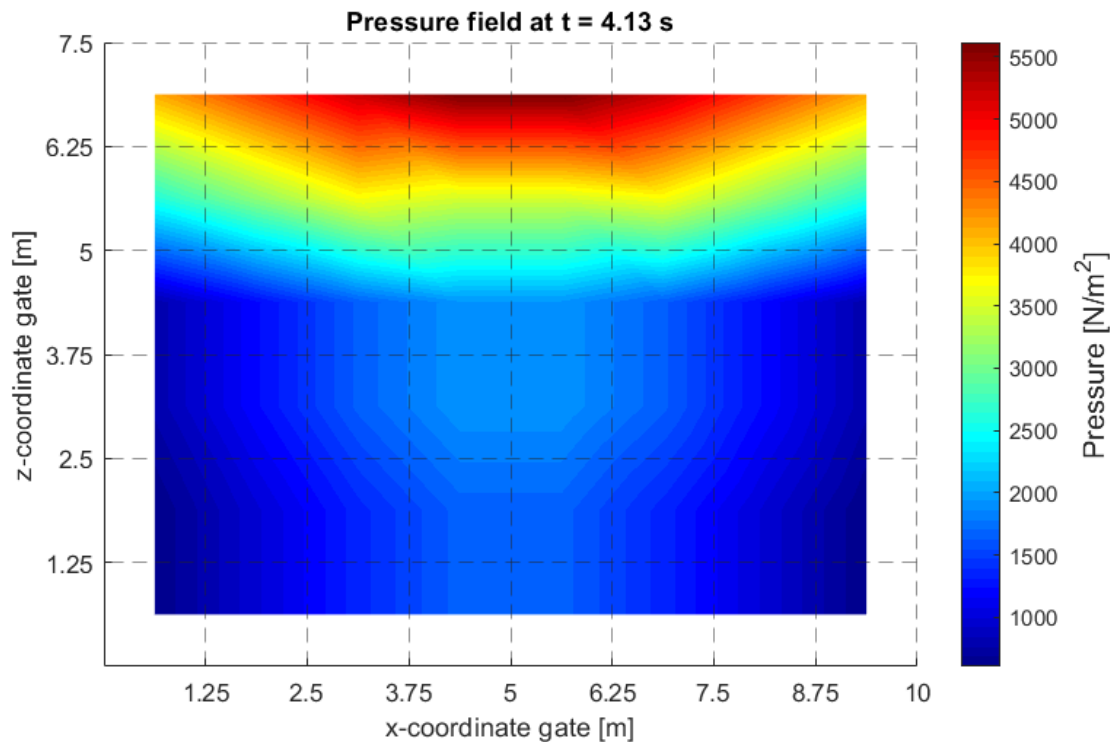


Figure 90: Mirrored 3D pressure field over the full gate surface during the maximum impact force (scaled, $\lambda = 12.5$), wave 1

H.3 Definition of individual waves in time

The force-time signal that is obtained with the scale measurements consists of approximately a thousand waves. For the analysis with the semi-analytical model the force-time signal has to be split shorter signals for individual waves, so that the model can be run separately for each individual wave. To obtain this individual time signals, first in Matlab the zero-crossings of the quasi-static wave signal are obtained. The quasi-static wave signal is used for this, because this data contains less oscillations than the wave impact data (due to the entrapped air/air bubbles during the wave impacts). It is assumed that the waves start and end halfway two zero-crossing points. The definition of the individual waves in time is shown in Figure 91. The data measured with loadcell 2 is used for the definition of the individual waves. This individual wave definition in time (based on load cell 2) is also used for the other data points on the gate.

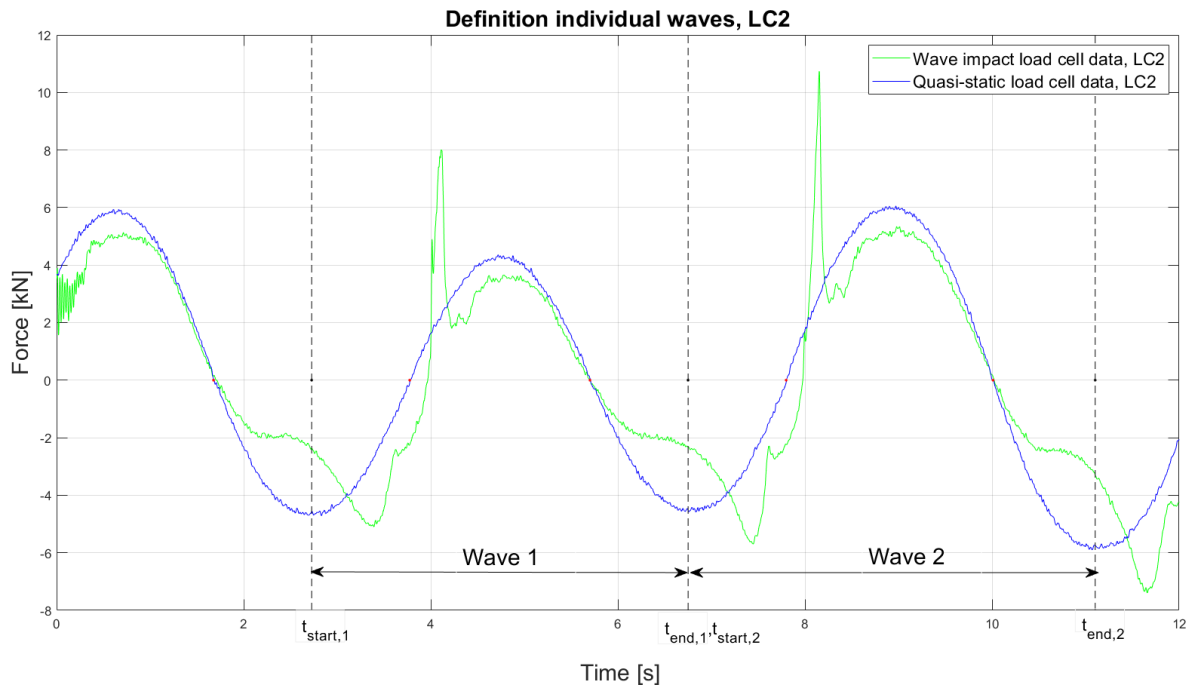


Figure 91: Definition individual waves, based on load cell 2 data (scaled, $\lambda = 12.5$)

In Figure 92 the histograms of the wave durations and impact durations for load cell data 2 are shown. From this two histograms it can be seen that the wave impacts are really short compared to the duration of the whole wave.

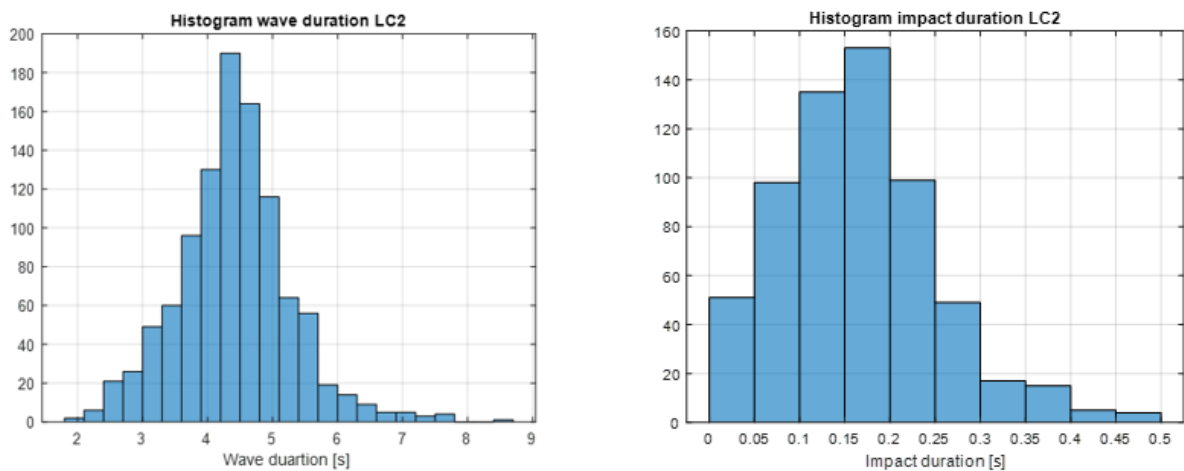


Figure 92: Histogram wave duration (left), histogram impact duration (right), based on load cell data 2 (scaled, $\lambda = 12.5$)

Skewness parameter analysis

1.1 Correction factor average force

From Figure 71, in section 7.4.1, it can be seen that the symmetrical skewness definition increases the average force compared to the uniform case. The asymmetrical skewness definition gives the same average force as for the uniform case. To be able to compare the maximum deflections for the different gates and different skewness values, a correction factor is used. This correction factor is determined based on the force, and corrects the force so that the average force is the same as for the uniform case. The force and deflection are related, so that for instance a ten times higher force gives a ten times higher deflection. So, the correction factor that is determined for the force can also be used to correct the maximum deflection that will be obtained in the next section. As already said, the asymmetrical skewness definition does not increase the average force, so no correction of the maximum deflections is needed for this definition. In Table 13 the uncorrected and corrected values of the maximum deflections that are determined with the semi-analytical and SDOF model for the different values of the symmetrical skewness, and gates are given.

Table 13: Correction factor average force, maximum deflections

s [-]	Correction factor average force [-]	$\tau/T = 0.1$		$\tau/T = 1.1$		$\tau/T = 5.0$	
		$W_{\max, \text{uncorrected}}$ [mm]	W_{\max} [mm]	$W_{\max, \text{uncorrected}}$ [mm]	W_{\max} [mm]	$W_{\max, \text{uncorrected}}$ [mm]	W_{\max} [mm]
-0.5	0.71	122.2	171.1	3.9	5.5	0.135	0.189
2	2.14	284.6	132.8	9.0	4.2	0.315	0.147
4	3.29	414.6	126.2	13.1	4.0	0.458	0.140
8	5.57	674.9	121.1	21.3	3.8	0.745	0.134

s [-]	Correction factor average force [-]	$W_{\max, \text{SDOF, uncorrected}}$ [mm]		$W_{\max, \text{SDOF}}$ [mm]		$W_{\max, \text{SDOF, uncorrected}}$ [mm]		$W_{\max, \text{SDOF}}$ [mm]	
		$W_{\max, \text{SDOF, uncorrected}}$ [mm]	$W_{\max, \text{SDOF}}$ [mm]	$W_{\max, \text{SDOF, uncorrected}}$ [mm]	$W_{\max, \text{SDOF}}$ [mm]	$W_{\max, \text{SDOF, uncorrected}}$ [mm]	$W_{\max, \text{SDOF}}$ [mm]	$W_{\max, \text{SDOF, uncorrected}}$ [mm]	$W_{\max, \text{SDOF}}$ [mm]
-0.5	0.71	71.8	100.5	4.2	5.9	0.137	0.192		
2	2.14	168.4	78.6	9.9	4.6	0.321	0.150		
4	3.29	245.8	74.8	14.5	4.4	0.470	0.143		
8	5.57	400.6	71.9	23.4	4.2	0.763	0.137		

1.2 Structural modal shapes case study gate

In Figure 93 several normed structural modal shapes are shown for the case study gate ($L_x = 10\text{ m}$, $L_z = 7.5\text{ m}$, see Figure 58b) with support type FSSS (F = free edge, S = simply supported edge).

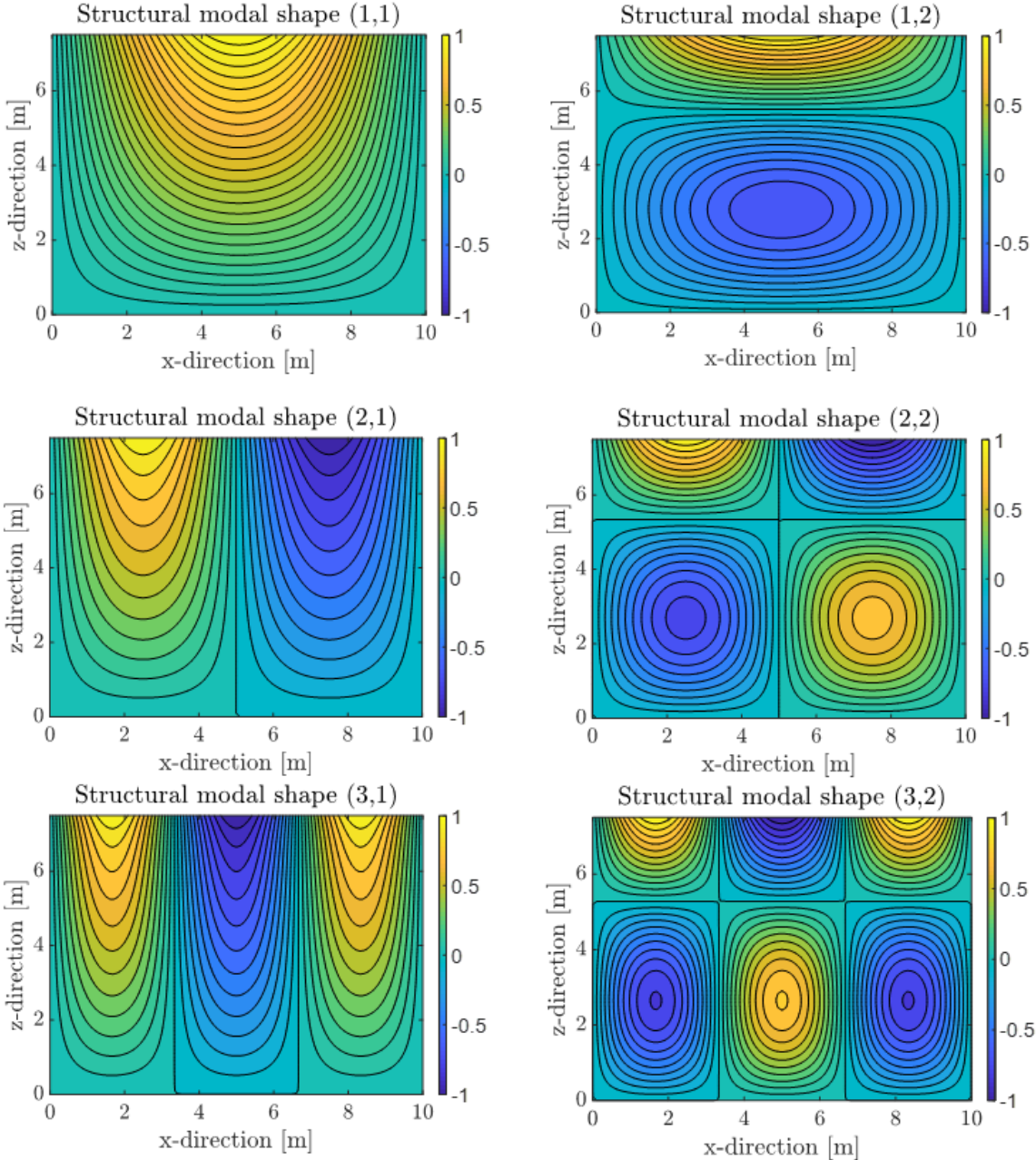


Figure 93: Structural modal shapes for case study gate

J Equivalent SDOF model

To be able to investigate the importance of taking higher modes of vibration into account for the determination of the maximum response of a gate, and to compare the results obtained with the semi-analytical model (MDOF model) in section 6.3.2 to the results obtained with an SDOF model, an equivalent SDOF model has to be set up. The semi-analytical model takes an infinite (or specified finite) number of modes into account, while an SDOF model only considers the first mode of vibration. The starting point of the derivation of the equivalent SDOF model is the plate equation of motion that is used for the semi-analytical model:

$$D\nabla^4 w(x, z, t) + (\rho_s + \rho_{s,w}) * \ddot{w}(x, z, t) = f_e(x, z, t) \quad (J.1)$$

In which: w = displacement of the mid-surface of the plate [m]
 ρ_s = distributed mass per unit area [kg/m²]
 $\rho_{s,w}$ = distributed added water mass per unit area [kg/m²]
 f_e = time signal of the external force distribution on the plate (for instance of a wave impact) [N/m²]

The distributed added water mass can be calculated with equation J.2 from Jongeling and Erdbrink (2010).

$$\frac{\rho_s + \rho_{s,w}}{\rho_s} = \left(\frac{f_{dry}}{f_{wet}} \right)^2 \quad (J.2)$$

In which: f_{dry} = the in-vacuo natural frequency of the gate [Hz]
 f_{wet} = the natural frequency of the submerged gate [Hz]

For the time signal of the external force, the 'model' signal composed in chapter 6 is used. As discussed earlier the response determined with the semi-analytical model consists of the summation of the response for an infinite number of modes. For the SDOF model it is assumed that all the energy goes to the first mode of vibration, so that the response can be simplified as indicated in equation J.3.

$$w(x, z, t) = \sum_{n=1}^{\infty} w_n(x, z) u_n(t) \approx w_0(x, z) * u_0(t) \quad (J.3)$$

In which: w_0 = an assumed shape function of the response
 u_0 = an assumed time function of the response

For the plate with boundary conditions as indicated in Figure 94a, the following shape function is assumed to obtain the first mode of vibration for the SDOF model:

$$w_0(x, z) = \sin\left(\frac{\pi x}{L_x}\right) \sinh\left(\frac{0.88z}{L_z}\right) \quad (J.4)$$

This shape function is shown in Figure 94b.

Support type: FSSS

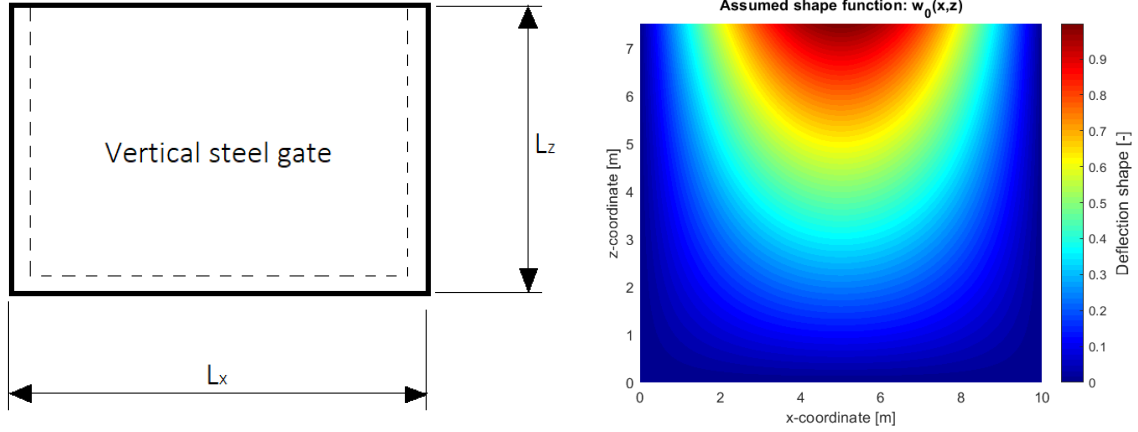


Figure 94: a) Boundary conditions of the case study gate, b) Assumed shape function $w_0(x,z)$ for the case study gate

When equation J.3 is substituted into the equation of motion (equation J.1), the following is obtained:

$$D\nabla^4 w_0(x, z) * u_0(t) + \rho_s w_0(x, z) * \ddot{u}_0(t) = f(x, z, t) \quad (J.5)$$

When the orthogonality condition is applied to equation J.5, this gives:

$$\begin{aligned} D \iint_S \nabla^4 w_0(x, z) * w_0(x, z) dS * u_0(t) + \rho_s \iint_S w_0(x, z) * w_0(x, z) dS * \ddot{u}_0(t) \\ = \iint_S \bar{f}(x, z) * w_0(x, z) dS * f(t) \end{aligned} \quad (J.6)$$

In which $\bar{f}(x, z)$ is the distribution of the wave impact force over the gate surface, and $f(t)$ is the corresponding course in time of this wave impact force.

The next step is to substitute equation J.7 into the homogeneous equation of motion. This results in equation J.8.

$$w(x, z, t) = w_0(x, z) * e^{i\omega t} \quad (J.7)$$

$$(D\nabla^4 w_0(x, z) - \rho_s \omega^2 w_0(x, z)) * e^{i\omega t} = 0 \rightarrow D\nabla^4 w_0(x, z) = \rho_s \omega^2 w_0(x, z) \quad (J.8)$$

When equation J.8 is substituted into the orthogonality equation (J.6), the following is obtained:

$$\rho_s \omega^2 \iint_S w_0(x, z) * w_0(x, z) dS * u_0(t) + \rho_s \iint_S w_0(x, z) * w_0(x, z) dS * \ddot{u}_0(t) = \bar{F}_0 * f(t) \quad (J.9)$$

$$\bar{F}_0 = \iint_S \bar{f}(x, z) * w_0(x, z) dS \quad \text{and} \quad L_0 = \iint_S w_0(x, z) * w_0(x, z) dS \quad (J.10)$$

$$L_0(\rho A \omega^2 u_0(t) + \rho_s \ddot{u}_0(t)) = \bar{F}_0 * f(t) \quad (J.11)$$

Equation J.11 can be rewritten as the following generalised SDOF equation of motion:

$$\ddot{u}_0(t) + \omega_n^2 u_0(t) = \frac{\bar{F}_0}{L_0 * \rho_s} * f(t) = \frac{\iint_S \bar{f}(x,z) * w_0(x,z) dS}{\rho_s \iint_S w_0(x,z)^2 dS} * f(t) \quad (J.12)$$

In which the factor in front of the time signal of the wave impact force at the right hand side of the equation, is a constant which can be calculated. Also, the natural frequency of the submerged gate indicated in Figure 94a is known from the semi-analytical model. For a gate with thickness of $t = 0.243$ m, the wet natural radial frequency is: $\omega_{n,w} = f_n * 2\pi = 6.71 * 2\pi = 42.16$ rad/s. With this data, Matlab can be used to solve equation J.12, and calculate the maximum response (deflection) for each wave impact from the 'model' force-time signal. This results are used to compare the SDOF model with the semi-analytical (MDOF) model in section 7.3.

The equivalent SDOF model is validated based on the semi-analytical model. The amount of modes that are taken into consideration can be set for the semi-analytical model, so to validate the equivalent SDOF model the semi-analytical has been run for only 1 mode. For this validation the options to include surface waves, and compressibility of the water are turned off in the semi-analytical model.